STUDY OF VISCOUS AND MATTER CREATION EFFECTS IN COSMOLOGY

A thesis submitted to

DELHI TECHNOLOGICAL UNIVERSITY

in partial fulfillment of the requirements for the award of the degree of

DOCTOR OF PHILOSOPHY

in

MATHEMATICS

By

AJAY KUMAR

Under the Supervision of

Prof. Chandra Prakash Singh

DEPARTMENT OF APPLIED MATHEMATICS

DELHI TECHNOLOGICAL UNIVERSITY

(Formerly Delhi College of Engineering)

BAWANA ROAD, DELHI-110 042, INDIA.

June, 2021 **Enroll. No. : 2K16/PHD/AM/02**

DECLARATION

I declare that the research work reported in this thesis entitled "**Study of Viscous and Matter Creation Effects in Cosmology**" for the award of the degree of *Doctor of Philosophy in Mathematics* has been carried out by me under the supervision of *Prof. Chandra Prakash Singh*, Department of Applied Mathematics, Delhi Technological University, Delhi, India.

The research work embodied in this thesis, except where otherwise indicated, is my original research. This thesis has not been submitted by me earlier in part or full to any other University or Institute for the award of any degree or diploma. This thesis does not contain other person's data, graphs, or other information unless specifically acknowledged.

Date : **(Ajay Kumar)**

CERTIFICATE

On the basis of a declaration submitted by **Mr. Ajay Kumar**, Ph.D. scholar, I hereby certify that the thesis titled **"Study of Viscous and Matter Creation Effects in Cosmology"** submitted to the Department of Applied Mathematics, Delhi Technological University, Delhi, India for the award of the degree of *Doctor of Philosophy in Mathematics*, is a record of bonafide research work carried out by him under my supervision.

I have read this thesis and that, in my opinion, it is fully adequate in scope and quality as a thesis for the degree of Doctor of Philosophy.

To the best of my knowledge, the work reported in this thesis is original and has not been submitted to any other Institution or University in any form for the award of any Degree or Diploma.

(Prof. Chandra Prakash Singh)
Associate Head and Supervisor
Department of Applied Mathematics
Delhi Technological University
Delhi.

(Prof. S. Sivaprasad Kumar)
Head
Department of Applied Mathematics
Delhi Technological University
Delhi.

ACKNOWLEDGEMENTS

It would not have been possible to write this doctoral thesis without the kind support and help of many individuals around me, to only some of whom it is possible to give a particular mention here. I would like to extend my sincere thanks to all of them.

First and foremost, praises and thanks to the GOD, the almighty, for His showers of blessings throughout my research work to complete the research successfully.

I would like to express my special gratitude and thanks to my supervisor Prof. Chandra Prakash Singh, Professor, Department of Applied Mathematics, Delhi Technological University (DTU), Delhi for the continuous support, for his patience, motivation, enthusiasm, and immense knowledge. His guidance helped me in all the time of research and writing of this thesis. It is indeed a great privilege and honor for me to work under his supervision. I am extremely grateful for what he has offered me. Without his guidance and persistent help, this thesis would not have been possible.

Besides my supervisor, I would like to thank Prof. S. Sivaprasad Kumar, Head, Department of Applied Mathematics, DTU for providing me the necessary facilities in the Department.

My sincere thanks also goes to Prof. H.C. Taneja, DRC chairman, Department of Applied Mathematics, DTU for his everlasting support and guidance. I am grateful to all faculty members of the Department of Applied Mathematics, DTU for their constant support and encouragement.

I also wish to extend my gratitude to Prof. Shri Ram, Ex. Head, Department of Mathematics, Indian Institute of Technology, Banaras Hindu University, Varanasi and Prof. J.K. Singh, Head, Department of Mathematics, Netaji Subhas University of Technology, New Delhi for their valuable guidance from the beginning of my Ph.D. research work.

I would like to acknowledge the academic and technical support of the Delhi Technological University, Delhi, and its staff, particularly the Academic-PG section for their all kinds of support. The library facilities of the University have been indispensable. I also thank everyone in the Department of Applied Mathematics for their support and assistance.

I am extremely grateful to my family and relatives for their love, prayers, caring, and sacrifices for educating me and preparing me for my future.

I place my acknowledge to Dr. Vijay Singh, Dr. Pankaj Kumar, Dr. Milan Srivastava, and Ms. Simran Kaur for valuable discussions on the subject matter and for their support. I also place on record, my sense of gratitude to one and all who, directly or indirectly, have lent their helping hand in this journey.

My acknowledgements would not be complete without thanking the University Grants Commission (UGC), Government of India, for providing fellowship (JRF and SRF) that made my Ph.D. work possible.

Date : **(AJAY KUMAR)**

Place : DTU, Delhi, India.

Dedicated

to

My Family

Contents

Preface

The general theory of relativity has far-reaching applications to cosmology, astrophysics, and particle physics. Consequently, scientists from diverse disciplines have started working on the applications of general relativity in their respective subjects. As a result, the general interest in general relativity has increased and is gradually increasing more and more. General relativity has changed our perception of the laws of the Universe remarkably and has developed a new branch of science called Cosmology. Steven Weinberg's famous book *The First Three Minutes* and Stephen Hawking's book *A Brief History of Time* has caused an avalanche of interest in this subject.

The modern cosmology has entered into the era of observational precision which is changing the frontiers of our knowledge about the Universe very rapidly. The twentieth century has not only witnessed the most exciting discovery of expanding Universe but it ended with the mysterious discovery through the observations of type Ia supernova in 1998 which evidence that the expansion of the Universe is accelerating. The recent discovery of gravitational waves by the LIGO probe and Black holes are some of the examples of it. At present, we have data coming from the probes like Type Ia supernova, Wilkinson Microwave Anisotropy Probe, Baryon Acoustic Oscillations, Sloan Digital Sky Survey, Planck collaboration, etc.

Nowadays, the quest to understand this late-time cosmic acceleration is one of the major challenges in cosmology. The standard cosmological model based on Einstein's general relativity is the most successful model but it does not account for the observed accelerated expansion of the Universe if the fluid content is taken only the standard matter and radiation. In fact, it needs to be supplemented by some exotic matter or modification in general relativity to accommodate the accelerated regime.

Since the discovery of the accelerated expansion of the Universe, several theories have been proposed to explain the accelerated phenomena. One of them is the assumption of the existence of a mysterious component with negative pressure, so-called *dark energy* (DE). The most natural and successful candidate of dark en-

ergy is the cosmological constant which was introduced by Einstein to obtain a static Universe. Many other dark energy candidates like scalar fields, chaplygin gas, holographic dark energy, Ricci dark energy, etc. have been proposed to explain the accelerated expansion of the Universe.

In the past few decades, a number of modified theories of gravity such as Gauss-Bonnet $f(G)$ theory, $f(R)$ theory, $f(R,G)$ theory, $f(T)$ theory, $f(R,T)$ gravity, etc. have also been proposed to explain the current epoch of cosmic acceleration. The study of dark energy models is of great interest in such modified gravity theories.

However, besides these two distinct approaches, in recent years, other alternatives to describe the current accelerating Universe have attracted special attention. Just like the early time cosmic acceleration associated with inflation, negative pressure can be seen as a possible driving mechanism for the late time accelerated expansion of the Universe as well. One of the earliest alternatives that could provide a mechanism producing such an accelerating Universe is through a negative pressure produced by viscous and/or matter creation. Some authors have explored that matter creation might be described equivalently in terms of a bulk viscous pressure in the cosmological fluid. Despite the fact that bulk viscous and matter creation cosmology apparently look similar, they have some fundamental differences. Bulk viscous cosmology is associated with a generalization of the hydrodynamics of ideal fluids for the case of non-ideal ones, with constitutive equations describing the viscous pressure built as additional correction terms to the equilibrium energy-momentum stress tensor. The matter creation process is classically described by a back reaction term in the Einstein field equations whose negative pressure may provide a self-sustained mechanism of cosmic acceleration.

Our aim, in this thesis, is to explore the effects of bulk viscosity and matter creation in holographic dark energy within the framework of a spatially homogeneous and isotropic flat Friedmann-Lemaître-Robertson-Walker metric. Chapter 1 is introductory in nature. Chapters 2 – 6 are based on the research work published in the form of research papers in reputed refereed journals. The abstract at the beginning of a chapter gives a brief outline of the work carried out in that chapter. I acknowledge the authors whose articles/research work and books have substantially helped me to write the thesis in the present form.

Date : **(AJAY KUMAR)**

Place : DTU, Delhi, India.

List of Figures

List of Tables

Chapter 1

Introduction

The introductory Chapter contains the fundamental concept of the General theory of relativity, cosmological principle, Einstein's field equations, cosmological parameters, modified theory of gravitation, dark energy, and accelerating Universe. The thermodynamics of the dissipative phenomenon (bulk viscosity and matter creation) are also studied in this chapter. Some latest observational data, like Type Ia supernova, observational Hubble data, baryon acoustic oscillations, cosmic microwave background data are discussed. This chapter also includes a brief discussion on some important cosmological and geometrical parameters. Finally, the motivation and plan of the research work are discussed.

General relativity is the theory of space-time and gravitation introduced by Albert Einstein in 1915 and published in 1916 [1]. It is one of the most beautiful and revolutionary conceptions of modern science. It describes that gravity is the geometry of four-dimensional curved space-time. Gravity governs the structure and evolution of the Universe on the largest scales of space-time. Cosmology is a branch of science which deals with the study of the origin of the Universe, its evolution, large scale structures and their dynamics, and its eventual fate. It is defined in the framework of General relativity. Therefore, cosmology is one of the most important applications of General relativity. In recent years, our understanding of the Universe has increased dramatically-both theoretically and observationally. The great observational progress in cosmology has revealed the existence of new mysterious components of the Universe: dark matter and dark energy. In the past twenty years, a standard model of cosmology, known as *Lambda-CDM model* has become mature, based on which we are able to describe the evolution of the Universe. However, certain aspects of this model are puzzling enough that may require new concepts that would go beyond this standard model. I will highlight some of the important topics in the following sections which explain the past and present progress in cosmology.

1.1 General Theory of Relativity

In the early twentieth century, Einstein developed two theories of relativity, namely the Special theory of relativity and the General theory of relativity. The special theory of relativity (STR) is a relativistic theory of space-time. It explains that the laws of physics are invariant for all non-accelerating observers. It only takes into account inertial systems in free space, where gravitational effects can be ignored. The speed of light is always constant regardless of the motion of the light source or the motion of the observer. To extend the principle of relativity for non-inertial systems Einstein [1] presented an extended theory, known as the General theory of relativity (GTR). GTR tells us that massive objects cause a distortion in space-time which causes gravity. The key idea of GTR is that gravity is not an ordinary force, but rather a property of space-time geometry. GTR is based on two basic principles: The principle of general covariance and the principle of equivalence.

The *principle of general covariance* states that the laws of physics remain covariant independent of the frame of reference. Einstein found tensor calculus an excellent

tool for the presentation of his general theory of relativity [1]. According to this principle, we must express all the physical laws of nature by means of equations in the covariant form, which are independent of the coordinate systems. Thus, the laws of nature can be expressed in the form of tensor equations because a tensor equation has exactly the same form in all coordinate systems.

The tensorial form of the line element is

$$ds^2 = g_{\mu\nu}dx^\mu dx^\nu, \quad (\mu,\ \nu = 0,1,2,3), \tag{1.1.1}$$

where $g_{\mu\nu}$ is a metric tensor of rank 2 obeying the transformation law

$$\bar{g_{ij}} = \frac{\partial x^\mu}{\partial \bar{x^i}}\frac{\partial x^\nu}{\partial \bar{x^j}}g_{\mu\nu}, \tag{1.1.2}$$

where the quantities carrying bar correspond to the new coordinate system. The metric tensor contains all the information about the gravitational field and is a symmetric tensor satisfying $g_{\mu\nu} = g_{\nu\mu}$. The contravariant tensor $g^{\mu\nu}$ corresponding to $g_{\mu\nu}$ is defined by $g_{\mu\nu}g^{\nu\lambda} = \delta^\lambda_\mu$, where δ^λ_μ is the Kronecker delta with $\delta^\lambda_\mu = 1$ when $\lambda = \mu$ and zero otherwise.

The line element (1.1.1) represents the curved geometry. Thus, according to GTR, space is curved in a gravitational field. Therefore, the geometry of space in a gravitational field is Riemannian which was originally developed by Riemann. In four-dimensional Riemannian space, the points are labeled by a general coordinate system $x^\mu = (x^0, x^1, x^2, x^3)$, where $x^0 = ct$ (c represents the speed of light) is a time coordinate and the other three are spatial coordinates. We will employ the 'space-like convention' for the metric, such that when it is diagonalized, it has the signature $(-,+,+,+)$. The metrics with this signature (one minus and the remainder plus) are called *Lorentzian*.

The *principle of equivalence* explains about 'equivalence of inertial mass and gravitational mass'. Einstein observed that the force due to gravity (gravitational force) experienced by a person standing on the massive objects (like earth) is equivalent to the pseudo-force experienced by the observer in the non-inertial frame of reference. According to local gravity experiments in the solar system, it is known that the equivalence principle between inertial and gravitational masses holds in high precision. The principle of equivalence is a very powerful tool in the general theory of relativity.

[1] The principal aim of tensor calculus is to investigate the relations which remain valid when we change from one coordinate system to any other.

1.2 Cosmological Principle

The cosmological principle states that the Universe is assumed to be homogeneous (no change during linear motion) and isotropic (non change during angular motion) at any instant of cosmic time t, when it is viewed on a large enough scale. It can be justified on the scales of larger than 100 MPc. Thus, following the Cosmological Principle, the Universe looks the same from all positions in space. Let us explain these two terms in brief.

Homogeneity means that the same observational evidence is available to observers at different locations in the Universe, i.e., there is no special place in the Universe. When it is viewed on the larger scales, homogeneity implies that the average density of matter in all locations in the Universe is around the same and the Universe is fairly smooth on large scales.

Isotropy means that the same observational evidence is available by looking in any direction in the Universe. That is, isotropy means there are no special directions to the Universe. An isotropic Universe also means that the Universe has no 'center'. A particular orientation (north and south poles) is formed by the Planet, but the Universe from every location appears the same. These two concepts sound identical, but they have very different characteristics.

Thus, according to cosmological principle, the laws of physics are universal. The same physical laws and models that apply here on the Earth also work in distant stars, galaxies, and all parts of the Universe. It is to be noted that it is assumed that physical constants (gravitational constant, the mass of the electron, speed of light) also do not change from place to place within the Universe, and over time. If we extend cosmological principle through time we have the 'perfect cosmological principle', i.e., the Universe is isotropic and homogeneous and has been for all time.

1.3 Cosmological Models

Let us begin with the space-time geometry of a homogeneous and isotropic cosmological model. Friedmann-Lemaître-Robertson-Walker (FLRW) metric, which is now widely known as Friedmann-Robertson-Walker (FRW) line element, is a metric for a spatially homogeneous and isotropic Universe. For a local observer, one can approx-

imate general relativity with the special relativity, described by Minkowski space-time with metric $\eta_{\mu\nu} = diag(-1,+1,+1,+1)$. The FLRW metric $g_{\mu\nu}$ can be approximated by $g_{\mu\nu} \approx \eta_{\mu\nu}$ only locally. The isotropy of the Universe implies that the off-diagonal terms, $g_{\mu\nu}$ vanishes with $\mu \neq \nu$, since there are no privileged directions. From the homogeneity of the Universe, we deduce that $g_{\mu\nu}$ (in cartesian coordinates) must be independent of the spatial coordinates since no position is preferable.

The most general spatially homogeneous and isotropic Friedmann-Lemaître-Robertson-Walker metric from (1.1.1) in spherical coordinates (r,θ,ϕ) can be written as [2]

$$ds^2 = -c^2dt^2 + a^2(t)\left[\frac{dr^2}{1-kr^2} + r^2(d\theta^2 + sin^2\theta d\phi^2)\right], \tag{1.3.1}$$

where k denotes the curvature of the space-time, $a(t)$ is the cosmic scale factor of the Universe which describes the expansion or contraction of the Universe. Different values of the curvature k define different geometry of space-time, i.e., a flat Universe for $k = 0$, a closed Universe for $k = +1$ and an open Universe for $k = -1$ [3, 4]. These different geometries also define the possible ultimate fate of the Universe. The closed geometry represents a Universe which collapses at the end and, open and flat geometries represent an ever expanding Universe. For a flat Universe, the FLRW line element can be written in the form [2]

$$ds^2 = -dt^2 + a^2(t)\left[dr^2 + r^2(d\theta^2 + sin^2\theta d\phi^2)\right]. \tag{1.3.2}$$

1.4 Einstein's Field Equations

In GTR, the geometry of the space-time is included in the metric tensor $g_{\mu\nu}$, while the matter content of the Universe is expressed by the energy-momentum tensor $T_{\mu\nu}$. The Einstein's field equation relates the energy-momentum tensor, $T_{\mu\nu}$ with the geometry of the Universe, $G_{\mu\nu}$ through the equation

$$G_{\mu\nu} = 8\pi G\, T_{\mu\nu}, \tag{1.4.1}$$

where G is Newton's gravitational constant and $G_{\mu\nu}$ is the Einstein tensor which is given by

$$G_{\mu\nu} = R_{\mu\nu} - \frac{1}{2}g_{\mu\nu}R, \tag{1.4.2}$$

[2] We consider the speed of light $c = 1$ throughout the thesis.

where R and $R_{\mu\nu}$ are the Ricci scalar and Ricci tensor, and are defined as follows:

$$R = g^{\mu\nu} R_{\mu\nu}, \tag{1.4.3}$$

$$R_{\mu\nu} = \frac{\partial \Gamma^{\lambda}_{\mu\nu}}{\partial x^{\lambda}} - \frac{\partial \Gamma^{\lambda}_{\mu\lambda}}{\partial x^{\nu}} + \Gamma^{\lambda}_{\mu\nu}\Gamma^{\delta}_{\lambda\delta} - \Gamma^{\delta}_{\mu\lambda}\Gamma^{\lambda}_{\nu\delta}, \tag{1.4.4}$$

where

$$\Gamma^{\lambda}_{\mu\nu} = \frac{1}{2} g^{\lambda\tau}(g_{\tau\mu,\nu} + g_{\tau\nu,\mu} - g_{\mu\nu,\tau}) \tag{1.4.5}$$

is the Christoffel symbol. With the help of (1.4.2), Eq. (1.4.1) can be expressed as

$$R_{\mu\nu} - \frac{1}{2} g_{\mu\nu} R = 8\pi G\, T_{\mu\nu}. \tag{1.4.6}$$

Equation (1.4.6) is the field equation of general relativity which is known as *Einstein's equation*. Thus, the general relativity says that space-time is a manifold M on which there is defined a Lorentz metric $g_{\mu\nu}$. The curvature of $g_{\mu\nu}$ is related to the matter distribution in space-time by Einstein's equation (1.4.6).

By contracting the Bianchi identity, one can deduce that the Einstein tensor $G_{\mu\nu}$ has zero divergence, i.e., $G^{\mu\nu}{}_{;\nu} = \left(R^{\mu\nu} - \frac{1}{2} g^{\mu\nu} R\right)_{;\nu} = 0$. Therefore, we see that Einstein's equations (1.4.6) are compatible with $T^{\mu\nu}{}_{;\nu} = 0$, which is the law of conservation of mass-energy and momentum. This conservation law is a physical requirement.

The Einstein field equation can also be obtained by varying the Einstein-Hilbert (EH) action with respect to $g^{\mu\nu}$. The EH action for gravity with the inclusion of matter fields is given by [2]

$$S = \int d^4x \sqrt{g} \left(\frac{1}{2\kappa} R + \mathscr{L}_m \right), \tag{1.4.7}$$

where $\mathscr{L}_m$ is the matter Lagrangian density of any matter fields and $\kappa = 8\pi G$.

At large scales and with high precision, matter inside a homogeneous and isotropic Universe can be described as a perfect fluid. It is clear that, if a fluid that is isotropic in some frame leads to a metric that is isotropic in some frame, the two frames will coincide; that is, the fluid will be at rest in comoving coordinates. Its energy-momentum tensor $T_{\mu\nu}$ contains all the information about the energy content of the Universe and is solely determined by its energy density $\rho(t)$ and isotropic pressure $p(t)$.

In general relativity, continuous matter distributions and fields are described by a energy-momentum tensor. The energy-momentum tensor for perfect fluid is defined as

$$T_{\mu\nu} = (\rho + p) u_{\mu}\, u_{\nu} + p\, g_{\mu\nu}, \tag{1.4.8}$$

where p is the pressure of the perfect fluid, ρ is the energy density and $u^\mu = \frac{dx^\mu}{dt}$ is the four-velocity normalized as $u_\mu u^\mu = -1$. Equation (1.4.8) satisfies the equation of motion

$$T^{\mu\nu}{}_{;\nu} = 0, \tag{1.4.9}$$

which yield

$$\dot{\rho} + 3\frac{\dot{a}}{a}(\rho + p) = 0, \tag{1.4.10}$$

where an overdot denotes derivative with respect to cosmic time t.

1.5 Friedmann Equations and its Solutions

To describe the dynamical evolution of the Universe, let us substitute the space-time metric (1.3.1) and energy-momentum tensor for perfect fluid (1.4.8) into the Einstein's equation (1.4.6). We will get 10 equations corresponding to the 10 independent components of a symmetric two-index tensor. However, on account of the space-time symmetries , there will be only two independent equations. Thus, the general evolution equations for homogeneous and isotropic cosmology, which are known as Friedmann equations [5], can be obtained as

$$\frac{\dot{a}^2}{a^2} = \frac{8\pi G}{3}\rho - \frac{k}{a^2}, \tag{1.5.1}$$

$$\frac{2\ddot{a}}{a} + \frac{\dot{a}^2}{a^2} = -8\pi G p - \frac{k}{a^2}, \tag{1.5.2}$$

where an overdot denotes differentiation with respect to cosmic time t. These two equations connect the evolution of the scale factor $a(t)$ to the content of the Universe and its curvature. Equation (1.5.1) serves as a definition of the Hubble parameter $H = \frac{\dot{a}}{a}$, which quantifies the relative expansion rate of the Universe.

Using the first Friedmann equation (1.5.1), the acceleration equation (1.5.2) can be rewritten as

$$\frac{\ddot{a}}{a} = -\frac{4\pi G}{3}(\rho + 3p), \tag{1.5.3}$$

which is sometimes called the Raychaudhuri equation. Depending on the sign of $\ddot{a}$ in (1.5.3), we can discriminate between an accelerating and a decelerating Universe and obtain a condition on the matter variables. The Universe decelerates for $\rho + 3p > 0$, while accelerates for $\rho + 3p < 0$.

We can choose an *equation of state* (EoS), a relationship between ρ and p to solve

the field equations. Often the perfect fluid relevant to cosmology obeys the simple equation of state

$$p = \omega\rho, \tag{1.5.4}$$

where ω is the EoS parameter which is the ratio of pressure to density. For a non-relativistic (dust-like) perfect fluid, $\omega = 0$ while for a relativistic (radiation-like) fluid, $\omega = 1/3$. With the help of (1.5.4), the condition from (1.5.3) can be transferred to the equation of state parameter implying $\omega > -1/3$ for deceleration and $\omega < -1/3$ for acceleration.

Using (1.5.4), the conservation equation (1.4.10) becomes

$$\frac{\dot{\rho}}{\rho} = -3(1+\omega)\frac{\dot{a}}{a}. \tag{1.5.5}$$

If ω is constant, this can be integrated to obtain

$$\rho \propto a^{-3(1+\omega)}. \tag{1.5.6}$$

Depending on the form of energy content of the Universe, i.e., the value of ω, the exact evolution of energy density can be determined. For a dust-like fluid, which is usually referred to as simply matter fluid, we have $p = 0$ and thus the evolution of energy density in this case is

$$\rho \propto a^{-3}, \tag{1.5.7}$$

while for a radiation-like fluid $p = \rho/3$ and thus the energy density evolves as

$$\rho \propto a^{-4}. \tag{1.5.8}$$

It is to be noted that the energy densities for both components depend on the scale factor. Both components are diluted as the Universe expands giving an a^{-3} dependence. The extra factor a^{-1} for the radiation comes from the red shifting of the photons as they travel through expanding space.

Friedmann equation (1.5.1) can be solved in conjunction with (1.5.6) to find the evolution of the scale factor as a function of the cosmic time which determines the dynamics of the Universe at background level. For a flat FLRW Universe

$$a \propto t^{\frac{2}{3(1+\omega)}}, \tag{1.5.9}$$

which reduces to the following equations depending on the values of ω

$$a \propto t^{\frac{2}{3}}, \text{ for matter} \tag{1.5.10}$$

$$a \propto t^{\frac{1}{2}}, \text{ for radiation} \tag{1.5.11}$$

From (1.5.10) and (1.5.11), one can deduce that a matter-dominated Universe expands faster than a radiation-dominated Universe, but both of them expands with a decelerated rate as $\ddot{a} < 0$ at any time.

1.6 Expanding Universe

Einstein in 1917 proposed a cosmic model based on his general relativistic field equation which is expressed as

$$R_{\mu\nu} - \frac{1}{2} g_{\mu\nu} R + \Lambda g_{\mu\nu} = 8\pi G\, T_{\mu\nu}, \tag{1.6.1}$$

where Λ is the cosmological constant.

Einstein added the cosmological constant in his original field equation in order to get the static Universe. The young mathematician Alexander Friedmann [5] voraciously studied the theory by assuming the structure of the Universe as a whole. He adopted Einstein's assumptions that the Universe was homogeneous and isotropic and that it had a closed spherical geometry. Then he took a radical step: he did not require that the Universe is static. With the requirement of a static Universe lifted, Friedmann found dynamical solutions to Einstein's equations which described the non-static Universe.

The Belgian priest Georges Lemaitre rediscovered the expanding Universe models in 1927, but his work also passed unnoticed [6]. All this changed in the late 1920s when Edwin Hubble [7] observed that the Universe is indeed expanding which was arguably the most unexpected discovery in the history of science. Hubble related the recession velocity of galaxies to their distance from us through Hubble's law which can be given in the following form:

$$v = H_0 D, \tag{1.6.2}$$

where v is the galaxy's recession velocity, which is usually expressed in Km/s, and D is the galaxy's proper distance from the observer, which is measured in megaparsecs (Mpc). The proportionality factor H_0 is the Hubble factor today also called the Hubble constant. Assuming the homogeneous and isotropic Universe (see Sect. 1.2), Hubble's law implies that galaxies are receding not only from us but also from each other; all galaxies are moving apart as the Universe itself expands. Just as the theoretical cosmology started after Einstein's model, so did Hubble's findings launch observational cosmology which deals with the observational studies of the Universe at the large-scale.

If the Universe is expanding and all galaxies are moving apart, we can imagine reversing time and watching them come together at some moment in the past: the Big Bang. The time when the condition $a = 0$ happened is called the Big Bang and the theory describing the Universe as generating from that moment is known as the Big Bang theory. According to this theory, the Universe began around 13.8 billion years ago from an infinite energy density, i.e., in the past, the distances were really small and all the matter and energy content of the Universe were located into a small amount of space and consequently, the mean energy (or temperature) was much higher than the mean energy observed today. The Universe came into existence after the Big Bang and eventually started to cool as it expanded from a state of higher temperature and density [2]. The Big Bang theory is indeed in astonishing agreement with observations and it is considered a perfectly good model of our Universe for times ranging from few fractions of a second to billions of years (i.e. today) after the Big Bang. The ΛCDM is the current "standard model" of Big Bang cosmology that can account for various measurements and observational data.

1.7 Inflationary Universe

The standard Big Bang model has been successful in presenting a theoretical explanation for several important experimental observations. It describes cosmic evolution starting from a fraction of a second after the Big Bang, accurately predicts the primordial nuclear abundances and the properties of the microwave background radiation, and explains how galaxies and clusters were formed over billions of years. But we should note that this model is far from a complete model of the Universe. It is not able to account for the state of the Universe at much earlier times when it was significantly

hotter and must assume certain very finely-tuned initial conditions that just clamor for an explanation. The cosmological inflation theory is not a replacement for the Big Bang theory, but rather an extra add-on idea that is supposed to apply during some very early stage of the Universe's expansion. Before describing the idea of inflation, let us cover some of the historical motivations which led to its introduction. We start the discussion by listing some of the unsatisfactory aspects of the Big Bang theory.

- **The Horizon Problem:** If one regards the fundamental assumption for the FLRW Universe, then there is a problem with the hot Big Bang model. This fundamental assumption known as the cosmological principle which states that the Universe is very homogeneous and isotropic on large scales, which does indeed seem to agree with the measurements. If one considers two different parts of the Universe that are outside of each other's horizons. They are so far apart that no light signal sent from one at beginning of the Universe could have reached the other. Yet they are observed to have similar properties. This suggests their being in thermal contact sometime in the past. Since the radiation from two distant opposite parts could not possibly be causally connected because information can not travel faster than the speed of light. Nor could the regions they traveled from even have been in communication. The problem of horizons originates from the Cosmic Microwave Background radiation (CMB), the afterglow from the Big Bang, emitted at $z \approx 1100$. When pointing our instrument to measure the CMB, we obtain the same black body temperature in all directions. Such a problem is known as the horizon problem.

- **The Flatness Problem:** The Friedmann equation $(1.5.1)$ in terms of density parameter is given by

$$\Omega - 1 = \frac{k}{a^2}, \tag{1.7.1}$$

  where Ω denotes the density parameter which is defined as $\Omega = \frac{\rho}{\rho_c}$. Here, $\rho_c = 3H^2/8\pi G$ is the critical energy density required for a flat, i.e., $k = 0$ for a given value of H. It has been observed that the current density of the Universe is very close to the critical density. From the current observational data of CMB and Baryon Acoustic Oscillations (BAO), we know that the Universe is very nearly spatially flat ($|\Omega - 1| \lesssim 0.005$) [8], however, in the framework of the standard Big Bang model, the comoving Hubble radius, $(aH)^{-1}$, is increasing as the Universe evolves. As such, $\Omega = 1$ is an unstable critical point, which means that for $|\Omega - 1|$

to have its present observed value Ω must have been extremely close to unity at much earlier times. This value can only be obtained through extremely fine-tuning and leaves one questioning why nature would have chosen parameters so precisely. This is the so-called Flatness Problem.

- **The Monopole Problem:** The Grand Unified Theory (GUT) of particle physics also predicts an abundance of 'relics', typically leftover from the radiation epoch, e.g. magnetic monopoles, domain walls, etc. If such relics existed in the early Universe, then their energy densities would have decreased as a matter component, thus they would have been diluted by cosmic expansion much more slowly than radiation. As such, these massive relics can easily come to dominate the dynamics of the Universe and would cause it to rapidly close in on itself. This is not what is observed, and none of these relics have currently been experimentally observed. However, the Big Bang model has no way of disposing of them without also disturbing conventional matter in the Universe. This is the so-called Monopole (or Relic) Problem.

To deal with these problems in the Big Bang model an additional theory that provides a more complete description is needed. To date, the prevailing theory offering solutions to these problems is that of inflation, initially proposed in 1981 by Alan H. Guth [9] in his study of the cosmological implications of the grand unified theories (GUTs) of particle interactions. He suggests that one could solve these problems by introducing an epoch of accelerated, or inflationary, expansion in the early Universe. The original motivation for this theory was to explain the non-existence of magnetic monopoles, and this theory was further developed by Linde [10, 11] and Albrecht and Steinhardt [12, 13]. The idea of inflation is to introduce a phase of decreasing co-moving Hubble radius, $(aH)^{-1}$, in the very early Universe,

$$\frac{d}{dt}[(aH)^{-1}] < 0. \tag{1.7.2}$$

Note that this implies that the Universe was subject to an accelerated expansion during this period, i.e. $\ddot{a} > 0$. With the help of equations (1.7.1) and (1.7.2), we observe that such an accelerated expansion dynamically drives Ω to unity, and thus the Universe to spatial flatness. Accordingly, so long as the inflationary period is sufficiently long, Ω will be forced arbitrarily close to one, such that, despite its value being driven away from one for the remaining post-inflationary evolution of the Universe, its value

will remain extremely near to unity up to the present. Thus, inflation provides an elegant solution to the flatness problem.

This is clear from the fact that equation (1.7.2) implies that the comoving Hubble radius decreases with time, and comoving scales become bigger than the horizon during inflation. As consequence inflation solves the problem of horizons: The light cones of different points in the CMB intersected before the 'Big Bang'. In the context of inflation, the Big Bang is not understood as the beginning of the Universe, but as the point of transition between an inflationary Universe, and the Universe of increasing comoving Hubble radius. Finally, Inflation also solves the problem of relics such as magnetic monopoles since their density can be diluted away during inflation and quickly become negligible.

Scientists are still not sure about the cause of the inflationary phase, however, it is believed that there is some kind of a negative "vacuum energy density" which is triggered by the separation of strong nuclear force from the other elementary forces at that time. A natural candidate for the driving force of inflation was supposed to be the scalar field, which decayed into radiation and matter to stop this scenario. During inflation, the kinetic energy of the scalar field was dominant which allowed de Sitter-like expansion of the Universe. Inflation happened for a very short time in the very early Universe during which the Universe experienced a very rapid expansion. Due to the very rapid expansion of the Universe, the small size Universe was increased to a much larger size. Thus, the Universe that was able to reach thermal equilibrium prior to inflation has been expanded to an enormous scale, perhaps much larger than our observable Universe.

1.8 Accelerating Universe

In the late 1990s, two groups (one led by Adam Riess [14] and the other by Saul Perlmutter [15]) reported plausible evidence based on supernova explosions that the expansion of the Universe is not slowing down, as predicted by the simplest models, but accelerating. "This is not what we expected," said Riess, who won the Nobel Prize for physics in 2011 (along with Brian Schmidt and Saul Perlmutter) for his finding. Thus, the second[3] cosmic accelerated phase which is known as the late-time cosmic acceleration, is assumed to have started after the decelerated phase. This transition

[3]the first cosmic accelerated phase is the inflationary phase which has been discussed in section 1.7

from decelerating phase to the accelerating phase has been confirmed by a number of observations such as Wilkinson Microwave Anisotropy Probe (WMAP) [16, 17], Sloan Digital Sky Survey (SDSS) [18], Planck collaboration [19, 20], Cosmic Microwave Background (CMB) [21], the Baryon Acoustic Oscillations (BAO) [22], etc. The only thing that could be accelerating the expansion (i.e. more than countering the braking force of the mutual gravitational pull of the galaxies) is space itself, suggesting that perhaps it is not empty after all but contains some mysterious, repulsive force called "dark energy" (DE), currently unknown to science.

Since the discovery of the accelerating Universe, people are trying to explain this observational fact in two different ways - either by introducing some unknown kind of matter in the framework of Einstein gravity or by modifying the Einstein gravity itself. The first kind of models is called the DE models whereas the second type of models is called modified theories of gravity models. Let us study the evolution of the Universe based on these two concepts.

1.8.1 Dark Energy Models

As discussed in Section 1.8, the discovery of Riess et al. in 1998 [14] and Perlmutter et al. in 1999 [15] changed the concept about the Universe. They observed that the distant supernovae at $z \sim 0.5$ and $\Delta m \sim 0.25$ magnitude are fainter than ones expected for a decelerating Universe in the absence of cosmological constant. This observation showed that the Universe is currently expanding with accelerating rate. The present epoch of this evolution is dominated by exotic energy known as 'dark energy' (DE), which has negative pressure and occupies approximately 68.3% of the total energy density of the Universe and play an important role in the formation and evolution of the Universe. The rest matter of the Universe is assumed to be dark matter (DM) and the baryonic matter[4], which occupies about 26.8% and 4.9% of total matter density, respectively.

These observations inspire theorists to understand the mechanism of the accelerated expansion of the Universe. Therefore, the theorists have proposed various cosmological models of dark energy to explain this bizarre phenomenon. Among the many possible proposals, possibly a cosmological constant (Λ) is the simplest answer to explain the late-time cosmic acceleration [23] because of its weird repulsive gravity. The cosmological constant provides a pretty good explanation for the expan-

[4]In cosmology, 'baryonic matter' is used to describe protons, neutrons, and electrons.

sion of the Universe being accelerated. However, this also brings some theoretical difficulties, which are how to explain its origin, right magnitude, and why it comes to dominate just now [24–26]. Therefore, it is natural to look for alternative models which can explain the accelerated expansion of the Universe.

In order to alleviate these problems and explain the accelerated expansion of the Universe, cosmologists have tried to explore various dynamical dark energy models like a quintessence, quiessence, K-essence, tachyon, phantom, Chaplygin gas model, holographic dark energy (HDE), holographic Ricci dark energy (HRDE), etc. A negative pressure term is always taken into account. Such as, the cosmological constant model with equation of state $\omega_\Lambda = p_\Lambda/\rho_\Lambda = -1$, where p_Λ and ρ_Λ are pressure and density of the dark energy, respectively, the quiessence whose equation of state is a constant between -1 and $-1/3$, and the quintessence which is described in terms of a scalar field ϕ. From equation (1.5.3), we understand that for accelerating Universe we require $\ddot{a} > 0$. Thus, in order to explain the current acceleration of the Universe, we require exotic energy dubbed dark energy with the equation of state satisfying $\omega < -1/3$.

Nowadays, there are many candidates for dark energy. Considering the purpose of the works to be presented in this thesis, we would discuss only those candidates, which are having significant relevance to the thesis. A plethora of literature is available where various candidates for dark energy have been discussed [27–29]. In a review paper, Copeland et al. [28] discussed various features of dark energy in an extensive manner. The standard ΛCDM model and dynamical DE models will be briefly discussed in the following sections.

The Standard ΛCDM Model

The simplest explanation of the cosmic acceleration of our Universe is given by the Lambda Cold Dark Matter (ΛCDM) model. The ΛCDM model is a mathematical parametrization of Big Bang cosmology which is described by general relativity and FLRW equations. This models assumes that the Universe is photons, neutrinos, ordinary matter(baryon) and cold (non-relativistic) dark matter and a cosmological constant, which is responsible for the observed acceleration.

The history of the cosmological constant started when Einstein added a cosmological constant to the equations of motion for the metric in general relativity (i.e. to the Einstein equations) in order to construct a cosmological model for a static Universe. After the discovery of the expansion of the Universe, the cosmological constant has

been almost forgotten due to the fact that its contribution is not necessary to achieve a dynamical expansion in FLRW cosmology. However, after the 1998 observation that the Universe is accelerating, the cosmological constant has been revived as a model of dark energy. A cosmological constant, because of its effective negative pressure has a repulsive effect and could counterbalance ordinary matter and Einstein's solution.

One can observe from Einstein's modified equations (1.6.1) that the cosmological constant Λ was included in the geometric part of the equations (i.e., in the left-hand side) to make the cosmological model as static. Now, the cosmological constant is currently associated with a vacuum energy or dark energy in empty space that is used to explain the contemporary accelerating expansion of the Universe. Therefore, it may be considered on right side of field equation (1.6.1), i.e. towards matter part. As a result, the updated equations (1.6.1) can be written as

$$R_{\mu\nu} - \frac{1}{2} g_{\mu\nu} R = 8\pi G \, (T_{\mu\nu} + T^{\Lambda}_{\mu\nu}). \tag{1.8.1}$$

where $T^{\Lambda}_{\mu\nu}$ denotes the cosmological constant's energy–momentum tensor, and the energy is said to be the energy of space (vacuum). Throughout the evolution, it remains unchanged. The energy–momentum tensor of vacuum energy can be defined as

$$T^{(vac)}_{\mu\nu} = -\rho_{\Lambda} g_{\mu\nu} = T^{\Lambda}_{\mu\nu}. \tag{1.8.2}$$

The relation between the vacuum energy density and the cosmological constant is $\rho_{\Lambda} = \frac{\Lambda}{8\pi G}$. The EoS of the cosmological constant is given by $p_{\Lambda} = -\rho_{\Lambda}$, where $\omega = -1$ is the EoS parameter.

The ΛCDM model, while successful at explaining the observational measurements and providing accurate predictions from large-scale cosmological simulations, faces theoretical challenges like fine-tuning and cosmic coincidence problems. For the first time, Steinhardt [30] and Zlatev et al. [31] discussed the cosmological coincidence problem. The coincidence problem refers to the coincidence of densities of DM and DE, even though their evolutions are different, and the fine-tuning problem refers to the discrepancy between the theoretical and the observational value of the vacuum energy or cosmological constant. The observations predict a very tiny value in comparison to the theoretical value leading to the famous and very worrying a discrepancy of 122 orders of magnitude.

Dynamical Dark Energy Models

Taking the fine-tuning and coincidence problems into consideration, in recent times many attempts have been made to tackle these issues, particularly, the dynamical DE models [28]. *'Quintessence'* is one of the simplest and most popular candidates for dynamical DE, proposed immediately after the 1998 discovery of cosmic acceleration [31–39]. Unlike the constant $\omega = -1$ equation of state for the cosmological constant, in the case of dynamical dark energy (or quintessence) the equation of state dynamically changes with time [40, 41]. The concept of quintessence basically uses a *scalar particle field* [42, 43]. The quintessence model provides a solution to the fine-tuning problem and by means of tracker solutions, it provides a solution to the coincidence problem also. Quintessence is inspired by the most basic models of inflation, where a slow-rolling scalar field drives the rapid expansion of the early Universe [44]. Scalar fields are proposed as a candidate for the CDM, and are thought to be responsible for the creation of cosmological structures [45].

Due to the remarkable qualitative similarity between the present DE and the primordial DE that derives inflation in the early Universe, inflationary models based on scalar fields have also been used to characterise late-time cosmic acceleration [28,31,35–37,39,46,47]. As a result, in recent years, scalar field cosmological models have become more common. The evidence from different observational data [48–52] also predict a possibility of the existence of some strange kind of fields in the Universe such as the *phantom field* as proposed by Caldwell [53] with negative kinetic energy [54, 55]. Some other candidates of dynamical DE are also proposed in literature such as the quintom (a combination of quintessence and phantom scalar fields) [56], tachyonic field [57–59], k-essence [59–61], Chaplygin gas [62, 63], etc.

Using such forms of DE candidates as a responsible agent to explain the evolution of the Universe is a common issue nowadays [28,39,57,59,63–65]. Apart from these DE models, there are some other possible candidates using significant properties of quantum mechanics like HDE, HRDE, agegraphic dark energy, etc. Let us discuss briefly the theory of HDE and HRDE.

Holographic Dark Energy

As discussed above, a typical candidate of DE is the cosmological constant in GTR. For the first time in history, theorists are forced to justify not only why the cosmological constant is small, but also why it is comparable to the critical density [66]. An intrigu-

ing attempt has been made in recent years to align the vacuum energy density with the holographic principle [67–69] of quantum gravity. The holographic dark energy (HDE) model is based on the holographic principle in which the ultra-violet (UV) cutoff of DE is converted to an infrared (IR) cutoff. It's worth noting that the UV cutoff is related to vacuum energy, while the IR cutoff is related to the Universe's large-scale structure. The holographic principle says that the information contained in a volume of space can be represented as a hologram, which corresponds to a theory locating on the boundary of that space. In other words, the number of degrees of freedom of a gravity-dominated system must vary along with the area of the surface bounding the system. In cosmology, one can obtain the upper bound of the entropy contained in the Universe. Susskind [68] further discussed this principle in the context of string theory. The HDE is an interesting and simple idea of explaining the observed accelerated expansion of the Universe.

Cohen et al. [70] stated that for a system with size L, it is required that the total energy in a region of size L should not exceed the mass of a black hole of the same size for the quantum zero-point energy density associated with the ultraviolet cutoff, thus $L^3\rho_\Lambda \leq LM_p^2$, where ρ_Λ is the vacuum energy density caused by UV cutoff, M_p is the reduced Planck mass given by the relation $M_p \sim \frac{1}{\sqrt{8\pi G}}$ and L is the infrared cutoff. In his paper, Li [66] taken the largest possible L to saturate this inequality, we get the energy density related to HDE given by

$$\rho_d = 3b^2 M_p^2 L^{-2}, \tag{1.8.3}$$

where b is a numerical constant and coefficient 3 is for mathematical convenience.

A nice review and the physical basis of the holographic principle is available in a paper by Canfora and Vilasi [71], in which the authors explained how the holographic principle could have a prominent role in understanding why the observed value of the cosmological constant is so smaller than the one computed in quantum field theory. Several authors have worked to develop the idea of holographic dark energy [72–79] and the origin of holographic dark energy models have been reviewed by Myung and Seo [80].

In a paper, Saridakis [81] presented a generalized version of holographic dark energy in brane cosmology. The holographic dark energy model is an attempt to probe the nature of dark energy within the framework of a fundamental theory originating from some considerations of the features of quantum gravity theory [82]. Myung [83]

proved that holographic dark energy bound to come from the Bekenstein-Hawking bound for a weakly gravitating system. Setare [84] investigated holographic model of interacting dark energy to obtain the equation of state for the holographic dark energy density in a non-flat (closed) Universe. In another paper, Myung [85] investigated the difference between holographic dark energy, Chaplygin gas, and tachyon model with a constant potential.

The large scale of the Universe can be taken as, for example, Hubble horizon, event horizon, particle horizon, or Ricci scalar. The Hubble horizon is a natural candidate for IR cut–off which is also free from causality but in his paper, Hsu [86] discussed that the HDE model with Hubble horizon or particle horizon can not derive the accelerated expansion of the Universe. However, the HDE model with event horizon can derive the accelerated expansion of the Universe [87]. The drawback with event horizon is that it is a global concept of space-time and the existence of the Universe depends on the future evolution of the Universe. HDE model proposed by Li [66] resolves the fine-tuning problem but it leads to a wrong equation of state (EoS) of dark energy. The HDE with event horizon is also not compatible with the age of some old high redshift objects [88]. Later in their paper, Pav*ó*n and Zimdahl [89] observed that the identification of L with the Hubble horizon, $L = H^{-1}$ may give a suitable EoS for DE for an interacting HDE model. It was also shown that there must be a constant ratio of the energy densities of HDE and DM irrespective of the type of interaction.

In the study of the generalized model of HDE, Nojiri and Odintsov [90] found that a unified model of the Universe may be achieved and they also claimed that in a generalized HDE model the coincidence problem may be resolved. Thus, HDE models may be able to solve the cosmic coincidence problem, giving them an advantage over other DE models. Different versions of the cut-off, corresponding to various generalized HDE, have been considered in Refs. [91–100]. The HDE model is able to explain the current accelerated expansion and is in agreement with the observational data [101–105]. The HDE is of interest from a phenomenological point of view, since it can be connected to the observations.

Holographic Ricci Dark Energy

It is important to note that in the literature, various scenarios of HDE have been studied via considering different system's infrared (IR) cutoff. Inspired by the holographic dark energy models, Gao et al. [96] proposed a HDE model in which the future event horizon is replaced by the inverse of the Ricci scalar curvature so that the dark energy

$\rho_\Lambda \propto R$, where $R = -6(2H^2 + \dot{H} + \frac{k}{a^2})$ and named it as "holographic Ricci dark energy (HRDE) model". The energy density for HRDE is given by

$$\rho_d = 3\alpha \left(\dot{H} + 2H^2 + \frac{k}{a^2} \right). \tag{1.8.4}$$

In flat FLRW Universe, $k = 0$, we have

$$\rho_d = 3\alpha \left(\dot{H} + 2H^2 \right), \tag{1.8.5}$$

where α is a dimensionless parameter replacing b^2 of the Li model [66], H is the Hubble parameter, a is the scale factor and k is the curvature. An overdot denotes derivative with respect to cosmic time t. It has been found that this model does not only avoid the causality problem but also naturally solves the coincidence problem [106]. HRDE model fits with the observational data and is suitable to describe the current acceleration of the Universe [107–110]. The HRDE model has been studied extensively to explain the accelerated expansion of the Universe in refs. [111–125].

Although, the DE models are able to explain the recent cosmic acceleration very well and also are in agreement with the observational data but the origin and evolution of DE are still mysterious and unknown. They also suffer from many other problems like the fine-tuning problem, coincidence problem, etc. These problems with DE models compel us to think beyond the standard model and other DE models. The modified gravity models are also suitable candidates to explain such cosmic acceleration. In the next subsection, let us discuss the modified theories of gravity in detail.

1.8.2 Modified Theories of Gravity

An alternative approach is to modify the laws of gravity itself to explain the cosmic acceleration. In the past few years, the interest in modified theories of gravity has been grown up. These theories imply a modification to Einstein's gravity to study the behavior of the Universe. A large number of models within modified theories can explain the DE phenomena. The first modification of Einstein's GTR was done by Weyl [126] by proposing the scale-invariant theory, and then Eddington [127] presented his theory of connections. There are examples of higher dimensional theories such as Kaluza–Klein theory [128, 129] and string theory [130, 131]. The theories like the scalar-tensor theories [132, 133] are an example of extra fields included in the field equations. In the last two decades, considerable developments have been made in

string theory, which has been considered a potential candidate of quantum gravity. One of the well established and extensively studied theories of gravity are the scalar-tensor theories, which often used to model Newton's constant G as a variable.

$f(R)$ theories of gravity, which can be mapped into scalar-tensor theories, have been extensively studied, where the EH action is generalized by using a more general function of the Ricci scalar R. To modify GTR, Utiyama and De Witt [134] used higher-order terms of scalar curvature R. In 1980, an inflationary model using the higher-order corrections to GTR was presented by Starobinsky [135], which has been a remarkably successful model of inflation. Buchdahl [136] was first to present a more general model of modified gravity by considering the general function of Ricci scalar R in the EH action $(1.4.7)$. This $f(R)$ theory coincide with observations [137–139].

In the recent years, various modified gravity theories have been proposed [139–148]. Some of modified theories of gravity are: $f(R)$ theories [138, 140, 144, 149, 150], Gauss-Bonnet $f(G)$ theory [151, 152], Brans–Dicke theory [153, 154], Brane world gravity [155, 156], Horava–Lifshitz gravity [157, 158], $f(T)$ theory [159, 160], $f(R,T)$ theory [161, 162], etc. However, none of these theories is complete which can solve the mysteries of the Universe [163]. The search for a complete theory of gravity is still going on. In this thesis, we have done some work in the framework of modified $f(R,T)$ gravity theory to discuss the evolution of the Universe. So, let us discuss the background and field equations of the modified $f(R,T)$ gravity theory.

The Modified $f(R,T)$ Gravity Theory

In 2007, $f(R)$ gravity theory is generalized by Bertolami et al. [164] by assuming the maximal coupling between Ricci scalar R and matter Lagrangian $\mathscr{L}_m$. In 2008, Harko [165] extended this model to the case of the arbitrary couplings in both geometry and matter. Further in 2010, Harko and Lobo [166] proposed a theory, called $f(R,\mathscr{L}_m)$ where the gravitational Lagrangian as an arbitrary function of the Ricci scalar R and of the matter Lagrangian $\mathscr{L}_m$.

In 2011, Harko et al. [161] proposed a new modified gravity theory, named $f(R,T)$ theory as an extension to the $f(R)$ theories, where R is the Ricci scalar and T is the trace of the energy-momentum tensor. This modified theory presents a maximal coupling between geometry and matter. The reason for choosing T as an argument for the Lagrangian is from exotic imperfect fluids or quantum effects. The EH action

for $f(R,T)$ gravity in the unit $8\pi G = 1$ is modified as [161]

$$S = \int d^4x\sqrt{-g}\left[\frac{1}{2}f(R,T) + \mathscr{L}_m\right], \tag{1.8.6}$$

where $f(R,T)$ is an arbitrary function of Ricci scalar R and trace of energy–momentum tensor T, g is the determinant of the metric tensor $g_{\mu\nu}$ and $\mathscr{L}_m$ is the matter Lagrangian. The energy–momentum tensor of matter is defined as [167]

$$T_{\mu\nu} = -\frac{2}{\sqrt{-g}}\frac{\delta(\sqrt{-g}\mathscr{L}_m)}{\delta g^{\mu\nu}}, \tag{1.8.7}$$

and its trace by $T = g^{\mu\nu}T_{\mu\nu}$. We assume that the matter Lagrangian density depends only on the metric tensor components $g_{\mu\nu}$ so that

$$T_{\mu\nu} = g_{\mu\nu}\mathscr{L}_m - 2\frac{\partial\mathscr{L}_m}{\partial g^{\mu\nu}}. \tag{1.8.8}$$

By varying action (1.8.6) with respect to the metric, one obtains the field equations of $f(R,T)$ theory as

$$f_R(R,T)R_{\mu\nu} - \frac{1}{2}f(R,T)g_{\mu\nu} + (g_{\mu\nu}\Box - \nabla_\mu\nabla_\nu)f_R(R,T) = T_{\mu\nu} - f_T(R,T)(T_{\mu\nu} + \ominus_{\mu\nu}), \tag{1.8.9}$$

where $f_R = \frac{\partial f}{\partial R}$, $f_T = \frac{\partial f}{\partial T}$. Here $\Box \equiv \triangledown^\mu\triangledown_\mu$ is the d'Alembert operator and $\triangledown_\mu$ is the covariant derivative. The tensor $\ominus_{\mu\nu}$ is defined as

$$\ominus_{\mu\nu} \equiv g^{ij}\frac{\delta T_{ij}}{\delta g^{\mu\nu}}, \qquad i,j = 0,1,2,3. \tag{1.8.10}$$

Using (1.8.8) into (1.8.10), we obtain

$$\ominus_{\mu\nu} = -2T_{\mu\nu} + g_{\mu\nu}\mathscr{L}_m - 2g^{ij}\frac{\partial^2\mathscr{L}_m}{\partial g^{\mu\nu}\partial g^{ij}}. \tag{1.8.11}$$

Due to the coupling of the matter and geometry, this $f(R,T)$ gravity model depends on a source term which is a function of the matter Lagrangian $\mathscr{L}_m$. Therefore, the choice of $\mathscr{L}_m$ will decide the field equations of the model. Harko et al. [161] proposed that the matter Lagrangian $\mathscr{L}_m$ may be chosen as $\mathscr{L}_m = -p$, where p is the thermodynamical pressure of matter content of the Universe. Then, Eq. (1.8.11) becomes

$$\ominus_{\mu\nu} = -2T_{\mu\nu} - pg_{\mu\nu}. \tag{1.8.12}$$

As $f(R,T)$ gravity depends on the source term, various theoretical models may be obtained depending on the choices of different matter sources. In this thesis, we have assumed the form $f(R,T) = R + f(T)$, with $f(T)$ being a generic function of T. Therefore, the field equations (1.8.9) now reduce to

$$R_{\mu\nu} - \frac{1}{2}R\, g_{\mu\nu} = T_{\mu\nu} - 2f'(T)T_{\mu\nu} - 2f'(T)\ominus_{\mu\nu} + f(T)g_{\mu\nu}, \tag{1.8.13}$$

where the prime denotes a derivative with respect to T. Using (1.8.12) the field equations (1.8.13) become

$$R_{\mu\nu} - \frac{1}{2}R\, g_{\mu\nu} = T_{\mu\nu} + 2f'(T)T_{\mu\nu} + [2pf'(T) + f(T)]g_{\mu\nu}, \tag{1.8.14}$$

Taking the covariant divergence of (1.8.9) and using the following identity

$$\nabla^{\mu}[f_R(R,T)R_{\mu\nu} - \frac{1}{2}f(R,T)g_{\mu\nu} + (g_{\mu\nu}\Box - \nabla_{\mu}\nabla_{\nu})f_R(R,T)] = 0, \tag{1.8.15}$$

We obtain the divergence of $T_{\mu\nu}$ as

$$\nabla^{\mu}T_{\mu\nu} = -\frac{f_T(R,T)}{1+f_T(R,T)}\left[(T_{\mu\nu}+\ominus_{\mu\nu})\nabla^{\mu}\ln f_T(R,T) + \nabla^{\mu}\ominus_{\mu\nu} - \frac{1}{2}g_{\mu\nu}\nabla^{\mu}T\right]. \tag{1.8.16}$$

Thus, one of the common features of this modified gravity is the non-conservation of the matter EMT. This extra terms is generated by the non-minimal geometry-matter coupling which is considered as particle production, with the gravitational field acting as a particle source.

Using the value of $\ominus_{\mu\nu}$ defined above, Eq. (1.8.16) for a perfect fluid $T_{\mu\nu} = (\rho + p)u_{\mu}u_{\nu} + pg_{\mu\nu}$ with energy density ρ, thermodynamical pressure p and normalized four velocity u^{ν}, satisfying the condition $u_{\nu}u^{\nu} = -1$, gives

$$\dot{\rho} + 3(\rho+p)H = -\frac{f_T(R,T)}{1+f_T(R,T)}\left[(\rho+p)\nabla_{\mu}\ln f_T(R,T) + \nabla_{\nu}\frac{\rho-p}{2}\right]. \tag{1.8.17}$$

Thus, the divergence of the energy-momentum tensor is nonzero. Let us interpret Eq. (1.8.17) from a thermodynamic point of view as describing adiabatic irreversible particle creation in a cosmological context. The above equation can be written as

$$\dot{\rho} + 3(\rho+p)H = (\rho+p)\,\Gamma, \tag{1.8.18}$$

where

$$\Gamma = -\frac{f_T(R,T)}{1+f_T(R,T)}\left[\nabla_\mu \ln f_T(R,T) + \nabla_\nu \frac{\rho - p}{2(\rho+p)}\right], \tag{1.8.19}$$

describes the particle creation rate.

Many authors have studied modified $f(R,T)$ theory in a different context to explain the early and late time evolution of the Universe. $f(R,T)$ gravity models have been investigated by Houndjo et al. [168] to reproduce the four known finite-time future singularities. A quintessence-like behavior has been obtained with a particular model $f(R,T) = \mu R + \nu T$ by Pasqua et al. [162] which exhibits a transition from a decelerated to an accelerated phase. Sharif and Zubair [169] investigated thermodynamical aspects with the apparent horizon in $f(R,T)$ gravity under the FLRW Universe. Azizi [170] discussed the wormhole geometries in $f(R,T)$ gravity and showed that the effective stress-energy may be considered as a possible candidate for violation of the null energy condition in $f(R,T)$ gravity. By assuming that the conservation equation holds for $f(R,T)$ gravity, Chakraborty [171] has discussed the energy conditions with a perfect fluid. The evolution of scalar cosmological perturbations in $f(R,T)$ gravity has been discussed by Alvarenga et al. [172] in the metric formalism under the assumption of a specific model that guarantees the standard continuity equation. The dynamics and stability of the model in $f(R,T)$ gravity has been discussed by Baffou et al. [173]. They showed that the model presents stability for both the de Sitter and power-law solutions and satisfies the observational data for both the low and high redshift regimes.

In their paper, Shabani and Farhoudi [174] have investigated the solar system consequences of the $f(R,T)$ gravity along with the cosmological consequences. In a paper by Fayaz et al. [175], the HDE and new agegraphic DE models were discussed in the anisotropic cosmological model under the framework of $f(R,T)$ gravity. The generalization of the conservation equation of $f(R,T)$ gravity is discussed by Harko [176] by using the concept of irreversible matter creation in open thermodynamic systems. Many authors [177–180] have successfully explained the history of the Universe by reconstructing the $f(R,T)$ gravity with various type of matter content. A number of authors have also discussed the evolution of the Universe in $f(R,T)$ gravity by considering different energy contents and formalism, see refs. [181–189].

Thus, a number of pioneer papers in the literature have motivated us to analyze the evolutionary behavior of the Universe in $f(R,T)$ gravity. In this thesis, we will discuss HRDE in $f(R,T)$ gravity to investigate the different aspects of the evolution of the

Universe.

1.9 Viscous Cosmology

The perfect fluid in cosmological models constitutes an idealized case, but not always. A perfect fluid is able to explain many aspects of the evolution of the Universe but without the investigation of dissipative phenomena arising in the cosmic fluid, some processes can't be explained. It is well known that viscosity is a concept in fluid mechanics which is related to an exotic fluid with some thermodynamical features such as bulk and/or shear viscosities. In cosmology shear viscosity is related to the anisotropy of space-time whereas the bulk viscosity usually related to the isotropic Universe.

The physical origin of bulk viscosity in a system can be traced to deviations from local thermodynamic equilibrium. In a cosmological fluid, the bulk viscosity may arise when the fluid expands (or contracts) too fast so that the system does not have enough time to restore its local thermodynamical equilibrium. The bulk viscosity arises an effective pressure restoring the system to its thermal equilibrium. So, in an accelerated expanding Universe it may be natural to assume the possibility that the expansion process is actually a collection of states out of thermal equilibrium in a small fraction of time due to the existence of bulk viscosity. It is natural for such a term to exist in expanding Universe anytime the fluid is out of equilibrium.

Since, the influence of dissipative processes including bulk viscosity, shear viscosity, and heat transport plays an important role in the cosmic expansion. The introduction of viscosity coefficients in cosmology has itself a long history. The physical importance of these phenomenological parameters has traditionally been assumed to be weak. Viscous cosmology has been investigated to observe the early inflation and the recent expansion of the Universe. The general theory of dissipation in relativity was put on a firm foundation by Eckart [190], and, in a somewhat different formulation by Landau and Lifshitz [191]. This is only the first order deviation from equilibrium and may have a causality problem. As per Eckart's theory, if p is the thermodynamic pressure of matter content and cosmic fluid has viscosity then the effective pressure is given by

$$\tilde{p} = p + \Pi, \tag{1.9.1}$$

where Π represents the dissipative pressure and is equal to $-3\zeta H$. Here, ζ is the coefficient of bulk viscosity. Now, the energy-momentum tensor (1.4.8) with viscous fluid modifies to

$$T_{\mu\nu} = (\rho + \tilde{p})u_\mu\, u_\nu + \tilde{p}\, g_{\mu\nu}, \tag{1.9.2}$$

In this thesis, the homogeneous and isotropic FLRW models have been considered to study the cosmological models. Therefore, the dissipative process is modeled as a bulk viscosity in this case [192–199]. In cosmology, the viscosity concept was first discussed by Misner [200] in 1968.

Israel and Stewart [201] developed a relativistic second-order theory, known as the full causal theory, which has been studied in the evolution of the early Universe. The dissipative variables were included in this theory to explain non-equilibrium states, making it causal and stable. The full Israel-Stewart transport equation is given by [202]

$$\tau\dot{\Pi} + \Pi = -3\zeta H - \frac{\varepsilon\tau\Pi}{2}\left[3H + \frac{\dot{\tau}}{\tau} - \frac{\dot{\zeta}}{\zeta} - \frac{\dot{T}}{T}\right], \tag{1.9.3}$$

where τ represents relaxation time associated with the dissipative effect.

Scalar dissipation processes in cosmology may be treated via the relativistic theory of bulk viscosity. To reduce the equilibrium pressure in an expanding Universe bulk viscosity can be useful. Therefore, the effective pressure could be made negative using sufficiently large bulk viscous pressure. Thermodynamics states with negative pressure are detestable and cannot be excluded by any law of nature. These thermodynamic states are connected with phase transitions. It is known that there is a problem of singularity either in GTR or modified gravity models. The bulk viscosity removes the initial singularity as shown by many authors [202–204]. The idea of modified gravity models with bulk viscosity has been presented in different ways to understand the evolution of the Universe. However, because of the simple form of Eckart theory, it has been widely used by several authors to characterize the bulk viscous fluid. The idea of viscous DE models was presented in different ways to understand the evolution of the Universe. Many authors [205–222] have studied the DE phenomenon as an effect of the bulk viscosity in the cosmic medium.

All these cited works are pioneer papers on bulk viscosity which show that, for an appropriate viscosity coefficient, an accelerated cosmology can be achieved without the need for a cosmological constant [223]. Since we do not know much about the nature of the Universe's content clearly, concern about the bulk viscosity is reason-

able and practical. To our knowledge, such type possibility has been discussed only in the context of the primordial Universe, concerning also the search for non-singular models. But many investigations show that the viscous pressure can play the role of an agent that drives the present acceleration of the Universe. Therefore, the interest in viscosity theories in cosmology has increased in recent years, for various reasons, perhaps especially from a fundamental viewpoint.

1.10 Matter Creation Cosmology

The study of matter creation in the relativistic cosmological models has drawn the attention of a number of authors. Parker [224] investigated the material content of the Universe and stated that it might have had its origin in the continuous creation of radiation and matter from the gravitational field of the expanding cosmos acting on the quantum vacuum, regardless of the relativistic theory of gravity assumed. However, these models were never fully realized due to the lack of a well-defined prescription of how matter creation is to be incorporated in classical Einstein's field equations.

Prigogine et al. [225, 226] was the first to give a theoretical approach to the adiabatic matter creation in the framework of GTR. They proposed an interesting type of cosmological history including large-scale entropy production by considering the cosmological thermodynamics of open systems. They used the generalized form of the first law of thermodynamics to describe the flow of energy from the gravitational field to the matter field, resulting in the creation of particles. The authors argued that the creation of particles can occur only as an irreversible process at the expense of the gravitational field. This phenomenon of matter creation has been studied by many authors in detail within the context of GTR [227–233].

A model with adiabatic matter creation was proposed in order to interpret the cosmological entropy and to solve the Big-Bang singularity problem. However, after the discovery of the accelerating expansion of the Universe, this model was reconsidered to explain the expansion of the Universe and got some unexpected results. It has been pointed out that matter creation can play the role of a dark energy component and lead to driving the accelerating expansion of the Universe. Because of its ability to generate an effective negative pressure, several authors [234–240] reconsidered the idea of irreversible matter development.

The matter formation model has been defined in the literature in terms of a bulk

viscous stress on a phenomenological level [204, 241]. However, Prigogine et al. [225, 226] came to the conclusion that bulk viscosity and matter formation are two separate processes that result in different Universe evolution histories. Further, the equivalence between bulk viscosity and matter creation is discussed by Triginer and Pavón [242], and Brevik and Stokkan [243]. Several authors have noted that while the dynamics of both ideas could be similar, they each had a different thermodynamic feature of the Universe. In a paper, the observational consequence of matter creation in the early Universe has been studied by Singh and Beesham [244].

In the gravitationally induced matter creation mechanism, the number of fluid particles is not conserved, i.e., $N^{\mu}_{;\mu} \neq 0$. In this case, the particle flux vector $N^{\mu} = n\,u^{\mu}$ is assumed to satisfy the balance equation [228]

$$N^{\mu}_{;\mu} \equiv \dot{n} + 3nH = n\Gamma, \tag{1.10.1}$$

where N is the total particle number in a comoving volume V, $n = N/V$ is the particle density and Γ is the rate of matter creation from the gravitational field with dimension $time^{-1}$. In principle, $\Gamma > 0$ represents the matter creation, $\Gamma < 0$ is for matter annihilation, and $\Gamma = 0$ is the case when there is no matter creation. The balance equation can be rewritten as $\frac{\dot{N}}{N} = \Gamma$, showing that Γ drives the matter creation rate in the comoving volume. In the case of adiabatic particle production, the particles and entropy are generated but the entropy per particle does not vary. Under such 'adiabatic condition', the creation pressure can be written as [231, 234, 242, 245]:

$$p_c = -\left(\frac{\rho + p}{3H}\right)\Gamma, \tag{1.10.2}$$

where p_c is the pressure due to the matter creation. Now, we can describe the dynamics of the Universe only if the matter creation rate is known. The nature of Γ is unknown as the associated quantum field theory (QFT) is yet to be developed. In general, there is no bound to choose some particular choices for Γ. Therefore, one can assume some phenomenological but general choices for Γ. In the literature, various forms of Γ, e.g., $\Gamma = constant$ [246], $\Gamma \propto H$ [247], $\Gamma \propto H^2$ [230, 248], and a linear combination [249], have been presented to explain the early and present-day acceleration of the Universe. However, the linear and quadratic forms of Γ are not compatible with the current cosmology, i.e., these models do not show transition redshift. Therefore, a natural extension is to consider the linear combinations of H, H^2..., and the derivative

of the Hubble parameter. Finally, one can use observational data to test the viability of such models.

The second law of thermodynamics inevitably leads to a change of the energy-momentum tensor (1.4.8) due to the presence of matter creation. So, the energy-momentum tensor of perfect fluid (1.4.8) empowered with the mechanism of matter creation modifies to

$$T_{\mu\nu} = (\rho + p + p_c)u_\mu\, u_\nu + (p + p_c)\, g_{\mu\nu}. \tag{1.10.3}$$

The entropy flux vector has the form $\mathbb{S}^\mu = n\sigma u^\mu \equiv su^\mu$, with $\sigma = \mathbb{S}/N$ being the basic entropy per particle and $\mathbb{S} = sa^3$ being the entropy in a comoving amount. The second law of thermodynamics imposes a relationship

$$\mathbb{S}^\mu_{;\mu} = n\dot{\sigma} + \sigma n\Gamma \geq 0. \tag{1.10.4}$$

The divergence of $\mathbb{S}^\mu$ is reduced to $\mathbb{S}^\mu_{;\mu} = \sigma n\Gamma$ if the creation process is such that the specific entropy per particle is constant. However, since matter creation and bulk viscosity are two distinct processes, the viscous term's specific entropy rate per particle is calculated as [242]

$$\dot{\sigma} = \frac{\zeta\theta^2}{n\mathbb{T}}, \tag{1.10.5}$$

where $\mathbb{T}$ is the temperature. It is obvious that the existence of Γ has no bearing on the production of entropy per particle, which is solely dependent on the nature of bulk viscosity. As previously stated, if $\zeta = 0$, the entropy per particle is constant.

1.11 Cosmological Parameters

Cosmological parameters play a very important role to understand the evolution of the Universe. A bunch of terminology is associated with the cosmological parameters, and we will just go over the basics here.

1.11.1 Hubble Parameter

The expansion rate of the Universe is described by the Hubble parameter, denoted by $H(t)$, defined as

$$H(t) = \frac{\dot{a}(t)}{a(t)}. \tag{1.11.1}$$

The value of the Hubble parameter at the present epoch is the Hubble constant, H_0. Current measurements lead us to believe that the Hubble constant is 70 ± 10 $kms^{-1}Mpc^{-1}$ (Mpc stands for megaparsec, which is 3.09×10^{26} m). Since there is still some uncertainty in this value, we often parameterize the Hubble constant as $H_0 = 100h\ kms^{-1}Mpc^{-1}$, so that $h \approx 0.7$.

The Hubble parameter (1.11.1) is the rate of change of the scale factor $a(t)$ which provides a way to link the observations with a proposed model using the scale factor. It is to be noted that we can expect the constant expansion rate throughout its history, $H(t) = H_0$ only in an empty space.

1.11.2 Critical Density

The density of matter that would be required to halt the expansion of the Universe is known as critical density. Let us rewrite the Friedmann equation (1.5.1) as

$$\frac{\dot{a}^2}{a^2} - \frac{k}{a^2} = \frac{8\pi G}{3}\rho. \tag{1.11.2}$$

This equation determines how the scale factor of the Universe (essentially the size of the Universe) changes with time in terms of energy density ρ, and k, a measure of the curvature of the Universe. The above equation reduces to

$$H^2 + \frac{k}{a^2} = \frac{8\pi G}{3}\rho. \tag{1.11.3}$$

Dividing by H^2 into both sides, we get

$$\frac{k}{a^2H^2} = \frac{8\pi G}{3H^2}\rho - 1 = \frac{\rho}{\rho_c} - 1, \tag{1.11.4}$$

where,

$$\rho_c = \frac{3H^2}{8\pi G} \tag{1.11.5}$$

is known as critical density. The critical density of the Universe depends on the Hubble parameter H. As the Hubble parameter is a time-dependent function, so the critical density also evolves with time. Using the value of H_0, the present value of the critical density may be calculated. Recent measurements indicate that the actual density of our Universe is very close to the critical density, and this is achieved if we take $k = 0$ (the Universe is flat).

1.11.3 Density Parameter

The density parameter Ω is commonly used to express cosmological quantities and cosmic field equations. The density parameter is typically defined as the ratio of matter density to critical density at the same time.

$$\Omega = \frac{8\pi G}{3H^2}\rho = \frac{\rho}{\rho_c}, \tag{1.11.6}$$

where ρ represents the density of matter/DE/scalar field, etc.
Using (1.11.6) into (1.11.4), the Friedmann equation can be written

$$\Omega - 1 = \frac{k}{a^2H^2}. \tag{1.11.7}$$

The sign of k is therefore determined by whether Ω is greater than, equal to, or less than, one. Thus, the density parameter determines the geometry of the Universe, i.e., a closed, flat, or open Universe. Determining it observationally is of crucial importance; recent measurements of the cosmic microwave background anisotropy lead us to believe that Ω is very close to unity.

The total energy content of the Universe is considered to be matter (Baryonic + Dark matter) and DE for which the densities can be represented by ρ_m and ρ_Λ, respectively. The total density is given by $\rho = \rho_m + \rho_\Lambda$. The density parameters for matter and DE are defined as

$$\Omega_m = \frac{\rho_m}{\rho_c}; \qquad \Omega_\Lambda = \frac{\rho_\Lambda}{\rho_c}; \qquad \Omega = \frac{\rho}{\rho_c}, \tag{1.11.8}$$

where $\Omega = \Omega_m + \Omega_\Lambda$.

1.11.4 Deceleration Parameter

An important cosmological quantity is the deceleration parameter (DP) q, which is an indicator of the accelerating/decelerating nature of the evolution of the Universe. It is defined as

$$q = -\frac{a\ddot{a}}{\dot{a}^2} = -\frac{\dot{H}}{H^2} - 1\,, \tag{1.11.9}$$

which measures the rate of change of the rate of expansion. The positive value of q represents the decelerated phase of the Universe whereas the negative value represents the accelerated phase. Our Universe has gone through two phases: early time inflation, followed by decelerated expansion, and finally decelerated expansion,

followed by late-time accelerated expansion. The change in sign of DP shows the phase transition.

1.11.5 Redshift

The fractional Doppler shift of an object's emitted light caused by radial motion is its redshift z. The spectral lines of atoms in light from distant stars and galaxies are distinct. These spectra are observed to be shifted towards the red end of the spectrum when analysed. The term "redshift" refers to this shift in the spectrum. In fact, redshift appears to be a Doppler shift, indicating that almost all galaxies are moving away from the more distant ones. It is measured by the quantity

$$z = \frac{\lambda_0 - \lambda_e}{\lambda_e} = \frac{\nu_e - \nu_0}{\nu_0}, \tag{1.11.10}$$

where ν_0 and λ_0 are the observed frequency and wavelength, and ν_e and λ_e are the emitted frequency and wavelength, respectively.

The scale factor $a(t)$, or the size of the Universe, is directly related to cosmological redshift. For an object at redshift z

$$1 + z = \frac{a(t_0)}{a(t_e)}, \tag{1.11.11}$$

where $a(t_0)$ is the size of the Universe at the moment the object's light is observed, and $a(t_e)$ is the size of the Universe at the time it was emitted.

1.12 Geometrical Parameters

Since various cosmological parameters show similar results for different DE models so it is not possible to discriminate them. Therefore, in order to have a better understanding of the DE models, higher-order time derivatives of $a(t)$ are required. Rapid progress in observational cosmology has led to the creation of the first precision cosmological model, which includes many of the key cosmological parameters. Geometrical parameters have long been used in cosmology to better understand the evolution of the Universe and to distinguish between different DE models. In this thesis, we will address certain geometrical parameters that are used to analyse cosmological phenomena.

1.12.1 Statefinder Parameter

Various dynamical dark energy models are developed in the recent past to explain the accelerating expansion of the Universe. In order to differentiate these models, a diagnostic proposal that makes use of parameter $\{r,s\}$, the so-called *statefinder*, was introduced by Sahni et al. [250] and Alam et al. [251] and defined as follows:

$$r \equiv \frac{\dddot{a}}{aH^3} \quad \text{and} \quad s \equiv \frac{r-1}{3(q-1/2)}. \tag{1.12.1}$$

In the sense that it is dependent on the expansion factor and thus on the metric representing space-time, the statefinder is a "geometrical" diagnostic. These two parameters are used to compare the goodness of various dark energy models with ΛCDM model. This statefinder diagnostic can distinguish various types of dark energy models because different cosmological models involving dark energy exhibit qualitatively different evolutionary trajectories in the $r-s$ plane. For the spatially flat ΛCDM cosmological model, the statefinder parameters correspond to a fixed point $\{r,s\}=\{1,0\}$ and $SCDM$ scenario gives a fixed point $\{1,1\}$ in the statefinder diagnostic pair $\{r,s\}$ plane, with which the distance of other DE models from ΛCDM can therefore be established on the $r-s$ plane [250, 251]. To distinguish between different DE models, we can plot trajectories in the $r-s$ and $r-q$ planes. In the modern period, when there are a plethora of DE models available in the literature, the statefinder parameters $\{r,s\}$ are crucial in distinguishing between them.

1.12.2 Cosmographic Parameters

The geometrical investigation discussed in previous subsection on the dark energy model has been further extended by considering the Taylor series expansion of the scale factor about the present time. As a result some new models independent dimensionless geometrical parameters, called cosmographic parameters (CP), have been defined as [252, 253]

$$j = \frac{1}{aH^3}\frac{d^3a}{dt^3}\ ,\ s = \frac{1}{aH^4}\frac{d^4a}{dt^4}\ ,\ l = \frac{1}{aH^5}\frac{d^5a}{dt^5}. \tag{1.12.2}$$

The cosmographic parameters defined in (1.12.2) are called as $jerk\ (j)$, $snap\ (s)$, and $lerk\ (l)$ parameter, respectively. Here r and j are same; but the s parameter defined in (1.12.2) is not same with one defined in (1.12.1). The study of the above parame-

ters for a particular DE model together with the Hubble parameter H and deceleration parameter q is known as the cosmography of the model. We can deduce from the equation (1.12.2) that any cosmological model's cosmography will be true as long as the Hubble parameter is fourth-order differentiable.

1.12.3 *Om* Diagnostic

To examine the dynamics of the dark energy models one more diagnostic, called Om, has been introduced in [254] with the help of Hubble parameter $H(z)$ and redshift z. Om-diagnostic is used to check different periods of the Universe. Many authors [255–257] have studied the DE models based on *Om(z)* diagnostic. We plot the trajectory in $Om(z) - z$ plane to discriminate the behavior of the DE models. The constant value of $Om(z)$ tells that DE behaves like a cosmological constant (ΛCDM). The positive slope of Om diagnostic means that the model behaves phantom-like while the negative slope indicates the behavior of the quintessence model. $Om(z)$ parameter for spatially flat Universe is defined as

$$Om(z) = \frac{\frac{H^2(z)}{H_0^2} - 1}{(1+z)^3 - 1}. \tag{1.12.3}$$

Om-diagnostic involves only the first-order derivative of the scale factor thus it is easier to reconstruct from observational data. We know that the curvature of $Om(z)$ can reliably distinguish dynamical DE from the cosmological constant, both with and without matter density as a reference.

1.13 Data Analysis

It has been understood that we live in an expanding Universe since Edwin Hubble developed Hubble's law in the late 1920s, which compared the recession velocity of galaxies to their distance from us. Latest findings, on the other hand, show that not only is the Universe expanding, but that it is also expanding faster. Since the acceleration cannot be accommodated in a Universe made up of radiation and matter, this section briefly discusses these findings, since they are the foundation of the field of dark energy. In this thesis, we will study various models that explain the late evolution of the Universe and test it using the most recent cosmological observations. This section introduces the statistical methods used to perform the data analysis. Even

though there are many promising cosmological probes that can be used to fit the cosmological models, but we will stick to some of the observations, which are important in the context of late-time cosmic acceleration. These are the observations of type Ia supernova, observational measurement of Hubble parameter, the baryon acoustic oscillation, and the cosmic microwave background radiation.

1.13.1 Supernova type Ia

Thermonuclear explosions of white dwarves in binary systems with red giants are known as supernova type Ia (SNIa). The red giant extends as it progresses through stellar stages, eventually expanding beyond its Roche lobe, which determines the area where matter remains attached to the red giant. As a result, matter begins to flow from the red giant to the white dwarf. The matter accumulates until the white dwarf exceeds the Chandrasekhar mass, which is about 1.4 solar masses. It becomes unstable at this stage and explodes in a thermonuclear explosion. Since SNIa are described by the explosion of a 1.4 solar mass white dwarf, one would expect these supernovae to be regular candles, with the same luminosity every time. SNIa is one of the best probes for confirming the redshift-distance relation under this hypothesis, as they provide a clear measurement of the luminosity distance independent of redshift determination. As a result, SNIa can be used to constrain the history of the Universe's expansion.

Since, SNIa are used as standard candles, and we can hence infer their distance from us. They were the objects observed when dark energy was discovered in 1998. They are still widely used to infer the expansion of the Universe. In this thesis, we use data from the compressed Joint Light-curve Analysis (cJLA) compilation, which is composed of 31 binned data points within the range $0.01 < z < 1.3$ [258]. We measure the distances of a supernova at different redshift z in the form of distance modulus $\mu_b(z)$ which is actually the difference between the apparent magnitude m_b and the absolute magnitude M_b of the B-band (wavelength band of the blue line) of the observed spectrum of the supernova and directly tells us about the expansion history.

$$\mu_b(z) = m_b - M_b = 5 \log\left(\frac{d_L(z)}{Mpc}\right) + M, \tag{1.13.1}$$

where M is the normalization parameter. In the above equation d_L is the luminosity distance which is defined by

$$d_L = c(1+z)\int_0^z \frac{dz'}{H(z',\theta)}, \tag{1.13.2}$$

where c is the speed of light and θ is the representation of model parameters.

We adopt the χ^2-statistics in order to estimate the free parameters in cosmological models from the observational data. The likelihood is evaluated by using the χ^2 statistics:

$$\chi^2_{SNIa} = x^T C_b^{-1} x, \tag{1.13.3}$$

where $x = \mu_b - M - 5\,log_{10}d_L$ and C_b is the covariance matrix of μ_b for which see Table F.2 in [258].

1.13.2 Observational Hubble Data

In order to study the expansion timeline of the Universe, the determination of the Hubble parameter using observational data is the other important part of fitting parameters. In the recent past, the measurement of Hubble parameter $H(z)$ got much attention from the researchers due to its model-independent nature. The observational Hubble data are based on differential ages of the galaxies [259]. Observational data presents the Hubble parameter estimated at different redshift z. In the statistical analysis, we have used 43 data points of the Hubble parameter in the redshift range $0 < z < 2.5$ [260].

The χ^2 function is defined as the following

$$\chi^2_{OHD} = \sum_{i=1}^{n} \frac{[H(z_i) - H_{obs}(z_i,\theta)]^2}{\sigma_i^2}, \tag{1.13.4}$$

where $H(z_i)$ and $H_{obs}(z_i,\theta)$ represents the theoretical and observed values of Hubble parameter, respectively. The standard deviation in the observed value is denoted by σ_i.

1.13.3 Baryon Acoustic Oscillations and Cosmic Microwave Background

The measurement of the baryon acoustic scale in the distribution of galaxies on large scales is another direct expansion background probe. Until recombination, the acous-

tic oscillations in the baryon-photon fluid imprint a fixed comoving length scale in the statistics of galaxies distribution, which is provided by the comoving sound horizon at recombination,

$$r_s(z_*) = \int_{z_*}^{\infty} \frac{c_s(z)}{H(z)} dz, \tag{1.13.5}$$

in which c_s is the sound speed and z_* indicates the photons decoupling redshift and holds the value $z_* = 1090$ as per the Planck 2015 results [20]. This scale determines the peak positions in the CMB anisotropy power spectrum. The baryons decouple from the photons after recombination, and their perturbations evolve under the influence of only gravity, which is dominated by dark matter due to its density being around a factor of six higher than the baryon density. Both baryon and dark matter perturbations eventually adopt the same power spectrum, with the acoustic oscillations function diluted in comparison to the CMB but still present and observable. The BAO scale can be used as a (statistical) standard ruler where supernova is standardizable candles. The adjustment in the size of this scale can be used to determine the Universe's expansion history, making it a useful tool for constraining dark energy.

The BAO systematics are relatively clean in comparison to other probes, with the key problems being the modelling of the impact of non-linear evolution and galaxy bias on peak position. One disadvantage is that large samples of galaxies must be measured in large amounts of space in order to obtain strict constraints. In this thesis, we will consider the combined BAO and CMB data from different observational missions [261]. We have taken the sample of BAO distances measurements from SDSS(R) [262], the 6dF Galaxy survey [263], BOSS CMASS [264] and three parallel measurements from WiggleZ survey [265]. We combine these results with the Planck 2015 [20].

In the context of BAO, the angular diameter, $d_A(z,\theta)$ is defined as

$$d_A(z_*,\theta) = c\int_0^{z_*} \frac{dz'}{H(z',\theta)}, \tag{1.13.6}$$

where $D_v(z,\theta)$ represents the dilation scale which is given by $D_v(z,\theta) = \left(\frac{d_A^2(z,\theta)cz}{H(z,\theta)}\right)^{1/3}$.

The distant redshift d_z is given by

$$d_z = \frac{r_s(z_*)}{D_v(z,\theta)}, \tag{1.13.7}$$

where $r_s(z_*)$ is defined as the co-moving sound horizon at the time when photons decouple, which is assumed to be the same as it is considered in Ref. [261].

With this information, the χ^2 function for BAO/CMB can be written as [261]

$$\chi^2_{BAO/CMB} = A^T C^{-1} A \tag{1.13.8}$$

where A is the matrix

$$A = \begin{bmatrix} \frac{d_A(z_*,\theta)}{D_v(0.106,\theta)} - 30.84 \\ \frac{d_A(z_*,\theta)}{D_v(0.35,\theta)} - 10.33 \\ \frac{d_A(z_*,\theta)}{D_v(0.57,\theta)} - 6.72 \\ \frac{d_A(z_*,\theta)}{D_v(0.44,\theta)} - 8.41 \\ \frac{d_A(z_*,\theta)}{D_v(0.6,\theta)} - 6.66 \\ \frac{d_A(z_*,\theta)}{D_v(0.73,\theta)} - 5.43 \end{bmatrix}$$

and C^{-1} is the inverse of the covariance matrix [261] given by

$$C^{-1} = \begin{bmatrix} 0.52552 & -0.03548 & -0.07733 & -0.00167 & -0.00532 & -0.00590 \\ -0.03548 & 24.97066 & -1.25461 & -0.02704 & -0.08633 & -0.09579 \\ -0.07733 & -1.25461 & 82.92948 & -0.05895 & -0.18819 & -0.20881 \\ -0.00167 & -0.02704 & -0.05895 & 2.91150 & -2.98873 & 1.43206 \\ -0.00532 & -0.08633 & -0.18819 & -2.98873 & 15.96834 & -7.70636 \\ -0.00590 & -0.09579 & -0.20881 & 1.43206 & -7.70636 & 15.28135 \end{bmatrix}$$

We have taken the correlation coefficient from Ref. [16].

1.14 Model Selection Criterion

The reduced chi-squared, denoted by χ^2_{red}, is a very popular method for model assessment, model comparison, convergence diagnostic, and error estimation in astronomy. If ν is the number of degree of freedom, the reduced χ^2 is then defined as

$$\chi^2_{red} = \frac{\chi^2_{min}}{\nu}. \tag{1.14.1}$$

If $\mathbb{N}$ is the data points and d is the free parameters, the number of degree of freedom $\nu = \mathbb{N} - d$. If a model is fitted to data and the resulting χ^2_{red} is larger than one, it is considered a “bad” fit, whereas if χ^2_{red} is less than one, it is considered an over-fit. The fit model is that one whose value of χ^2_{red} is closest to one.

Statistical analysis can be used to decide the models are “better”, taking into account the number of parameters required and how well the models complement the data. We use the Akaike Information Criterion (AIC) [266] and the Bayesian or Schwarz Information Criterion (BIC) [267] to evaluate the goodness of our model in comparison to a given reference model and analyse whether our model is favored by these parameters. The AIC parameter is defined as follows [266]

$$AIC = -2\ ln\mathscr{L}_{max} + 2d, \tag{1.14.2}$$

where $\mathscr{L}_{max} = e^{-\chi^2_{tot}/2}$ is the maximum likelihood obtained for the cosmological model. The “preferred model” for this criterion is the one with the smaller value of AIC. We measure $\Delta AIC_{kl} = AIC_k - AIC_l$ to compare the model k with the model l, which can be interpreted as “evidence in favor” of the model k over the model l. We have “strong evidence in favor” of model k for $0 \leq \Delta AIC_{kl} < 2$, “average evidence in favor” of model k for $2 < \Delta AIC_{kl} < 4$, “less evidence in favor” of model k for $4 < AIC_{kl} \leq 7$, and “no evidence in favor” of model k for $\Delta AIC_{kl} > 10$ [268].

The bayesian criterion, on the other hand, is established by the relation [267]

$$BIC = -2\ ln\mathscr{L}_{max} + d\ lnN, \tag{1.14.3}$$

Similar to ΔAIC_{kl}, $\Delta BIC_{ij} = BIC_i - BIC_j$ can be interpreted as “evidence favor” the model i compared to the model j. For $0 \leq \Delta BIC_{ij} < 2$ there is “not enough evidence against” the model i, for $2 \leq \Delta BIC_{ij} < 6$ there is “evidence against” the model i and for $6 \leq \Delta BIC_{ij} < 10$ there is “strong evidence against” model i [268].

1.15 Motivation

Cosmological observations carried out by many researchers [14–20] show that the Universe recently went transition from a decelerating to an accelerating expansion. These data are consistent with a flat FLRW cosmology whose dominant components at present consist of matter (cold dark matter plus baryons) and a cosmological constant or, equivalently, the energy density of the vacuum; the ΛCDM concordance model. Radiation and matter predominate early in the Universe’s evolution, resulting in decelerating expansion, while the cosmological constant or vacuum energy portion predominates more recently, resulting in accelerating expansion. The mech-

anism or substances behind the present cosmic acceleration, on the other hand, are unknown, and this poses a difficult problem for modern cosmology. There are primarily two well-known approaches to explain the Universe's accelerating phase. One is the introduction of a component known as dark energy, which has a strong negative pressure and an equation of state $\omega < -1/3$, and the other is modifications to standard General Relativity.

In relativistic cosmology, an accelerating Universe is obtained by assuming the existence of a DE component (an exotic fluid endowed with negative pressure in order to violate the strong energy condition). To investigate the behavior of the DE, several theoretical cosmological models of the Universe have been proposed. The two most accepted DE models are that of a *cosmological constant* (ΛCDM) or a non-zero vacuum energy density and a slowly varying rolling scalar field (quintessence models). The ΛCDM model, on the other hand, faces a number of difficulties. For example, the data requires a fine-tuned value for the energy density of the vacuum ($\Omega \approx 0.26$). To validate and constrain the ΛCDM model, the astronomical community is working on a number of major observational projects. It's critical to find and investigate a number of physical processes that could explain the Universe's late-time acceleration.

In this regard, it's worth noting that the existence of negative pressure is a crucial component for accelerating the expansion. When physical systems deviate from their thermodynamic equilibrium states, this type of stress occurs naturally in a variety of situations. In general, such states are connected with phase transitions, and for some systems, the existence of negative pressure seems to be inevitable.

It has been noted by several works that a bulk viscous fluid can produce an accelerating cosmology without the need for any cosmological constant or dark energy components. In the context of inflation, some authors [241, 269] studied the effect of bulk viscosity and found that the bulk viscous fluid is capable of producing an accelerated expansion of the Universe. This idea was extended to explain the late-time acceleration of the Universe [270–275]. Therefore, it is required to analyze a viable mechanism for the origin of the bulk viscosity. The deviation from the local thermodynamic equilibrium is the source of bulk viscosity in a physical system. As the cosmic fluid expands in an expanding Universe, the bulk viscosity can be thought of as a measure of the pressure needed to restore equilibrium. It's possible that in an accelerated expanding Universe, the expansion process is simply a set of states that are out of thermal equilibrium in a short amount of time. As a result, in a more practical explanation of the accelerated Universe today, it is normal to presume the presence of bulk

viscosity. Bulk viscosity is the only viscous effect capable of changing the background dynamics in a homogeneous and isotropic Universe (for detail, see Sec. 1.9).

The macroscopic foundation of the negative pressure accompanying matter creation can be derived using relativistic non-equilibrium thermodynamics. The second law of thermodynamics determines how an irreversible process of quantum origin can be incorporated into classical Einstein's field equation. It was demonstrated that the matter creation is an irreversible process completely different from bulk viscosity mechanism [276]. The irreversible development process is characterised by two new ingredients in comparison to the standard equilibrium equations: a balance equation for the particle number density and a negative pressure term in the stress tensor. The second law of thermodynamics establishes a clear relationship between these quantities. According to this law, matter creation at the cost of the gravitational field can only take place as an irreversible mechanism limited by the normal non-equilibrium thermodynamics requirements.

After the discovery of the accelerating Universe the particle creation was reconsidered to explain it and got the unexpected results. The work on matter creation has recently attracted a lot of interest in cosmology. The matter creation pressure, which is negative, might play the role of the dark energy component. Lima et al. [276] presented the late-time evolution of the class of models with matter creation which is qualitatively very different from that of the standard ΛCDM model. They showed that it is quantitatively possible to account for a recent transition from decelerated to accelerated expansion in late-time evolution without a cosmological constant.

In recent years, holographic dark energy has been discussed extensively as a possible candidate for dark energy. The model is built on the basis of the holographic principle and some features of the theory of quantum gravity. In this principle, the ultraviolet cut-off is related to the infrared cut-off. Depending on the infrared cut-off, e.g., the Hubble horizon, event horizon, particle horizon, Ricci scalar, or Granda-Oliveros cut-off, different models have been constructed to study the late-time evolution of the Universe. The HDE model with different IR cut-off has proven to be a promising dark energy candidate. Thus, the HDE model attracts a lot of interests in studying the late-time evolution of the Universe.

Despite these excellent DE cosmological models, we still have some problems to work out, and the quest for a concrete model continues. This encourages physicists to consider alternative gravity theories. Modified theories of gravity provide a very promising gravitational alternative to dark energy. These theories present a very

natural unification of the early-time inflation and late-time cosmic acceleration. The $f(R,T)$ theory [161] is one of the efficient modified gravity theories to describe the recent accelerated expansion of the Universe. This modified theory presents a maximal coupling between geometry and matter. It is worth considering the $f(R,T)$ modified theories of gravity to study the cosmological models.

Since the astronomical community has been working on a number of large observational projects to test and constrain the standard ΛCDM model, it is critical to define and investigate a number of physical mechanisms that may also be responsible for the Universe's late time acceleration.

In this thesis, we have investigated the effects of dissipative processes (bulk viscosity and matter creation) in the modified theory of gravity and holographic dark energy within the framework of a flat FLRW metric. We have considered bulk viscosity and matter creation as independent physical phenomena. Bulk viscosity is associated with a generalization of the hydrodynamics of ideal fluids for the case of non-ideal ones, with constitutive equations describing the viscous pressure. The matter creation is based on the non-equilibrium thermodynamics where the Universe is assumed to be an open thermodynamical system. The study of bulk viscosity and matter creation provides us to improve the dynamical cosmic evolution of the existing dark energy models.

The thesis entitled **"Study of Viscous and Matter Creation Effects in Cosmology"** comprises seven chapters. The bibliography and the list of publications have been given at the end of the thesis.

Chapter 1 titled *"Introduction"* provides a brief review of the general theory of relativity, expanding Universe, inflationary Universe, and accelerating Universe. It gives a brief overview of the candidates for explaining the Universe's accelerated expansion that have been proposed in the literature. The thermodynamics of dissipative processes of bulk viscosity and matter creation has been discussed. A brief survey of modified $f(R,T)$ gravity and holographic dark energy has been carried out. The cosmological parameters have been briefly discussed, as they play an important role in the study of cosmological models. Some of the latest observational data such as Type Ia supernova (SNe), Observational Hubble parameter data (OHD), Baryon acoustic oscillations (BAO), and cosmic microwave background (CMB) data are discussed. The motivation of the work in this thesis has been discussed at the end. Thus, the current chapter establishes a context, explains the purpose of the thesis work, and

offers tools for achieving the objectives.

Chapter 2 titled *"Holographic Ricci dark energy model with bulk viscosity"* deals with viscosity effect on holographic Ricci dark energy (HRDE) model within the framework of the standard Eckart theory of relativistic thermodynamics. We assume that the flat Friedmann-Lemaître-Robertson-Walker Universe is filled with pressureless dark matter and viscous HRDE. Non-viscous and viscous HRDE models have been discussed. In the non-viscous model, we have obtained a power-law form of scale factor which gives a constant value of the deceleration parameter. Thus, the phase transition is not possible in non–viscous model. The statefinder pair is also constant and it does not discriminate from ΛCDM model. However, the model shows the transition from the decelerated phase to the accelerated phase due to the presence of the bulk viscous term. The viscous HRDE model is compatible with the quintessence- and Chaplygin gas-like model in early time for small viscous values and approaches to ΛCDM model.

The chapter is based on a published research paper "Ricci dark energy model with bulk viscosity, *The European Physical Journal Plus* **133**, 312 (2018)".

In **Chapter 3** titled *"Holographic Ricci dark energy with bulk viscosity in $f(R,T)$ gravity"*, we have extended the work of the previous chapter to study the HRDE model with bulk viscosity in modified $f(R,T)$ gravity. We have assumed that the Universe is filled with pressureless dark matter and viscous HRDE. The bulk viscous coefficient ζ has been assumed to be of the form $\zeta = \zeta_0 + \zeta_1 H$, i.e., proportional to the velocity of the expansion of the Universe. The exact solutions of the field equations have been obtained by assuming the simplest form of $f(R,T) = R + \lambda T$ with constant and variable bulk viscous coefficients. We have discussed how the presence of viscous fluid can cause late-time acceleration. The viscous HRDE model produces a time-dependent deceleration parameter that demonstrates phase transition. We have discussed the behavior of the deceleration parameter by constraining ζ. We have plotted the trajectories in $r-s$, $r-q$, and *Om(z)* $-z$ planes to discriminate the viscous HRDE model from the existing dark energy model.

The thermodynamics of non-viscous and viscous HRDE models have also been discussed. We have explored the obvious violation of energy-momentum tensor in $f(R,T)$ gravity and have provided a thermodynamic interpretation of the extra terms generated by the non-minimal geometry-matter coupling as describing as a particle production.

The content of this chapter is based on **two** research papers entitled "Holographic

Ricci dark energy with constant bulk viscosity in $f(R,T)$ gravity, *Gravitation and Cosmology* **25**, 58 (2019)" and "Viscous Ricci dark energy and generalized second law of thermodynamics in modified $f(R,T)$ gravity, *Modern Physics Letters A* **33**, 1850225 (2018)".

In **Chapter 4** titled *"Holographic Dark Energy with matter creation"*, we have discussed holographic dark energy model with adiabatic matter creation in the framework of homogeneous and isotropic flat FLRW Universe filled with holographic dark energy and pressureless dark matter with matter creation. We have discussed the basic terminology and solved the field equations by considering various forms of particle creation rate Γ. For the first case, we have taken $\Gamma = 3\beta H$ which gives a power-law form of the scale factor. We have also calculated the deceleration parameter for this form of Γ which is constant and hence there is no transition redshift throughout the evolution. The HDE model with Hubble horizon as an infrared cut-off also does not show the transition regime.

In order to solve such problem we have considered a class of such models where the particle creation rate is assumed to be of the form $\Gamma = constant$ and $\Gamma = 3\delta H_0 + 3\beta H$. We have discussed the observational analysis in both cases by employing the MCMC package EMCEE on a different combination of publicly available data sets. The best-fit values of model parameters have been obtained with different combinations of data sets. We have analyzed the thermodynamics of matter creation in the HDE model. It has been observed that the GSL is valid with the apparent horizon as the boundary under certain conditions.

The chapter is based on **two** research papers "Observational constraints on holographic dark energy with matter creation, *Astrophysics and Space Science* **365**, 84 (2020)" and "Holographic dark energy, matter creation, and cosmic acceleration, *Physical Review D* **102**, 123537 (2020)".

Chapter 5 titled *"Holographic Ricci dark energy model with bulk viscosity and matter creation"*, explores the effect of bulk viscosity and matter creation in holographic Ricci dark energy model within the framework of a flat FLRW Universe. We have assumed the bulk viscosity coefficient as $\zeta = \zeta_0 + \zeta_1 H$ and the particle creation rate as $\Gamma = 3\beta H$ to obtain the exact solutions for the scale factor and various physical quantities. We have considered these two dissipative phenomenons as independent irreversible processes. It has been observed that the assumption $\Gamma \propto H$ does not describe the present-day Universe (transition phase) in the absence of bulk viscos-

ity. Therefore, to overcome this problem we have introduced the bulk viscosity along with matter creation to observe the present-day Universe and we have succeeded to obtain such a model. We have obtained the function Hubble parameter in terms of redshift which is used to obtain the free parameters of the HRDE model.

We have performed the statistical analysis for our model using the latest observational data of SNe, OHD, and combined data of BAO and CMB. We have employed publicly available EMCEE codes for the implementation of the MCMC method. We have obtained the best-fit values for the model parameters. Using best-fit values of model parameters we have presented the evolution of various cosmological parameters and have studied various geometrical diagnostics and cosmographic parameters analytically and graphically. The deceleration parameter shows a signature flipping behavior thereby indicating the evolution of the Universe from early deceleration to present late-time acceleration. We have examined the energy conditions of our model to analyze the physical viability of the model. It has been observed that the NEC, WEC, and DEC are satisfied but SEC fails to hold for our model. The best-fitting results have shown that this HRDE model yields theoretical prediction values at an acceptable level by working out the numerical processing to the joint observational data sets of SNe, OHD, and BAO/CMB.

This chapter comprises the result of a research paper “Viscous Ricci dark energy model with matter creation: exact solution and observational tests, *Pramana Journal of Physics* **94**, 129 (2020)”.

In **Chapter 6** titled *“Cosmology of matter creation in FLRW model"*, we have discussed the matter-dominated model with matter creation cosmology in FLRW model as an alternative to explain the cosmic acceleration. As matter creation models are phenomenological and the literature contains a variety of models, so a generalized model could be a better choice to start for any study. Thus, we have generalized the form of particle creation rate Γ in order to produce a clear image about the matter creation models aiming to realize the early physics and its compatibility with the current astronomical data. We have performed the fitting of free parameters using joint observational data of SNe, OHD, and BAO/CMB.

We have investigated the model analytically and numerically in which the matter creation process provides the late-time accelerating phase of the cosmic expansion without the need for any dark energy. We have performed the information criterion of AIC and BIC to discriminate our model with ΛCDM model. We have discussed the

thermodynamic behavior of the model by calculating the total entropy for the matter creation. We have established the general conditions for any matter creation model that ensure the validity of the generalized second law of thermodynamics. Our analysis shows that the model is close to the standard ΛCDM model.

The work presented in this chapter comprises the result of a published paper, “Quintessence behavior via matter creation cosmology, *The European Physical Journal C* **80**, 106 (2020)”.

Chapter 7 titled *“Conclusion and Future Scope"* presents the conclusion of the thesis work and future research plan. In the present thesis, we have studied the effects of bulk viscosity and gravitationally induced matter creation in some of the cosmological models. In one of the works, we have proposed a new form of particle creation rate Γ to discuss the early and late-time evolution of the Universe. This form of Γ may play an important role in the study of the Universe in the framework of other cosmological models/theories. We believe that this form has a lot of potential in the study of different cosmic phenomena. We hope to expand the thesis work in the future to include other modified theories. The cosmological perturbation is also an intriguing field where dissipative processes could be used to do a lot of work.

Finally, the thesis concludes with a bibliography and a list of the author’s publications.

****

Chapter 2

Holographic Ricci Dark Energy Model with Bulk Viscosity

In this chapter [1]*, we explore the bulk viscosity in holographic Ricci dark energy (HRDE) model within the framework of a flat FLRW metric. We obtain the exact solution for non-viscous and viscous HRDE models, respectively. In the non-viscous HRDE model, a power-law form of expansion is obtained which gives constant deceleration parameter and statefinder pair. In the viscous HRDE model, we consider all possible forms of bulk viscous coefficient and discuss the cosmological evolution in detail. We obtain the exponential expansion of scale factor which gives time-dependent deceleration parameter and statefinder pair. The model shows a transition from decelerated phase to accelerated phase depending on the values of the viscous term. We plot the evolution of cosmological parameters to observe the physical behaviors of the viscous model.*

[1]This chapter is based on a published research paper “Ricci dark energy model with bulk viscosity, *The European Physical Journal Plus* **133**, 312 (2018)".

2.1 Introduction

Many observational experiments [14, 15] show that DE plays an important role in the evolution of the Universe and gives rise to accelerated expansion. These observations inspire theorists to understand the mechanism of the accelerated expansion of the Universe. Therefore, the theorists have proposed various cosmological models of dark energy to explain this bizarre phenomenon. In recent years, an interesting attempt was developed to link the vacuum energy density with the holographic principle [67–69] of quantum gravity. This class of model is called holographic dark energy (HDE) in which the ultra-violet (UV) cutoff of DE is converted to an infra-red (IR) cutoff. It is to be noted that the UV cutoff is related to the vacuum energy, and the IR cutoff is related to the large-scale structure of the Universe. The HDE is an interesting and simple idea of explaining the observed accelerated expansion of the Universe. Based on the choices of IR cutoff like Hubble horizon, particle horizon, event horizon, or Ricci scalar, different types of HDE models have been proposed in recent past years. The HDE model suffers the choice of IR cut-off problem. Gao et al. [96] put forward an HDE model the so-called *holographic Ricci dark energy (HRDE)* model by assuming the IR cut-off as a function of Ricci scalar as defined and explained in section 1.8.1. Gao et al. [96] showed that this model does not only avoid the causality problem but also naturally solves the coincidence problem of DE. The HRDE model has been studied extensively to explain the accelerated expansion of the Universe in refs. [107, 111–125].

In general, various cosmological models have been discussed by considering that the Universe has to be filled with perfect fluid. Even though, it is most important to investigate more realistic models in which the dissipative processes due to viscosity have been taken into account. The influence of dissipative processes including bulk viscosity, shear viscosity, and heat transport play the important role in the cosmic expansion. The general theory of dissipation in the relativistic imperfect fluid was proposed by Eckart [190], and later on, modified by Landau and Lifshitz [191]. Israel and Stewart [201] developed a relativistic second-order theory, known as full causal theory. Misner [200] was the first to discuss the viscosity concept in cosmology. He suggested that the early era neutrino viscosity could have significantly decreased the current anisotropy of black-body radiation during the evolution process. Murphy [203] demonstrated that the bulk viscosity in the FLRW model would drive the initial

singularity to the infinite past.

The general problems associated with viscous cosmology have been discussed in Refs. [196, 283]. The DE models with the viscous term have been studied in Refs. [192, 193, 198, 271, 275, 277, 284–290]. The viscous model is also consistent with astrophysical observations at lower redshifts, and a viscous cosmic model favors a standard cold dark matter model ($SCDM$) with cosmological constant (ΛCDM) in the later cosmic evolution [194]. The viscous model also shows the phantom crossing behavior, i.e., the transition from quintessence to phantom region [209, 210]. Feng and Li [206] have investigated the HRDE model with viscous term directly proportional to the square root of energy density. The authors have analyzed that the age problem can be alleviated once the viscosity is taken into account.

The motive of this chapter is to study the HRDE model within the framework of a spatially flat FLRW space-time filled with dark matter and viscous HRDE. We find the solution for non-viscous and viscous HRDE models, and analyze the evolutionary behavior of the scale factor and deceleration parameter. We also discuss the statefinder and *Om* diagnostics to discriminate the model with other dark energy models. We plot the trajectories of this model for the statefinder parameters and *Om*. It is found that the HRDE model approaches ΛCDM for different parameters. The *Om* diagnostic is carried out to discriminate the model with other DE models.

In addition to the literature surveyed above, this study is largely motivated by the work of Cataldo et al. [210], which investigate dissipative processes in the Universe within the framework of the standard Eckart theory of relativistic irreversible thermodynamics, and in the full causal Israel-Stewart-Hiscock theory. Another inspirational work is the work by Feng and Li [206] who considered HRDE in the presence of bulk viscosity.

Chapter 2 has been organized as follows: In section 2.2, we have considered the non-viscous HRDE model containing two perfect fluids, the pressureless DM and HRDE. The scale factor, deceleration parameter, and statefinder of the HRDE model have been obtained and their behaviors have been discussed. Section 2.3 has presented the viscous HRDE model with all possible forms of the viscous term. This section has been divided into two subsections 2.3.1 and 2.3.2. The scale factor, deceleration parameter, statefinder, and *Om* diagnostic have been obtained and their behaviors have been discussed in each subsection. We have plotted the trajectories of deceleration parameter, statefinder, and *Om* to analyze the effect of bulk viscosity

on the HRDE model. We have also plotted trajectories to see the effect of the model parameter on the HRDE model. In the final section 2.4, we have summarized our results and discuss various problems.

2.2 Non-Viscous HRDE Model

We consider the following spatially homogeneous and isotropic flat FLRW line element

$$ds^2 = -dt^2 + a^2(t)[dr^2 + r^2(d\theta^2 + \sin^2\theta d\phi^2)], \tag{2.2.1}$$

where $a(t)$ is the cosmic scale factor.

The Einstein field equations in the units of $8\pi G = c = 1$ take the usual form

$$R_{\mu\nu} - \frac{1}{2}R\, g_{\mu\nu} = T_{\mu\nu}, \tag{2.2.2}$$

where the symbols have their usual meaning. The stress-energy-momentum tensor of perfect fluid is given by

$$T_{\mu\nu} = (\rho + p)u_\mu u_\nu + p\, g_{\mu\nu}, \tag{2.2.3}$$

where ρ and p are the energy density and pressure respectively. Let us consider the Universe filled with DM (excluding the baryon matter) and HRDE. So, we assume $\rho = \rho_m + \rho_d$ and $p = p_m + p_d$ (as we consider the pressureless DM, $p_m = 0$). Here, ρ_m and ρ_d are respectively the energy density of DM and HRDE, p_m and p_d are the pressure of DM and HRDE, respectively.

A relation between ρ_d and p_d is given by the equation of state (EoS)

$$p_d = \omega_d \rho_d, \tag{2.2.4}$$

where ω_d is the EoS parameter of HRDE.

The field equations (2.2.2), for line element (2.2.1) and energy-momentum tensor (2.2.3), yield the Friedmann equations

$$3H^2 = \rho = \rho_m + \rho_d, \tag{2.2.5}$$

and

$$2\dot{H}+3H^2=-p=-p_d, \tag{2.2.6}$$

where $H=\dot{a}/a$ is the Hubble parameter. An overdot stands for derivative with respect to cosmic time t. The conservation equation is given by

$$\dot{\rho}+3H(\rho+p)=0. \tag{2.2.7}$$

Gao et al. [96] proposed the IR cutoff of HDE density as a function of the Ricci scalar which is defined in Eq. (1.8.5). The HRDE density is given by

$$\rho_d=3\alpha(\dot{H}+2H^2), \tag{2.2.8}$$

where α is a dimensionless parameter.

Using (2.2.8), the field equations (2.2.5) and (2.2.6) yield

$$\dot{H}+\frac{3(1+2\alpha\omega_d)}{(2+3\alpha\omega_d)}H^2=0. \tag{2.2.9}$$

The solution of (2.2.9) is given by

$$H=\frac{1}{c_0+\frac{3(1+2\alpha\omega_d)}{(2+3\alpha\omega_d)}t}, \tag{2.2.10}$$

where c_0 is an integration constant. Equation (2.2.10) can be rewritten as

$$H=\frac{H_0}{\left\{1+\frac{3H_0(1+2\alpha\omega_d)}{(2+3\alpha\omega_d)}(t-t_0)\right\}}, \tag{2.2.11}$$

where H_0 is the present value of the Hubble parameter at $t=t_0$, the cosmic time where the HRDE starts to dominate. Integrating the above equation to solve for the scale factor, we get

$$a=a_0\left\{1+\frac{3H_0(1+2\alpha\omega_d)}{(2+3\alpha\omega_d)}(t-t_0)\right\}^{\frac{(2+3\alpha\omega_d)}{3(1+2\alpha\omega_d)}}, \alpha\neq-\frac{1}{2\omega_d} \tag{2.2.12}$$

where a_0 is the present value of the scale factor at $t=t_0$. It is observed that the Universe expands as power-law, $a\propto t^m$, where m is a positive constant. This form of scale factor provides phase description of the Universe. For $m<1$, the non-viscous HDRE model expands with decelerated rate, $m=1$ gives the marginal inflation whereas the

model expands with accelerated rate for $m > 1$. It is possible to identify the constraints on parameter which correspond to a Universe that would start with a decelerated epoch, then making a transition into accelerated epoch in late times. The Universe decelerates for $\omega_d > -\frac{1}{3\alpha}$, accelerates for $\omega_d < -\frac{1}{3\alpha}$ or expands with marginal inflation for $\omega_d = -\frac{1}{3\alpha}$. Equation (2.2.12) shows that when $\alpha = 0$, i.e., in the absence of HRDE, the scale factor obeys $a = a_0(1 + \frac{3}{2}H_0(t - t_0))^{2/3}$, which corresponds to dark matter dominated Universe. Hence, one can see that the parameter α plays a significant role for the evolution of the HRDE.

A second order derivative of the scale factor with time is given by

$$\frac{d^2a}{dt^2} = -\frac{(1+3\alpha\omega_d)a_0H_0^2}{(2+3\alpha\omega_d)}\left[1+\frac{3H_0(1+2\alpha\omega_d)}{(2+3\alpha\omega_d)}(t-t_0)\right]^{-\frac{(4+9\alpha\omega_d)}{3(1+2\alpha\omega_d)}}. \tag{2.2.13}$$

This shows that the Universe will undergo an eternal deceleration. The time elapsed since the Big-Bang, t_B, is calculated as

$$t_B = t_0 - \frac{(2+3\alpha\omega_d)}{3H_0(1+2\alpha\omega_d)}. \tag{2.2.14}$$

The result regarding the evolution of the Universe can be further verified by studying the evolution of the deceleration parameter q, which is defined in equation (1.11.9). For this model, we get

$$q = \frac{3(1+2\alpha\omega_d)}{(2+3\alpha\omega_d)} - 1. \tag{2.2.15}$$

This equation shows that the value of q is constant and this is due to the power-law form of scale factor. Therefore, this HRDE model does not show transition phase throughout the evolution of the Universe. For $\omega_d = -\frac{1}{3\alpha}$, the deceleration parameter $q = 0$. The Universe expands with decelerated rate if $q > 0$, i.e., $\omega_d > -\frac{1}{3\alpha}$ and accelerated rate for $q < 0$, i.e., $\omega_d < -\frac{1}{3\alpha}$. The parameter α is the main characteristic of HRDE model which can be determined only by the observations.

In order to constraint the parameter α in HRDE model, Zhang [117] found the best-fit result with 1σ and 2σ errors of parameter $\alpha = 0.359^{+0.024}_{-0.025}(1\sigma)^{+0.040}_{-0.040}(2\sigma)$ for HRDE model from the latest observational data including the Union sample of 307 type Ia supernovae, the shift parameter of cosmic microwave background given by the five-year Wilkinson Microwave Anisotropy Probe observations, and the baryon acoustic oscillation measurement from Sloan Digital Sky Survey. In the current work, we shall take the value of α in 2σ range, $\alpha = (0.319, 0.399)$, e.g., $\alpha = 0.34$, EoS parameter

$\omega_d = -\frac{1}{3\alpha}$ gives $\omega_d = -0.9804$ which is very closed to the result obtained by del Campo et al [124]. Therefore, for $\alpha = 0.34$ and $\omega_d = -0.9804$, the HRDE model inflates with marginal rate for which $q = 0$ whereas for $\alpha = 0.34$ and $\omega_d > (or <) -0.9804$, we get $q > (or <)\ 0$ respectively.

In order to bring about the discrimination between the various contenders, we use the statefinder pair $\{r,s\}$ defined by Sahni et al. [250] and Alam et al. [251] as in (1.12.1). For this model, the statefinder parameter are obtained as

$$r = 1 - \frac{9(1+2\alpha\omega_d)}{2(1+\frac{3}{2}\alpha\omega_d)} + \frac{9(1+2\alpha\omega_d)^2}{2(1+\frac{3}{2}\alpha\omega_d)^2} \tag{2.2.16}$$

and

$$s = \frac{1+2\alpha\omega_d}{1+\frac{3}{2}\alpha\omega_d}. \tag{2.2.17}$$

Different models on the $r-s$ plane accordingly show different trajectories, e.g., the spatially flat ΛCDM scenario corresponds to a fixed point $\{1,0\}$ and $SCDM$ scenario gives a fixed point $\{1,1\}$ in the statefinder diagnostic pair $\{r,s\}$ plane, with which the distance of other DE models from ΛCDM can therefore be established on the $r-s$ plane. From the Eqs. (2.2.16) and (2.2.17), we observe that the HRDE model may approach to ΛCDM as $\alpha \to -\frac{1}{2\omega_d}$. HRDE model may correspond to $\{r,s\} \to \{1,0\}$, but there is no such value of parameters which would clearly show the ΛCDM. However, in the absence of dark energy, i.e., $\alpha = 0$, the model gives the pair $\{1,1\}$ of $SCDM$.

2.3 Viscous HRDE Model

According to the observations, the phase transition plays a vital role in describing the evolution of the Universe. However, in section 2.2, we have observed that the non-viscous HRDE model does not show the phase transition as the deceleration parameter is constant. Therefore, in this section, our aim is to discuss the viscous HRDE model to find whether it would show the phase transition and act as a possible candidate for the accelerating Universe.

The stress-energy-momentum tensor (2.2.3) after considering bulk viscosity modifies to

$$T_{\mu\nu} = (\rho + p)u_\mu u_\nu + p\, g_{\mu\nu} - 3\zeta H\, h_{\mu\nu}, \tag{2.3.1}$$

where ζ is the bulk viscous coefficient, and $h_{\mu\nu} = g_{\mu\nu} + u_\mu u_\nu$ is the projection tensor. Using (2.3.1), the field equations (2.2.5) and (2.2.6) for the viscous RDE model modify

to

$$3H^2 = \rho_m + \rho_d, \tag{2.3.2}$$

$$2\dot{H} + 3H^2 = -\tilde{p_d}, \tag{2.3.3}$$

where $\tilde{p_d}$ is an effective pressure with $\tilde{p_d} = p_d - 3H\zeta$. On thermodynamical grounds, ζ is conventionally chosen to be a positive quantity and generically depends on the cosmic time t, or redshift z, or the scale factor a, or the energy density ρ, or a more complicated combination form.

It is to be noted that the Eckart theory [190] has some problems in its formulation, for example, all the equilibrium states in this theory are unstable, another issue is that signals can propagate through the fluids faster than the speed of light. To correct the problems of the Eckart theory, Israel and Stewart [201] developed a more consistent and general theory that avoids these issues from which the Eckart theory is the first-order limit when the relaxation time goes to zero. In this limit, the Eckart theory is a good approximation to the Israel-Stewart theory.

In spite of the problems of the Eckart theory, but taking advantage of the equivalence of both theories at this limit, it has been widely used by several authors because it is simpler to work with this than with the Israel-Stewart one. In particular, it has been used to model bulk viscous dark fluids as responsible for the observed acceleration of the Universe assuming that the approximation of vanishing relaxation time is valid for this purpose. Moreover, Hiscock and Salmonson [291] have shown that Eckart theory can be favored over the Israel-Stewart theory, in explaining the inflationary acceleration of FLRW Universe with a bulk viscous fluid. This motivates us to use Eckart results, especially when one tries to look at the phenomenon of the recent acceleration of the Universe. Another compelling reason to use Eckart's theory is that Israel-Stewart theory can not produce a recent accelerating epoch as argued by many authors. Therefore, we study the non-causal approximation of the bulk viscosity in this chapter.

Following [277], we consider a parameterized bulk viscous coefficient ζ of the form,

$$\zeta = \zeta_0 + \zeta_1 H, \tag{2.3.4}$$

where ζ_0 and ζ_1 are positive constants. In Eq. (2.3.4), ζ is a linear combination of two terms: the first term is a constant ζ_0 and the second term is proportional to the Hubble parameter, which characterizes the dependence of the bulk viscosity on the

expansion rate of the Universe. The motivation of considering this bulk viscosity is that by fluid mechanics we know the transport/viscosity phenomenon is involved with the velocity $\dot{a}$, which is related to the expansion $\theta = 3\dot{a}/a$.

Using linear EoS for DE (2.2.4) and (2.3.4), a linear combination of (2.3.2) and (2.3.3) gives a single evolution equation for H as

$$(2+3\alpha\omega_d)\dot{H} + 3(1+2\alpha\omega_d)H^2 - 3\zeta H = 0. \tag{2.3.5}$$

Equation (2.3.5) may be integrated directly as a function of the bulk viscosity. For $\alpha \neq -\frac{1}{2\omega_d}$, the solution has the form

$$H(t) = \frac{e^{\frac{3}{(2+3\alpha\omega_d)}\int \zeta(t)\,dt}}{c_1 + \frac{3(1+2\alpha\omega_d)}{(2+3\alpha\omega_d)}\int e^{\frac{3}{(2+3\alpha\omega_d)}\int \zeta(t)\,dt}\,dt}, \tag{2.3.6}$$

where c_1 is the constant of integration. Thus, for a given $\zeta(t)$ we have the expressions for various physical parameters. In the following subsections, we present different viscous HRDE models arises due to the choice of bulk viscous coefficient ζ.

2.3.1 HRDE Model with Constant Bulk Viscosity

In this case, we parameterize the functional form of ζ as $\zeta = \zeta_0 = constant$ by taking $\zeta_1 = 0$ in equation (2.3.4) (hereafter *VHRDE1 model*). It is the simplest parameterizations for bulk viscous coefficient. Using this form of ζ into (2.3.6) and simplifying, we get

$$H(t) = H_0 e^{\frac{3\zeta_0(t-t_0)}{(2+3\alpha\omega_d)}}\left[1 + \frac{H_0(1+2\alpha\omega_d)}{\zeta_0}\left\{e^{\frac{3\zeta_0(t-t_0)}{(2+3\alpha\omega_d)}} - 1\right\}\right]^{-1}. \tag{2.3.7}$$

The scale factor of the Universe $a(t)$, normalized to unity at the present epoch, evolves with time as

$$a = \left[1 + \frac{H_0(1+2\alpha\omega_d)}{\zeta_0}\left\{e^{\frac{3\zeta_0(t-t_0)}{(2+3\alpha\omega_d)}} - 1\right\}\right]^{\frac{(2+3\alpha\omega_d)}{3(1+2\alpha\omega_d)}}, \tag{2.3.8}$$

where $\zeta_0 \neq 0$ and $\alpha \neq -1/2\omega_d$. From equation (2.3.8), we obtained the Hubble parameter in terms of scale factor a as

$$H(a) = \frac{H_0}{(1+2\alpha\omega_d)}\left[\frac{\zeta_0}{H_0} + \left\{(1+2\alpha\omega_d) - \frac{\zeta_0}{H_0}\right\}a^{-\frac{3(1+2\alpha\omega_d)}{(2+3\alpha\omega_d)}}\right]. \tag{2.3.9}$$

We observe that the model starts from a non-singular state and constant bulk viscous coefficient gives rise to exponential expansion. As $(t-t_0)\to 0$, the scale factor reduces to

$$a \to \left[1+\frac{3H_0(1+2\alpha\omega_d)}{(2+3\alpha\omega_d)}(t-t_0)\right]^{\frac{(2+3\alpha\omega_d)}{3(1+2\alpha\omega_d)}}, \tag{2.3.10}$$

which shows power-law expansion in early time. In limiting conditions, as $(t-t_0)\to\infty$, the scale factor tends to $a(t)\to e^{\frac{3\zeta_0(t-t_0)}{(2+3\alpha\omega_d)}}$, which corresponds to acceleration similar to the de Sitter phase, implies that the VHRDE1 model behaves similar to the cosmological constant model as $(t-t_0)\to\infty$. This shows that the Universe has an earlier deceleration phase followed by an acceleration phase in the later stage of the evolution. Equation (2.3.8) reveals that the time elapsed since the Big-Bang is

$$t_B = t_0 + \frac{(2+3\alpha\omega_d)}{3\zeta_0}\, ln\left(1-\frac{\zeta_0}{H_0(1+2\alpha\omega_d)}\right). \tag{2.3.11}$$

Therefore, the Universe begins with a Big-Bang followed by an eternal expansion and this expansion begins with a decelerated rate followed by an eternal accelerated one. Hence, the age of the Universe since Big-Bang is,

$$t_0 - t_B = -\frac{(2+3\alpha\omega_d)}{3\zeta_0}\, ln\left(1-\frac{\zeta_0}{H_0(1+2\alpha\omega_d)}\right). \tag{2.3.12}$$

We can calculate the transition between the decelerated-accelerated expansion depending on the value of ζ_0. To compute the scale factor where the transition happens, we take the derivative of $\dot{a}$ with respect to a using (2.3.9) to give [272]

$$\frac{d\dot{a}}{da} = \frac{H_0}{(1+2\alpha\omega_d)}\left[\frac{\zeta_0}{H_0} - \left\{(1+2\alpha\omega_d)-\frac{\zeta_0}{H_0}\right\}\left(\frac{1+3\alpha\omega_d}{2+3\alpha\omega_d}\right)a^{-\frac{3(1+2\alpha\omega_d)}{(2+3\alpha\omega_d)}}\right]. \tag{2.3.13}$$

Equating (2.3.13) to zero, we get the transition scale factor a_{tr} as [272]

$$a_{tr} = \left[\frac{(1+3\alpha\omega_d)\{(1+2\alpha\omega_d)H_0-\zeta_0\}}{(2+3\alpha\omega_d)\zeta_0}\right]^{\frac{(2+3\alpha\omega_d)}{3(1+2\alpha\omega_d)}}. \tag{2.3.14}$$

The corresponding transition redshift z_{tr}, where $a=(1+z)^{-1}$, is

$$z_{tr} = \left[\frac{(1+3\alpha\omega_d)\{(1+2\alpha\omega_d)H_0-\zeta_0\}}{(2+3\alpha\omega_d)\zeta_0}\right]^{-\frac{(2+3\alpha\omega_d)}{3(1+2\alpha\omega_d)}} - 1. \tag{2.3.15}$$

From (2.3.14) or (2.3.15), we observe that for $\zeta_0 = \frac{(1+3\alpha\omega_d)H_0}{3}$, the transition from decelerated phase to accelerated phase occurs at $a_{tr}=1$ or $z_{tr}=0$, which corresponds

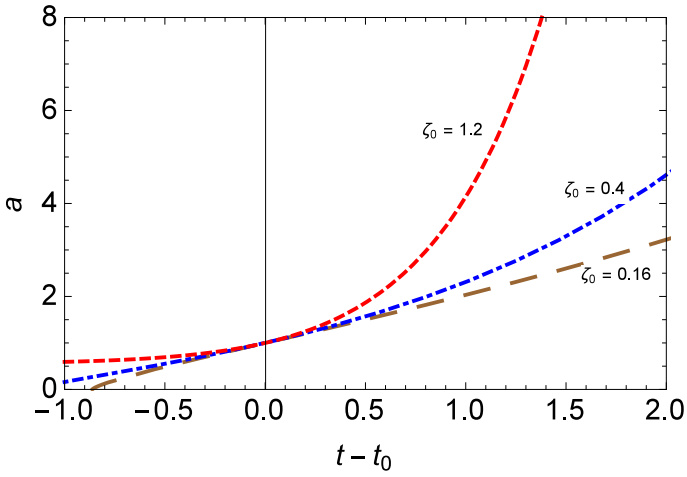

Figure 2.1: The evolution of scale factor for different values of $\zeta_0 > 0$ with fixed $\alpha = 0.34$ and $\omega_d = -0.5$ in VHRDE1 model.

to the present time of the Universe. When $\zeta_0 \to 0$, the value of a_{tr} tends to infinity in the future. If we take the observed value of $\alpha = 0.34$ with $H_0 = 1, \omega_d = -0.5$, we obtain $\zeta_0 = 0.16$. So, we observe that for $0 < \zeta_0 \leq 0.16$, the scale factor a expands initially with decelerated rate and with accelerated in late time and for $\zeta_0 > 0.16$, a will accelerates from early time. This can be verified from the evolution of scale factor as shown in Fig. 2.1. We can see from Fig. 2.1 that as the values of ζ_0 increases, the transition from deceleration to acceleration occurs in past.

Now, the deceleration parameter q is given by

$$q = \frac{3\left\{(1+2\alpha\omega_d) - \frac{\zeta_0}{H_0}\right\}}{2(1+\frac{3}{2}\alpha\omega_d)} e^{-\frac{3\zeta_0(t-t_0)}{2(1+\frac{3}{2}\alpha\omega_d)}} - 1. \tag{2.3.16}$$

Equation (2.3.16) represents the time-dependent DP, which describes the phase transition at time $t = t_0$, which is time at which the VHRDE1 starts to dominate. The DP in terms of scale factor a is given by

$$q(a) = \frac{3(1+2\alpha\omega_d) - 3\zeta_0}{(2+3\alpha\omega_d)} \left[\frac{(1+2\alpha\omega_d)}{\{a^{\frac{3(1+2\alpha\omega_d)}{(2+3\alpha\omega_d)}} - 1\}\zeta_0 + (1+2\alpha\omega_d)}\right] - 1. \tag{2.3.17}$$

The DP in terms of redshift z can be written as

$$q(z) = \frac{3(1+2\alpha\omega_d) - 3\zeta_0}{(2+3\alpha\omega_d)} \left[\frac{(1+2\alpha\omega_d)}{\{(1+z)^{\frac{-3(1+2\alpha\omega_d)}{(2+3\alpha\omega_d)}} - 1\}\zeta_0 + (1+2\alpha\omega_d)}\right] - 1. \tag{2.3.18}$$

We can observe that for $\zeta_0 = 0$, we have DP (2.2.15) for non-viscous HRDE model. When the bulk viscous parameter and all other parameters are zero, we get $q = 1/2$, which corresponds to a decelerating matter-dominated Universe. As $(t - t_0) \to 0$, we get $q \to \frac{(1+3\alpha\omega_d)H_0 - 3\zeta_0}{(2+3\alpha\omega_d)H_0}$. When $\zeta_0 = \frac{(1+3\alpha\omega_d)H_0}{3}$, i.e., at the value of transition of ζ_0, we have $q = 0$, i.e., marginal inflation occurs. As $(t - t_0) \to \infty$, we have $q \to -1$ that approaches to de Sitter Universe. Thus, DP is decreasing function with a transition from positive to negative value of q for the value of scale factor a_{tr} given in equation (2.3.14). From (2.3.17), we get DP at present as $q_0 = q(a = 1) = \frac{(1+3\alpha\omega_d) - 3\zeta_0}{(2+3\alpha\omega_d)}$. It is to be noted that when $\zeta_0 = \frac{(1+3\alpha\omega_d)H_0}{3}$, we get $q_0 = 0$, i.e., the transition from decelerated phase to accelerated phase takes place at present. For $\zeta_0 < (1 + 3\alpha\omega_d)H_0/3$ we have $q_0 > 0$, i.e., the decelerated phase in the present and it would enter the accelerating phase in future. The current $q_0 < 0$ if $\zeta_0 > (1 + 3\alpha\omega_d)H_0/3$ we have an accelerated phase at present time and it entered this epoch at an early stage.

The variation of q with a for two sets (various values of ζ_0 and fixed α, and various

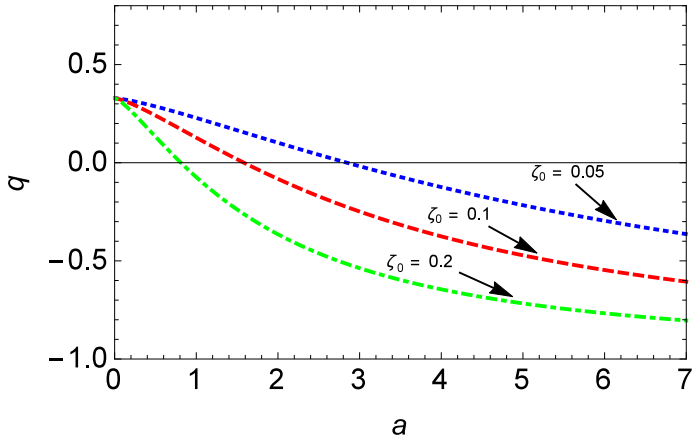

Figure 2.2: The evolution of the deceleration parameter q in terms of the scale factor a for different values of $\zeta_0 > 0$ with fixed $\omega_d = -0.5$ and $\alpha = 0.34$ in VHRDE1 model.

values of α and fixed ζ_0) are shown in Fig. 2.2 and Fig. 2.3, respectively. Fig. 2.2 plot the evolution of DP with a for different values of ζ_0 and fixed $\alpha = 0.34$. We can observe that as the values of ζ_0 increases, the transition occurs in early time. We also observe that for large α, the transition takes place in early time as shown in Fig. 2.3. We observe that q changes its sign from positive to negative, i.e., shows the transition from decelerated to accelerated phase in both the figures. It is also observed that $q \to -1$ in the late time of evolution.

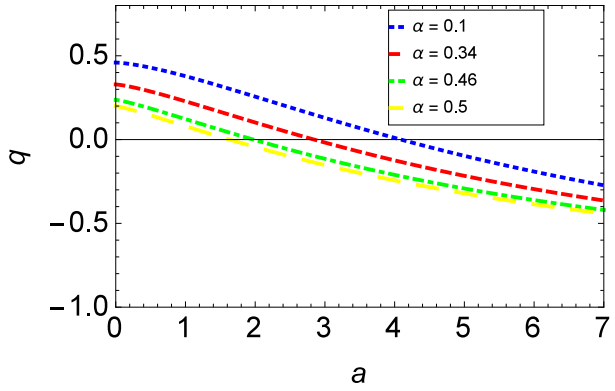

Figure 2.3: The evolution of the deceleration parameter q in terms of the scale factor a for different values of $\alpha > 0$ with fixed $\omega_d = -0.5$ and $\zeta_0 = 0.05$ in VHRDE1 model.

Statefinder analysis

In Section 2.2 for the non-viscous case, we find that the statefinder pair is constant and is not much of use to discriminate with other models. In this section, we present our analysis to the VHRDE1 model to distinguish it from other DE models. In VHRDE1 model, the statefinder parameter can be obtained as

$$r = 1 + \frac{9\left(\frac{\zeta_0}{H_0} - (1+2\alpha\omega_d)\right)\left(1 - \frac{(1+2\alpha\omega_d)}{(2+3\alpha\omega_d)}\right)}{(2+3\alpha\omega_d)} e^{\frac{-3\zeta_0(t-t_0)}{(2+3\alpha\omega_d)}} + \frac{9\left(\frac{\zeta_0}{H_0} - (1+2\alpha\omega_d)\right)^2}{(2+3\alpha\omega_d)^2} e^{\frac{-6\zeta_0(t-t_0)}{(2+3\alpha\omega_d)}}, \tag{2.3.19}$$

and

$$s = \frac{\frac{\left(\frac{\zeta_0}{H_0} - (1+2\alpha\omega_d)\right)\left(1 - \frac{1+2\alpha\omega_d}{(2+3\alpha\omega_d)}\right)}{(1+\frac{3}{2}\alpha\omega_d)} e^{\frac{-3\zeta_0(t-t_0)}{(2+3\alpha\omega_d)}} + \frac{\left(\frac{\zeta_0}{H_0} - (1+2\alpha\omega_d)\right)^2}{2(1+\frac{3}{2}\alpha\omega_d)^2} e^{\frac{-6\zeta_0(t-t_0)}{(2+3\alpha\omega_d)}}}{\frac{\left((1+2\alpha\omega_d) - \frac{\zeta_0}{H_0}\right)}{(1+\frac{3}{2}\alpha\omega_d)} e^{\frac{-3\zeta_0(t-t_0)}{(2+3\alpha\omega_d)}} - 1}. \tag{2.3.20}$$

The above equations show that in the limit $(t-t_0) \to \infty$, the statefinder parameters $\{r,s\} \to \{1,0\}$, which corresponds to the ΛCDM model. Thus, the present model resembles the ΛCDM model in the future. The $\{r,s\}$ and $\{r,q\}$-planes trajectory of the present model are shown in Fig. 2.4 and Fig. 2.5, respectively for different values of ζ_0 with fixed $\omega_d = -0.5$ and $\alpha = 0.34$. In Fig. 2.4, the fixed points $\{r,s\} = \{1,1\}$ and $\{r,s\} = \{1,0\}$ are shown as $SCDM$ model and ΛCDM model, respectively.

In Fig. 2.4, the trajectory is divided into two region. In one of the region on left side of vertical line, the trajectories for large viscous term in $\{r,s\}$ plane lie in region $r > 1$,

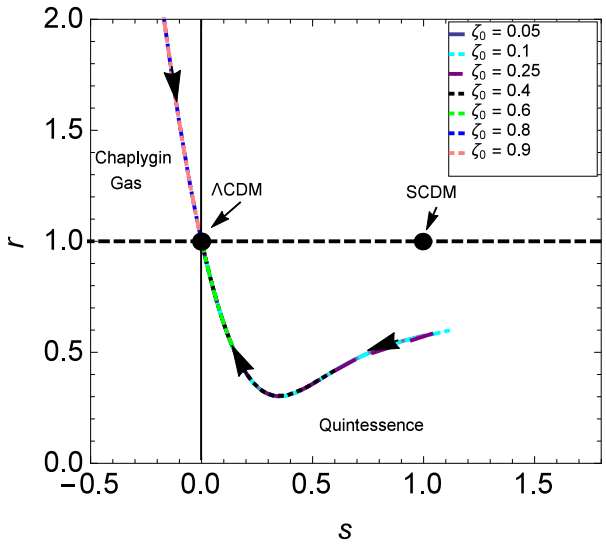

Figure 2.4: The evolution of $\{r,s\}$ in the $r-s$ plane for different values of $\zeta_0 > 0$ with fixed $\omega_d = -0.5$ and $\alpha = 0.34$ in VHRDE1 model . The curves are coinciding with each other in Chaplygin gas and quintessence models. The arrows represent the direction of the evolution of statefinder diagnostic pair with time.

$s < 0$, a feature similar to the chaplygin gas (CG) model of DE [278]. In other region of $\{r,s\}$ plane on the right side of vertical line, the trajectory for small values of ζ_0 in $\{r,s\}$ plane lie in the region $r < 1$, $s > 0$, a feature similar to the quintessence model (Q) [250, 251]. The arrows in the figure give the direction of the evolution. In other words, for $0 < \zeta_0 < 0.66$, the trajectories starts in quintessence region during early time and approaches to ΛCDM in late time. However, the trajectories starts from Chaplygin gas model if $\zeta_0 > 0.66$ and approaches to ΛCDM in late time. Thus, the VHRDE1 model is compatible with quintessence model for small values of ζ_0 whereas it is compatible with Chaplygin gas model for large values of ζ_0. In both cases, the VHRDE1 model resembles to ΛCDM model in late time. The trajectory in both region are coinciding for all different values of ζ_0. The VHRDE1 model can also be discriminated from HDE model with event horizon as the infra-red cut-off, in which the $r-s$ evolution starts from a region $r \sim 1$, $s \sim 2/3$ and end on the ΛCDM point.

Fig. 2.5 shows the trajectory of evolutionary behavior of VHRDE1 model in $\{r,q\}$ plane. The trajectories have been plotted for different values of ζ_0 with fixed $\alpha = 0.34$, $\omega_d = -0.5$ and $H_0 = 1$. The $SCDM$ model and steady-state (SS) model correspond to fixed point $\{r,q\} = \{1, 0.5\}$ and $\{r,q\} = \{1,-1\}$, respectively. It can be seen that there is a sign change of q from positive to negative in the quintessence region which explains the recent phase transition from decelerated to accelerated phase. The trajectories

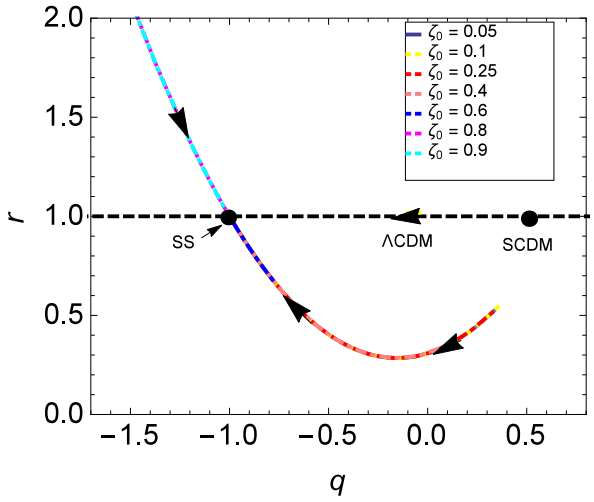

Figure 2.5: The evolution of $\{r,q\}$ in the $r-q$ plane for different values of $\zeta_0 > 0$ with fixed $\omega_d = -0.5$ and $\alpha = 0.34$ in VHRDE1 model. The arrows represent the direction of the evolution pair $r-q$ with time.

show that VHRDE1 models commence evolving from different points for different values of ζ_0 with respect to ΛCDM which starts from $SCDM$ fixed point. In the phantom region, the evolution of q starts from negative and tends to $q = -1$ in late time. Therefore, the VHRDE1 model always converges to SS model as ΛCDM, quintessence, and phantom models in the late-time evolution of the Universe. Thus, the constant VHRDE1 model behaves quintessence-like and phantom-like in early time and ΛCDM in the late time of evolution depending upon the value of ζ_0.

The above discussion concludes the effect of the viscous term in the HRDE model. Let us discuss the model from the viewpoint of model parameter α. Fig. 2.6 and Fig. 2.7 show the trajectories in $r-s$ and $r-q$ planes, respectively, for the different values of α with constant $\omega_d = -0.5$, $H_0 = t_0 = 1$ and $\zeta_0 = 0.05$. The arrows in the diagram denote the evolution directions of the statefinder trajectories and $r-q$ trajectories. In Fig. 2.6, we observe that for the fixed value of ζ_0, the VHRDE1 model always corresponds to the Q model. It may start from the vicinity of $SCDM$ model in the early time of evolution for some values of α, e.g., $\alpha = 0.34$. In the late-time of evolution, the model always converges to ΛCDM model for any values of α .

Fig. 2.7 shows the time evolution of the $r-q$ trajectories in $r-q$ plane. The horizontal line at $r = 1$ corresponds to the time evolution of the ΛCDM model. The signature change from positive to negative in q clearly explains the phase transition of the Universe. The constant VHRDE1 model may start from the vicinity of the $SCDM$ model ($\{r,q\} = \{1, 0.5\}$) for some values of α, e.g., $\alpha = 0.34$. However, the constant VHRDE1

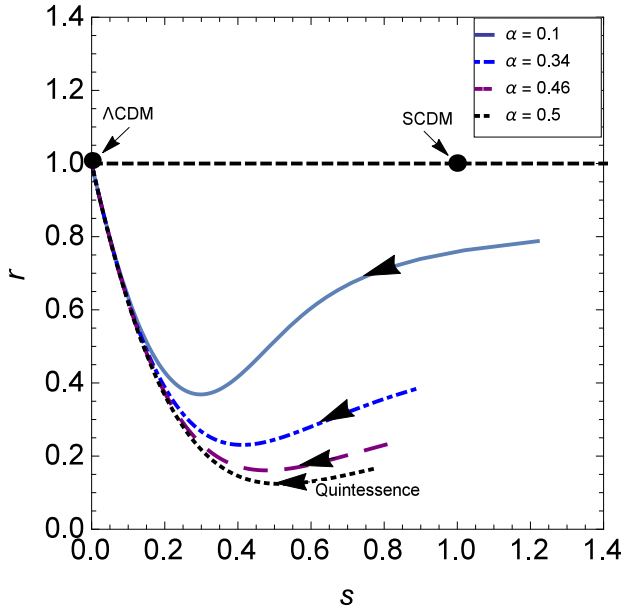

Figure 2.6: The $r-s$ trajectories in $r-s$ plane for different values of α with $\omega_d = -0.5$ and $\zeta_0 = 0.05$ in VHRDE1 model. The arrows represent the direction of the evolutions of the statefinder diagnostic pair with time.

model approaches the SS model as the ΛCDM and Q models in the future. Thus, the VHRDE1 model is compatible with the ΛCDM and Q models with variable model parameters and constant value of ζ_0.

From the above analysis we conclude that our model corresponds to both Q and CG models for the different values of viscous coefficient ζ_0 whereas for the different values of model parameters α with respect to the fixed value of ζ_0, our model only corresponds to Q model. We can say that the bulk viscous coefficient and model parameter play the important role in the evolution of the Universe, i.e., they both determine the evolutionary behavior as well as the ultimate fate of the Universe.

Om Diagnostics

As a complementary to $\{r,s\}$, a new diagnostic called Om has been proposed by Sahni et al. [254] as discussed and defined in section 1.12.3 by Eq. (1.12.3), which helps to distinguish the present matter density contrast Ω_{0m} in different models more effectively. This is also a geometrical diagnostic that explicitly depends on redshift

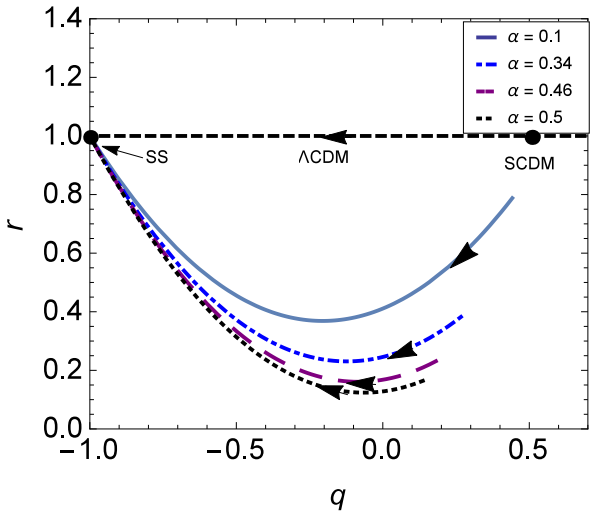

Figure 2.7: The $r-q$ trajectories in $r-q$ plane for different values of α with $\omega_d = -0.5$ and $\zeta_0 = 0.05$ in VHRDE1 model. The arrows represent the direction of the evolutions with time.

and the Hubble parameter. Using (2.3.9), the value of $Om(z)$ is given by

$$Om(z) = \frac{\left[\frac{\zeta_0}{H_0} + \{(1+2\alpha\omega_d) - \frac{\zeta_0}{H_0}\}(1+z)^{\frac{3(1+2\alpha\omega_d)}{2+3\alpha\omega_d}}\right]^2 - (1+2\alpha\omega_d)^2}{(1+2\alpha\omega_d)^2[(1+z)^3-1]}. \tag{2.3.21}$$

To analyse evolution of the *Om(z)* due to viscosity effect, we plot the graph of $Om(z)$ versus redshift z for different values of $\zeta_0 > 0$ by fixing the values of α, ω_d and H_0 as shown in Fig. 2.8. It is observed that for $0 < \zeta_0 < 0.66$, the $Om(z)$ trajectory shows the negative slope which corresponds to the quintessence model of dark energy and for $\zeta_0 > 0.66$, we observe the positive slope of $Om(z)$ which corresponds to the phantom.

In Fig. 2.9, we plot the $Om(z)$ trajectory with respect to z for different values of α to see the contribution from this parameter on the evolution with fixed $\zeta_0 = 0.05, \omega_d = -0.5$ and $H_0 = 1$. We observe that the $Om(z)$ trajectory shows the negative curvature which corresponds to the quintessence model of DE. For the case of $z = -1$, $Om(z) = 1 - \frac{\zeta_0^2}{H_0^2(1+2\alpha\omega_d)^2}$, which is constant, so it will correspond to ΛCDM.

The above analysis from evolution of scale factor, DP, statefinder pair and $Om(z)$, it is obvious that the constant bulk viscous coefficient ζ_0 (or model parameter α) play an important role in the evolution of the Universe. The Universe shows transition from decelerated to accelerated phase and for some values of this coefficient the acceleration starts from past. The VHRDE1 model behaves like quintessence for small ζ_0 and Chaplygin gas like for large values of this parameter. However, the model parameters

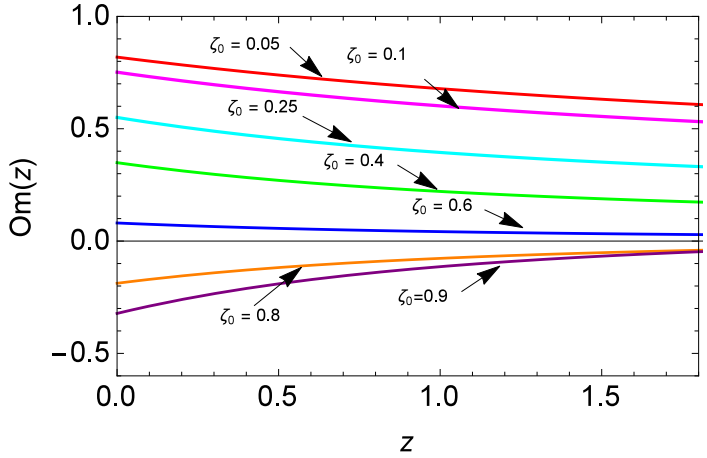

Figure 2.8: The evolution of $Om(z)$ versus the redshift z for different values of $\zeta_0 > 0$ with $\omega_d = -0.5$, $\alpha = 0.34$ in VHRDE1 model.

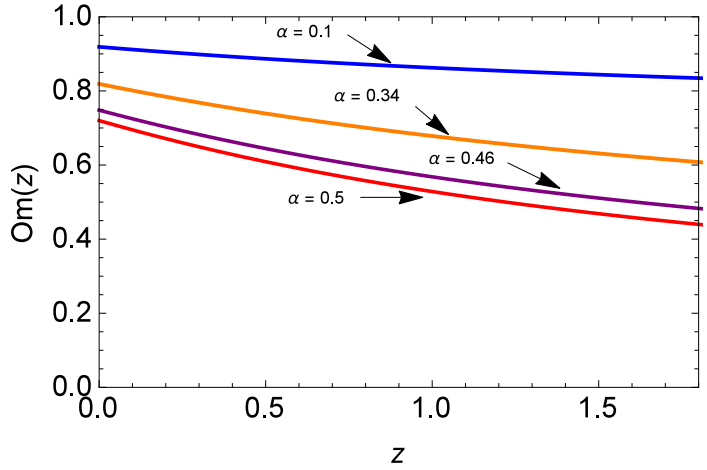

Figure 2.9: The evolution of $Om(z)$ versus the redshift z for different values of α with $\zeta_0 = 0.05$ and $\omega_d = -0.5$ in VHRDE1 model.

gives only quintessence like model. In both cases, the VHRDE1 model resembles to ΛCDM model in late time.

2.3.2 HRDE Model with Variable Bulk Viscosity

In this subsection we consider two cases for bulk viscous coefficient: (i) $\zeta = \zeta_1 H$ and (ii) $\zeta = \zeta_0 + \zeta_1 H$.

Case (i): $\zeta = \zeta_1 H$

The parameterized form of $\zeta = \zeta_1 H$ can be obtained from equation (2.3.4) by taking

$\zeta_0 = 0$ (hereafter VHRDE2 model. Using this form in (2.3.5) we get

$$\dot{H} + \frac{3(1-\zeta_1+2\alpha\omega_d)}{(2+3\alpha\omega_d)}H^2 = 0. \tag{2.3.22}$$

On solving above equation we get

$$H = \frac{H_0}{\left\{1+\frac{3H_0(1-\zeta_1+2\alpha\omega_d)}{(2+3\alpha\omega_d)}(t-t_0)\right\}}. \tag{2.3.23}$$

The scale factor, normalized to unity at present epoch, can be obtained as

$$a = \left\{1+\frac{3H_0(1-\zeta_1+2\alpha\omega_d)}{(2+3\alpha\omega_d)}(t-t_0)\right\}^{\frac{(2+3\alpha\omega_d)}{3(1-\zeta_1+2\alpha\omega_d)}}; \text{ for } \zeta_1 \neq (1+2\alpha\omega_d),\ \alpha \neq -2/3\omega_d \tag{2.3.24}$$

Equation (2.3.24) shows that the scale factor is of the power-law form. The behavior of this model is similar to the model as discussed in section 2.2 for non-viscous HRDE model. The Universe decelerates for $\zeta_1 < (1+3\alpha\omega_d)/3$, shows marginal inflation if $\zeta_1 = (1+3\alpha\omega_d)/3$ and accelerates for $\zeta_1 > (1+3\alpha\omega_d)/3$. It is to be noted that for $\alpha = 0$, the scale factor reduces to $a = a_0\left\{1+\frac{3H_0(1-\zeta_1)}{2}(t-t_0)\right\}^{\frac{2}{3(1-\zeta_1)}}$, where $\zeta_1 \neq 1$. When $\zeta_1 = 0$ we recover the usual matter-dominated Universe. For this model the DP is given by

$$q = \frac{3(1-\zeta_1+2\alpha\omega_d)}{(2+3\alpha\omega_d)} - 1, \tag{2.3.25}$$

which is constant. The positive or negative value of q depends on $\zeta_1 < (1+3\alpha\omega_d)/3$ or $\zeta_1 > (1+3\alpha\omega_d)/3$ respectively. We get $q = 0$ for $\zeta_1 = (1+3\alpha\omega_d)/3$.
Now, the statefinder parameter can be evaluated as

$$r = 1 - \frac{9(1-\zeta_1+2\alpha\omega_d)}{2(1+\frac{3}{2}\alpha\omega_d)} + \frac{9(1-\zeta_1+2\alpha\omega_d)^2}{2(1+\frac{3}{2}\alpha\omega_d)^2} \tag{2.3.26}$$

and

$$s = \frac{1-\zeta_1+2\alpha\omega_d}{1+\frac{3}{2}\alpha\omega_d}. \tag{2.3.27}$$

The above equations show that in the limit $\zeta_1 \to (1+2\alpha\omega_d)$ the statefinder parameters $\{r,s\} \to \{1,0\}$ but there is no such values of parameters which would clearly show ΛCDM. For $\zeta_1 = \frac{\alpha\omega_d}{2}$, the VHRDE2 model behaves as SCDM, i.e., $\{r,s\} = \{1,1\}$.

Case (ii): $\zeta = \zeta_0 + \zeta_1 H$

This parameterized form of ζ is the general form involving the combination of two terms: constant and function of Hubble parameter (*hereafter VHRDE3 model*). Using this general form of bulk viscous coefficient into equation (2.3.5), we get

$$\dot{H} + \frac{3(1-\zeta_1+2\alpha\omega_d)}{(2+3\alpha\omega_d)}H^2 - \frac{3\zeta_0}{(2+3\alpha\omega_d)}H = 0. \tag{2.3.28}$$

On solving the above equation, we get

$$H = H_0 e^{\frac{3\zeta_0(t-t_0)}{(2+3\alpha\omega_d)}}\left[1+\frac{H_0(1-\zeta_1+2\alpha\omega_d)}{\zeta_0}\left\{e^{\frac{3\zeta_0(t-t_0)}{(2+3\alpha\omega_d)}}-1\right\}\right]^{-1}. \tag{2.3.29}$$

From above equation, the scale factor, normalized to unity at present epoch, evolves with time as

$$a = \left[1+\frac{H_0(1-\zeta_1+2\alpha\omega_d)}{\zeta_0}\left\{e^{\frac{3\zeta_0(t-t_0)}{(2+3\alpha\omega_d)}}-1\right\}\right]^{\frac{(2+3\alpha\omega_d)}{3(1-\zeta_1+2\alpha\omega_d)}}, \tag{2.3.30}$$

where $\zeta_0 \neq 0$ and $\zeta_1 \neq (1+2\alpha\omega_d)$. The Hubble parameter in terms of scale factor a is given by

$$H = \frac{H_0}{(1-\zeta_1+2\alpha\omega_d)}\left[\frac{\zeta_0}{H_0}+\left\{(1-\zeta_1+2\alpha\omega_d)-\frac{\zeta_0}{H_0}\right\}a^{\frac{-3(1-\zeta_1+2\alpha\omega_d)}{(2+3\alpha\omega_d)}}\right], \tag{2.3.31}$$

When $\zeta_1 = 0$, H reduces to equation (2.3.9) which is the case of constant viscosity.

From (2.3.30), we get exponential form of the scale factor which may show transition from one phase to other. As $(t-t_0) \to 0$, the scale factor behaves as

$$a \to \left[1+\frac{3H_0(1-\zeta_1+2\alpha\omega_d)(t-t_0)}{(2+3\alpha\omega_d)}\right]^{\frac{(2+3\alpha\omega_d)}{3(1-\zeta_1+2\alpha\omega_d)}}, \tag{2.3.32}$$

which shows power-law expansion in early time. On the other hand, if $\zeta_0 = H_0(1-\zeta_1+2\alpha\omega_d)$ or $(t-t_0) \to \infty$, we obtain

$$a(t) = \exp\left(\frac{3\zeta_0(t-t_0)}{(2+3\alpha\omega_d)}\right). \tag{2.3.33}$$

This case corresponds the de Sitter Universe which shows accelerated expansion in the later time of evolution. The derivative of $\dot{a}$ with respect to a can be obtained

from (2.3.31), which is given by

$$\frac{d\dot{a}}{da}=\frac{H_0}{(1-\zeta_1+2\alpha\omega_d)}\left[\frac{\zeta_0}{H_0}-\left\{(1-\zeta_1+2\alpha\omega_d)-\frac{\zeta_0}{H_0}\right\}\left(\frac{1-3\zeta_1+3\alpha\omega_d}{2+3\alpha\omega_d}\right)a^{-\frac{3(1-\zeta_1+2\alpha\omega_d)}{(2+3\alpha\omega_d)}}\right]. \tag{2.3.34}$$

Equating (2.3.34) to zero to get the transition scale factor a_{tr} as

$$a_{tr}=\left[\frac{(1-3\zeta_1+3\alpha\omega_d)\{(1-\zeta_1+2\alpha\omega_d)H_0-\zeta_0\}}{(2+3\alpha\omega_d)\zeta_0}\right]^{\frac{(2+3\alpha\omega_d)}{3(1-\zeta_1+2\alpha\omega_d)}}. \tag{2.3.35}$$

The corresponding transition redshift z_{tr} is given by

$$z_{tr}=\left[\frac{(1-3\zeta_1+3\alpha\omega_d)\{(1-\zeta_1+2\alpha\omega_d)H_0-\zeta_0\}}{(2+3\alpha\omega_d)\zeta_0}\right]^{-\frac{(2+3\alpha\omega_d)}{3(1-\zeta_1+2\alpha\omega_d)}}-1. \tag{2.3.36}$$

From (2.3.35) and (2.3.36), we observe that for $\zeta_0+\zeta_1H_0=\frac{(1+3\alpha\omega_d)H_0}{3}$, the transition from decelerated phase to accelerated phase occurs at $a_{tr}=1$ or $z_{tr}=0$, which corresponds to the present time of the Universe. By considering the observational value $\alpha=0.34$ along with $\omega_d=-0.5$, $H_0=1$, we get $(\zeta_0+\zeta_1)=0.16$. A plot of the evolution of the scale factor is given in Fig. 2.10. Thus, for $0<(\zeta_0+\zeta_1)\leq 0.16$ the scale factor has earlier deceleration phase followed by an acceleration phase in later stage of the evolution. The transition from the decelerated to accelerated expansion depends on the viscosity coefficient ζ_0 and ζ_1 as shown above. For $(\zeta_0+\zeta_1)>0.16$, the transition takes place in past of the Universe and the scale factor increases with accelerated rate forever.

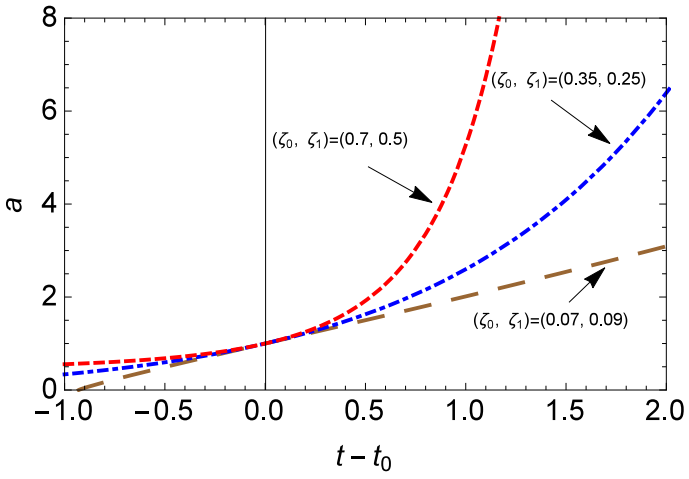

Figure 2.10: Plot of a versus $t-t_0$ for different values of ζ_0 and ζ_1 in the range $0<(\zeta_0+\zeta_1)\leq 0.16$ (the bottom curve) and $(\zeta_0+\zeta_1)>0.16$ (middle and top curves) with fixed $\omega_d=-0.5$, $H_0=1$ and $\alpha=0.34$ in VHRDE3 model.

The transition may also be discussed through the evolution of DP. In this case, we get

$$q=\frac{3\left\{(1-\zeta_1+2\alpha\omega_d)-\frac{\zeta_0}{H_0}\right\}}{2(1+\frac{3}{2}\alpha\omega_d)}e^{-\frac{3\zeta_0(t-t_0)}{2(1+\frac{3}{2}\alpha\omega_d)}}-1, \tag{2.3.37}$$

which is a time-dependent value of DP, which may describe the transition phase of the Universe. It can be observed that DP must change its sign at $t=t_0$. This time can be achieved if $3(\zeta_0+\zeta_1H_0)=\{1+3\alpha\omega_d\}H_0$. The sign of q is positive for $t<t_0$ and it is negative for $t>t_0$. The values of ζ_0 and ζ_1 can be obtained for a given values of ω_d and α which may be obtained from observation, or vice-versa.

From (2.3.30), the DP in terms of scale factor a is given by

$$q(a)=\frac{3(1-\zeta_1+2\alpha\omega_d)-3\zeta_0}{(2+3\alpha\omega_d)}\left[\frac{(1-\zeta_1+2\alpha\omega_d)}{\{a^{\frac{3(1-\zeta_1+2\alpha\omega_d)}{(2+3\alpha\omega_d)}}-1\}\zeta_0+(1-\zeta_1+2\alpha\omega_d)}\right]-1. \tag{2.3.38}$$

In terms of red shift z, the above equation becomes

$$q(z)=\frac{3(1-\zeta_1+2\alpha\omega_d)-3\zeta_0}{(2+3\alpha\omega_d)}\left[\frac{(1-\zeta_1+2\alpha\omega_d)}{\{(1+z)^{\frac{-3(1-\zeta_1+2\alpha\omega_d)}{(2+3\alpha\omega_d)}}-1\}\zeta_0+(1-\zeta_1+2\alpha\omega_d)}\right]-1. \tag{2.3.39}$$

The variation of q with a for varying ζ_0 and ζ_1 with constant α and others is shown in Fig. 2.11. We can observe the sign change from positive to negative in q. It is to be noted that for $(\zeta_0+\zeta_1)<0.16$, the transition takes place in late time and for $(\zeta_0+\zeta_1)>0.16$, the transition would occur in very early time. If we take higher values of (ζ_0,ζ_1), q is always negative, i.e, the model accelerates forever. It is to be noted that $q\to-1$ in late times for all cases.

We also plot q versus a in Fig. 2.12 for different model parameter α with fixed ζ_0, ζ_1 and others to observe the effect of α. In this case, we find that q changes its sign from positive to negative, i.e., there is transition from decelerated to accelerated phase. It is found that transition takes place in late time or early depending on the values of model parameter α.

When all the bulk viscous parameters and model parameter are zero, the DP $q=1/2$, which corresponds to a decelerating matter dominated Universe. However, when only $\zeta_0=0$ and $\zeta_1\neq0$, the value of q reduces to (2.3.25) of the case $\zeta=\zeta_1H$, and when $\zeta_0\neq0$ and $\zeta_1=0$, equation (2.3.38) reduces to (2.3.17) of the case $\zeta=\zeta_0$.

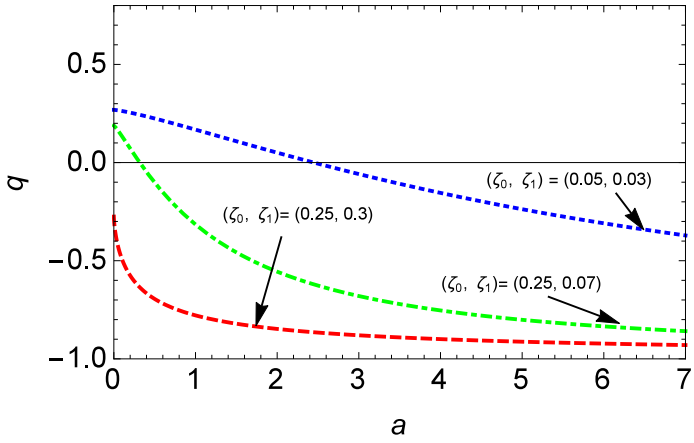

Figure 2.11: Behavior of the deceleration parameter q in terms of the scale factor a for different values of $\zeta_0 > 0$ and $\zeta_1 > 0$ with fixed $\omega_d = -0.5$ and $\alpha = 0.34$ in VHRDE3 model.

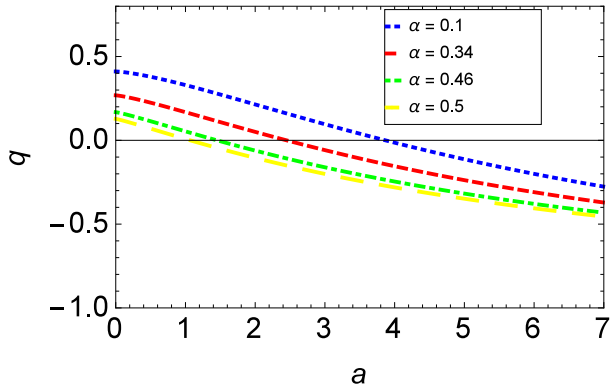

Figure 2.12: Behavior of the deceleration parameter q in terms of the scale factor a for different values of α with fixed $\omega_d = -0.5$, $\zeta_0 = 0.05$ and $\zeta_1 = 0.03$ in VHRDE3 model.

The present value of DP corresponding to $z = 0$ or $a = 1$ is given by

$$q_0 = q(a=1) = \frac{3(1-\zeta_1+2\alpha\omega_d)-3\zeta_0}{(2+3\alpha\omega_d)} - 1. \tag{2.3.40}$$

It is observed that if $3(\zeta_0+\zeta_1) = [1+3\alpha\omega_d]$, the deceleration parameter $q = 0$. This implies that the transition into the accelerating phase would occur at the present time. The current DP $q_0 < 0$ if $3(\zeta_0+\zeta_1) > [1+3\alpha\omega_d]$, implying that the present Universe is in the accelerating epoch and it entered this epoch at an early stage. But $q_0 > 0$ if $3(\zeta_0+\zeta_1) < [1+3\alpha\omega_d]$ implying that the present Universe is decelerating and it will be entering the accelerating phase at a future time. For the observational value $\alpha = 0.34$ with $\omega_d = -0.5$ and $H_0 = 1$, we get $(\zeta_0+\zeta_1) = 0.16$ which gives $q_0 = 0$. Thus for this value set, the transition into the accelerating phase would occur at present time. If $(\zeta_0+\zeta_1) > 0.16$, $q_0 < 0$, i.e., the Universe is in an accelerating phase and it entered

this epoch at an early stage. If $(\zeta_0+\zeta_1)<0.16$, $q_0>0$, i.e., the Universe is in decelerating epoch and it will enter into the accelerated phase in the future. From the above discussion, we say that both viscous coefficients and model parameters have their own role in the evolution of the Universe. Some values of the bulk viscous term give the accelerated phase from the beginning and continue to be accelerated in late time.

Statefinder analysis

The statefinder parameters $\{r,s\}$ can be obtained as

$$r=1+\frac{9\left(\frac{\zeta_0}{H_0}-(1-\zeta_1+2\alpha\omega_d)\right)\left(1-\frac{(1-\zeta_1+2\alpha\omega_d)}{(2+3\alpha\omega_d)}\right)}{(2+3\alpha\omega_d)}e^{\frac{-3\zeta_0(t-t_0)}{(2+3\alpha\omega_d)}}+\frac{9\left(\frac{\zeta_0}{H_0}-(1-\zeta_1+2\alpha\omega_d)\right)^2}{(2+3\alpha\omega_d)^2}e^{\frac{-6\zeta_0(t-t_0)}{(2+3\alpha\omega_d)}} \tag{2.3.41}$$

and

$$s=\frac{\frac{2\left(\frac{\zeta_0}{H_0}-(1-\zeta_1+2\alpha\omega_d)\right)\left(1-\frac{1-\zeta_1+2\alpha\omega_d}{(2+3\alpha\omega_d)}\right)}{(2+3\alpha\omega_d)e^{\frac{3\zeta_0(t-t_0)}{(2+3\alpha\omega_d)}}}+\frac{2\left(\frac{\zeta_0}{H_0}-(1-\zeta_1+2\alpha\omega_d)\right)^2}{(2+3\alpha\omega_d)^2e^{\frac{6\zeta_0(t-t_0)}{(2+3\alpha\omega_d)}}}}{\frac{2\left((1-\zeta_1+2\alpha\omega_d)-\frac{\zeta_0}{H_0}\right)}{(2+3\alpha\omega_d)e^{\frac{3\zeta_0(t-t_0)}{(2+3\alpha\omega_d)}}}-1}. \tag{2.3.42}$$

The above equations show that in the limit $(t-t_0)\to\infty$, the statefinder parameters $\{r,s\}\to\{1,0\}$, which corresponds to the ΛCDM model. Let us observe the effect of ζ_0 and ζ_1 in VHRDE3 model. Fig. 2.13 shows that $\{r,s\}$ trajectory is divided into two region, namely in $r<1$ and $s>0$ as we know this is the region of quintessence (Q) like model [250] and other region is on left side of vertical line which is $r>1$ and $s<0$, known as Chaplygin gas model (CG) [278]. The model behaves as Q-model for $0<(\zeta_0+\zeta_1)\leq 0.66$ and CG model for $(\zeta_0+\zeta_1)>0.66$. We have assumed $H_0=t_0=1$, $\alpha=0.34$ and $\omega_d=-0.5$. The arrows show the direction of the evolution of the model. The trajectory in both regions converge to ΛCDM model in late time of the evolution.

Fig. 2.14 plot the time evolution of $\{r,q\}$ for different combinations of (ζ_0,ζ_1) with $H_0=t_0=1$, $\alpha=0.34$ and $\omega_d=-0.5$ The fixed points $\{r,q\}$ =$\{1,0.5\}$ and $\{r,q\}$ =$\{1,-1\}$ represent the $SCDM$ and SS models, respectively. It can be seen that q changes its sign from positive to negative showing the transition from decelerated to accelerated phase. In this figure also, the region is divided into two parts, namely quintessence and phantom regions. The VHRDE3 model starts from both regions depending on the values of (ζ_0,ζ_1). But, it always converges to SS model as ΛCDM, Q and CG models

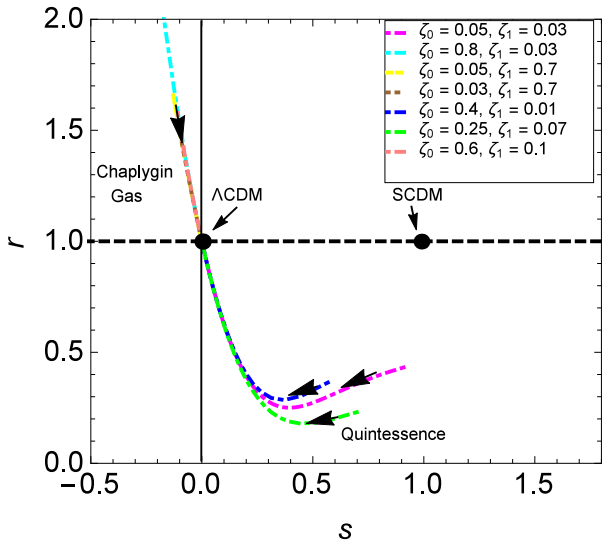

Figure 2.13: The $r-s$ trajectories for different values of $\zeta_0 > 0$ and $\zeta_1 > 0$ with fixed $\alpha = 0.34$, $\omega_d = -0.5$ in VHRDE3 model. The arrows represent the directions of the evolutions of $\{r,s\}$ with time.

converge in late time. Thus, the bulk viscosity is able to behave like Q and CG models for different combinations of ζ_0 and ζ_1. It also explain the phase transition of the Universe.

Let us see the effect of model parameter α with fixed bulk viscous coefficient and others. Fig. 2.15 and Fig. 2.16 represent the $r-s$ and $r-q$ trajectories for different values of α with fixed $\zeta_0 = 0.05$, $\zeta_1 = 0.03$ and $\omega_d = -0.5$. The evolutionary directions in both the figures are shown by arrows. Fig. 2.15 shows that the trajectory lies in the region $r < 1$ and $s > 0$ which behaves like the Q model. Some trajectory for α starts from the vicinity of $SCDM$ in early evolution. However, all the trajectories approach to ΛCDM in late time. The $r-q$ trajectory is shown in Fig. 2.16 for various values of α by fixing other parameters. The sign of q changes from positive to negative which shows the transition from decelerated to accelerated phase. In late time the VHRDE3 model approaches to SS model like ΛCDM and Q models. Thus, we observe that the VHRDE3 model is compatible with Q and CG models in early time with various viscous coefficients with fixed model parameter whereas the VHRDE3 model behaves like Q model in early time and SS model in late time.

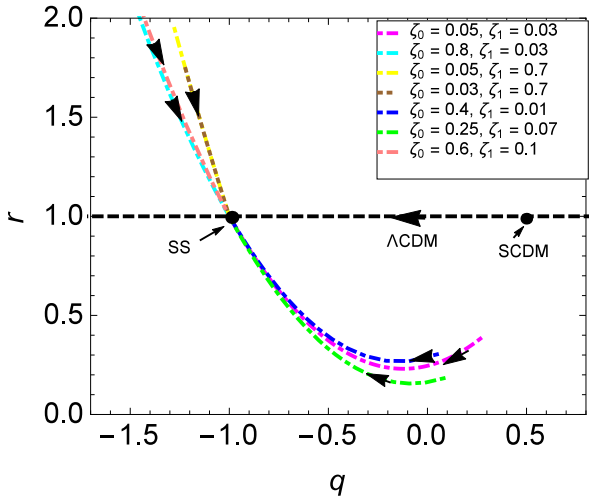

Figure 2.14: The $r-q$ trajectories for different values of $\zeta_0 > 0$ and $\zeta_1 > 0$ with fixed $\alpha = 0.34$, $\omega_d = -0.5$ in VHRDE3 model. The arrows represent the directions of the evolutions of $\{r, q\}$ with time.

***Om* Diagnostic**:

Using the value of the $H(z)$ from equation (2.3.31), we get

$$Om(z) = \frac{\left[\frac{\zeta_0}{H_0} + \{(1-\zeta_1+2\alpha\omega_d) - \frac{\zeta_0}{H_0}\}(1+z)^{\frac{3(1-\zeta_1+2\alpha\omega_d)}{2+3\alpha\omega_d}}\right]^2 - (1-\zeta_1+2\alpha\omega_d)^2}{(1-\zeta_1+2\alpha\omega_d)^2[(1+z)^3-1]}. \quad (2.3.43)$$

Fig. 2.17 shows the *Om(z)* trajectory for different values of pair (ζ_0, ζ_1) with fixed $\alpha = 0.34$, $\omega_d = -0.5$. For $0 < (\zeta_0 + \zeta_1) < 0.66$, the trajectory represents negative curvature, i.e., the VHRDE3 model behaves as quintessence like. The trajectory shows positive curvature, i.e., phantom like for $(\zeta_0 + \zeta_1) > 0.66$. As $z \to -1$, i.e., in late time we get *Om(z)* $= 1 - \frac{\zeta_0^2}{H_0^2(1-\zeta_1+2\alpha\omega_d)^2}$, which is constant value. This means that VHRDE3 model corresponds to ΛCDM for $z \to -1$.

In Fig. 2.18, we plot the $Om(z)$ trajectory for different values of α with fixed $(\zeta_0, \zeta_1) = (0.05, 0.03)$. It is observed that we get negative curvature for any values of model parameter α. Therefore, the model shows quintessence like behavior for varying parameter α. Hence we conclude that the bulk viscous RDE model behaves quintessence and phantom like depending on the quantities of viscous term for fixed α whereas it behaves quintessence like for varying model parameter by fixing viscous term. Therefore, both the factors effect the evolution of the Universe.

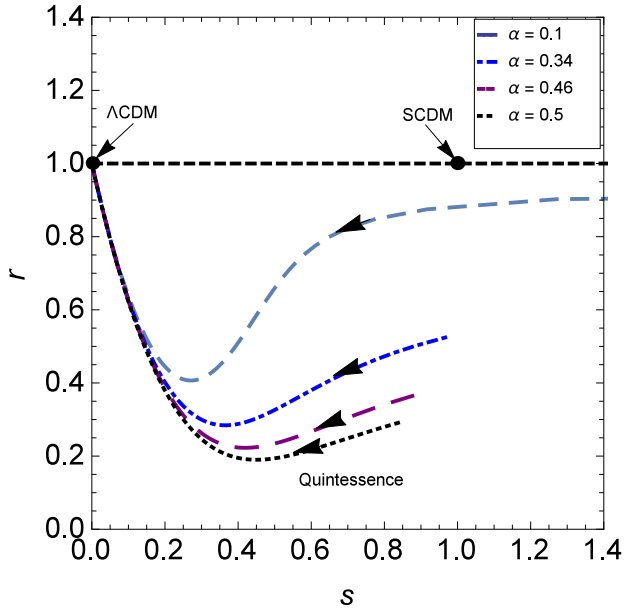

Figure 2.15: The $r-s$ trajectories in $r-s$ plane for different values of α with $\omega_d = -0.5$, $\zeta_0 = 0.05$ and $\zeta_1 = 0.03$ in VHRDE3 model. The arrows represent the direction of the evolution of statefinder diagnostic pair with time.

2.4 Conclusion

We have discussed the behaviors of some viscous HDRE models on the scale factor, deceleration parameter, the statefinder pair, and *Om* diagnostics for the purpose to mimic HRDE characters, with the hope to demonstrate that cosmic viscosity can also play the role as a possible candidate for DE. For this purpose, we have discussed non-viscous and viscous HRDE models. In what follows, we summarize the results obtained in both cases one by one.

In the non-viscous HRDE model, we have calculated the relevant cosmological parameters and discussed their evolutions. We have obtained the power-law form of scale factor and explained the evolution by putting the constraint on the physical parameters. This power-law form gives a constant deceleration parameter which does not describe the phase transition. The model decelerates or accelerates depending on the constraint of the model. The statefinder pair is also constant and it does not discriminate with ΛCDM or $SCDM$. There are no such values of parameters that would clearly show ΛCDM. It has been found that the model approaches $\{r,s\} \to \{1,0\}$ in the limit $\alpha \to \frac{-1}{2\omega_d}$, but this is nonphysical as the scale factor does not allow this value to exist.

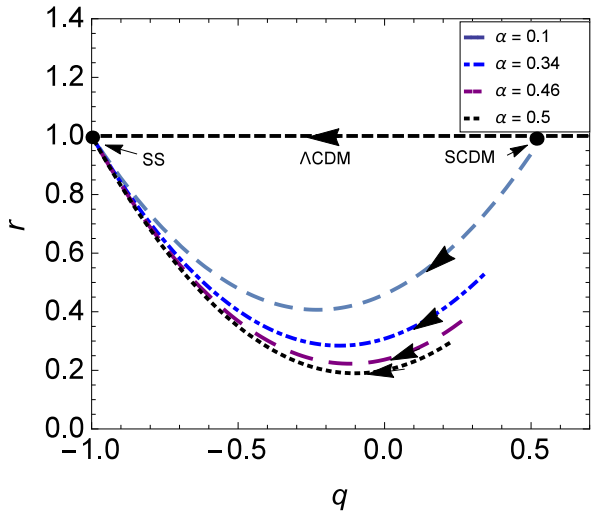

Figure 2.16: The $r-q$ trajectories in $r-q$ plane for different values of α with $\omega_d = -0.5$, $\zeta_0 = 0.05$ and $\zeta_1 = 0.03$ in VHRDE3 model. The arrows represent the direction of the evolution of the pair $\{r,q\}$ with time.

In section 2.3, we have explored the HRDE model with different forms of bulk viscosity, namely $\zeta = \zeta_0$, $\zeta = \zeta_1 H$ and $\zeta = \zeta_0 + \zeta_1 H$ to observe whether the bulk viscosity can accelerate the Universe and hence possible candidate of DE. Let us discuss these three cases with their physical significance.

In subsection 2.3.1, we have discussed the viscous HRDE model with a constant bulk viscous coefficient (VHRDE1 model). We have found the expression of the Hubble parameter in terms of the scale factor. The exact solution of scale factor in terms of cosmic time t is found which is in the exponential form. In the early time when $(t-t_0) \to 0$, the scale factor gives power-law form which shows that the model decelerates and as $(t-t_0) \to \infty$, it accelerates exponentially. This shows that the VHRDE1 model has an earlier deceleration phase followed by an accelerated phase in the late time of evolution. The time elapsed and age of the Universe since the Big-Bang have been calculated. We have also calculated the scale factor a_{tr} and corresponding redshift z_{tr}, where the transition takes place. We have observed that for $3\zeta_0 = (1+3\alpha\omega_d)$, the transition from decelerated phase to accelerated phase occurs at $a_{tr} = 1$ or $z_{tr} = 0$. We have calculated the range in which the VHRDE1 model shows different expansion history. For $0 < \zeta_0 \leq 0.16$, the scale factor expands initially with decelerated rate and then with an accelerated rate in late time. As $\zeta_0 > 0.16$, the scale factor accelerates too early and expands as de Sitter-like model as shown in Fig. 2.1. We have calculated the deceleration parameter in terms of t as well as in a, which is not constant.

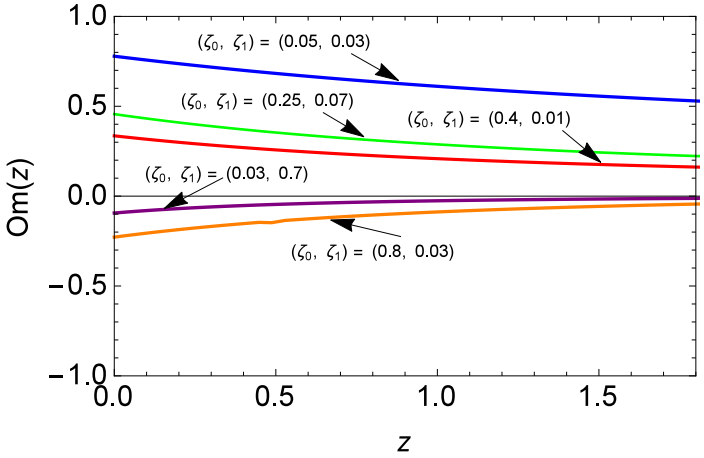

Figure 2.17: The evolution of $Om(z)$ versus the redshift z for different values of $\zeta_0 > 0$ and $\zeta_1 > 0$ with $\omega_d = -0.5$, $\alpha = 0.34$ in VHRDE3 model.

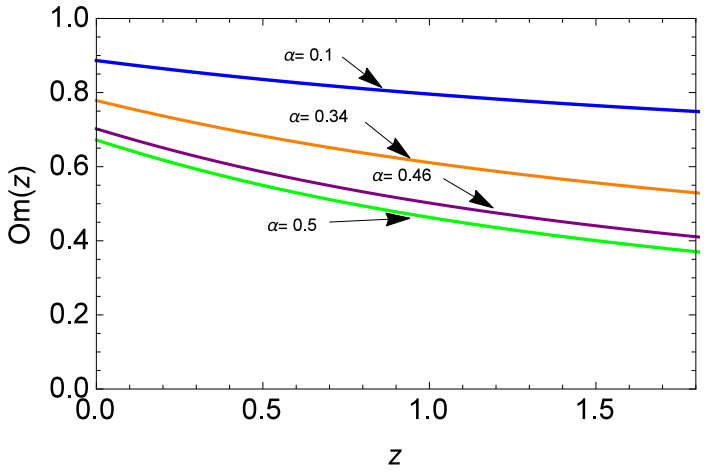

Figure 2.18: The evolution of $Om(z)$ versus the redshift z for different values of α with $\zeta_0 = 0.05, \zeta_1 = 0.03$ and $\omega_d = -0.5$ in VHRDE3 model.

This explains the phase transition of the Universe. We have found the present q_0 at $a_{tr} = 1$ from where the transition from deceleration to acceleration begins at present. We have plotted the evolution of q versus a in Fig. 2.2 for different values of ζ_0 with fixed α and in Fig. 2.3 for different values of α with fixed ζ_0. The sign of q changes from positive to negative depending on ζ_0 or α. This means that the VHRDE1 model shows a transition from decelerated to accelerated phase in some cases early or late depending on the values of ζ_0 or α.

To discriminate the VHRDE1 model with the existing DE models, we have considered two independent geometrical diagnostics, namely statefinder pair and *Om* analysis. Let us first discuss the result obtained in the statefinder pair. We have plotted the trajectories of $\{r,s\}$ and $\{r,q\}$ in $r-s$ and $r-q$ planes, respectively for different values of ζ_0 with fixed α as shown in Fig. 2.4 and Fig. 2.5. The present model re-

sembles to ΛCDM model as $(t-t_0)\to\infty$, the $\{r,s\}\to\{1,0\}$. The region of $r-s$ plane is divided in two regions as $r<1$, $s>0$ and $r>1$, $s<0$. The first region describes the quintessence region whereas the second region left to vertical line corresponds to the Chaplygin gas. We see that the evolution starts in both the region depending on the small or large values of ζ_0, but in late time it approaches ΛCDM. This VHRDE1 model also discriminates from viscous Ricci dark energy [107] where the value of s is constant. It also discriminates from the HDE model with event horizon as an infra-red cut-off. Fig. 2.5 shows that q changes its sign from positive to negative. The plane $r-q$ is divided into two regions, namely quintessence and phantom. The viscous HRDE with constant bulk viscous coefficient behaves quintessence-like and phantom-like in early time and resembles SS in late time. We have also discussed the $r-s$ and $r-q$ with different values of model parameter α with fixed ζ_0. In $r-s$ plane the evolution starts from quintessence region ($r<1$, $s>0$) during early time and approaches to $\{r,s\}=\{1,0\}$ in late time. In the $r-q$ plane, the trajectory evolves from the region of $SCDM$, some may start from the vicinity of $SCDM$ and approaches to SS model in late time as ΛCDM approaches to SS through $SCDM$.

We have studied *Om* diagnostic due to viscosity by plotting the trajectory in $Om-z$ plane in Fig. 2.8 for different values of ζ_0 with fixed $\alpha=0.34$. It is observed that for $0<\zeta_0<0.66$, the $Om(z)$ trajectory shows the negative slope which corresponds to that VHRDE1 model behaves as quintessence, and for $\zeta_0>0.66$, we observe the positive slope of $Om(z)$ which corresponds that VHRDE1 model behaves as the phantom. In Fig. 2.9, the trajectory of *Om* has been plotted for different values of model parameter α for fixed ζ_0. In this case, we have found only the negative curvature showing the behavior of quintessence.

In subsection 2.3.2, we have studied two case: $\zeta=\zeta_1 H$ (VHRDE2 model) and $\zeta=\zeta_0+\zeta_1 H$ (VHRDE3 model). In the case of the VHRDE2 model, we get a power-law form of expansion of the Universe similar to the non-viscous case in section 2.2. The DP is constant which does not show the transition of the Universe. The statefinder pair is also constant. In the case of the VHRDE3 model, we have obtained an exponential form of scale factor which shows that the Universe starts from a finite volume and expands exponentially. At the beginning as $(t-t_0)\to 0$, the scale factor expands with power-law form, i.e., with decelerated phase and in late time when $(t-t_0)\to\infty$, it expands like de Sitter, i.e., with accelerated rate. We have calculated the transition of scale factor and redshift and found the value of $(\zeta_0+\zeta_1 H)$ where the transition takes place at present time. An evolutionary graph of the scale factor is plotted in Fig.

2.10, which shows that for $0 < (\zeta_0 + \zeta_1) \leq 0.16$ the scale factor has an earlier deceleration phase followed by an acceleration phase in the later stage of the evolution. For $(\zeta_0 + \zeta_1) > 0.16$, the transition takes place in the past of the Universe and the scale factor increases with accelerated rate forever.

The transition has also been discussed by explaining DP in terms of t, a, and z. The DP is exponentially time-dependent which shows phase transition. An evolutionary graph of DP is plotted in $q - a$ plane in Fig. 2.11 for different values of (ζ_0, ζ_1) with fixed α, where it shows sign change from positive to negative. It is to be noted that for $(\zeta_0 + \zeta_1) < 0.16$, the transition takes place in late time and for $(\zeta_0 + \zeta_1) > 0.16$, the transition would occur in very early time. For $(\zeta_0 + \zeta_1) = 0.16$, the transition occurs at present time. If we take higher values of (ζ_0, ζ_1), q is always negative, i.e, the model accelerates forever. It is to be noted that $q \to -1$ in late time for all cases. We have also plotted q versus a in Fig. 2.12 for different values of α with fixed ζ_0 and ζ_1. It is found that transition takes place in late time or early depending on the values of model parameter α. We have also calculated the current value of q and discussed the transition phase in detail in subsection 2.3.2.

At last we have discussed the statefinder and *Om* diagnostics for VHRDE3 models when the viscous coefficient is in the form of $\zeta = \zeta_0 + \zeta_1 H$. To discriminate with other DE models we have plotted $r - s$ and $r - q$ trajectories in Fig. 2.13 and Fig. 2.14. As discussed in subsection 2.3.2, a detailed comparison has been carried out and found that the viscous HRDE model behaves quintessence like for small pair of (ζ_0, ζ_1) whereas it behaves Chaplygin gas like for large (ζ_0, ζ_1). The model resembles ΛCDM in late time from both models. Similarly, in $r - q$ plane, the trajectory starts from positive q and ends to SS model at a late time. Similar behavior can be observed from phantom side for large (ζ_0, ζ_1). We have also plotted $r - s$ and $r - q$ as shown in Fig. 2.15 and Fig. 2.16 for different values of α with fixed ζ_0 and ζ_1 to observe the effect of model parameter. The model starts from quintessence in early time and approaches to ΛCDM in late time. In $r - q$ plane, the sign of q changes from positive to negative which shows the transition from decelerated to accelerated phase. In late time the VHRDE3 model approaches to SS model like ΛCDM and Q models.

We have calculated the *Om(z)* for $\zeta = \zeta_0 + \zeta_1 H$ and analyzed the nature of *Om(z)*. The trajectory in Fig. 2.17 has positive or negative curvature showing quintessence or phantom-like depending on the choices of pair (ζ_0, ζ_1). However, if we vary α by fixing ζ_0 and ζ_1, we get only negative curvature and the model behaves like quintessence.

In concluding remarks, we can say that bulk viscosity affects the evolution of the Uni-

verse. The model shows the transition from decelerated phase to accelerated phase due to the presence of bulk viscous term. The viscous HRDE model is compatible with quintessence and Chaplygin gas-like model in early for small viscous values and approaches to ΛCDM in late time. This work is totally different from the work done by Feng for viscous Ricci dark energy [107] in which the parameter s of statefinder pair is constant but here we have obtained a curved trajectory. It also discriminates from the HDE model with event horizon [278]. In this model, the model parameter α also plays an important role in the evolution of the Universe and we have observed that the viscous HRDE model is compatible with quintessence like in early time and ΛCDM in late time. It is to be noted that this work gives good consistent results with bulk viscosity.

****

Chapter 3

Holographic Ricci Dark Energy with Bulk Viscosity in $f(R,T)$ Gravity

---

In this chapter [1]*, we extend the study of previous chapter in the modified* $f(R,T)$ *gravity theory within the framework of a flat FLRW model with bulk viscosity. The exact solution of the field equations is obtained by assuming constant and variable bulk viscous coefficients. Further, we assume the form of* $f(R,T) = R + \lambda T$*, where* λ *is a constant. We find the scale factor and deceleration parameter, and classify all possible evolution of the Universe. The behaviors concerning the cosmic expansion depend on the coupling parameter of* $f(R,T)$ *and bulk viscous term. The physical and geometrical significance of the models is studied in detail. We analyze the time evolution of the total entropy and generalized second law of thermodynamics of viscous HRDE model in* $f(R,T)$ *theory inside the apparent horizon.*

---

[1] Chapter 3 is based on **two** research papers entitled "Holographic Ricci dark energy with constant bulk viscosity in $f(R,T)$ gravity, *Gravitation and Cosmology* **25**, 58 (2019)" and "Viscous Ricci dark energy and generalized second law of thermodynamics in modified $f(R,T)$ gravity, *Modern Physics Letters A* **33**, 1850225 (2018)".

3.1 Introduction

In recent years, various modified gravity theories have been proposed: some of them are $f(R)$ theories in which the Ricci scalar R is replaced by a general function $f(R)$. This theory is consistent with the observations [139, 279]. Harko et al. [161] proposed a new modified theory known as $f(R,T)$ gravity theory, where R is the Ricci Scalar and T stands for the trace of the energy-momentum tensor. This modified theory presents a maximal coupling between geometry and matter. A brief introduction about modified $f(R,T)$ gravity theory has already been discussed in Sect.1.8.2 of Chapter 1. Many authors [171, 173, 176, 180, 180, 199, 280–282, 292–294] have studied modified $f(R,T)$ theory in different context to explain early and late time evolution of the Universe. Harko and Lobo [295] have reviewed a plethora of modified theories of gravity with generalized curvature-matter couplings. Chattopadhyay [125] has studied the HRDE model in modified $f(R,T)$ gravity theory. It is worth considering that the modified theories have the corresponding description in the fluid-like form, and the study of HRDE viscous fluids is one of the easiest ways to understand some general features of such a kind of alternative theory. Therefore, our aim is to study the HRDE model with bulk viscosity in modified $f(R,T)$ gravity theory to explain the accelerated expansion of the Universe.

Singh and Kumar [198] have studied a cosmological model with bulk viscosity in modified $f(R,T)$ gravity theory. Here, we have investigated the dynamics of the viscous HRDE model in modified $f(R,T)$ gravity. We have considered that the Universe is filled with pressureless dark matter and viscous HRDE. We have explored the effect of bulk viscosity in explaining the early and late time acceleration of the Universe by assuming the bulk viscous coefficient ζ to be of the form $\zeta = \zeta_0 + \zeta_1 H$, i.e., proportional to the velocity of the expansion of the Universe. The exact solution of the field equations has been obtained by assuming the simplest form of $f(R,T) = R + \lambda T$, where λ is a constant, with constant and variable bulk viscous coefficients. We have discussed the expansion history of the Universe for all possible scenarios depending upon the value of model parameter α and under the constraints on ζ. We have discussed the behavior of the deceleration parameter for various ranges of λ and constraints on ζ. We have discussed the presence of finite-time singularity, like Big-Rip. We have also obtained the statefinder pair and *Om* to discriminate our model with other existing DE models. We have also studied the validity of the generalized second law of ther-

modynamics for a viscous HRDE (VHRDE) in a Universe enveloped by the apparent horizon.

Chapter 3 has been organized as follows: In Section 3.2, we have presented the field equations of the VHRDE model in modified $f(R,T)$ gravity theory. Subsection 3.2.1 have presented the solution and physical and geometrical interpretation of the VHRDE model with the constant bulk viscous coefficient. In Subsection 3.2.2, we have discussed the VHRDE model with variable bulk viscous coefficient in $f(R,T)$ gravity. We have also discussed the evolution of the cosmological parameters in detail. The thermodynamical analysis of the model has also been studied. The main results of both models have been summarized in Section 3.3.

3.2 Viscous HRDE Model in $f(R,T)$ Gravity

Let us consider a homogeneous and isotropic flat FLRW metric defined in equation (2.2.1). We assume that the Universe is filled with pressureless DM (excluding baryonic matter) and viscous HRDE. The existence of viscous fluid leads to modify the perfect fluid energy-momentum tensor which is given by (2.3.1).

The field equations of modified $f(R,T)$ theory is given by

$$f_R(R,T)R_{\mu\nu}-\frac{1}{2}f(R,T)g_{\mu\nu}+(g_{\mu\nu}\Box-\nabla_\mu\nabla_\nu)f_R(R,T)=T_{\mu\nu}-f_T(R,T)(T_{\mu\nu}+\ominus_{\mu\nu}), \tag{3.2.1}$$

where $f_R=\frac{\partial f}{\partial R}$, $f_T=\frac{\partial f}{\partial T}$. Here $\Box\equiv\nabla^\mu\nabla_\mu$ is the d'Alembert operator and ∇_μ is the covariant derivative. The tensor $\ominus_{\mu\nu}$ is defined as $\ominus_{\mu\nu}=-2T_{\mu\nu}-pg_{\mu\nu}$.

Assuming the ansatz for the function $f(R,T)$ as $f(R,T)=R+f(T)$, where $f(T)$ is an arbitrary function of T. We assume the simple form of $f(T)=\lambda T$, where λ is an arbitrary constant [161]. Such a functional form for $f(R,T)$ has been broadly investigated and resulted in well-behaved cosmological models. Now, the field equations (3.2.1) reduce to

$$R_{\mu\nu}-\frac{1}{2}Rg_{\mu\nu}=T_{\mu\nu}+\lambda(T_{\mu\nu}+pg_{\mu\nu})+\frac{1}{2}\lambda Tg_{\mu\nu}. \tag{3.2.2}$$

When the effective pressure is considered in $f(R,T)$ theory, the matter Lagrangian is $\mathscr{L}_m=-\tilde{p_d}$ in place of $\mathscr{L}_m=-p$. The tensor $\ominus_{\mu\nu}$ modifies to $\ominus_{\mu\nu}=-2T_{\mu\nu}-\tilde{p_d}g_{\mu\nu}$, where the trace has now the form of $T=\rho_m+\rho_d-3\tilde{p_d}$, where $\tilde{p_d}=p_d-3\zeta H$.

Using line element (2.2.1) and energy-momentum tensor (2.3.1), the field equations

(3.2.2) yield

$$3H^2 = \rho_m + \rho_d + \lambda(\rho_m + \rho_d + p_d - 3H\zeta) + \frac{1}{2}\lambda T, \tag{3.2.3}$$

$$2\dot{H} + 3H^2 = -p_d + 3H\zeta + \frac{1}{2}\lambda T. \tag{3.2.4}$$

If an equation of state (EoS) connecting ρ_d and p_d is chosen in the form $p_d = \omega_d \rho_d$, where ω_d is the EoS parameter. From equations (3.2.3) and (3.2.4), we get a single evolution equation for H as

$$2\dot{H} + (1+\lambda)[\rho_m + (1+\omega_d)\rho_d] - 3(1+\lambda)\zeta H = 0. \tag{3.2.5}$$

Using the value of ρ_d given in (2.3.4) into (3.2.3), we get

$$\rho_m = \frac{3}{(2+3\lambda)}\Big[(\lambda\alpha\omega_d - 3\lambda\alpha - 2\alpha)\dot{H} + 2(1 - 2\alpha - 3\lambda\alpha + \lambda\alpha\omega_d)H^2 - \lambda\zeta H\Big]. \tag{3.2.6}$$

Using the values of ρ_m and ρ_d from equations (3.2.6) and (2.3.4), respectively into equation (3.2.5), we get

$$\dot{H} + l_1 l_2 H^2 - (1+2\lambda) l_1 \zeta H = 0, \tag{3.2.7}$$

where $l_1 = 3(1+\lambda)/[2+3\lambda+3\alpha(1+\lambda)(1+2\lambda)\omega_d]$ and $l_2 = 1 + 2\alpha\omega_d + 4\lambda\alpha\omega_d$.

Let us consider the bulk viscosity [192, 273, 277] in the form,

$$\zeta = \zeta_0 + \zeta_1 H, \tag{3.2.8}$$

where ζ_0 and ζ_1 are positive constants. We define the dimensionless bulk viscous parameters ξ_0, ξ_1 and total dimensionless viscous parameter ξ as,

$$\xi = \frac{\zeta}{H_0}, \quad \xi_0 = \frac{\zeta_0}{H_0}, \quad \xi_1 = \zeta_1, \tag{3.2.9}$$

where H_0 is the current value of Hubble parameter. Using the above transformation, we obtain the dimensionless form of bulk viscosity from (3.2.8),

$$\xi = \xi_0 + \xi_1 h, \tag{3.2.10}$$

where $h = \frac{H}{H_0}$ is the dimensionless Hubble parameter. Using the above dimensionless quantities, we obtain a dimensionless equation from (3.2.7) as

$$h' + l_1 l_2 h - (1+2\lambda) l_1 \xi = 0. \tag{3.2.11}$$

where $'$ denote the differentiation with respect to conformal time $ln\, a$. In the following subsections, we consider two different cases of ξ to solve equation (3.2.11).

3.2.1 HRDE Model with Constant Bulk Viscosity

In this section, we assume the bulk viscous coefficient as a constant, *i.e.*, $\xi = \xi_0 = constant$ (hereafter *VHRDE4 model*).

Solving (3.2.11) with $\xi = \xi_0$, we get

$$h(a) = \frac{(1+2\lambda) l_1 \xi_0}{l_1 l_2} + \left(1 - \frac{(1+2\lambda) l_1 \xi_0}{l_1 l_2}\right)\left(\frac{a}{a_0}\right)^{-l_1 l_2} \tag{3.2.12}$$

where $l_1 l_2 \neq 0$. On integration of equation (3.2.12), we get the scale factor,

$$a(t) = \left[1 + \frac{l_2}{(1+2\lambda)\xi_0}\left(e^{(1+2\lambda) l_1 \xi_0 H_0 (t-t_0)} - 1\right)\right]^{\frac{1}{l_1 l_2}}. \tag{3.2.13}$$

It is observed that the constant bulk viscous coefficient gives rise to exponential expansion. We can observe the phase transition in the evolution of the Universe. In early time, the scale factor can be approximated as

$$a(t) \to \left[1 + l_1 l_2 H_0 (t-t_0)\right]^{\frac{1}{l_1 l_2}}, \tag{3.2.14}$$

which is the power-law expression. In limiting conditions, as $(t - t_0) \to \infty$, the scale factor behaves as

$$a(t) \to exp\left[(1+2\lambda) l_1 \xi_0 H_0 (t-t_0)\right] \tag{3.2.15}$$

which corresponds to acceleration similar to the de Sitter phase, implies that the bulk viscous dark energy behaves similar to the cosmological constant model. This shows that the Universe has an earlier deceleration phase followed by an acceleration phase in the later stage of the evolution.

Fig. 3.1 shows the behavior of scale factor with $H_0(t - t_0)$ for the values of model parameter $\alpha = 0.34$ [117], $\omega_d = -0.5$ and $\lambda = 0.06$. We can also assume the negative

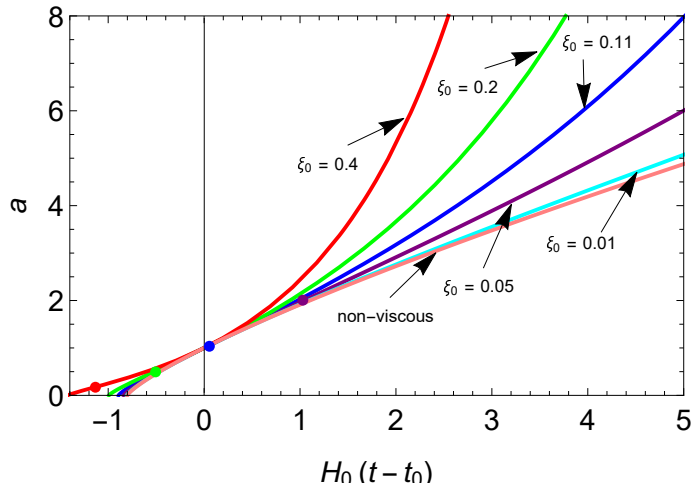

Figure 3.1: The scale factor evolution with respect to $H_0(t-t_0)$ for $\alpha = 0.34$, $\omega_d = -0.5$ and $\lambda = 0.06$ in VHRDE4 model. The dots on each curve denotes the transition time.

value of λ, but the evolution of the scale factor would be similar. The value of the scale factor at which the transition from the decelerated to the accelerated expansion occur, is depend on the bulk viscosity coefficient ξ_0.

The Hubble parameter in terms of cosmic time t can be obtained as

$$H(t) = \frac{H_0 e^{(1+2\lambda)l_1\xi_0 H_0(t-t_0)}}{\left[1+\frac{l_2}{(1+2\lambda)\xi_0}\left\{e^{(1+2\lambda)l_1\xi_0 H_0(t-t_0)}-1\right\}\right]}, \tag{3.2.16}$$

Taking derivative of $\dot{a}$ in (3.2.12) with respect to a, to get

$$\frac{d\dot{a}}{da} = H_0\left[\frac{(1+2\lambda)\xi_0}{l_2} + \left(1-\frac{(1+2\lambda)\xi_0}{l_2}\right)(1-l_1l_2)a^{-l_1l_2}\right] \tag{3.2.17}$$

Equating (3.2.17) to zero, we can obtain the transition scale factor a_{tr}, which is given by

$$a_{tr} = \left[\frac{(1+2\lambda)l_1\xi_0}{(l_1l_2-1)[l_1l_2-(1+2\lambda)l_1\xi_0]}\right]^{-\frac{1}{l_1l_2}}, \tag{3.2.18}$$

Using the relation $a = (1+z)^{-1}$, where z is the redshift, we can obtain the corresponding transition redshift z_{tr} as

$$z_{tr} = \left[\frac{(1+2\lambda)l_1\xi_0}{(l_1l_2-1)[l_1l_2-(1+2\lambda)l_1\xi_0]}\right]^{\frac{1}{l_1l_2}} - 1 \tag{3.2.19}$$

From (3.2.18) and (3.2.19), we observe that for $\xi_0 = \frac{1+3(1+\lambda)(1+2\lambda)\alpha\omega_d}{3(1+\lambda)(1+2\lambda)}$, the transition from decelerated phase to accelerated phase occurs at $a_{tr} = 1$ or $z_{tr} = 0$, which corresponds to the present time of the Universe. Especially, substituting the observational values of model parameter $\alpha = 0.34$ along with $\omega_d = -0.5$, we get the present value

of $\xi_0 = 0.11$ for $\lambda = 0.06$ and $\xi_0 = 0.233$ for $\lambda = -0.06$. For $\xi_0 = 0.11$, the transition takes place at present time and for $\xi_0 > 0.11$, it occurs at early time. For $\xi_0 < 0.11$, the scale factor has a deceleration phase followed by an accelerated phase in late time as shown in Fig. 3.1. The first trajectory of a is for non-viscous HRDE model, i.e., $\xi_0 = 0$.

Now, the second order derivative of (3.2.13) with respect to t can be obtain as

$$\frac{d^2a}{dt^2} = H_0^2 e^{(1+2\lambda)l_1\xi_0 H_0(t-t_0)}\left[e^{(1+2\lambda)l_1\xi_0 H_0(t-t_0)} - l_1 l_2 + (1+2\lambda)l_1\xi_0\right] \times \left[1 + \frac{l_2}{(1+2\lambda)\xi_0}\left(e^{(1+2\lambda)l_1\xi_0 H_0(t-t_0)} - 1\right)\right]^{\frac{1}{l_1 l_2}-2}, \tag{3.2.20}$$

Equating (3.2.20) to zero to get the transition cosmic time, t_{tr} from decelerated to accelerated epochs, which is equals to

$$t_{tr} = t_0 + \frac{1}{(1+2\lambda)l_1\xi_0 H_0}\ \ln\left\{l_1 l_2 - (1+2\lambda)l_1\xi_0\right\}. \tag{3.2.21}$$

In the absence of bulk viscosity, i.e., $\xi = 0$, one can obtain the scale factor from (3.2.7) as

$$a(t) = \left[1 + l_1\, l_2\, H_0\, (t-t_0)\right]^{\frac{1}{l_1 l_2}}. \tag{3.2.22}$$

We observe that the scale factor evolves according to power-law form, i.e., $a(t) \propto t^m$ with $m = [2+3\lambda+3\alpha(1+\lambda)(1+2\lambda)\omega_d]/3(1+\lambda)(1+2\alpha\omega_d+4\lambda\alpha\omega_d)$. The Universe decelerates for $m < 1$, i.e., $1+3\alpha(1+\lambda)(1+2\lambda)\omega_d > 0$ and accelerates for $m > 1$, i.e., $1+3\alpha(1+\lambda)(1+2\lambda)\omega_d < 0$. The Universe shows the marginal inflation for $m = 1$, i.e., $1+3\alpha(1+\lambda)(1+2\lambda)\omega_d = 0$. Equation (3.2.22) shows that when $\alpha = 0$, i.e., in the absence of HRDE, the scale factor reduces to $a(t) = \left[1 + \frac{3(1+\lambda)H_0}{(2+3\lambda)}(t-t_0)\right]^{\frac{(2+3\lambda)}{3(1+\lambda)}}$. In the absence of parameter λ, we obtain the case of matter-dominated phase in general relativity as the scale factor becomes $a(t) = \left[1 + \frac{3H_0}{2}(t-t_0)\right]^{\frac{2}{3}}$.

Deceleration parameter

The decelerated or accelerated expansion of the Universe is characterized by the deceleration parameter (DP) q, which is calculated as

$$q(t) = -1 + \left\{l_1 l_2 - (1+2\lambda)l_1\xi_0\right\}e^{-(1+2\lambda)l_1\xi_0 H_0(t-t_0)}. \tag{3.2.23}$$

Table 3.1: Variation of q for $\omega_d = -0.5$, $\alpha = 0.34$

λ	Constraints on ξ_0	q	Evolution of the Universe
$\lambda > 2.1277$	For all $\xi_0 > 0$	Positive	Decelerated expansion
$0.272 \leq \lambda \leq 2.1277$	For all $\xi_0 > 0$	Negative	Accelerated expansion
$-0.5 < \lambda < 0.272$	$0 < \xi_0 < \frac{1-0.51(1+\lambda)(1+2\lambda)}{3(1+\lambda)(1+2\lambda)}$	$+$ve to $-$ve	Transition from dec. to acc.
	$\xi_0 \geq \frac{1-0.51(1+\lambda)(1+2\lambda)}{3(1+\lambda)(1+2\lambda)}$	Negative	Accelerated expansion
$-0.6865 \leq \lambda \leq -0.5$	For all $\xi_0 > 0$	Positive	Decelerated expansion
$-1 \leq \lambda < -0.6865$	For all $\xi_0 > 0$	Negative	Accelerated expansion
$-1.7712 \leq \lambda < -1$	$0 < \xi_0 < \frac{1-0.51(1+\lambda)(1+2\lambda)}{3(1+\lambda)(1+2\lambda)}$	$-$ve to $+$ve	Transition from acc. to dec.
	$\xi_0 \geq \frac{1-0.51(1+\lambda)(1+2\lambda)}{3(1+\lambda)(1+2\lambda)}$	Positive	Decelerated expansion
$\lambda < -1.7712$	For all $\xi_0 > 0$	Positive	Decelerated expansion

The above equation shows that the deceleration parameter is time-dependent, which may describe the phase transition of the Universe. In the non-viscous HDRE model, we get $q = (l_1\ l_2 - 1)$, which is constant throughout the evolution of the Universe. When all parameters are zero, we obtains the matter-dominated Universe with null bulk viscosity. As $(t - t_0) \to \infty$, we find that $q \to -1$. The model shows late time acceleration.

In terms of the scale factor, Eq. (3.2.23) can be written as

$$q(a) = -1 + \frac{[l_1 l_2 - (1+2\lambda) l_1 \xi_0]}{\left[1 + \frac{(1+2\lambda)\xi_0}{l_2}(a^{l_1 l_2} - 1)\right]}, \tag{3.2.24}$$

whereas, in terms of redshift z, it can be obtained as

$$q(z) = -1 + \frac{[l_1 l_2 - (1+2\lambda) l_1 \xi_0]}{\left[1 + \frac{(1+2\lambda)\xi_0}{l_2}((1+z)^{-l_1 l_2} - 1)\right]}. \tag{3.2.25}$$

For $z = 0$ or $a = 1$, we get the present value of q as

$$q_0 = -1 + [l_1 l_2 - (1+2\lambda) l_1 \xi_0]. \tag{3.2.26}$$

Tables 3.1–3.3 summarize the behavior of q for $\omega_d = -0.5$, $\omega_d = -1$ and $\omega_d = -1.215$ with $\alpha = 0.34$, respectively. The behavior of q and evolution have been observed for different ranges of λ, which put the constraints on ξ_0. We observe that the Universe accelerates, decelerates and shows phase transition for various ranges of λ and a suitable constraints on ξ_0.

Table 3.2: Variation of q for $\omega_d = -1$, $\alpha = 0.34$

λ	Constraints on ξ_0	q	Evolution of the Universe
$\lambda > 0.6785$	For all $\xi_0 > 0$	Positive	Decelerated expansion
$0 \leq \lambda \leq 0.6785$	For all $\xi_0 > 0$	Negative	Accelerated expansion
$-0.5 < \lambda < 0$	$0 < \xi_0 < \frac{1-1.02(1+\lambda)(1+2\lambda)}{3(1+\lambda)(1+2\lambda)}$	$+$ve to $-$ve	Transition from dec. to acc.
	$\xi_0 \geq \frac{1-1.02(1+\lambda)(1+2\lambda)}{3(1+\lambda)(1+2\lambda)}$	Negative	Accelerated expansion
$-0.708 \leq \lambda \leq -0.5$	For all $\xi_0 > 0$	Positive	Decelerated expansion
$-1 \leq \lambda < -0.708$	For all $\xi_0 > 0$	Negative	Accelerated expansion
$-1.493 \leq \lambda < -1$	$0 < \xi_0 < \frac{1-1.02(1+\lambda)(1+2\lambda)}{3(1+\lambda)(1+2\lambda)}$	$-$ve to $+$ve	Transition from acc. to dec.
	$\xi_0 \geq \frac{1-1.1055(1+\lambda)(1+2\lambda)}{3(1+\lambda)(1+2\lambda)}$	Positive	Decelerated expansion
$\lambda < -1.493$	For all $\xi_0 > 0$	Positive	Decelerated expansion

Table 3.3: Variation of q for $\omega_d = -1.215$, $\alpha = 0.34$

λ	Constraints on ξ_0	q	Evolution of the Universe
$\lambda \geq 0.4280$	For all $\xi_0 > 0$	Positive	Decelerated expansion
$-0.067 \leq \lambda < 0.4280$	For all $\xi_0 > 0$	Negative	Accelerated expansion
$-0.5 < \lambda < -0.067$	$0 < \xi_0 < \frac{1-1.239(1+\lambda)(1+2\lambda)}{3(1+\lambda)(1+2\lambda)}$	$+$ve to $-$ve	Transition from dec. to acc.
	$\xi_0 \geq \frac{1-1.239(1+\lambda)(1+2\lambda)}{3(1+\lambda)(1+2\lambda)}$	Negative	Accelerated expansion
$-0.7174 \leq \lambda \leq -0.5$	For all $\xi_0 > 0$	Positive	Decelerated expansion
$-1 \leq \lambda < -0.7174$	For all $\xi_0 > 0$	Negative	Accelerated expansion
$-1.4326 \leq \lambda < -1$	$0 < \xi_0 < \frac{1-1.239(1+\lambda)(1+2\lambda)}{3(1+\lambda)(1+2\lambda)}$	$-$ve to $+$ve	Transition from acc. to dec.
	$\xi_0 \geq \frac{1-1.239(1+\lambda)(1+2\lambda)}{3(1+\lambda)(1+2\lambda)}$	Positive	Decelerated expansion
$\lambda < -1.4326$	For all $\xi_0 > 0$	Positive	Decelerated expansion

Statefinder diagnostic

Let us investigate the statefinder diagnostic for viscous HRDE model. In this case, we get

$$r = 1 + \frac{(l_1 l_2 - 3)(l_1 l_2 - (1+2\lambda) l_1 \xi_0)}{e^{(1+2\lambda) l_1 \xi_0 H_0 (t-t_0)}} + \frac{(l_1 l_2 - (1+2\lambda) l_1 \xi_0)^2}{e^{2(1+2\lambda) l_1 \xi_0 H_0 (t-t_0)}} \tag{3.2.27}$$

and

$$s = \frac{(l_1 l_2 - (1+2\lambda) l_1 \xi_0) \left[2(l_1 l_2 - 3) + \frac{2(l_1 l_2 - (1+2\lambda) l_1 \xi_0)}{e^{(1+2\lambda) l_1 \xi_0 H_0 (t-t_0)}} \right]}{6(l_1 l_2 - (1+2\lambda) l_1 \xi_0) - 9 e^{(1+2\lambda) l_1 \xi_0 H_0 (t-t_0)}} \tag{3.2.28}$$

We get the time-dependent values of the statefinder pair for the viscous model. To discriminate from other dark energy models, let us plot the $r-s$ and $r-q$ trajectories as shown in Figs. 3.2, 3.3, 3.4 and 3.5 respectively for different values of ξ_0 and fixed

positive and negative values of λ. We assume $\alpha = 0.34$ and $\omega_d = -0.5$ in both cases. In Figs. 3.2 and 3.3, the $r-s$ trajectories are divided into two regions through a vertical line. The region $r > 1$, $s < 0$ in $r-s$ plane shows the behavior similar to Chaplygin gas (CG) [278], whereas the region $r < 1$, $s > 0$ shows the behavior similar to quintessence model $(Q-model)$ [250, 251].

In Fig. 3.2, the $r-s$ trajectory for $\lambda = 0.06$ shows CG like behavior for larger values of ξ_0, i.e., for $\xi_0 > 0.55$, while it shows $Q-model$ like behavior for the smaller values of ξ_0, i.e., for $0 < \xi_0 \leq 0.55$. In both the cases, our model approaches to ΛCDM in late time.

In Fig. 3.3 where $\lambda = -0.06$, the $r-s$ trajectory shows the behavior of $Q-model$ in early time for $0 < \xi_0 \leq 0.79$ and approaches to ΛCDM in late time. However, the model shows behavior of CG in early time for $\xi_0 > 0.79$ and approaches to ΛCDM in late time.

The trajectory in both regions are coinciding for all different values of ξ_0 irrespective of choice of λ, whether positive or negative. The current values of $\{r,s\}$ of viscous HRDE become closer to the ΛCDM model for some values of ξ_0.

As a complementary, we plot the evolution trajectory in $r-q$ plane. In Figs. 3.4 and 3.5, the $r-q$ trajectories are divided into two regions through a point $(r,q) = (1,-1)$. The region $r > 1$, $q < -1$ in $r-q$ plane shows the behavior similar to phantom model, whereas the region $r < 1$, $q > -1$ shows the behavior similar to quintessence model $(Q-model)$.

Figs. 3.4 and 3.5 show the trajectories of evolution behavior of our model in $r-q$ plane. The trajectories are plotted for $\lambda = 0.06$ and $\lambda = -0.06$, respectively, for different values of ξ_0. In both the figures the stars represents respectively the fixed points $\{r,q\} = \{1, 0.5\}$ and $\{r,q\} = \{1,-1\}$ of $SCDM$ and Steady State (SS) models. It can be observed that there is a sign change of q from positive to negative in $Q-region$ for small values of ξ_0, i.e. $0 < \xi_0 \leq 0.55$ when we take $\lambda = 0.06$, and $0 < \xi_0 \leq 0.79$ when $\lambda = -0.06$. This shows that the viscous HRDE model transits from decelerated to accelerated phase. The q has always negative value starting from $q < -1$ and tends to $q = -1$ in late time for large values of ξ_0, i.e., $\xi_0 > 0.55$ and $\xi_0 > 0.79$ for positive and negative values of λ, respectively.

It can also be observed from Figs. 3.4 and 3.5 that our model always converges from both regions to SS model in late-time evolution as ΛCDM model starting from $SCDM$ and tends to SS model. In Fig 3.5, it is observed that some trajectories start from the vicinity of $SCDM$ and approach to SS model.

The present viscous HRDE model can be discriminated from the holographic dark

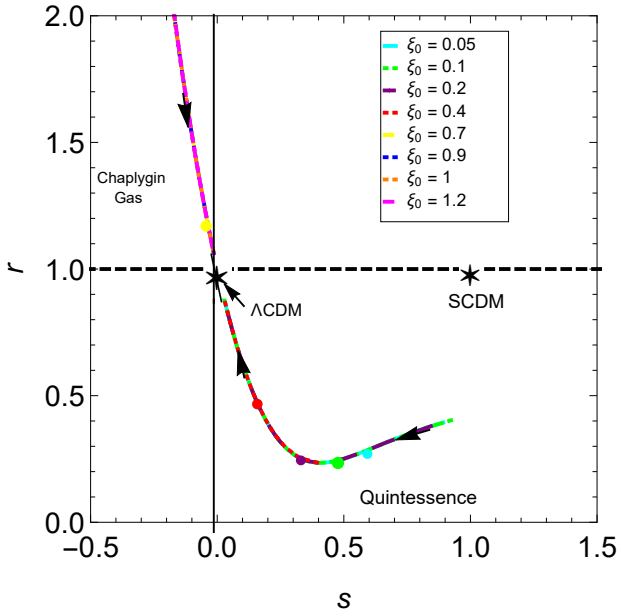

Figure 3.2: Evolution trajectories in the statefinder $r-s$ plane for different values of ξ_0 with $\omega_d = -0.5$, $\alpha = 0.34$ and $\lambda = 0.06$. The arrows represent the directions of the evolution of statefinder diagnostic pair with time. The color dots are the location of respective current point of (r,s). The star is the ΛCDM and $SCDM$ fixed point.

energy model with event horizon as the infrared cutoff, in which the $r-s$ evolution starts from a region $r \sim 1$, $s \sim 2/3$ and ends on the ΛCDM point [296]. It can also be discriminated from Ricci dark energy model [107], in which (r,s) trajectory is a vertical segment, i.e., s is a constant during the evolution of the Universe.

For the non-viscous HRDE model, $\{r,s\}$ can be calculated as

$$r = 1 - 3\,l_1\,l_2 + 2(l_1\,l_2)^2, \qquad s = 2\,l_1\,l_2/3. \tag{3.2.29}$$

We observe that the pair $\{r,s\}$ is constant and it depends on λ, α and ω_d. We find that the fixed point of $SCDM$, i.e., $\{r,s\} = \{1,1\}$ is obtained for $\alpha = \frac{\lambda}{(1+\lambda)(1+2\lambda)\omega_d}$. The non-viscous HRDE model does not show the behavior of ΛCDM model, i.e., $\{r,s\} = \{1,0\}$.

Om(z) diagnostic

In addition to statefinder $\{r,s\}$, another diagnostic method, *Om(z)*, is obtained using (3.2.16) into (1.12.3) as

$$Om(z) = \frac{\left[\frac{(1+2\lambda)\xi_0}{l_2} + \left(1 - \frac{(1+2\lambda)\xi_0}{l_2}\right)(1+z)^{l_1 l_2}\right]^2 - 1}{(1+z)^3 - 1} \tag{3.2.30}$$

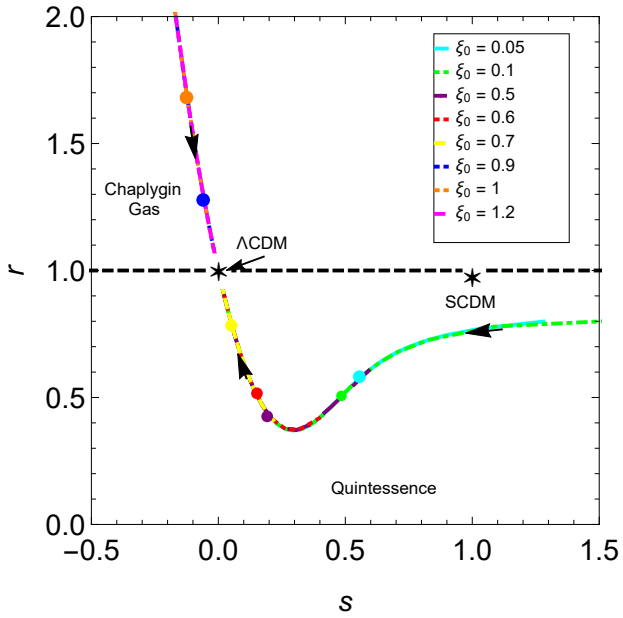

Figure 3.3: Evolution trajectories in the statefinder $r-s$ plane for different values of ξ_0 with $\omega_d = -0.5$, $\alpha = 0.34$ and $\lambda = -0.06$. The arrows represent the directions of the evolution of statefinder diagnostic pair with time. The color dots are the location of the respective current point of (r,s). The star is the ΛCDM and $SCDM$ fixed point.

We plot the evolution of *Om(z)* in Figs. 3.6 and 3.7 to analyze the evolution due to viscosity effect for different values of ξ_0 and fixed positive and negative values of λ with model parameter $\alpha = 0.34$ and $\omega_d = -0.5$. In Fig. 3.6, for $0 < \xi_0 < 0.55$, the negative slope of *Om(z)* trajectories show quintessence like, whereas, for $\xi_0 > 0.55$, the positive slope of the *Om* trajectory is observed, i.e., in this range the model behaves as phantom like.

In Fig. 3.7, we plot the *Om(z)* trajectories for the negative value of λ (e.g., $\lambda = -0.06$). In this case, we observed that the negative curvature for $0 < \xi_0 < 0.8$ and the positive curvature for $\xi_0 > 0.8$. In the late time of evolution when $z = -1$, we get $Om(z) = 1 - \frac{(1+2\lambda)^2\xi_0^2}{(1+2\alpha\omega_d+4\lambda\alpha\omega_d)^2}$, which is the constant value of *Om(z)*, i.e., zero curvature. Thus, for $z = -1$ the DE corresponds to ΛCDM.

Thermodynamics and local entropy

The EMT of a relativistic fluid with bulk viscosity as the only dissipative phenomena is given by Eq. (2.3.1). The energy non-conservation equation (1.8.17) in the presence of bulk viscous dissipative processes in $f(R,T)$ gravity gives

$$\dot{\rho} + 3(\rho + \tilde{p_d})H = -\frac{f_T(R,T)}{1 + f_T(R,T)}\left[(\rho + \tilde{p_d})\nabla_\mu \ln f_T(R,T) + \nabla_\nu \frac{\rho - \tilde{p_d}}{2}\right], \qquad (3.2.31)$$

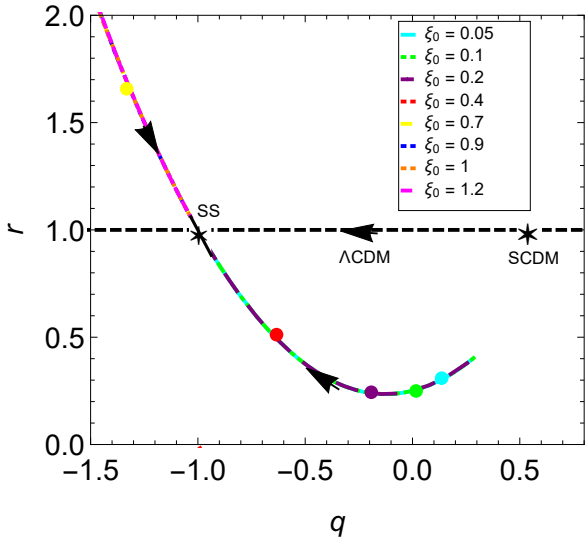

Figure 3.4: Evolution of trajectories in $r-q$ plane for different values of ξ_0 with $\omega_d = -0.5$, $\alpha = 0.34$ and $\lambda = 0.06$. The black dashed line denotes the ΛCDM model. The arrows represent the directions of the evolution of $\{r,q\}$ with time. The current points are represented by color dots for each respective values of ξ_0.

where $\rho = \rho_m + \rho_d$ and $\tilde{p_d} = p_d - 3\zeta H$. Using the assumption $f(R,T) = R + \lambda T$, Eq. (3.2.31) gives

$$\dot{\rho} + 3(\rho + \tilde{p_d})H = -(\rho + \tilde{p_d})\left[\frac{\lambda}{2(1+\lambda)}\frac{(\dot{\rho} - \dot{\tilde{p_d}})}{(\rho + \tilde{p_d})}\right]. \tag{3.2.32}$$

From the above equation, we find that the particle creation is equivalent to the effective bulk viscous pressure in the energy-momentum tensor. Hence, the bulk viscous pressure acts as a particle creation pressure. However, in an open thermodynamic system, these two terms are different which is associated with the entropy production rate. Let us now focus on thermodynamics, and especially on the production of entropy. In the FLRW line element, the law of generation of the entropy production is given by [2, 297]

$$\mathbb{T}\nabla_\nu s^\nu = \zeta(\nabla_\nu u^\nu)^2 = 9H^2\zeta, \tag{3.2.33}$$

where $\mathbb{T}$ is the temperature and $\nabla_\nu s^\nu$ is the rate at which entropy is being generated in unit volume. In the viscous processes, thermodynamic interpretation $\nabla_\nu s^\nu$ is quadratic in creation pressure, i.e., $\nabla_\nu s^\nu \propto p_c^2/\zeta\mathbb{T}$. The second law of thermodynamics can be written as

$$\mathbb{T}\nabla_\nu s^\nu \geq 0, \tag{3.2.34}$$

which implies from (3.2.33) that $9H^2\zeta \geq 0$. Since the Hubble parameter H is positive in an expanding Universe, then $\zeta = \zeta_0$ has to be positive in order to preserve the validity

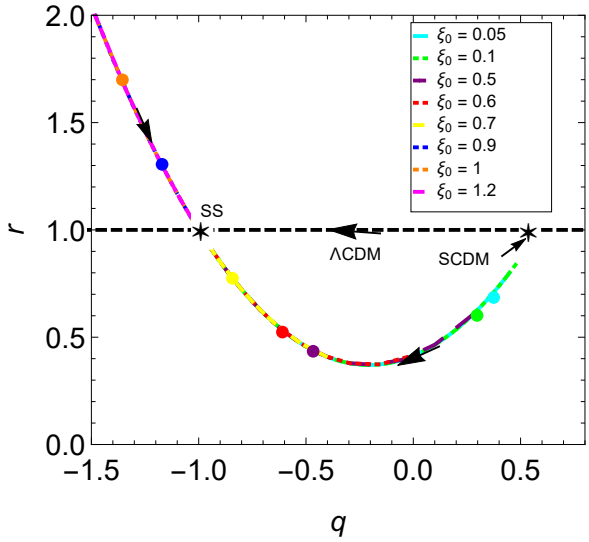

Figure 3.5: Evolution of trajectories in $r-q$ plane for different values of ξ_0 with $\omega_d = -0.5$, $\alpha = 0.34$ and $\lambda = -0.06$. The black dashed line denotes the ΛCDM model. The arrows represent the directions of the evolution of $\{r,q\}$ with time. The current points are represented by color dots for each respective values of ξ_0.

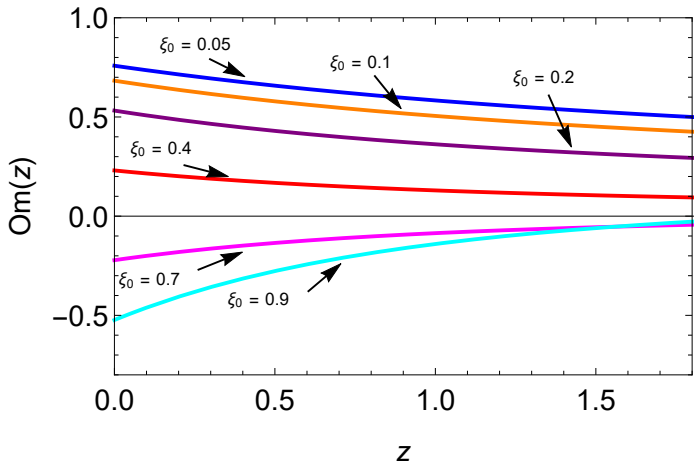

Figure 3.6: The *Om(z)* trajectories are plotted for different values of ξ_0 with $\omega_d = -0.5$, $\alpha = 0.34$ and $\lambda = 0.06$.

of the second law of thermodynamics. Thus, equation (3.2.34) implies that

$$\zeta = \zeta_0 \geq 0. \tag{3.2.35}$$

Therefore, ζ_0 always remains positive throughout the evolution of the Universe as $\zeta_0 > 0$ and hence satisfying the local second law of thermodynamics.

In non-viscous case, we obtain the particle creation rate from (1.8.19) as

$$\Gamma = \frac{\Gamma_0}{[1+l_1\, l_2\, H_0(t-t_0)]}, \tag{3.2.36}$$

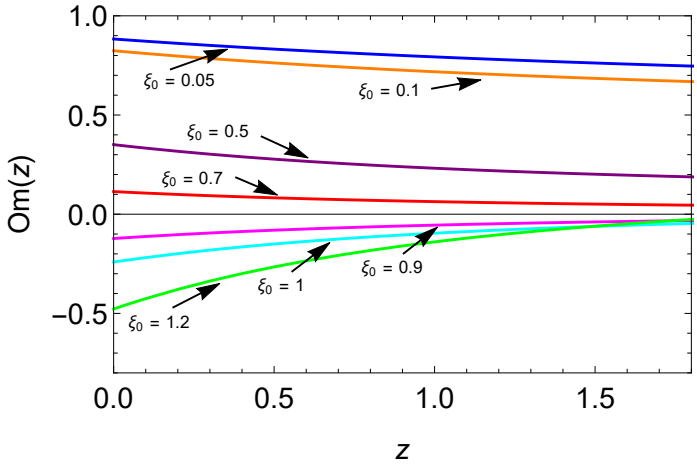

Figure 3.7: The *Om(z)* trajectories are plotted for different values of ξ_0 with $\omega_d = -0.5$, $\alpha = 0.34$ and $\lambda = -0.06$.

where $\Gamma_0 = \frac{l_1\lambda[1+(l_1-2)(1+\lambda)\alpha\omega_d+2l_1\alpha^2\omega_d^2(1+\lambda)(1+2\lambda)]H_0}{(1+\lambda)(1-l_1\alpha\omega_d-2l_1\lambda\alpha\omega_d)}$. From the second law of thermodynamics, the time variation of the entropy is given by [176]

$$\mathbb{S}(t) = S_0 \exp\left[\int_0^t \Gamma(t')dt'\right], \tag{3.2.37}$$

where S_0 is an arbitrary constant of integration. Using (3.2.36) into (3.2.37), we get

$$\mathbb{S}(t) = S_0[1 + l_1\, l_2\, H_0(t-t_0)]^{\frac{\Gamma_0}{l_1\, l_2\, H_0}}, \tag{3.2.38}$$

which shows that the entropy varies as power function of t. The entropy production rate is given by [176]

$$\mathbb{T}\nabla_\mu \mathbb{S}^\mu = (\rho + p)\,\Gamma. \tag{3.2.39}$$

Since Γ and $(\rho + p)$ are always positive, therefore, the model satisfies the second law of thermodynamic, i.e., $\nabla_\mu \mathbb{S}^\mu \geq 0$.

3.2.2 HRDE Model with Variable Bulk Viscosity

In this section, we assume the general form of bulk viscous coefficient ξ as given in (3.2.10) (hereafter *VHRDE5 model*).

Substituting (3.2.10) into (3.2.11), we obtain

$$h' + l_3 h = (1+2\lambda)l_1\xi_0 \tag{3.2.40}$$

where $l_3 = l_1 l_2 - (1+2\lambda) l_1 \xi_1$.

On solving (3.2.40), we get

$$h(a) = \frac{(1+2\lambda) l_1 \xi_0}{l_3} + \left(1 - \frac{(1+2\lambda) l_1 \xi_0}{l_3}\right) \left(\frac{a}{a_0}\right)^{-l_3} \tag{3.2.41}$$

where $l_3 \neq 0$. Now, the scale factor is given by

$$a(t) = \left[1 + \frac{l_3}{(1+2\lambda) l_1 \xi_0} \left(e^{(1+2\lambda) l_1 \xi_0 H_0 (t-t_0)} - 1\right)\right]^{\frac{1}{l_3}}, \tag{3.2.42}$$

where $\xi_0 \neq 0$ and $\lambda \neq -1/2$.

Taking $a(t) = 0$, we obtain the cosmic time t_B when the Big-Bang happens

$$t_B = t_0 + \frac{1}{(1+2\lambda) l_1 \xi_0 H_0} \ln\left[1 - \frac{(1+2\lambda) l_1 \xi_0}{l_3}\right]. \tag{3.2.43}$$

Hence, the age of the Universe since Big-Bang is given by $t_0 - t_B$. The Hubble parameter with respect to t reads

$$H(t) = \frac{H_0 e^{(1+2\lambda) l_1 \xi_0 H_0 (t-t_0)}}{\left[1 + \frac{l_3}{(1+2\lambda) l_1 \xi_0} \left(e^{(1+2\lambda) l_1 \xi_0 H_0 (t-t_0)} - 1\right)\right]}. \tag{3.2.44}$$

Differentiating (3.2.41) with respect to a to obtain

$$\frac{d\dot{a}}{da} = H_0 \left[\frac{(1+2\lambda) l_1 \xi_0}{l_3} + \left(1 - \frac{(1+2\lambda) l_1 \xi_0}{l_3}\right) (1 - l_3) a^{-l_3}\right] \tag{3.2.45}$$

We can obtain the transition scale factor a_{tr} by equating (3.2.45) equal to zero, and

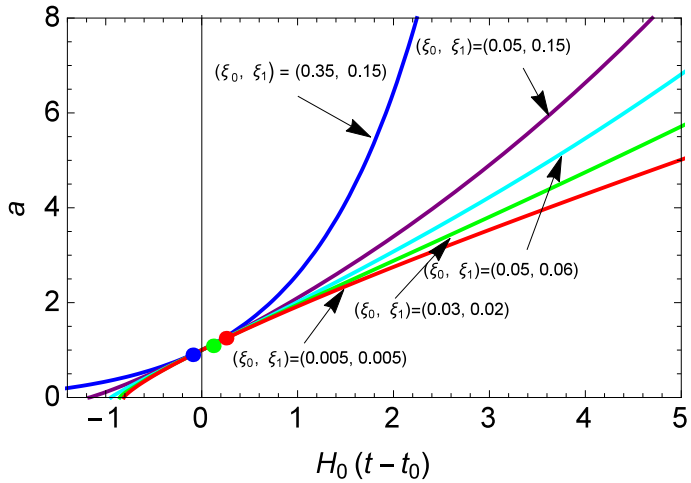

Figure 3.8: The evolution of scale factor with respect to $H_0(t-t_0)$ for different values of ξ_0 and ξ_1 with $\omega_d = -0.5$, $\lambda = 0.06$ and $\alpha = 0.34$ in VHRDE5 model.

given by

$$a_{tr} = \Big[\frac{(1+2\lambda)l_1\xi_0}{(l_3-1)[l_3-(1+2\lambda)l_1\xi_0]}\Big]^{-\frac{1}{l_3}}, \tag{3.2.46}$$

and its corresponding transition redshift z_{tr} is

$$z_{tr} = \Big[\frac{(1+2\lambda)l_1\xi_0}{(l_3-1)[l_3-(1+2\lambda)l_1\xi_0]}\Big]^{\frac{1}{l_3}} - 1 \tag{3.2.47}$$

We plot the evolution of scale factor with respect to $H_0(t-t_0)$ in Fig. 3.8 for the values of model parameter $\alpha = 0.34$, $\omega_d = -0.5$ and $\lambda = 0.06$. We get the similar behavior if negative value of λ is taken. The transition from decelerated phase to accelerated phase of the Universe depends on the values of ξ_0 and ξ_1.

It is observed from Fig. 3.8 that small combinations of (ξ_0, ξ_1) give late time acceleration whereas large combinations of (ξ_0, ξ_1) give the early acceleration of the Universe. The model predicts an eternally expanding Universe that begins with a Big-Bang followed by a decreasing decelerated expansion until a time when the deceleration vanishes and then there is a transition to an accelerated expansion epoch that is going to continue forever, so that $a \to \infty$ when $t \to \infty$. The dot represents the time at which the Universe transits from decelerated phase to accelerated phase. The Universe starts acceleration with finite past for some combination of (ξ_0, ξ_1). We can observe the similar behavior for negative value of λ.

Now, we compute the second order derivative of the scale factor $a(t)$ with respect to cosmic time t as

$$\frac{d^2a}{dt^2} = H_0^2 e^{(1+2\lambda)l_1\xi_0 H_0(t-t_0)}\left[e^{(1+2\lambda)l_1\xi_0 H_0(t-t_0)} - l_3 + (1+2\lambda)l_1\xi_0\right] \times \left[1 + \frac{l_3}{(1+2\lambda)l_1\xi_0}\Big(e^{(1+2\lambda)l_1\xi_0 H_0(t-t_0)} - 1\Big)\right]^{\frac{1}{l_3}-2}, \tag{3.2.48}$$

Equating (3.2.48) equal to zero, we can obtain the transition cosmic time t_{tr}, given by

$$t_{tr} = t_0 + \frac{1}{(1+2\lambda)l_1\xi_0 H_0}\ \ln\left\{l_3 - (1+2\lambda)l_1\xi_0\right\}. \tag{3.2.49}$$

Future finite-time singularity

Let us examine VHRDE5 model with accelerating cosmological solutions ending at the future finite-time singularities. The presence of viscous fluids could bring the future

finite-time singularities. In literature, many authors [207, 279, 290] have studied the future finite-time singularity. The future finite-time singularities can be classified in to four types. The detailed classification was firstly developed in Refs. [298, 299] and we now present in brief the essential features of this classification scheme.

- Type I (The Big-Rip Singularity): This singularity occurs when the cosmic time approaches $t \to t_s$, the scale factor a, the effective energy density ρ_{eff} and finally the effective pressure $|p_{eff}|$ diverge, that is, $a \to \infty$, $\rho_{eff} \to \infty$, and $|p_{eff}| \to \infty$.

- Type II (The Sudden Singularity): This singularity occurs when the cosmic time approaches $t \to t_s$, where only the scale factor a and the effective energy density ρ_{eff} tend to a finite value, that is, $a \to a_s$, $\rho_{eff} \to \rho_s$, but the effective pressure diverges, $|p_{eff}| \to \infty$.

- Type III : This singularity occurs when the cosmic time $t \to t_s$, $a \to a_s$, $\rho_{eff} \to \infty$, and $|p_{eff}| \to \infty$.

- Type IV : This singularity is not of the crushing type and it is the most mild among the four types of finite time cosmological singularities. In this case, as $t \to t_s$, $a \to a_s$, $\rho_{eff} \to 0$, and $|p_{eff}| \to 0$. This also includes the case when p_{eff} (ρ_{eff}) or both of them tend to some finite values.

Here, t_s, a_s, and ρ_s are constants with $a_s \neq 0$. Meng et al. [192], Sebastiani [212], Myrzakul et al. [300] and Khadekar et al. [301] studied finite-time future singularity in viscous FLRW models. Let us discuss the above four singularities in our viscous HRDE model.
The total energy density $\rho = \rho_d + \rho_m$ is given by

$$\begin{aligned}\rho &= \frac{3\xi_0}{(2+3\lambda)} e^{(1+2\lambda)l_1\xi_0 H_0(t-t_0)} \Bigg[-\lambda l_3 (e^{(1+2\lambda)l_1\xi_0 H_0(t-t_0)} - 1) \\ &\quad + l_1^2 \lambda \alpha \omega_d \xi_0 H_0^2 (1+2\lambda)^2 + (1+2\lambda) l_1 \{ -\lambda (H_0^2 l_3 \alpha \omega_d + \xi_0) \\ &\quad + (2H_0^2(1+\lambda\alpha\omega_d) - \lambda\xi_1) e^{(1+2\lambda)l_1\xi_0 H_0(t-t_0)} \} \Bigg] \\ &\quad \times \left[1 + \frac{l_3}{(1+2\lambda)l_1\xi_0} \left(e^{(1+2\lambda)l_1\xi_0 H_0(t-t_0)} - 1 \right) \right]^{-2} \end{aligned} \tag{3.2.50}$$

The total pressure of the HRDE in the presence of viscosity is $p_{eff} = p_d - 3\zeta H$, can be evaluated as

$$\begin{aligned} p_{eff} &= 3\xi_0 e^{(1+2\lambda)l_1\xi_0 H_0(t-t_0)}\Bigg[-l_3\{e^{(1+2\lambda)l_1\xi_0 H_0(t-t_0)} - 1 + l_1 H_0^2\alpha\omega_d(1+2\lambda)\} \\ &\quad +(1+2\lambda)l_1\{(l_1 H_0^2\alpha\omega_d(1+2\lambda)-1)\xi_0 + (2H_0^2\alpha\omega_d - \xi_1)e^{(1+2\lambda)l_1\xi_0 H_0(t-t_0)}\}\Bigg] \\ &\quad \times\left[1+\frac{l_3}{(1+2\lambda)l_1\xi_0}\left(e^{(1+2\lambda)l_1\xi_0 H_0(t-t_0)}-1\right)\right]^{-2}. \end{aligned} \tag{3.2.51}$$

Assuming $\omega_d = -0.5$ and $\alpha = 0.34$, we obtain that for $-1 < \lambda < -0.686548$ or $0.78205 < \lambda < 2.12772$ (as calculated by Mathematica software), we have $a \to \infty$, $\rho \to \infty$ and $|p_{eff}| \to \infty$, which shows the Type I Big-Rip singularity at a finite-time

$$t_s = \frac{1}{(1+2\lambda)l_1\xi_0 H_0}\ln\left[1-\frac{(1+2\lambda)l_1\xi_0}{l_3}\right] + t_0. \tag{3.2.52}$$

For other values of λ (excluding the mentioned interval), we obtain that at this finite time $a \to 0$, $\rho \to \infty$ and $|p_{eff}| \to \infty$, which shows the Type III singularity.

In the absence of model parameter α, the Big-Rip singularity depends on only λ. Thus for $\lambda < -2/3$ we have $a \to \infty$, $\rho \to \infty$ and $|p_{eff}| \to \infty$ at finite-time

$$t_s = \frac{(2+3\lambda)}{3(1+\lambda)(1+2\lambda)\xi_0 H_0}\, ln\left(1-\frac{(1+2\lambda)\xi_0}{\{1-(1+2\lambda)\xi_1\}}\right) + t_0. \tag{3.2.53}$$

Evolution of deceleration parameter

The deceleration parameter q in VHRDE5 model is obtained as

$$q(t) = -1 + \Big\{l_3 - (1+2\lambda)l_1\xi_0\Big\}e^{-(1+2\lambda)l_1\xi_0 H_0(t-t_0)}. \tag{3.2.54}$$

which is time-dependent and may describe the phase transition of the Universe.

In terms of the scale factor a, The q can be written as

$$q(a) = -1 + \frac{[l_3 - (1+2\lambda)l_1\xi_0]}{\left[1+\frac{(1+2\lambda)l_1\xi_0}{l_3}(a^{l_3}-1)\right]}, \tag{3.2.55}$$

Table 3.4: Variation of q for $\omega_d = -0.5$, $\alpha = 0.34$

λ	Constraints on ξ_0 and ξ_1	q	Evolution of the Universe
$\lambda > 2.1277$	For all $\xi_0, \xi_1 > 0$	Positive	Decelerated expansion
$0.272 \leq \lambda \leq 2.1277$	For all $\xi_0, \xi_1 > 0$	Negative	Accelerated expansion
$-0.5 < \lambda < 0.272$	$0 < \xi_0 + \xi_1 < \frac{\{1-0.51(1+\lambda)(1+2\lambda)\}}{3(1+\lambda)(1+2\lambda)}$	$+$ve to $-$ve	Transition from dec. to acc.
	$\xi_0 + \xi_1 \geq \frac{\{1-0.51(1+\lambda)(1+2\lambda)\}}{3(1+\lambda)(1+2\lambda)}$	Negative	Accelerated expansion
$-0.6865 \leq \lambda \leq -0.5$	For all $\xi_0, \xi_1 > 0$	Positive	Decelerated expansion
$-1 \leq \lambda < -0.6865$	For all $\xi_0, \xi_1 > 0$	Negative	Accelerated expansion
$-1.7712 \leq \lambda < -1$	$0 < \xi_0 + \xi_1 < \frac{\{1-0.51(1+\lambda)(1+2\lambda)\}}{3(1+\lambda)(1+2\lambda)}$	$-$ve to $+$ve	Transition from acc. to dec.
	$\xi_0 + \xi_1 \geq \frac{\{1-0.51(1+\lambda)(1+2\lambda)\}}{3(1+\lambda)(1+2\lambda)}$	Positive	Decelerated expansion
$\lambda < -1.7712$	For all $\xi_0, \xi_1 > 0$	Positive	Decelerated expansion

which can also be written in terms of redshift z as

$$q(z) = -1 + \frac{[l_3 - (1+2\lambda) l_1 \xi_0]}{\left[1 + \frac{(1+2\lambda) l_1 \xi_0}{l_3}((1+z)^{-l_3} - 1)\right]}. \tag{3.2.56}$$

The present value of DP which corresponds to $z = 0$ or $a = 1$, is

$$q_0 = -1 + [l_3 - (1+2\lambda) l_1 \xi_0]. \tag{3.2.57}$$

Now, $q_0 = 0$ gives $(\xi_0 + \xi_1) = \frac{\{1+3(1+\lambda)(1+2\lambda)\alpha\omega_d\}}{3(1+\lambda)(1+2\lambda)}$. The transition into accelerating phase would occur at present time for this sum of ξ_0 and ξ_1. Especially, for $\alpha = 0.34$, $\omega_d = -0.5$ and $\lambda = 0.06$, we get $\xi_0 + \xi_1 = 0.11$ which gives $q_0 = 0$. For $\xi_0 + \xi_1 < 0.11$, $q > 0$, we have decelerating phase today and for $\xi_0 + \xi_1 \geq 0.11$, we have $q < 0$, i.e., the model expands with acceleration today. In case of $\lambda = -0.06$, we get $\xi_0 + \xi_1 = 0.23$ for which $q = 0$.

Table 3.4 gives the evolution and behavior of q for $\alpha = 0.34$ and $\omega_d = -0.5$. We observe that the Universe shows the deceleration for the ranges $\lambda > 2.1277$, $-0.6865 \leq \lambda \leq -0.5$ and $\lambda < -1.7712$, whereas shows acceleration for the ranges $0.272 \leq \lambda \leq 2.1277$ and $-1 \leq \lambda < -0.6855$. The Universe also shows the phase transition from deceleration to acceleration for small values of $\xi_0 + \xi_1$ and acceleration for large values of $\xi_0 + \xi_1$ in the range $-0.5 < \lambda < 0.272$ and phase transition from acceleration to deceleration for small values of $\xi_0 + \xi_1$ and deceleration for large values of $\xi_0 + \xi_1$ in the range $-1.7712 \leq \lambda < -1$.

Table 3.5: Variation of q for $\omega_d = -1$, $\alpha = 0.34$

λ	Constraints on ξ_0 and ξ_1	q	Evolution of the Universe
$\lambda > 0.6785$	For all $\xi_0, \xi_1 > 0$	Positive	Decelerated expansion
$0 \leq \lambda \leq 0.6785$	For all $\xi_0, \xi_1 > 0$	Negative	Accelerated expansion
$-0.5 < \lambda < 0$	$0 < \xi_0 + \xi_1 < \frac{\{1-1.02(1+\lambda)(1+2\lambda)\}}{3(1+\lambda)(1+2\lambda)}$	$+$ve to $-$ve	Transition from dec. to acc.
	$\xi_0 + \xi_1 \geq \frac{\{1-1.02(1+\lambda)(1+2\lambda)\}}{3(1+\lambda)(1+2\lambda)}$	Negative	Accelerated expansion
$-0.708 \leq \lambda \leq -0.5$	For all $\xi_0, \xi_1 > 0$	Positive	Decelerated expansion
$-1 \leq \lambda < -0.708$	For all $\xi_0, \xi_1 > 0$	Negative	Accelerated expansion
$-1.493 \leq \lambda < -1$	$0 < \xi_0 + \xi_1 < \frac{\{1-1.02(1+\lambda)(1+2\lambda)\}}{3(1+\lambda)(1+2\lambda)}$	$-$ve to $+$ve	Transition from acc. to dec.
	$\xi_0 + \xi_1 \geq \frac{\{1-1.1055(1+\lambda)(1+2\lambda)\}}{3(1+\lambda)(1+2\lambda)}$	Positive	Decelerated expansion
$\lambda < -1.493$	For all $\xi_0, \xi_1 > 0$	Positive	Decelerated expansion

Table 3.6: Variation of q for $\omega_d = -1.215$, $\alpha = 0.34$

λ	Constraints on ξ_0 and ξ_1	q	Evolution of the Universe
$\lambda \geq 0.4280$	For all $\xi_0, \xi_1 > 0$	Positive	Decelerated expansion
$-0.067 \leq \lambda < 0.4280$	For all $\xi_0, \xi_1 > 0$	Negative	Accelerated expansion
$-0.5 < \lambda < -0.067$	$0 < \xi_0 + \xi_1 < \frac{\{1-1.239(1+\lambda)(1+2\lambda)\}}{3(1+\lambda)(1+2\lambda)}$	$+$ve to $-$ve	Transition from dec. to acc.
	$\xi_0 + \xi_1 \geq \frac{\{1-1.239(1+\lambda)(1+2\lambda)\}}{3(1+\lambda)(1+2\lambda)}$	Negative	Accelerated expansion
$-0.7174 \leq \lambda \leq -0.5$	For all $\xi_0, \xi_1 > 0$	Positive	Decelerated expansion
$-1 \leq \lambda < -0.7174$	For all $\xi_0, \xi_1 > 0$	Negative	Accelerated expansion
$-1.4326 \leq \lambda < -1$	$0 < \xi_0 + \xi_1 < \frac{\{1-1.239(1+\lambda)(1+2\lambda)\}}{3(1+\lambda)(1+2\lambda)}$	$-$ve to $+$ve	Transition from acc. to dec.
	$\xi_0 + \xi_1 \geq \frac{\{1-1.239(1+\lambda)(1+2\lambda)\}}{3(1+\lambda)(1+2\lambda)}$	Positive	Decelerated expansion
$\lambda < -1.4326$	For all $\xi_0, \xi_1 > 0$	Positive	Decelerated expansion

In Table 3.5, which corresponds to $\omega_d = -1$, the behavior of the expansion of the Universe shows deceleration phase for the ranges $\lambda > 0.6785$, $-0.708 \leq \lambda \leq -0.5$ and $\lambda < -1.493$, whereas shows acceleration for the ranges $0 \leq \lambda \leq 0.6785$ and $-1 \leq \lambda < -0.708$. The phase transition from deceleration to acceleration is obtained for small values of $\xi_0 + \xi_1$ and acceleration for large values of $\xi_0 + \xi_1$ in $-0.5 < \lambda < 0$, whereas the phase transition from acceleration to deceleration is obtained for small values of $\xi_0 + \xi_1$ and deceleration for large values of $\xi_0 + \xi_1$ in the range $-1.493 \leq \lambda < -1$.

In Table 3.6, which summarizes the behavior of the Universe for $\omega_d = -1.215$, we observe that the Universe decelerates in the ranges $\lambda \geq 0.4280$, $-0.7174 \leq \lambda \leq -0.5$ and $\lambda < -1.4326$ and accelerates in the ranges $-0.067 \leq \lambda < 0.4280$ and $-1 \leq \lambda < -0.7174$. It can also be observed that the Universe shows phase transition from deceleration to

acceleration for small values of $\xi_0+\xi_1$ and acceleration for large values of $\xi_0+\xi_1$ in $-0.5<\lambda<-0.067$, whereas the phase transition from acceleration to deceleration is obtained for small values of $\xi_0+\xi_1$ and deceleration for large values of $\xi_0+\xi_1$ in the range $-1.4326\leq\lambda<-1$.

Statefinder and *Om* diagnostics

For VHRDE5 model, the statefinder pair is given by

$$r=1+\frac{(l_3-3)(l_3-(1+2\lambda)l_1\xi_0)}{e^{(1+2\lambda)l_1\xi_0H_0(t-t_0)}}+\frac{(l_3-(1+2\lambda)l_1\xi_0)^2}{e^{2(1+2\lambda)l_1\xi_0H_0(t-t_0)}} \tag{3.2.58}$$

and

$$s=\frac{(l_3-(1+2\lambda)l_1\xi_0)\left[2(l_3-3)+\frac{2(l_3-(1+2\lambda)l_1\xi_0)}{e^{(1+2\lambda)l_1\xi_0H_0(t-t_0)}}\right]}{6(l_3-(1+2\lambda)l_1\xi_0)-9e^{(1+2\lambda)l_1\xi_0H_0(t-t_0)}} \tag{3.2.59}$$

The present value of the statefinder pair $\{r_0,s_0\}$ can be obtained as

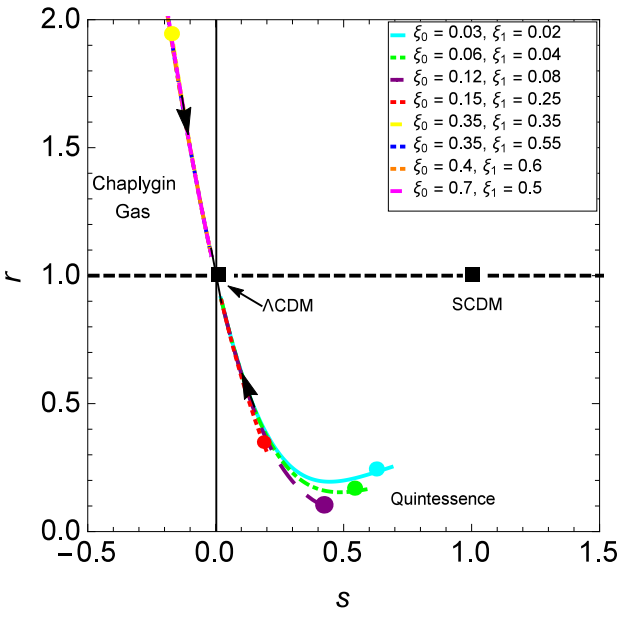

Figure 3.9: The $r-s$ trajectories are plotted in $s-r$ plane for different values of ξ_0 and ξ_1 with $\omega_d=-0.5$ and $\lambda=0.06$ along with the observational value of $\alpha=0.34$. The arrows represent the direction of the evolution of statefinder diagnostic pair with time. The dot represents the present values of $\{r_0,s_0\}$.

$$r_0=1+(l_3-3)(l_3-(1+2\lambda)l_1\xi_0)+(l_3-(1+2\lambda)l_1\xi_0)^2, \tag{3.2.60}$$

and

$$s_0 = \frac{2(l_3-(1+2\lambda)l_1\xi_0)\left[(l_3-3)+(l_3-(1+2\lambda)l_1\xi_0)\right]}{6(l_3-(1+2\lambda)l_1\xi_0)-9}. \tag{3.2.61}$$

From (3.2.58) and (3.2.59), we find that as $(t-t_0)\to\infty$, $\{r,s\}\to\{1,0\}$, a value cor-

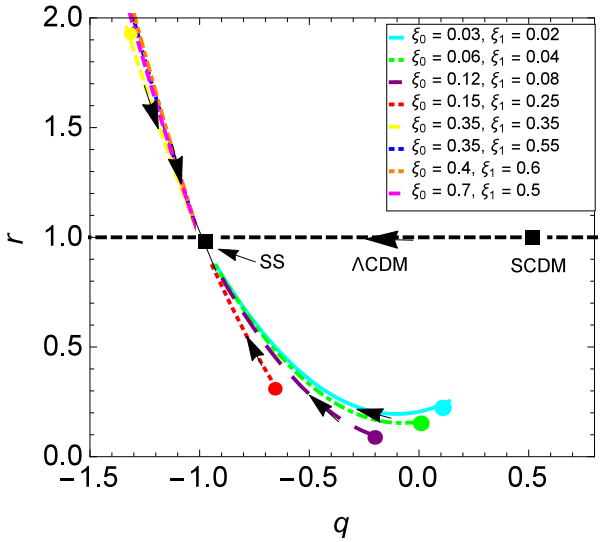

Figure 3.10: The $r-q$ trajectories are plotted in $q-r$ plane for different values of ξ_0 and ξ_1 with $\omega_d=-0.5$ and $\lambda=0.06$ along with the observational value of $\alpha=0.34$. The arrows represent the directions of the time evolution of pair $\{r,q\}$ with time. The dot represents the present values of $\{r_0,q_0\}$.

responding to ΛCDM model. We plot the $r-s$ and $r-q$ trajectories to analyze the evolution of viscous HRDE model. It is to be noted that $\{r,s\}$ depends on the choice of (ξ_0,ξ_1) and coupling parameter λ. The $r-s$ and $r-q$ trajectories for different combinations for (ξ_0,ξ_1) and $\lambda=0.06$ with $\omega_d=-0.5$ and $\alpha=0.34$ are shown in Figures 3.9 and 3.10, respectively.

In Fig. 3.9, the dark-box represents the fixed point of the ΛCDM and $SCDM$ models at $\{r,s\}=\{1,0\}$ and $\{r,s\}=\{1,1\}$, respectively. The dots represent the present value $\{r_0,s_0\}$ of the statefinders for different combinations of (ξ_0,ξ_1) and the arrows shows the direction of the evolution of the statefinders. It is observed that the $r-s$ trajectories show the behavior similar to the CG for $(\xi_0+\xi_1)>0.55$, and behaves as $Q-model$ for $0<(\xi_0+\xi_1)\leq 0.55$. The model approaches to ΛCDM in late time from both the regions.

Fig. 3.10 represents the $q-r$ plane trajectories for different values of (ξ_0,ξ_1) with $\lambda=0.06$. The dark-box denote the fixed point $\{r,q\}=\{1,0.5\}$ for $SCDM$ and $\{r,q\}=\{1,-1\}$ for Steady State (SS) models, respectively and the arrows represents the direction of the evolution. It can be observed from the figures that q changes its sign

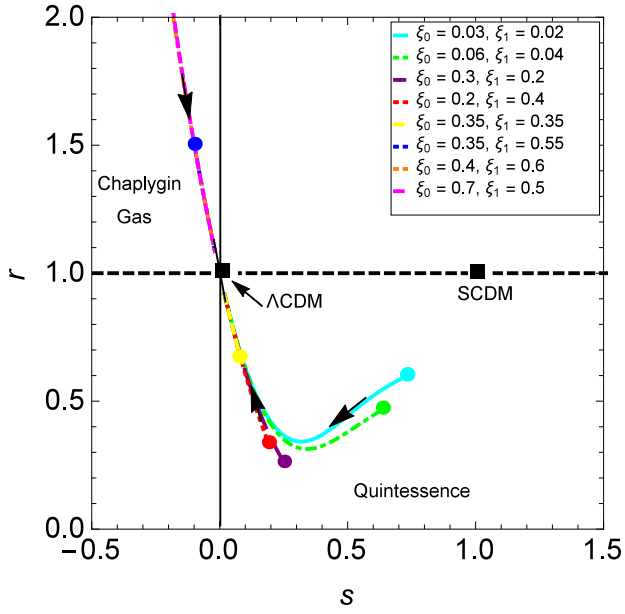

Figure 3.11: The $r-s$ trajectories are plotted in $r-s$ plane for different values of ξ_0 and ξ_1 with $\omega_d = -0.5$ and $\lambda = -0.06$ along with the observational value of $\alpha = 0.34$. The arrows represent the direction of the evolution of statefinder diagnostic pair with time.

from positive to negative for $0 < (\xi_0 + \xi_1) \leq 0.55$ which clearly shows the phase transition from deceleration to acceleration. For $(\xi_0 + \xi_1) > 0.55$, q is always negative. It can also be seen that our model always converges to SS model in late time from both the regions as ΛCDM approaches to SS model.

A similar trajectories of $r-s$ and $r-q$ can be observed for $\lambda = -0.06$ and different combinations of (ξ_0, ξ_1) as shown in Figs. 3.11 and 3.12. However, the constraint of $\xi_0 + \xi_1$ for quintessence region is $0 < (\xi_0 + \xi_1) \leq 0.79$ and for Chaplygin gas model, it is $(\xi_0 + \xi_1) > 0.79$. The dot represents the present values of $\{r_0, s_0\}$.

The present VHRDE5 model can also be discriminated from the holographic dark energy model with event horizon as the infrared cutoff, in which the $r-s$ evolution starts from a region $r \sim 1$, $s \sim 2/3$ and ends on the ΛCDM point [296]. It can also be discriminated from Ricci dark energy model in which (r,s) trajectory is a vertical segment, i.e., s is a constant during the evolution of the Universe [107].

For this model, $Om(z)$ can be calculated as

$$Om(z) = \frac{\left[\frac{(1+2\lambda)l_1\xi_0}{l_3} + \left(1 - \frac{(1+2\lambda)l_1\xi_0}{l_3}\right)(1+z)^{l_3}\right]^2 - 1}{(1+z)^3 - 1} \tag{3.2.62}$$

We plot the evolution of Om-diagnostic with respect to redshift z in Fig. 3.13 for differ-

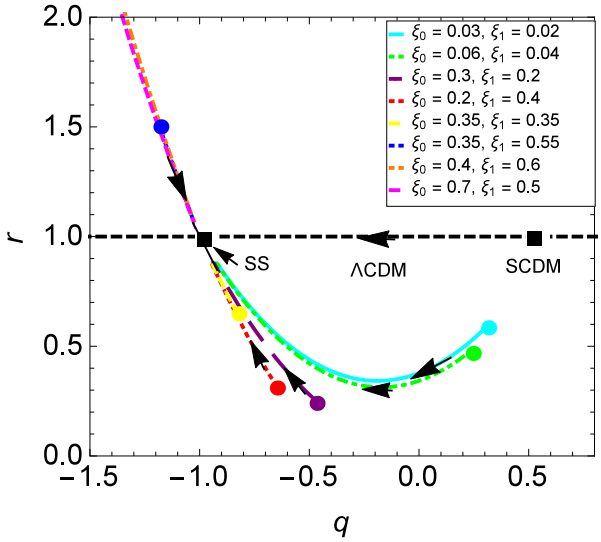

Figure 3.12: The $r-q$ trajectories are plotted in $r-q$ plane for different values of ξ_0 and ξ_1 with $\omega_d = -0.5$ and $\lambda = -0.06$ along with the observational value of $\alpha = 0.34$. The arrows represent the direction of the time evolution of pair $\{r,q\}$ with time.

ent values of (ξ_0, ξ_1) and fixed positive values of λ, e.g., $\lambda = 0.06$. It can be observed from the figure that the $Om(z)$ trajectories shows positive and negative slopes for different values of (ξ_0, ξ_1). Fig. 3.13 shows the negative slope of $Om(z)$ trajectories for $0 < (\xi_0 + \xi_1) \leq 0.55$, which corresponds to $Q - model$, whereas for $(\xi_0 + \xi_1) > 0.55$, $Om(z)$ trajectories shows positive slope, i.e., model behaves as phantom.

Entropy and generalized second law of thermodynamics

Let us discuss the entropy and generalized second law (GSL) of thermodynamics of VHRDE5 model. Using (3.2.41) into (3.2.10), we obtain the evolution of bulk viscosity,

$$\xi(a) = \xi_0 + \xi_1 \left\{ \left(1 - \frac{(1+2\lambda)l_1\xi_0}{l_3}\right) a^{-l_3} + \frac{(1+2\lambda)l_1\xi_0}{l_3} \right\}. \tag{3.2.63}$$

Since the Hubble parameter H is positive in an expanding Universe, therefore ξ_0 and ξ_1 has to be positive in order to preserve the second law of thermodynamics. Figure 3.14 shows the behavior of ξ with respect to the scale factor for different combinations of ξ_0 and ξ_1 corresponding to the positive value of λ. We observe that the total bulk viscosity is always positive and decreases to zero for small values of $0 < (\xi_0 + \xi_1) \leq 0.55$. These curves have been shown above the line (0,0). Therefore, the model does not violate the entropy law for these ranges. The figures also show that the total bulk viscous coefficient is evolving from negative to a positive value for

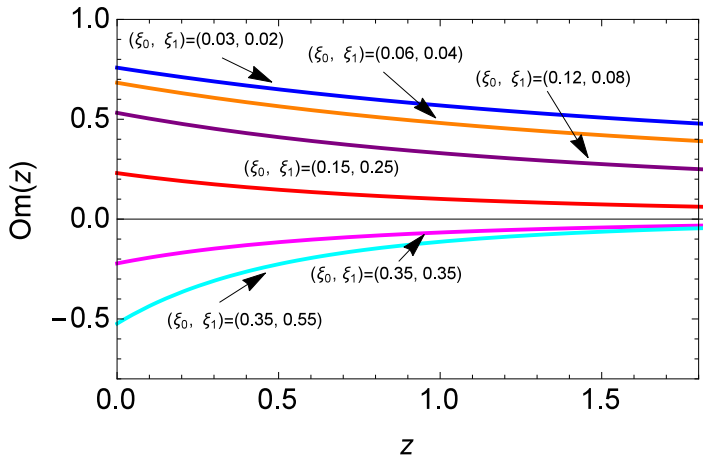

Figure 3.13: The $Om-z$ trajectories are plotted in $Om-z$ plane for different values of ξ_0 and ξ_1 with $\omega_d = -0.5$ and $\lambda = 0.06$ along with the observational value of $\alpha = 0.34$.

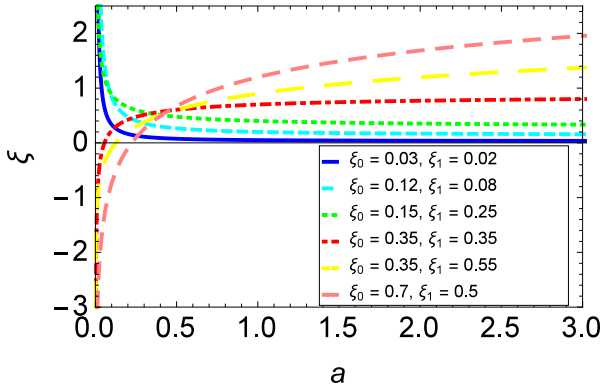

Figure 3.14: The evolution of $\xi(a)$ for different combinations of (ξ_0, ξ_1) and $\lambda = 0.06$. We take $\omega_d = -0.5$ and $\alpha = 0.34$.

$(\xi_0 + \xi_1) > 0.55$. Thus, the rate of entropy production is negative for large values of $\xi_0 + \xi_1$ in the early epoch and positive in the later epoch. Hence the entropy law violates in the early epoch and obeys in the later epoch.

Let us investigate the generalized second law (GSL) of thermodynamics in the viscous HRDE model in the framework of modified $f(R,T)$ gravity theory at the apparent horizon of FLRW Universe. The dynamical apparent horizon is derived by the relation $h^{\alpha\beta}\partial_\alpha r \partial_\beta r = 0$, which gives radius of apparent horizon for flat FLRW Universe as

$$r_{hor} = \frac{1}{H_0 h}. \tag{3.2.64}$$

The entropy of the apparent horizon in $f(R,T)$ gravity is expressed as [302]

$$\mathbb{S}_{hor} = \frac{\tilde{A}}{4G_{eff}} = \frac{8\pi^2 r_{hor}^2}{1+\lambda}, \tag{3.2.65}$$

where G_{eff} is the effective gravitational coupling given by $G_{eff} = G + \frac{f_T(R,T)}{8\pi}$, which can be further written as $G_{eff} = \frac{1+\lambda}{8\pi}$ for our model and $\tilde{A} = 4\pi r_{hor}^2$ is the area of the apparent horizon.

Consider $\mathbb{S}_i = \mathbb{S}_m + \mathbb{S}_d$ is the amount of entropy of the dark matter-dark energy components, where $\mathbb{S}_m$ is the entropy of dark matter and $\mathbb{S}_d$ is the entropy of DE. As we know from the first law of thermodynamics that the infinitesimal difference of the entropy, energy density and volume in modified $f(R,T)$ gravity have the following relation [281].

$$\mathbb{T}_i d\mathbb{S}_i = d(\rho_i V) + p_i dV - \mathbb{T}_i d\mathbb{S}_p, \tag{3.2.66}$$

where $\mathbb{T}_i$ is the temperature, ρ_i is the sum of densities of matter and DE, $\mathbb{S}_p$ is the entropy production and V represents the volume of the horizon enclosed, which is given as $V = \frac{4}{3}\pi r_{hor}^3$.

In case of a thermal equilibrium between the fluids and the horizon, we have $\mathbb{T}_i = \mathbb{T}_{hor}$. Using this relation and solving Eq. (3.2.66), we get

$$\mathbb{T}_{hor}(\dot{\mathbb{S}}_m + \dot{\mathbb{S}}_d + \dot{\mathbb{S}}_p) = 4\pi r_{hor}^2(\dot{r}_{hor} - 1)(\rho + \omega_d\rho_d - 3\xi h). \tag{3.2.67}$$

As we have considered the thermal equilibrium for our system, we take the temperature $\mathbb{T}_{hor} = \frac{bH_0h}{2\pi} = \frac{b}{2\pi r_{hor}}$ [303], which is equal to the Hawking temperature of the horizon with the assumption that the fluid within the horizon is in equilibrium with horizon so that there is no effective flow of fluid towards the horizon [304]. Therefore, we have

$$\mathbb{T}_{hor}\dot{\mathbb{S}}_{hor} = \frac{8\pi b}{1+\lambda}\dot{r}_{hor}, \tag{3.2.68}$$

According to GSL of thermodynamics, during the evolution of the Universe the rate of change of the sum of all the entropies of the fluid within the Universe and that of the horizon must always greater than or equal to zero. Thus, GSL states that

$$\dot{\mathbb{S}}_{tot} = \dot{\mathbb{S}}_m + \dot{\mathbb{S}}_d + \dot{\mathbb{S}}_p + \dot{\mathbb{S}}_{hor} \geq 0. \tag{3.2.69}$$

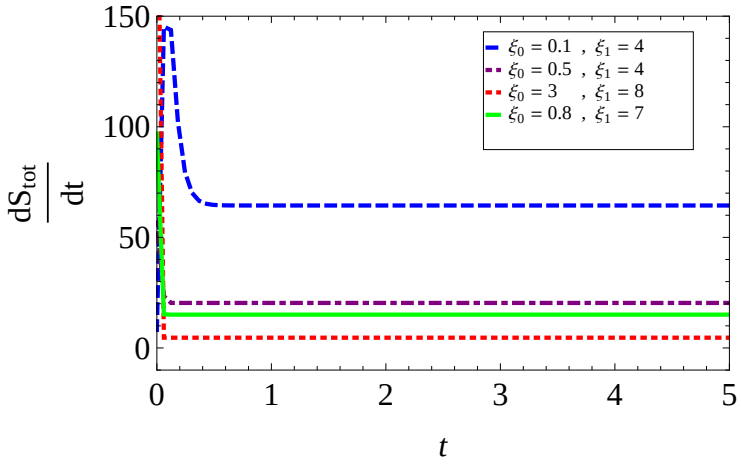

Figure 3.15: The change in total entropy $\frac{dS_{tot}}{dt}$ with respect to time t for different combination of ξ_0 and ξ_1 with $\alpha = 0.34$, $\omega_d = -0.5$, $H_0 = 72$ and $\lambda = 0.06$.

Using above equations, the change in total entropy is given by

$$\begin{aligned}\dot{\mathbb{S}}_{tot} = &\frac{16\pi^2}{H_0 e^{2(1+2\lambda)l_1\xi_0 H_0(t-t_0)}}\left[1+\frac{l_3}{(1+2\lambda)l_1\xi_0}\left(e^{(1+2\lambda)l_1\xi_0 H_0(t-t_0)}-1\right)\right]\\
&\times\left[\frac{l_3-(1+2\lambda)l_1\xi_0}{1+\lambda}+\frac{3}{(2+3\lambda)bH_0^2}\left(\frac{(l_3-(1+2\lambda)l_1\xi_0)}{e^{(1+2\lambda)l_1\xi_0 H_0(t-t_0)}}-1\right)\right.\\
&\left\{\frac{((1+2\lambda)l_1H_0^2\alpha\omega_d-1)((1+2\lambda)l_1\xi_0-l_3)}{l_1}\right.\\
&\left.\left.+\left((1+2\alpha\omega_d+4\lambda\alpha\omega_d)H_0^2-\frac{l_3+l_1\xi_1+2l_1\lambda\xi_1}{l_1}\right)e^{(1+2\lambda)l_1\xi_0 H_0(t-t_0)}\right\}\right] \qquad (3.2.70)\end{aligned}$$

We plot the evolution of the rate of total entropy $\dot{\mathbb{S}}_{tot}$ with respect to cosmic time t in Fig. 3.15. It can be observed from the figure that the rate of total entropy is positive under the constraint $\xi_0 > 0.03$ and $\xi_1 > 3.7$ for $\lambda = 0.06$, $\alpha = 0.34$, $\omega_d = -0.5$ and $H_0 = 72\,Km/sec/Mpc$. Hence, the GSL of thermodynamics always valid for this model under some constraints of ξ_0 and ξ_1 with the apparent horizon. The total rate of change of entropy approaches to zero in the late time evolution for the larger values of ξ_0 and ξ_1.

3.3 Conclusion

In this chapter, we have explored the effect of bulk viscosity in the HRDE model in the background of modified $f(R,T)$ gravity. We have assumed the simplest form of $f(R,T) = R+\lambda T$ to solve the field equations. We have found the exact solution of the

scale factor and have calculated the deceleration parameter, statefinder, and *Om(z)* diagnostic parameters. We have plotted the trajectories in $r-s$, $r-q$, and *Om(z)* planes to discriminate the viscous HRDE model from the existing dark energy model. The thermodynamics of viscous HRDE models have been discussed. We have also explored the obvious violation of EMT in $f(R,T)$ gravity and have provided a thermodynamic interpretation of the extra terms generated by the non-minimal geometry-matter coupling as describing as a particle production. Let us summarize the results as follows:

In the VHRDE4 model, the scale factor varies exponentially which gives a time-dependent deceleration parameter. Fig. 3.1 shows the evolution of the scale factor for different values of ξ_0 and positive λ. We have calculated the transition scale factor a_{tr} and redshift z_{tr} to find the present time transition. It has been observed that the Universe has an earlier decelerated phase followed by an accelerated phase in the later stage of the evolution. We have observed that there is early acceleration for large ξ_0 and late-time acceleration for small values of ξ_0. We have also calculated the transition cosmic time for the scale factor. We have discussed the behavior of the deceleration parameter which is time-dependent. The DP implies that our model shows phase transition from one epoch to another. It is also observed that as $(t-t_0)\to\infty$, we get $q\to-1$. Thus the model accelerates in late time.

We have also discussed the geometrical diagnostics of statefinder and *Om(z)* in the VHRDE4 model, which distinguishes it from other DE models. The evolution of the $r-s$ and $r-q$ trajectories for various values of ξ_0 with positive and negative values of λ have been analyzed as shown in Figs. 3.2–3.5. In Figs. 3.2 and 3.3, we have observed that our model behaves like Q-model for small values of ξ_0 whereas it behaves CG-like for larger values of ξ_0 and finally approaches to ΛCDM in late time. From Figs. 3.4 and 3.5 for $r-q$ trajectories, we have observed that there is a sign change of q from positive to negative in Q-region for small values of ξ_0, which shows that our model transits from decelerated phase to accelerated phase. Our model always converges to the SS model as the ΛCDM model approaches from $SCDM$ in late time. We have also plotted $Om(z)-z$ trajectories in Fig. 3.6 and 3.7 for different values of ξ_0 and fixed positive and negative values of λ. In Fig. 3.6, the evolution of $Om(z)-z$ trajectories have negative slope for $0<\xi_0\leq 0.55$, which corresponds to $Q-model$, whereas for $\xi_0>0.55$, $Om(z)$ trajectories shows positive slope, i.e., model behaves as $phantom$. Similarly, the $Om(z)-z$ trajectories show a negative slope for $0<\xi_0\leq 0.8$, which corresponds to $Q-model$, whereas shows a positive slope for $\xi_0>0.8$, i.e., model behaves

as $phantom$. We have also discussed the entropy and thermodynamics for the HRDE model with constant bulk viscosity. We have found that a non-vanishing particle production rate is equivalent to a bulk viscous pressure. It has been observed that the validity of the second law of thermodynamics preserves for $\zeta_0 = \xi_0 \geq 0$.

In the case of the VHRDE5 model, we have assumed the bulk viscosity coefficient as the most general form, $\zeta = \zeta_0 + \zeta_1 H$. We have observed the evolution of the scale factor time-dependent and varies exponentially. Fig. 3.8 shows the evolution of the scale factor with respect to $H_0(t - t_0)$ for different values of ξ_0 and ξ_1 with positive value of λ. The Universe has earlier decelerated phase followed by an accelerated phase in the late time. The transition from decelerated phase to the accelerated phase of the Universe depends on the values of ξ_0 and ξ_1. For the present time, the transition takes place for $\xi_0 + \xi_1 = 0.11$. For $0 < (\xi_0 + \xi_1) < 0.11$, the Universe expands with decelerated rate followed by the accelerated rate in late time. The transition takes place at early time for $(\xi_0 + \xi_1) > 0.11$. We have calculated the cosmic time when the Big-Bang happens. We have also calculated the transition time when it transits from decelerated phase to the accelerated phase. We have briefly discussed how the presence of viscous fluid could produce the finite-time future singularity. It is found that Big Rip and type III finite-time singularities appear in the viscous HRDE model. We have evaluated the deceleration parameter which is time-dependent. This means that it can show the phase transition from one epoch to another. It is observed that as $(t - t_0) \to \infty$, we get $q \to -1$. Thus the model accelerates in late time. It has been found that $q = 0$ at present time $t = t_0$ for $(\xi_0 + \xi_1) = 0.11$. Thus, at present time when $0 < (\xi_0 + \xi_1) < 0.11$, $q > 0$, the Universe would decelerates and when $(\xi_0 + \xi_1) > 0.11$, $q < 0$, it accelerates.

In the VHRDE5 model, we have also discussed the statefinder parameters and Om and plotted their trajectories for various combinations of ξ_0 and ξ_1 with positive and negative values of λ as shown in Figs. 3.9–3.13. In Figs. 3.9 and 3.11, we have found that our model behaves like Q-model for small values of $\xi_0 + \xi_1$ whereas it behaves CG-like for larger values of $\xi_0 + \xi_1$. In both cases, our model approaches ΛCDM in late time. In Figs. 3.10 and 3.12, we have observed from the $r - q$ trajectories that there is a sign change of q from positive to negative in Q-region for small values of $\xi_0 + \xi_1$, which shows that our model changes the phase from deceleration to acceleration. Our model always converges to the SS model as the ΛCDM model approaches from $SCDM$ in late time. We have also discussed the Om diagnostic in terms of redshift z. We have plotted the evolution of Om-diagnostic with respect to redshift z in Fig.

3.13 for different values of (ξ_0, ξ_1) and fixed positive value of λ, i.e., for $\lambda = 0.06$. It shows negative slope of $Om(z)$ trajectories for $0 < (\xi_0 + \xi_1) \leq 0.55$, which corresponds to $Q - model$, whereas for $(\xi_0 + \xi_1) > 0.55$, $Om(z)$ trajectories shows positive slope, i.e., model behaves as $phantom$.

We have examined the entropy law in the viscous HRDE model. We have found that the bulk viscous coefficient is always positive and decreasing to zero for small values of $0 < \xi_0 + \xi_1 < 0.55$ as shown in Fig. 3.14. Therefore, the model does not violate the entropy law. However, for large $(\xi_0 + \xi_1) > 0.55$, $\xi(a)$ evolves from negative to positive which shows that the entropy law is violated in early time and obeys in late time. In the last part of our work, we have extended our study to examine the GSL of thermodynamics for this model in modified theory. We have calculated the rate of change of total entropy and plotted the evolution with respect to cosmic time t. We have observed that the rate of entropy is positive in the range of $\xi_0 > 0.03$ and $\xi_1 > 3.7$. Hence, the GSL of thermodynamics always valid with apparent horizon for this model under some constraint of ξ_0 and ξ_1.

We conclude that the dark energy phenomena can be explained in the presence of bulk viscosity, which shows that the accelerated expansion of the Universe strictly depends on the bulk viscosity coefficient. Our work implies a theoretical basis for future observations to constrain the viscous HRDE model.

****

Chapter 4

Holographic Dark Energy Model with Matter Creation

In this chapter [1]*, we study the adiabatic matter creation process in holographic dark energy (HDE) with the motivation of considering it as an alternative choice to explain the recent accelerating phase of the Universe. Exact solutions are obtained to discuss the evolution of the Universe by considering various forms of particle creation rate* Γ*. We obtain the best-fit values of the model parameters through the MCMC method by the use of the EMCEE python package on the latest observational data. We discuss the cosmographic parameters and* Om *to distinguish our model from other standard dark energy models. We analyze the model by applying the Akaike information criterion (AIC) and Bayesian information criterion (BIC) based on the penalization associated with the number of parameters. We also discuss the thermodynamics of the HDE model with matter creation and find that the model satisfies the GSL of thermodynamics under certain conditions.*

[1]This chapter is based on **two** research papers "Observational constraints on holographic dark energy with matter creation, *Astrophysics and Space Science* **365**, 84 (2020)" and "Holographic dark energy, matter creation, and cosmic acceleration, *Physical Review D* **102**, 123537 (2020)".

4.1 Introduction

As discussed in the earlier chapters, a new candidate to dynamical DE, based on the holographic principle of quantum gravity, was proposed by 't Hooft [67] to overcome the shortcomings of the standard ΛCDM model like fine-tuning and cosmic coincidence problem [35, 305]. According to the holographic principle, the number of degrees of freedom, which is finite in a bounded system, has a relation with the area of its boundary [68, 70]. This class of model is called the holographic dark energy (HDE) model in which the UV cutoff of DE is related to an IR cutoff. The HDE models have been defined and discussed in detail in section 1.8.1. The HDE model suffers the choice of IR cut-off problem. The HDE model with Hubble horizon as an IR cut-off is not able to explain the current accelerated expansion [66]. However, the HDE models with other IR cut-off, e.g., particle horizon, event horizon, apparent horizon, etc. describe the accelerated phenomena of the evolution of the Universe and are in agreement with the observational data [66, 72, 84, 86, 91–105, 306].

Just like the early-time cosmic acceleration associated with inflation, negative pressure can be seen as a possible driving mechanism for the late-time accelerated expansion of the Universe as well. One of the earliest alternatives that could provide a mechanism producing such accelerating phase is through a negative pressure produced by viscous or particle production effects. Adiabatic matter creation is a non-equilibrium thermodynamical process that makes use of ideas of the thermodynamics of open systems in the context of cosmology. The merits of the matter creation with respect to usual DE ideology are (a) the former has a strong physical basis namely non-equilibrium thermodynamics, while the latter (DE) has not, and (b) the matter creation mechanism unites the dark sector (DE and DM) since a single dark component (the dark matter) needs to be introduced into the cosmic fluid and thus it contains only one free parameter.

In gravitationally induced matter creation, by assuming that dark matter particles are produced by a time-varying gravitational field, it is possible to obtain a late-time acceleration composed only by pressureless fluids, like baryons and cold dark matter [225–229, 307, 308]. The particle creation scenario has a strong physical basis: non-equilibrium thermodynamics. Additionally, the study of the effects of adiabatic particle production in the cosmic microwave background level shows a close behavior to that of ΛCDM [309]. Many authors [230, 231] have explored the scenarios of matter

creation in cosmology, but here we are particularly interested in the gravitationally induced particle creation scenario in which some specific choices of the particle creation rate have been assumed. Some authors [236, 237, 239, 310–313] have discussed the matter creation cosmology with different forms of matter creation rate. In these works, it has been shown that phenomenological particle creation can explain not only the present era of cosmic acceleration but also provide a viable alternative to the concordance ΛCDM model. Recently, Singh and Kaur [314] have studied matter creation cosmology in Brans-Dicke theory and constrained the model with a combined set of observational data.

In this chapter, we consider the cosmological consequences due to adiabatic matter creation mechanism in HDE model with Hubble horizon as an IR cut-off. It has been observed that the HDE model with Hubble horizon as an IR cut-off is not consistent with the current observations. Therefore, instead of assuming other IR cut-offs, we have included the matter creation mechanism in the HDE model with the same Hubble horizon as an IR cut-off with the possibility that this model would be consistent with the current observations. We have considered constant and variable particle creation rates and have solved the field equations to obtain the exact solution. We have discussed the evolution and dynamics of the model by constraining the model parameters through the latest observational data. We have plotted the trajectories of the scale factor, matter density parameter, and deceleration parameter for best-fit values of model parameters. We have compared our model with the standard ΛCDM model. We have also plotted the trajectory of the Hubble evolution of our model and ΛCDM with an error bar from Hubble data. As a comparison, the models with matter creation have been examined with the selection criteria of AIC and BIC.

The chapter has been organized as follows: In Section 4.2, we have presented the HDE model with matter creation. Section 4.3 has divided into three subsections. In Subsection 4.3.1, we have presented the solution of the HDE model with creation rate, $\Gamma = 3\beta H$ and discussed the evolution of the model. In subsection 4.3.2, we have discussed the model with constant creation rate. Subsection 4.3.3 has dealt with a more general form of particle creation rate. Finally, we present the summary of our work in Section 4.4.

4.2 HDE Model with Matter Creation

In a spatially flat, homogeneous, and isotropic FLRW line element given by (2.2.1), the Friedmann and conservation equations can be written, respectively, as

$$3H^2 = \rho, \tag{4.2.1}$$

and

$$\dot{\rho} + 3H(\rho + p) = 0, \tag{4.2.2}$$

where $\rho = \rho_m + \rho_d$ and $p = p_c + p_d$ are the total energy density and pressure, respectively. Here, ρ_m is the energy density of dark matter, ρ_d the energy density of HDE, p_d is the pressure of HDE and p_c is the pressure due to the matter creation which is discussed in section 1.10 and defined by (1.10.2).

We consider that there is no interaction between the two fluids. Therefore, the energy conservation equation (4.2.2) for dark matter and HDE conserve separately, that is,

$$\dot{\rho}_m + 3\rho_m H = \rho_m \Gamma, \tag{4.2.3}$$

$$\dot{\rho}_d + 3(\rho_d + p_d)H = 0. \tag{4.2.4}$$

In this chapter, we consider the IR cut-off as the inverse of Hubble scale ($L = H^{-1}$) in the relation $\rho_d = 3b^2 M_p^2 L^{-2}$ given by (1.8.3) so that the corresponding energy density is given by [86]

$$\rho_d = 3b^2 H^2. \tag{4.2.5}$$

Cosmic inflation and the accelerated expansion of the Universe can be characterized by the equation of state (EoS) of dark energy. Since we consider the Universe to be filled with perfect fluid, therefore, we have a linear EoS, $p_d = \omega_d \rho_d$ for the dark energy, where ω_d is the EoS parameter. The condition for accelerated expansion $\ddot{a} > 0 \Rightarrow p < (-1/3)\rho$. It has been observed that the linear dark energy EoS reveals by Supernova [315].

Therefore, assuming the linear EoS for HDE, and using (1.10.2), (4.2.3) (4.2.4) and (4.2.5), Eq. (4.2.1) gives the following evolution equation:

$$\dot{H} + \frac{3}{2}\left[(1-b^2)\left(1 - \frac{\Gamma}{3H}\right) + (1+\omega_d)b^2\right] H^2 = 0. \tag{4.2.6}$$

Let us discuss how the matter creation rate, Γ modifies the evolution of the HDE model with matter creation as compared to the case of the HDE model without matter creation.

As already mentioned, the HDE model has been proposed on the basis of duality between UV cut-off and IR cut-off. The UV cut-off is related to the vacuum energy, and the IR cut-off is related to the large scale of the Universe. Hsu [86] studied the HDE model with Hubble horizon as an IR cut-off and found that the HDE model with Hubble horizon as an IR cut-off is not able to explain the current accelerated expansion. He found the dark energy EoS parameter $\omega_d = 0$, which is not consistent with the current observations. In what follows, let us review the HDE model with Hubble scale without matter creation.

In the absence of matter creation, i.e., taking $\Gamma = 0$, Eq. (4.2.6) gives the solution of the Hubble parameter,

$$H = H_0 \left(\frac{a_0}{a}\right)^{\frac{3k_0}{2}} = H_0(1+z)^{\frac{3k_0}{2}}, \tag{4.2.7}$$

where $k_0 = (1+b^2\omega_d)$. From the above equation, the scale factor can be obtained as

$$a = a_0 \left[1 + \frac{3k_0}{2} H_0 (t - t_0)\right]^{\frac{2}{3k_0}}, \tag{4.2.8}$$

which shows that the expansion of the Universe is of power-law form. The deceleration parameter gives

$$q = (3k_0 - 2)/2, \tag{4.2.9}$$

which is constant. Therefore, no transition redshift in the Universe will be achieved when the Hubble horizon is taken as the IR cut-off. The evolution of the scale factor is shown in Fig. 4.3, which shows decelerated expansion throughout the evolution.

To remedy the situation, many authors [101, 103, 306] proposed different IR cut-off like particle horizon, event horizon, Ricci scalar, etc., to discuss the accelerating Universe. However, the Hubble horizon is a natural choice of cosmological length scale. Therefore, instead of considering any other IR cut-off or interaction between the fluids as did by many authors, we restrict ourselves to the Hubble horizon as an infrared cut-off but in the presence of gravitationally induced matter creation to realize an accelerated expansion of the Universe, a transition from the past decelerated expansion to recent accelerated expansion and cosmic observational compatible model. The main advantage of considering HDE with matter creation is the introduction of another free parameter, thus providing an extra degree of freedom in the process of constructing a

physical interpretation of the solution. The evolution of the matter creation model has been tested by the latest observational data sets.

4.3 Solution of HDE Model with Matter Creation

In the presence of matter creation, Eq. (4.2.6) can be fully solved once the particle creation rate Γ is specified. In this chapter, we consider the HDE model driven by three different forms of the particle creation rate. First, we consider Γ as a function of the Hubble parameter and then for the second case we consider Γ as some constant, and finally, for the third case, we consider Γ as a linear combination of the current value of the Hubble parameter and the Hubble function.

4.3.1 HDE Model with $\Gamma = 3\beta H$

In order to investigate the effect of the particle creation on the Universe dynamics, we firstly consider the ansatz for the particle creation rate of the form [247] (hereafter *CHDE1 model*)

$$\Gamma = 3\beta H, \tag{4.3.1}$$

where β is a positive constant. Using (4.3.1) into (4.2.6), the solution of Hubble parameter in terms of redshift is given by

$$H(z) = H_0\,(1+z)^{\frac{3k_1}{2}}, \tag{4.3.2}$$

where $k_1 = (1-\beta+\beta b^2+b^2\omega_d)$. Integrating (4.3.2), we obtain the scale factor $a(t)$ as

$$a(t) = \left[1+\frac{3}{2}k_1 H_0(t-t_0)\right]^{\frac{2}{3k_1}}. \tag{4.3.3}$$

From the above equation, we can see that the scale factor is of power-law form, i.e. $a \propto t^m$ for positive constant m. While this model predicts acceleration for $k_1 < 2/3$, it does not allow a transition from deceleration to acceleration, as required by Type Ia supernova. Using the value of $a(t)$, the deceleration parameter is given by $q = (3k_1-2)/2$, which is constant. The constant value of q implies that the CHDE1 model does not show any transition throughout the evolution. Thus, the CHDE1 model with $\Gamma = 3\beta H$ shows contradiction with Type Ia supernovae observations.

4.3.2 HDE Model with $\Gamma = 3\delta H_0$

According to the observations, the phase transition plays a vital role in describing the evolution of the Universe. However, we have observed that HDE model with Hubble horizon as IR cutoff or HDE model with the particle creation rate $\Gamma = 3\beta H$ is unable to give the phase transition. Therefore, in this subsection our purpose is to discuss a suitable form of Γ that would give the phase transition.

We assume the particle creation rate of the form [246] (hereafter *CHDE2 model*)

$$\Gamma = 3\delta H_0, \tag{4.3.4}$$

where δ is order unity dimensionless constant and H_0 is the present value of the Hubble parameter.

Using (4.3.4) into (4.2.6), we obtain the following dimensionless equation:

$$h' + \frac{3}{2}k_0 h = \frac{3}{2}\delta(1-b^2), \tag{4.3.5}$$

where $h = \frac{H}{H_0}$ is the dimensionless Hubble parameter and a prime denotes $\frac{d}{d\,ln\,a}$.

Considering the relation $h(a_0) = 1$, we can solve equation (4.3.5) analytically to obtain

$$h(a) = \frac{(1-b^2)\delta}{k_0} + \left\{1 - \frac{(1-b^2)\delta}{k_0}\right\}\left(\frac{a}{a_0}\right)^{-\frac{3k_0}{2}}, \tag{4.3.6}$$

where $k_0 \neq 0$. Integrating (4.3.6), we obtain the scale factor $a(t)$ as

$$a(t) = \left[1 + \frac{k_0}{(1-b^2)\delta}\left\{e^{\frac{3}{2}(1-b^2)\delta H_0(t-t_0)} - 1\right\}\right]^{\frac{2}{3k_0}}. \tag{4.3.7}$$

From the above equation, we can see that at the early time (when $t \to 0$), the scale factor

$$a(t) \to \left[1 + \frac{3}{2}k_0 H_0(t-t_0)\right]^{\frac{2}{3k_0}}$$

which is of power-law form. In the late time (when $t \to \infty$), the scale factor $a(t) \to e^{\frac{(1-b^2)\delta H_0(t-t_0)}{k_0}}$ which corresponds to the de Sitter Universe. Thus, the CHDE2 model can explain early deceleration and late time accelerating phase with constant matter creation rate.

The Hubble parameter in terms of redshift z can be given as

$$\frac{H(z)}{H_0} = \left[\frac{(1-b^2)\delta}{k_0} + \left\{1 - \frac{(1-b^2)\delta}{k_0}\right\}(1+z)^{\frac{3}{2}k_0}\right]. \tag{4.3.8}$$

To study the decelerated or accelerated epochs and the transitions between them, we assume $H_0(t-t_0) = y$. The second order derivative of the scale factor $a(t)$ with respect to y gives

$$\frac{d^2a}{dy^2} \propto \left[2 - 3(1-\delta+\delta b^2 + b^2\omega_d)e^{\frac{3}{2}(b^2-1)\delta y}\right] \tag{4.3.9}$$

From (4.3.9), we can check the behavior of the scale factor so that the Universe shows decelerated expansion in the early time followed by a transition to accelerated expansion in the late time. The conditions satisfying above description are

$$(b^2-1)\delta > 0 \text{ and } (1-3\delta+3\delta b^2+3b^2\omega_d) < 0. \tag{4.3.10}$$

These conditions will be used to find the best fit values of model parameters.

In this model, the deceleration parameters can be obtained as

$$q = -1 + \frac{3}{2}[k_0 - (1-b^2)\delta]e^{\frac{-3}{2}(1-b^2)\delta H_0(t-t_0)} \tag{4.3.11}$$

In terms of redshift z, q is given by

$$q(z) = -1 + \frac{3}{2}\frac{k_0 - (1-b^2)\delta}{\left[1 + \frac{(1-b^2)\delta}{k_0}\left\{(1+z)^{\frac{-3}{2}k_0} - 1\right\}\right]}. \tag{4.3.12}$$

It can be seen that $q(z) \to -1$ as $z \to -1$. In the absence of matter creation ($\delta = 0$), this expression yields $q = (3k_0 - 2)/2$, which is same as given in equation (4.2.9). While, in the absence of dark energy ($b = 0$), we find

$$q(z) = -1 + \frac{3}{2}\frac{(1-\delta)}{\left[1 + \delta\left\{(1+z)^{-\frac{3}{2}} - 1\right\}\right]}. \tag{4.3.13}$$

Thus, we find that the existence of a transition redshift at late times depends exclusively on the δ parameter, i.e., on the matter creation. We can find the current value of q by putting $z = 0$ in (4.3.12) as

$$q_0 = \frac{(1-3\delta+3\delta b^2+3b^2\omega_d)}{2}. \tag{4.3.14}$$

Let us find the redshift, z_{tr}, at which the Universe transits from the decelerating phase and enters into the current accelerating phase, i.e., $q(z)=0$. It is given by

$$z_{tr}=-1+\left[1+\frac{k_0(1-3\delta+3\delta b^2+3b^2\omega_d)}{2\delta(1-b^2)}\right]^{\frac{-2}{3k_0}} \tag{4.3.15}$$

The cosmic time of transition 't_{tr}' between the decelerated to the accelerated epochs can be given by

$$t_{tr}=t_0+\frac{2}{3(b^2-1)\delta H_0}\ln\left(\frac{2}{3(1-\delta+\delta b^2+b^2\omega_d)}\right). \tag{4.3.16}$$

The effective equation of state parameter (EoS), ω_{eff} can be obtained using the standard relation [316]

$$\omega_{\text{eff}}=-1-\frac{1}{3}\frac{2a}{h}\frac{dh}{da}, \tag{4.3.17}$$

where $h=H/H_0$ is the weighted Hubble parameter. For this model, ω_{eff}, is given by

$$\omega_{\text{eff}}(z)=-1+\frac{k_0+(b^2-1)\delta}{\left[1+\frac{(1-b^2)\delta}{k_0}\left\{(1+z)^{-\frac{3}{2}k_0}-1\right\}\right]}. \tag{4.3.18}$$

The condition of EoS parameter, $\omega<-1/3$ for acceleration of the present Universe can be obtained by taking $z=0$ in (4.3.18), which is given by

$$3\omega_{\text{eff}}+1=(1-3\delta+3\delta b^2+3b^2\omega_d)<0. \tag{4.3.19}$$

Data analysis and results

We present the statistical analysis to constraint the CHDE2 model with constant matter creation. In order to extract the observational constraints and incorporate the data sets statistically, we use the Markov chain Monte Carlo (MCMC) package EMCEE to perform the numerical analysis of our model [317]. In our analysis, we have considered the value of the Hubble constant as $H_0=67.8$ *Km/s/Mpc* [20]. We also use the value of constant $b=0.50$ which is in the range $b=0.495\pm0.039$ obtained by Li et al. [318] from the Planck constraints on HDE model. Following are the publicly available data sets that we exploit in our statistical analysis (see, section 1.13 for detail).

- *Supernova Type Ia (SNe-JLA):* SNe data were the first to indicate that our Universe is accelerating. For CHDE2 model, we include the latest Joint Light Curve analysis (JLA) sample comprising 31 data points in the redshift range

$z \in [0.01, 1.3]$ [258].

- *Observational Hubble data (OHD):* For OHD data set, we use the 43 measurements of the Hubble parameter values in the interval $0 < z < 2.5$, see [260].

- *Baryon acoustic oscillations and cosmic microwave background (BAO/CMB):* We use the combined BAO/CMB data from different observational missions [261]. We take the sample of BAO distances measurements from SDSS(R) [262], the 6dF Galaxy survey [263], BOSS CMASS [264] and three parallel measurements from WiggleZ survey [265]. We combine theses results with the Planck 2015 [20].

We use the Chi-square method to find the best fit value of model parameters. The χ^2 is defined in equations (1.13.3), (1.13.4) and (1.13.8) for SNe, OHD and BAO/CMB, respectively. The parameters space for our model is $\{\delta, \omega_d, M\}$. Here, M is a free normalization parameter used in SNe Ia observation. We minimize χ^2_{tot} to obtain the best-fit values of the free parameters. We have presented the observational summary in Table 4.1 and one of the contour plots is shown in Fig. 4.1 with $1\sigma(68.3\%)$ and $2\sigma(95.4\%)$ confidence level.

We assess the viability of CHDE2 model against a given reference model. For

Table 4.1: The data fitting results of the free parameters in the CHDE2 model

Parameter	SNe+OHD+BAO/CMB	SNe+BAO/CMB	SNe+OHD
δ	$0.673^{0.010}_{-0.010}$	$0.584^{0.019}_{-0.021}$	$0.750^{0.023}_{-0.038}$
ω_d	$-0.002^{0.002}_{-0.003}$	$-0.010^{0.007}_{-0.015}$	$-0.051^{0.040}_{-0.085}$
M	$24.994^{0.018}_{-0.018}$	$25.020^{0.017}_{-0.019}$	$24.963^{0.019}_{-0.018}$

this purpose we use two standard information criteria- Akaike Information Criterion (AIC) [266] and Bayesian or Schwarz Information Criterion (BIC) [267] defined as in section 1.13 by Eqs. (1.14.2) and (1.14.3).

We present the obtained results of AIC and BIC in the Table 4.2 with consideration of the ΛCDM as the referring model. According to the values of ΔAIC and ΔBIC, we can see that $2 < \Delta AIC < 4$ for the combined data of $SNe + OHD$, and hence the CHDE2 model has average evidence in favor with respect to the reference model of ΛCDM cosmology corresponding to $SNe + OHD$. Concerning ΔBIC corresponding to

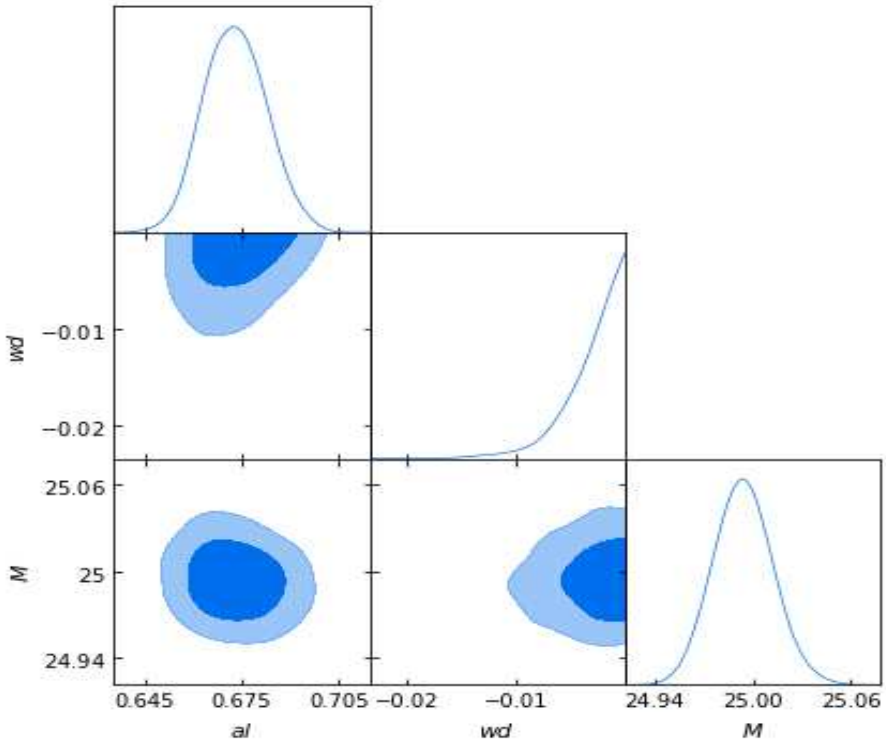

Figure 4.1: 1σ and 2σ confidence level contour plots for the CHDE2 model parameters using the observational data SNe+OHD+BAO/CMB. The labels *al* and *wd* denote δ and ω_d parameters, respectively.

combined data of SNe and OHD, the CHDE2 model has $2 < \Delta BIC < 6$ which means that it has positive evidence against it. For all other cases, the values of ΔAIC and ΔBIC are ruled out completely. The reduced $\chi^2_{red} = \chi^2_{min}/(\mathbb{N} - d)$, where $\mathbb{N}$ is the total number of data and d is the degree of freedom, listed in Table 4.2 shows that the CHDE2 model provides a very good fit to these data.

Next, we discuss the evolution, cosmographic and $Om(z)$ analysis of HDE model

Table 4.2: Summary of the AIC and BIC values and their differences for CHDE2 model from the reference model of ΛCDM

Data	χ^2	χ^2_{red}	AIC	BIC	ΔAIC	ΔBIC
SNe+OHD+BAO/CMB	86.72	1.09	90.72	95.50	58.83	59.01
SNe+BAO/CMB	34.45	0.91	38.45	41.72	16.16	16.15
SNe+OHD	33.78	0.46	37.78	42.39	3.33	3.18

with constant matter creation by considering the best-fit values given in Table 4.1.

Evolution of the model

We plot the evolution of the scale factor in Fig. 4.2 for the best-fit model parameters obtained from different observational data sets. From the figure, it can be observed

that the expansion starts with an accelerated rate in early time followed by deceleration and then the exponential acceleration in the late time. In Fig. 4.2, the dot on the trajectory denotes the transition point whose values are listed in Table 4.3.

In Fig. 4.3, we plot the evolution of the scale factor for a different combination of models to compare their behaviors. The evolution of the HDE with matter creation ($\delta \neq 0$ and $b \neq 0$) and matter-dominated model with matter creation ($\delta \neq 0$ and $b = 0$) approximately coincide to each other. These two trajectories show that both the models evolve with early acceleration, medieval deceleration, and then late-time acceleration. The other two evolutions, the HDE model without matter creation ($\delta = 0$ and $b \neq 0$) and matter-dominated model ($\delta = 0$ and $b = 0$) decelerate throughout their evolutions.

We also introduce the matter density parameter Ω_m, which is defined by $\Omega_m = \rho_m/\rho_c$, where $\rho_c = 3H_0^2$ is the critical energy density. Using (4.2.1) and (4.3.8), we obtain

$$\Omega_m(a) = (1-b^2)\left[\frac{(1-b^2)\delta}{k_0} + \left\{1 - \frac{(1-b^2)\delta}{k_0}\right\}\left(\frac{a}{a_0}\right)^{\frac{-3}{2}k_0}\right]^2, \tag{4.3.20}$$

where $\delta \neq 0$ and $b \neq 0$. From the above equation, it is to be noted that for $\delta = 0$ and $b = 0$, i.e., in the absence of both HDE and matter creation, the matter density parameter follows $\Omega_m \sim (a/a_0)^{-3}$, which corresponds to the matter dominated phase. However, in the absence of matter creation only, i.e. putting $\delta = 0$ and $b \neq 0$, $\Omega_m \sim (1-b^2)\left(\frac{a}{a_0}\right)^{\frac{-3}{2}k_0}$. In the presence of matter creation, i.e., $\delta \neq 0$ and $b = 0$, we have $\Omega_m \sim [\delta + (1-\delta)(a/a_0)^{-3}]$. The evolution of Ω_m with the scale factor for the best fit values are shown in Fig. 4.4 which shows that how does the matter creation influence the behavior of Ω_m. In each case, as $a \to 0$, the matter density diverges which indicates the existence of the Big-Bang at the origin of the Universe.

In Fig. 4.5, we plot the evolution of the deceleration parameter q with respect to the redshift z for the best-fitted values of the parameters. From the figure, we can observe that the trajectories of q change in sign from positive to negative as the redshift decreases. This implies that the CHDE2 model shows transition from decelerated phase to accelerated phase. In Fig. 4.5, a dot on each trajectory denotes the current value, q_0 at $z = 0$. The current values of q are given in Table 4.3 for different set of data, which lies in $-1 < q < 0$.

Using (4.3.18) we plot the trajectory for ω_{eff} with respect to the redshift z as shown in Fig. 4.6. It is observed that as $z \to -1$, $\omega_{\text{eff}} \to -1$, which means that the HDE

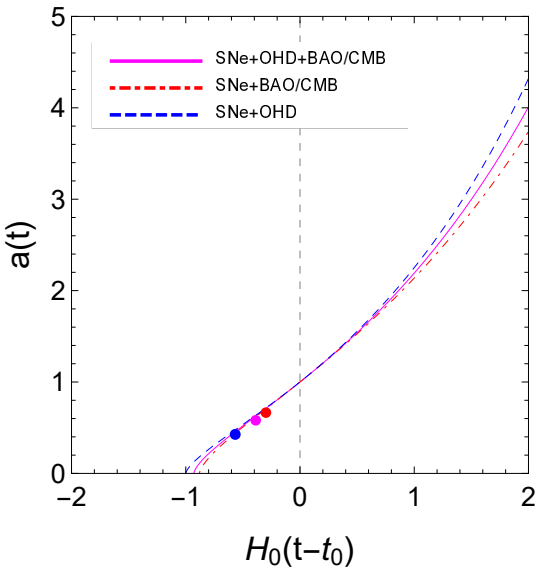

Figure 4.2: Evolution of the scale factor as a function of time for different combinations of data sets in CHDE2 model. A dot on each trajectory denotes the transition scale factor, a_{tr}.

model with constant matter creation behaves as a de Sitter model in late-time. It is also observed that the model is free from big-rip singularity as each of the trajectories does not cross the phantom divide line. A dot on each trajectory in the figure denotes the current EoS parameter value, $\omega_{\text{eff}}(z=0)$. The current values of ω_{eff} for the set of combined data are listed in Table 4.3.

In Fig. 4.7, we plot the error bars of the Hubble data set to compare our model with the ΛCDM model. The fitting achieved from our statistical analysis for combined data $SNe+OHD+BAO/CMB$ is more compatible with the Hubble data for the HDE model with constant matter creation whereas the cosmic expansion differs appreciably in the case of $SNe+OHD$ and $SNe+BAO/CMB$ with increasing z. The Hubble function is a monotonically increasing function of the redshift for all best-fit values of parameters.

Let us calculate the age of the Universe using best-fit values of parameters. The age of the Universe in terms of redshift is given by $t(z)=T(z)/H_0$, where

$$T(z)=\int_z^{\infty}\frac{dz'}{(1+z')(H(z')/H_0)}. \tag{4.3.21}$$

For ΛCDM model, the age parameter is [206]

$$T(z)=\int_z^{\infty}\frac{dz'}{(1+z')[\Omega_{m0}(1+z')^3+(1-\Omega_{m0})]^{1/2}} \tag{4.3.22}$$

Using equation (4.3.8) into (4.3.21), we plot the age of the Universe with respect to the redshift z for the best-fit values as shown in Fig. 4.8. The current ages of the

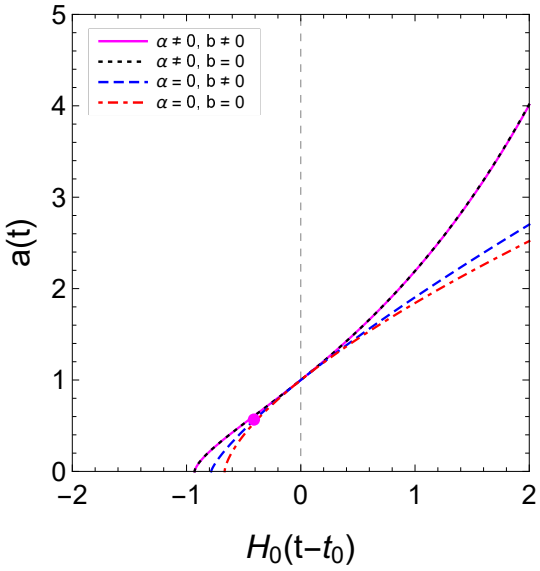

Figure 4.3: Evolution of the scale factor as a function of time for different models where the combined observational data of $SNe + OHD + BAO/CMB$ is used. A dot on the trajectory denotes the transition scale factor, a_{tr}.

Universe t_0 are given in Table 4.3 using different combined set of data. The age of the Universe corresponding to combined $SNe + OHD + BAO/CMB$ data set is found to be $t_0 = 13.393\ Gyr$, which is comparatively same as predicted by ΛCDM model.

Table 4.3: The numerical values of a_{tr}, z_{tr}, q_0, $\omega_{\text{eff}}(z=0)$ and $t_0(Gyr)$ using the best-fit result of CHDE2 model parameters

Data	a_{tr}	z_{tr}	q_0	$\omega_{\text{eff}}(z=0)$	t_0
SNe+OHD+BAO/CMB	0.620	0.611	-0.258	-0.505	13.393
SNe+BAO/CMB	0.737	0.356	-0.161	-0.440	12.691
SNe+OHD	0.504	0.982	-0.363	-0.575	14.414

Cosmographic and Om(z) analysis

Now, we present a comparative study of CHDE2 model with other standard models of dark energy. Using (4.3.8) in (1.12.1), the statefinder parameters are calculated to

$$r = 1 + \frac{9(\delta(1-b^2)-k_0)\left(1-b^2\omega_d\right)}{4\,e^{\frac{3}{2}\delta(1-b^2)H_0(t-t_0)}} + \frac{9(\delta(1-b^2)-k_0)^2}{4\,e^{3\delta(1-b^2)H_0(t-t_0)}} \tag{4.3.23}$$

$$s = \frac{\frac{(\delta(1-b^2)-k_0)\left(1-b^2\omega_d\right)}{2\,e^{\frac{3}{2}\delta(1-b^2)H_0(t-t_0)}} + \frac{(\delta(1-b^2)-k_0)^2}{2\,e^{3\delta(1-b^2)H_0(t-t_0)}}}{(k_0-\delta(1-b^2))e^{\frac{-3}{2}\delta(1-b^2)H_0(t-t_0)}-1} \tag{4.3.24}$$

Equations (4.3.23) and (4.3.24) show that in the limit $(t-t_0)\to\infty$, the statefinder parameters $\{r,s\}\to\{1,0\}$, a value corresponding to the ΛCDM model. Therefore, the HDE model resembles the ΛCDM model in the future. The trajectory for the $s-r$ plane

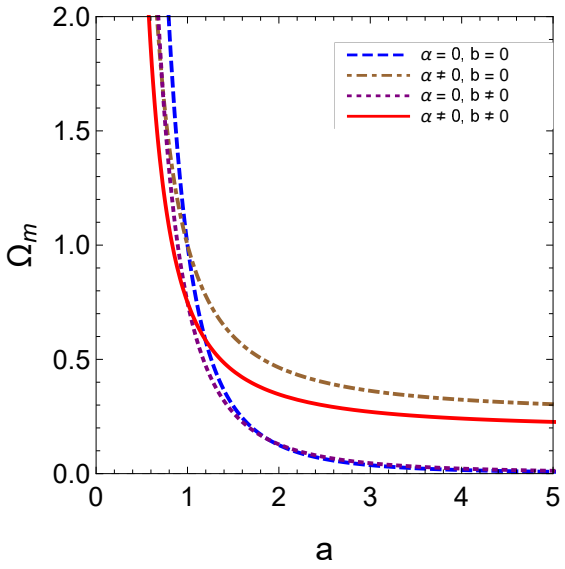

Figure 4.4: Evolution of the mass density parameter with the scale factor for different combinations of best fit values of the CHDE2 model parameters where the combined data $SNe+OHD+BAO/CMB$ is used.

for the best-fit parameters are shown in Fig. 4.9. From the figure, it can be observed that in early time the trajectories lying in the region corresponding to $r<1, s>0$, which represents the quintessence region. The model is converging to the ΛCDM model in the late time of its evolution.

We plot the trajectory of $\{r,q\}$ in $q-r$ plane for best-fit parameters obtained from a different set of observational data as shown in Fig. 4.10. The SCDM model and steady-state (SS) model correspond to fixed points $\{r,q\}=\{1,0.5\}$ and $\{r,q\}=\{1,-1\}$, respectively. The horizontal line at $r=1$ corresponds to the ΛCDM model. We can observe that the trajectories go from a positive value of q to a negative value, which explains the transition from decelerated phase to the accelerated one. The CHDE2 model approaches the SS model in late time.

The geometrical investigation discussed above on the dark energy model has been further extended by considering some new model-independent dimensionless geometrical parameters, called cosmographic parameters (CP), discussed in section 1.12.2 and defined by equation (1.12.2).

We discuss the variations of the cosmographic parameters with respect to redshift z by plotting their trajectories for combined data set of $SNe+OHD+BAO/CMB$ as shown in Fig. 4.11. From the figure, one can notice that during the entire evolution of the Universe, the trajectories of j and l remain positive, and for l it decreases sharply from the high value at the early epoch. The trajectory of s shows that it is negative in the early phase of the evolution and then gradually increases and becomes positive,

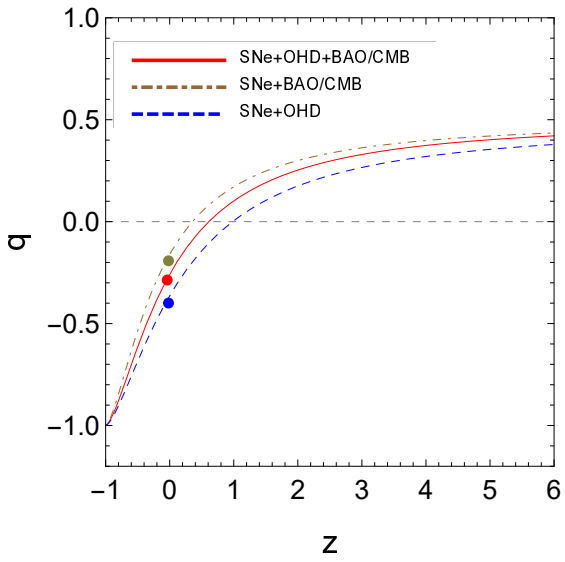

Figure 4.5: Plot of the deceleration parameter q as a function of redshift z for the best-fit values of parameters in CHDE2 model. A dot on each trajectory denotes the current value, q_0.

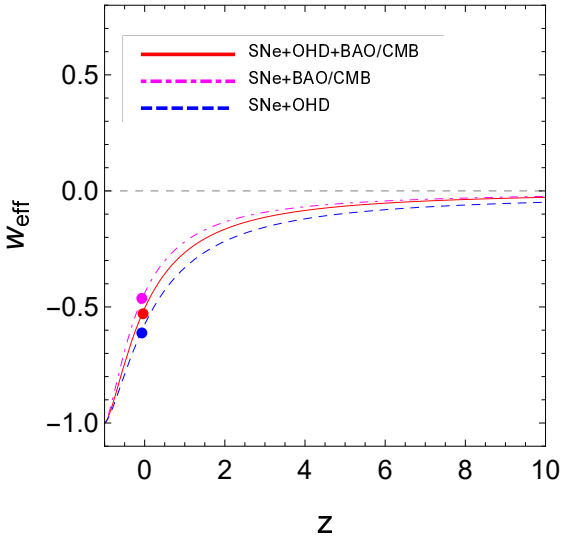

Figure 4.6: Behavior of effective equation of state parameter ω_{eff} with respect to the redshift z for best-fit values of parameters in the CHDE2 model. A dot on each trajectory denotes the current value, $\omega_{\text{eff}}(z=0)$.

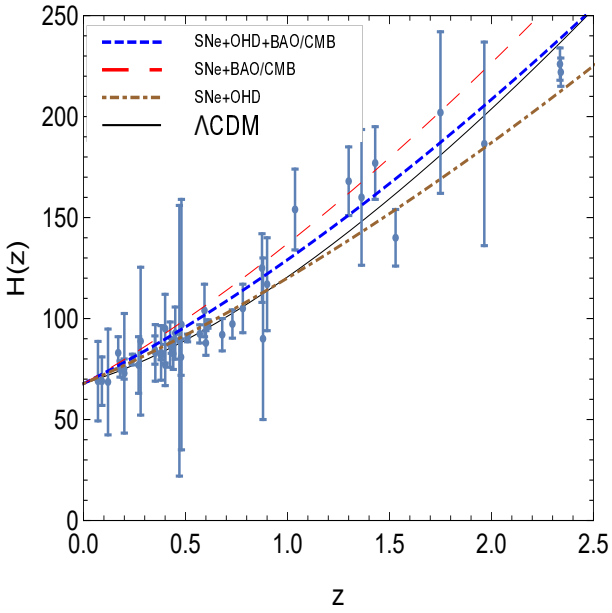

Figure 4.7: The Hubble evolution and Λ*CDM* model with error bar plots from Hubble data for CHDE2 model.

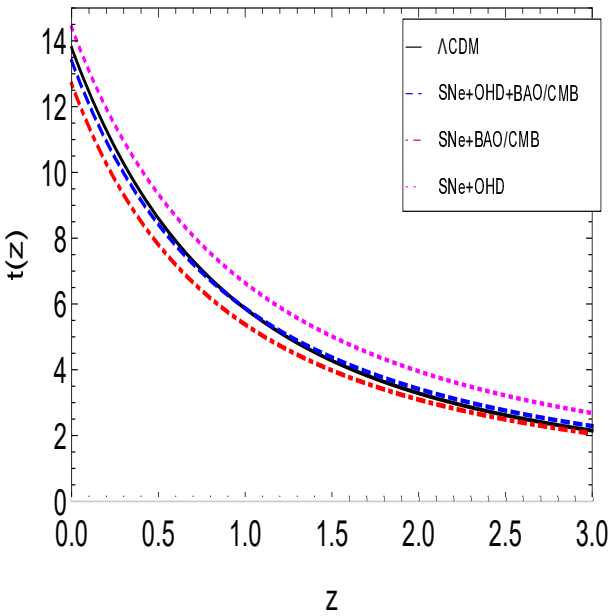

Figure 4.8: The age of Universe as a function of redshift for best fit values obtained from different combined observational data set in CHDE2 model. Black solid curve shows ΛCDM model, blue dashed curve for $SNe+OHD+BAO/CMB$, magenta dotted curve for $SNe+OHD$ whereas red dashed-dotted curve shows $SNe+BAO/CMB$.

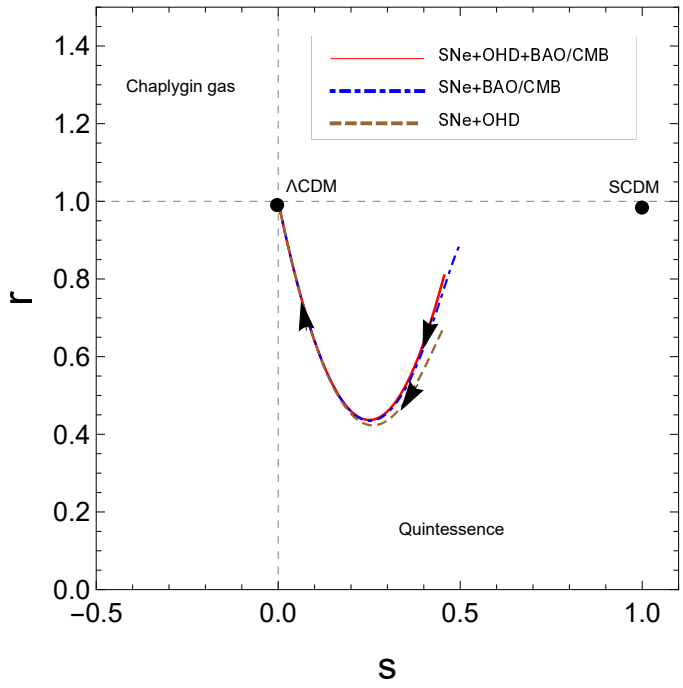

Figure 4.9: The evolutionary trajectories of $\{r,s\}$ in the $s-r$ plane corresponding to the best-fit parameters of CHDE2 model. The arrow shows the direction of the evolution of the trajectory. It can be observed that the evolution of $\{r,s\}$ are approximately coincide for the best estimates from $SNe+BAO/CMB$, $SNe+OHD$ and $SNe+OHD+BAO/CMB$ data set.

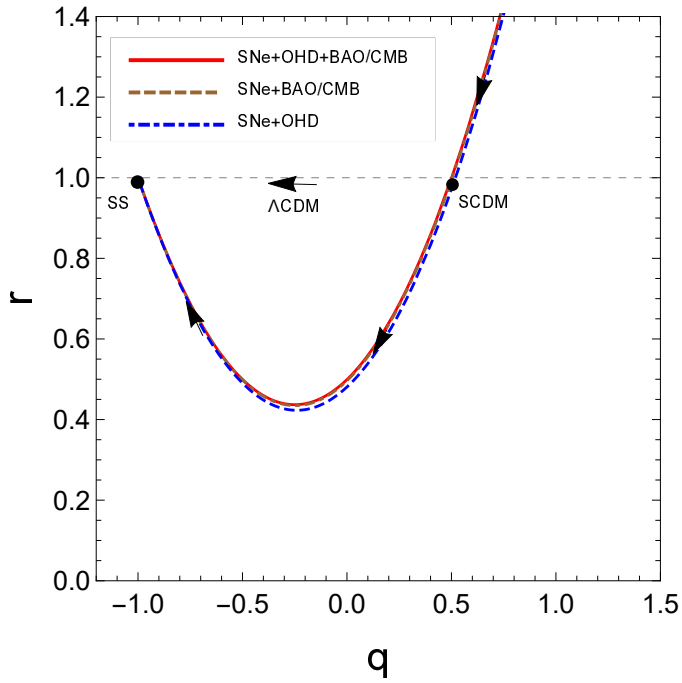

Figure 4.10: The evolutionary trajectories of $\{r,q\}$ in the $q-r$ plane corresponding to the best-fitted parameters of CHDE2 model. The arrow shows the direction of the evolution of the trajectory. The evolution of $\{r,q\}$ are approximately coincide for the best estimates from $SNe+BAO/CMB$, $SNe+OHD$ and $SNe+OHD+BAO/CMB$ data set.

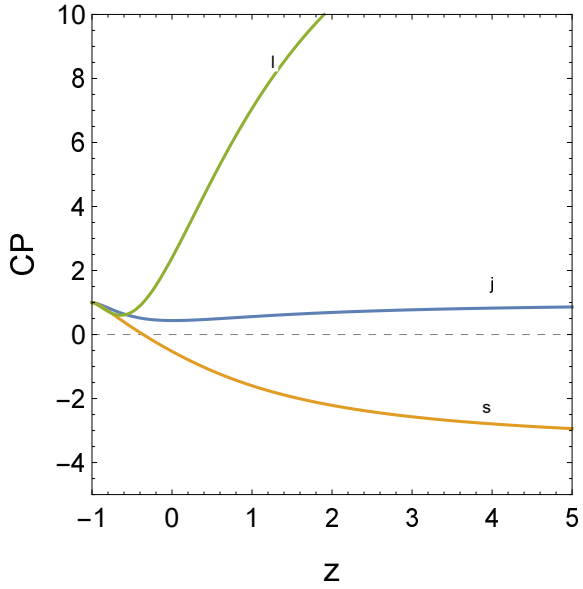

Figure 4.11: The cosmographic parameters j, s and l are plotted using the combined data of $SNe+OHD+BAO/CMB$ in CHDE2 model.

hence it shows the transition from negative values to positive values. In the late-time, j reaches 1 as z approaches to -1 which corresponds to the ΛCDM model. Similarly, other parameters s and l also approach 1 in the late-time of evolution. So, based on the cosmographic analysis, we can deduce that the CHDE2 model is different from the ΛCDM model at the present time $z=0$, but in the late-time, it converges to the ΛCDM model.

One more independent diagnostic parameter, called Om, was discussed in section 1.12.3 to differentiate the dark energy models from ΛCDM. Using (4.3.8) in (1.12.3), we obtain

$$Om(z)=\frac{\left[\frac{(1-b^2)\delta}{k_0}+\left(1-\frac{(1-b^2)\delta}{k_0}\right)(1+z)^{\frac{3}{2}k_0}\right]^2-1}{(1+z)^3-1}, \tag{4.3.25}$$

We plot the trajectories of Om-diagnostic against the redshift z in Fig. 4.12. The negative slope of the trajectories of $Om(z)-z$ plane indicates the behavior similar to the quintessence model.

4.3.3 HDE Model with $\Gamma=3\delta H_0+3\beta H$

Many authors [236, 237, 307, 314] have studied the flat FLRW model by adding the constant term to $\Gamma=3\beta H$. The advantage of such form is that it is analytically described, and due to this feature we will consider it as an interesting choice for HDE model. It has been shown that such form of Γ solves the age problem and is also generically capable of accounting for the Type Ia supernova observation. Therefore,

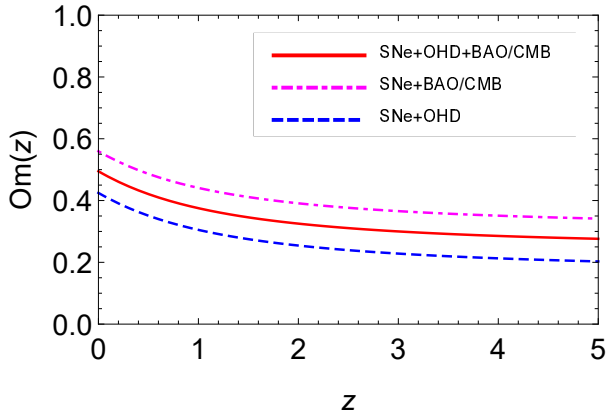

Figure 4.12: The evolutionary trajectories of $Om-z$ for best-fit model parameters of CHDE2 model.

we consider the following matter creation rate [236] (hereafter *CHDE3 model*)

$$\Gamma = 3\delta H_0 + 3\beta H. \tag{4.3.26}$$

where the parameter δ and β lies in the interval $[0,1]$. Using (4.3.26) into (4.2.6), we obtain the following dimensionless equation:

$$h' + \frac{3k_1}{2}h = \frac{3}{2}\delta(1-b^2), \tag{4.3.27}$$

where $k_1 = (1-\beta+\beta b^2+b^2\omega_d)$. We can solve equation (4.3.27) analytically to obtain

$$h(a) = \frac{(1-b^2)\delta}{k_1} + \left\{1 - \frac{(1-b^2)\delta}{k_1}\right\}\left(\frac{a}{a_0}\right)^{-\frac{3k_1}{2}}. \tag{4.3.28}$$

To obtain the scale factor $a(t)$, we integrate (4.3.28) in normalized unit at present time to get

$$a(t) = \left[1 + \frac{k_1}{(1-b^2)\delta}\left\{e^{\frac{3}{2}(1-b^2)\delta H_0(t-t_0)} - 1\right\}\right]^{\frac{2}{3k_1}}, \tag{4.3.29}$$

where $k_1 \neq 0$ and $b \neq \pm 1$. From (4.3.29), we can see that this model shows power-law form in the early time as the scale factor

$$a(t) \to \left[1 + \frac{3k_1}{2}H_0(t-t_0)\right]^{\frac{2}{3k_1}},$$

which is similar to that of $\Gamma = 3\beta H$. But as $t \to \infty$, the scale factor $a(t) \to e^{\frac{(1-b^2)\delta H_0(t-t_0)}{k_1}}$ which corresponds to the de Sitter Universe. This shows that the Universe has an

early deceleration followed by an accelerating phase in the late time of evolution. Thus, this form of the particle creation rate unifies the evolution of the Universe, i.e., transition from early deceleration to late time acceleration.

The Hubble parameter in terms of redshift z can be written as

$$H(z) = H_0 \left[\frac{(1-b^2)\delta}{k_1} + \left\{ 1 - \frac{(1-b^2)\delta}{k_1} \right\} (1+z)^{\frac{3k_1}{2}} \right]. \tag{4.3.30}$$

Next, we find the limiting conditions on the scale factor to study the transition of the Universe. Assuming $H_0(t-t_0) = y$, the second order derivative of the scale factor $a(t)$ with respect to y as

$$\frac{d^2a}{dy^2} \propto \left[2 - 3(k_1 - \delta + \delta b^2) e^{\frac{3}{2}(b^2-1)\delta y} \right]. \tag{4.3.31}$$

Now, the appropriate conditions which can explain early deceleration and followed by a transition to accelerated expansion in the late time, are given by

$$(1 - 3\delta - 3\beta + 3\delta b^2 + 3\beta b^2 + 3b^2\omega_d) < 0. \tag{4.3.32}$$

This condition will be used later on to find the best fit values of model parameters. The deceleration parameter q is obtained as

$$q(t) = -1 + \frac{3}{2}(k_1 - \delta + \delta b^2) e^{-\frac{3}{2}(1-b^2)\delta H_0 (t-t_0)}, \tag{4.3.33}$$

and in terms of redshift z, it is given by

$$q(z) = -1 + \frac{3}{2} \frac{(k_1 - \delta + \delta b^2)}{\left[1 + \frac{(1-b^2)\delta}{k_1} \left\{ (1+z)^{\frac{-3k_1}{2}} - 1 \right\} \right]}. \tag{4.3.34}$$

It is evident from Eq. (4.3.34) that $q(z)$ approaches to -1 in future. The present value of q can be obtained by putting $z = 0$ in (4.3.34) to get

$$q_0 = \frac{(1 - 3\delta - 3\beta + 3\delta b^2 + 3\beta b^2 + 3b^2\omega_d)}{2}. \tag{4.3.35}$$

The transition redshift z_{tr} can be obtained by putting $q = 0$ in (4.3.34) and given by

$$z_{tr} = \left[\frac{2\delta(1-b^2)}{2\delta(1-b^2) + k_1(1 - 3\delta - 3\beta + 3\delta b^2 + 3\beta b^2 + 3b^2\omega_d)} \right]^{\frac{2}{3k_1}} - 1. \tag{4.3.36}$$

It is to be noted that $q(z) = (3k_1 - 2)/2$ and $z_{tr} = -1$ for $\delta = 0$, which shows that the value of q is constant and there is no transition from deceleration to the acceleration phase. The transition would take place in infinite future. This gives a contradiction with Type Ia supernova observation (see, case I). This shows that the transition in finite late time is possible only if $\delta \neq 0$ or $b \neq \pm 1$.

The transition time 't_{tr}' can be obtained as

$$t_{tr} = t_0 + \frac{2}{3(b^2-1)\delta H_0} \ln\left(\frac{2}{3(k_1 - \delta + \delta b^2)}\right). \tag{4.3.37}$$

The effective equation of state (EoS) parameter can be obtained as

$$\omega_{\text{eff}}(z) = -1 + \frac{(k_1 - \delta + \delta b^2)}{\left[1 + \frac{(1-b^2)\delta}{k_1}\left\{(1+z)^{\frac{-3k_1}{2}} - 1\right\}\right]}. \tag{4.3.38}$$

For the present acceleration, ω_{eff} should satisfy the condition $\omega_{\text{eff}} < -1/3$ with $z = 0$ in (4.3.38), which is given by

$$3\omega_{\text{eff}} + 1 = (1 - 3\delta - 3\beta + 3\delta b^2 + 3\beta b^2 + 3b^2\omega_d). \tag{4.3.39}$$

Using (4.3.32), we find that $3\omega_{\text{eff}} + 1 < 0$.

Data analysis and results

In this section, we discuss the observational data sets that we employ to constraint the free parameters. We use the condition (4.3.32) to constraint the model parameters. Following are the publicly available data sets that we exploit in our statistical analysis.

- *Type Ia supernovae (Pantheon data):* Data from SNe Ia are an important tool for understanding the recent evolution of the Universe. For this model, we use the Pantheon sample, the latest compilation of SNe Ia, comprising 40 binned data points in the redshift region $z \in [0.014, 1.62]$ [319].
  The χ^2 for SNe Ia is defined as

$$\chi^2_{Pantheon} = \bar{m}^T C^{-1} \bar{m} \tag{4.3.40}$$

  where $\bar{m} = m_B - m_{th}$ with

$$m_{th} = 5\, log_{10} D_L + M, \tag{4.3.41}$$

and C is the covariance matrix of μ_{obs} given in [320]. The luminosity distance d_L is defined by $d_L = (c/H_0)D_L$, where

$$D_L = (1+z_{hel})\int_0^{z_{cmb}} \frac{H_0 dz'}{H(z',\theta)} \tag{4.3.42}$$

where θ represents the set of model parameters, z_{hel} is the heliocentric redshift and z_{cmb} is the redshift of the CMB rest frame.

- *Hubble Data (HD):* For the study of the cosmic expansion history, the measurement of Hubble parameter $H(z)$ got much attention from the researchers due to its model independent nature. In this paper, we use the 36 $H(z)$ measurements in which first 31 measurements are obtained from the cosmic chronometric method [321], three correlated measurements from the BAO signal in galaxy distribution [322], and the last two measurements determined from the BAO signal in Ly-α forest distribution alone or cross-correlated with quasistellar objects (QSOs) [323, 324].
  The χ^2 for 33 Hubble measurement is given by

$$\chi^2_{CC+Ly\alpha} = \sum_{i=1}^{33} \frac{[H_{obs}(z_i) - H_{th}(z_i)]^2}{\sigma_i^2}, \tag{4.3.43}$$

where $H_{th}(z_i)$ and $H_{obs}(z_i)$ represents theoretical and observed values respectively and σ_i^2 the standard deviation of each $H_{obs}(z_i)$.
The χ^2 for the 3 galaxy distribution measurements is given by

$$\chi^2_{gal} = A^T C^{-1} A \tag{4.3.44}$$

where C is the covariance matrix given by [322]

$$C = \begin{bmatrix} 3.65 & 1.78 & 0.93 \\ 1.78 & 3.65 & 2.20 \\ 0.93 & 2.20 & 4.45 \end{bmatrix}$$

and

$$A = \begin{bmatrix} H_{obs}(0.38) - H_{th}(0.38) \\ H_{obs}(0.51) - H_{th}(0.51) \\ H_{obs}(0.61) - H_{th}(0.61) \end{bmatrix}$$

Table 4.4: Fitting results for CHDE3 model

Parameters	Best-fit values
H_0	$67.516^{+1.396}_{-1.166}$
b	$0.049^{+0.106}_{-0.038}$
δ	$0.548^{+0.025}_{-0.030}$
β	$0.012^{+0.022}_{-0.009}$
ω_d	$-2.048^{+1.736}_{-5.073}$
M	$23.847^{+0.007}_{-0.009}$
χ^2_{min}	36.637
χ^2_{red}	0.516

So, the combined χ^2 for HD is

$$\chi^2_{HD} = \chi^2_{CC+Ly\alpha} + \chi^2_{gal} \tag{4.3.45}$$

- *Local Hubble constant:* Furthermore, we also include the recently measured local H_0 given by $H_0 = 73.5 \pm 1.4\ km\ s^{-1}Mpc^{-1}$ by SH0ES as reported in [325].

We use the Markov chain Monte Carlo (MCMC) method by employing EMCEE python package [317] for the model under consideration, and to constrain the free parameters of the model by utilizing combination of data sets: $SNeIa + HD + H_0$. The parameters space for the model is $\{H_0, b, \delta, \beta, \omega_d\}$, with one additional free normalization parameter M used in SNe Ia observation. We calculate the best-fit values by minimizing the combined χ^2 function of above defined data sets. Table 4.4 summarizes the main results of the statistical analysis for CHDE3 model carried out using the set of data $SNeIa + HD + H_0$. Figure 4.13 shows the $1\sigma(68.3\%)$ and $2\sigma(95.4\%)$ confidence contours for this model considering the set of data $SNeIa + HD + H_0$. The overall likelihood function peaks at $\delta = 0.548$, $\beta = 0.012$, $b = 0.049$, $\omega_d = -2.048$ with $\chi^2 = 36.637$. The present value of Hubble parameter H_0 comes out to be $H_0 = 67.516$ which is in good agreement with the latest obtained value for H_0 [8].

Table 4.5 gives a summary of the ICs and χ^2_{red} results. It is easy to observe that the ΛCDM has lower ICs, so the ΔAIC and ΔBIC are calculated with respect to the ΛCDM model. According to ICs, we notice a tension between AIC and BIC results: AIC indicates there is “less evidence in favour" while BIC indicates that there is “ very strong evidence against" (CHDE3) from current data. The CHDE3 model is punished by the ICs mainly because of large number of free parameters and thus is not favoured

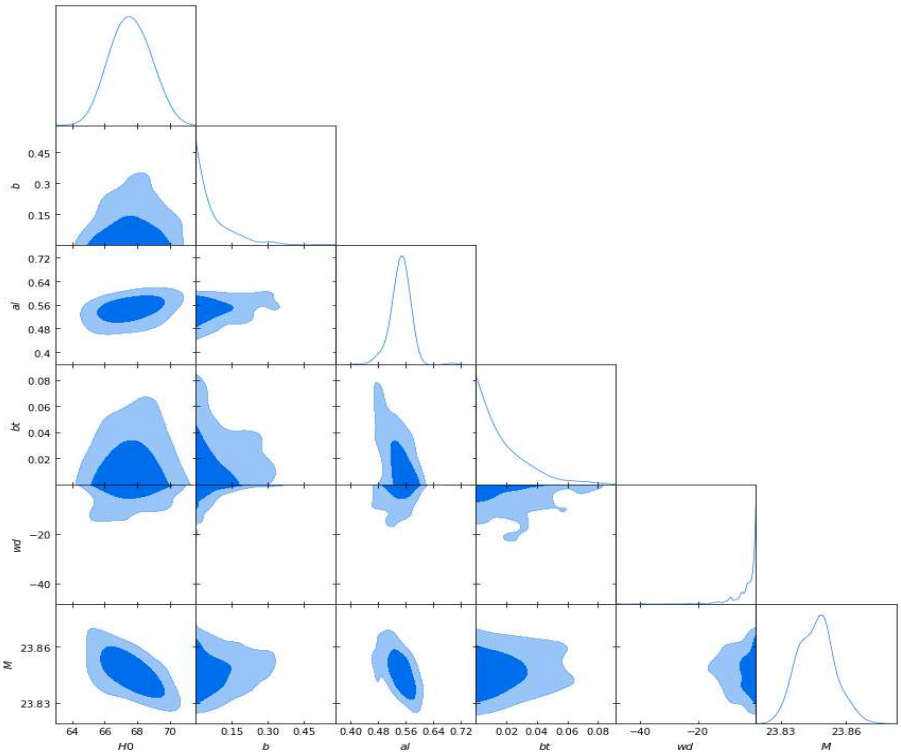

Figure 4.13: $1\sigma(68.3\%)$ and $2\sigma(95.4\%)$ confidence level contour plot for the CHDE3 model parameters using the observational data $SNeIa+OHD+H_0$. The labels al, bt and wd denote δ, β and ω_d parameters, respectively.

Table 4.5: Summary of χ^2, χ^2_{red}, AIC and BIC values and their differences from the reference model ΛCDM .

Model	χ^2_{min}	χ^2_{red}	AIC	BIC	ΔAIC	ΔBIC
ΛCDM	36.52	0.493	40.52	45.28	0	0
CHDE3	36.64	0.516	46.64	58.29	6.12	13.01

by the current joint data set from a model selection point of view. It is to be noted that ICs strongly penalizes models when they have more free parameters.

It is observed from Table 4.5 that for ΛCDM model, $\chi^2 = 36.52$, and $\chi^2_{red} = 0.493 < 1$, while for CHDE3 model with matter creation, $\chi^2 = 36.64$ and $\chi^2_{red} = 0.516 < 1$. It shows that CHDE3 model with matter creation gives good fit to the data from reduced chi-square point of view because the reduced chi-square does not contain the information of the complexity as ICs have.

Next, we investigate the cosmic history and cosmographic analysis of the CHDE3 model by the best fitting results as given in Table 4.4.

Table 4.6: The numerical values of a_{tr}, z_{tr}, q_0, $\omega_{\text{eff}}(z=0)$ and t_0 (Gyr) for the best-fitted values obtained using $SNeIa+HD+H_0$.

Model	a_{tr}	z_{tr}	q_0	$\omega_{\text{eff}}(z=0)$	t_0 (Gyr)
CHDE2	0.48	1.08	-0.39	-0.59	14.64
CHDE3	0.52	0.923	-0.34	-0.56	14.28

Evolution of the model

Let us examine the best fit values through the expansion history of the Universe to see whether they are consistent with the current data at the background level. Table 4.6 presents the numerical values of transition scale factor a_{tr}, transition redshift z_{tr}, the current values of q and ω_{eff}, and the age of the Universe. We plot the trajectory of the scale factor in Fig. 4.14 for all possible models using the best-fit values of model parameters to compare their evolutions. The inflection points are located at $a_{tr}=0.48$ for the CHDE2 model whereas it is at $a_{tr}=0.52$ for the CHDE3 model, slightly higher than the earlier one. The trajectories of these two models show that both the models evolve with the accelerated rate in early time followed by deceleration and then the exponential acceleration at late time. For other models including the general relativity (GR) case, we get decelerated expansion throughout the evolution as shown in Fig. 4.14.

To observe clearly how to realize cosmic acceleration from these models, we plot

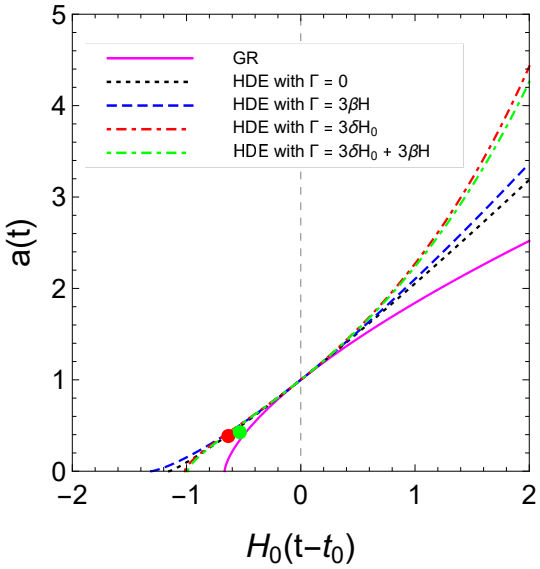

Figure 4.14: The evolution of the scale factor as a function of time for the best-fit value of the model parameters of different HDE models with and without matter creation. The dot denotes the transition point.

the deceleration parameter q versus redshift z for all possible models using best-fit

values of model parameters in Fig. 4.15. As expected, the CHDE2 and CHDE3 models give negative q at late times, and positive q at an earlier epoch, meaning that the expansion of the Universe slowed down in the past and speeded up recently. There are transition redshift $z_{tr} = 0.923$ and $z_{tr} = 1.08$, respectively between the two epochs which are substantially higher than the concordance model ($z_{tr} = 0.66$). The respective current value of q is $q_0 = -0.34$ and $q_0 = -0.39$, which are respectively higher than the corresponding WMAP value $q_0 = -0.60$ [326]. These results show that the HDE model with matter creation cannot be discriminated from the ΛCDM model by the deceleration parameter due to the insufficient observation accuracy. For the other models including the GR case, the trajectories do not show a transition from positive to negative as q has a constant value for each model.

To check the behavior of the effective EoS ω_{eff}, we plot the trajectories with re-

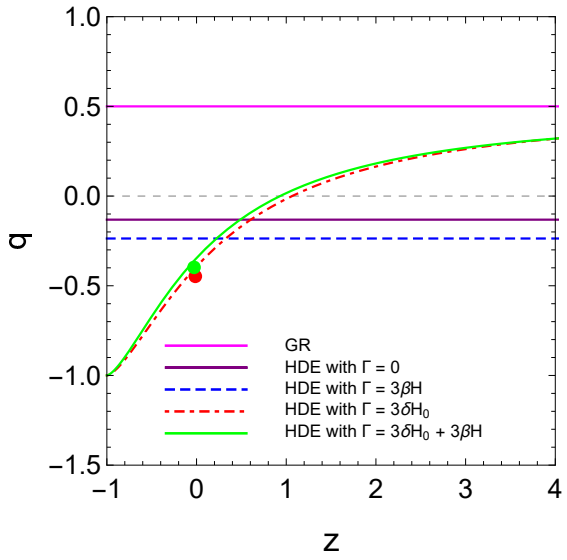

Figure 4.15: Plot of the deceleration parameter q as a function of redshift z for the best-fit value of parameters of different HDE models with and without matter creation. A dot on the trajectory shows the current value of q.

spect to the redshift z in Fig. 4.16 for different models using the best fit value of model parameters. It can be observed that the trajectories for CHDE2 and CHDE3 models show $\omega_{\text{eff}} \to -1$ in the late-time, which implies that these HDE models converge to de Sitter Universe in late-time. It is to be noted that the best fit value of CHDE3's EoS parameter ω_d is $\omega_d = -2.048^{+1.736}_{-5.073}$, which shows the phantom behavior. It may be due to the tension with the ΛCDM or maybe the conjunction of chance. Many authors [117, 327, 328] have also constrained the HDE and got the best fit value $\omega_d < -1$. However, the effective EoS parameter do not cross the phantom divide line $\omega_{\text{eff}} < -1$. This hint that the quantum vacuum and the particle creation rate may

indeed result in an effective EoS greater than -1 which shows the quintessence behavior. In other words, these HDE models, which are characterized by a particle production rate that grows throughout cosmic history, today present a significant effective EoS of quintessence type. The present value of the effective EoS is around $\omega_{\text{eff}}(z=0)=-0.59$ for CHDE2 model whereas it is $\omega_{\text{eff}}(z=0)=-0.56$ for CHDE3 model. These respective values are comparatively higher than that predicted by the joint analysis of $WMAP+BAO+H_0+SNe$ data, which is around $\omega(z=0)=-0.93$ [329]. The effective EoS for other models has a constant value ($\omega_{\text{eff}}>-1/3$), meaning that the model expands with decelerated rate.

In Fig. 4.17, we plot the reconstructed evolution history of $H(z)$ in the CHDE3

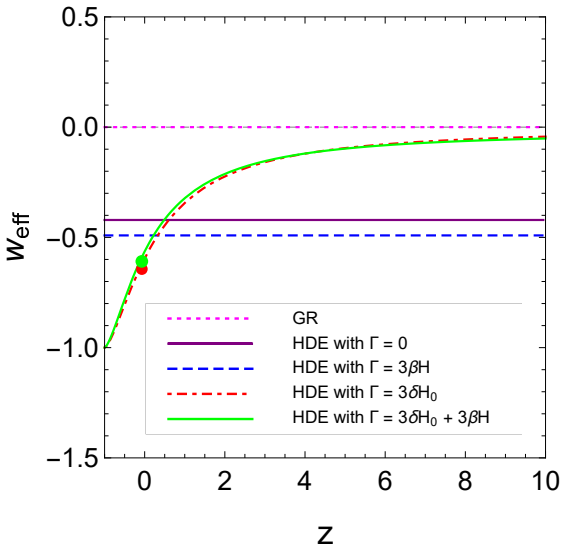

Figure 4.16: Behavior of effective equation of state parameter ω_{eff} with respect to the redshift z for the best-fit value of parameters of different HDE models with and without matter creation. A dot on the trajectory shows the current ω_{eff}.

model, constrained by observational data. We find that the fitting achieved from the combined observational data of $SNeIa+HD+H_0$ is compatible with the Hubble observational data.

The age of the Universe in terms of redshift z is discussed by plotting its trajectory. Using equation (4.3.21), we can calculate and plot the age of the Universe with respect to the redshift z for the best-fit values as shown in Fig. 4.18. The current ages of the Universe are found to be $t_0\sim 14.64$ and $t_0\sim 14.28$ Gyr in the case of CHDE2 and CHDE3 models, respectively, which are higher than the concordance model ($t_0\sim 13.7$ Gyr).

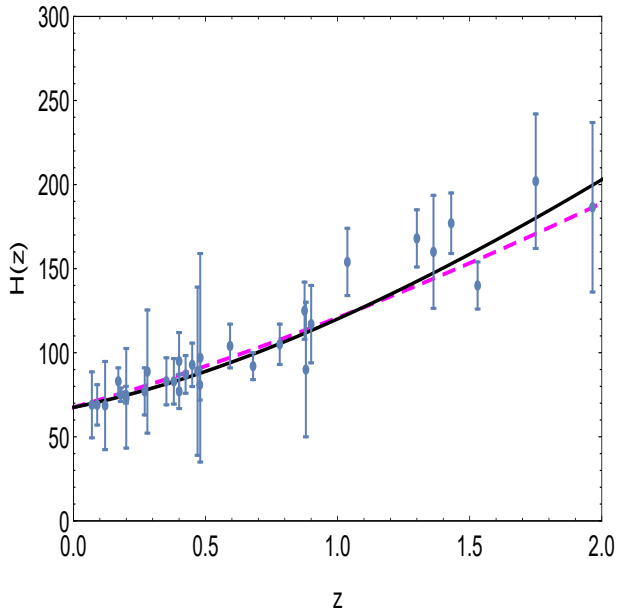

Figure 4.17: The comparison of the $z \sim H(z)$ curves. The solid grey line corresponds to the ΛCDM model and the dashed magenta line corresponds to the CHDE3 model. The $H_{obs}(z)$ data are also plotted with their error bars.

Cosmographic and Om(z) analysis

This subsection is devoted to the study of various cosmographic parameters for CHDE3 model which we use to discriminate between the various contenders of dark energy models. Firstly, we discuss geometrical analysis of our models using statefinder parameters $\{r,s\}$, which can be obtained as

$$r = 1 + \frac{9k_1(\delta - \delta b^2 - k_1)}{4\, e^{\frac{3}{2}\delta(1-b^2)H_0(t-t_0)}} + \frac{9(\delta - \delta b^2 - k_1)^2}{4\, e^{3\delta(1-b^2)H_0(t-t_0)}}, \tag{4.3.46}$$

$$s = \frac{\frac{k_1(\delta - \delta b^2 - k_1)}{2\, e^{\frac{3}{2}\delta(1-b^2)H_0(t-t_0)}} + \frac{(\delta - \delta b^2 - k_1)^2}{2\, e^{3\delta(1-b^2)H_0(t-t_0)}}}{(k_1 - \delta + \delta b^2)e^{\frac{-3}{2}\delta(1-b^2)H_0(t-t_0)} - 1}. \tag{4.3.47}$$

Using (4.3.46) and (4.3.47), the trajectory of $\{r,s\}$ in $s-r$ plane is shown in Fig. 4.19. The arrow represents the direction of the evolution of the trajectory. It can be observed that the trajectory of $\{r,s\}$ starts from a region $r < 1, s > 0$ in early time which corresponds to the quintessence model and tends to the ΛCDM point in the future. The current value of $\{r,s\}$ is found to be $\{r_0, s_0\} = \{0.430, 0.225\}$ which is different from ΛCDM. Thus, the CHDE3 model is obviously different from the ΛCDM model.

The change of sign from positive to negative is observed in the trajectory of $\{r,q\}$ in $q-r$ plane as shown in Fig. 4.20, which explains the transition from decelerated phase to accelerated one. In the $q-r$ plane, the fixed points $\{r,q\} = \{1, 0.5\}$ represents the

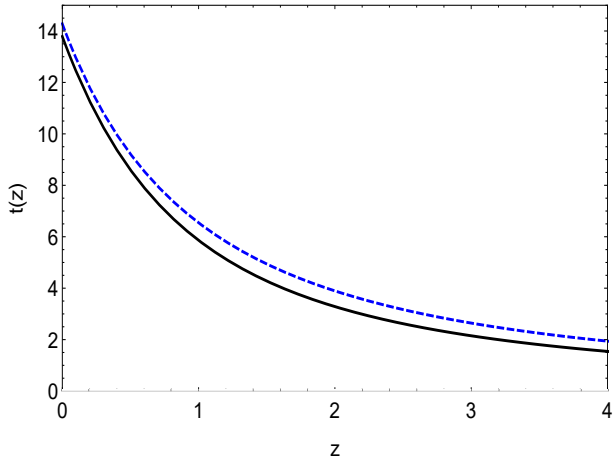

Figure 4.18: The age of Universe as a function of redshift for best-fit values of CHDE3 model. The black solid line represents the age of ΛCDM model whereas blue dashed line represents the age of CHDE3 model.

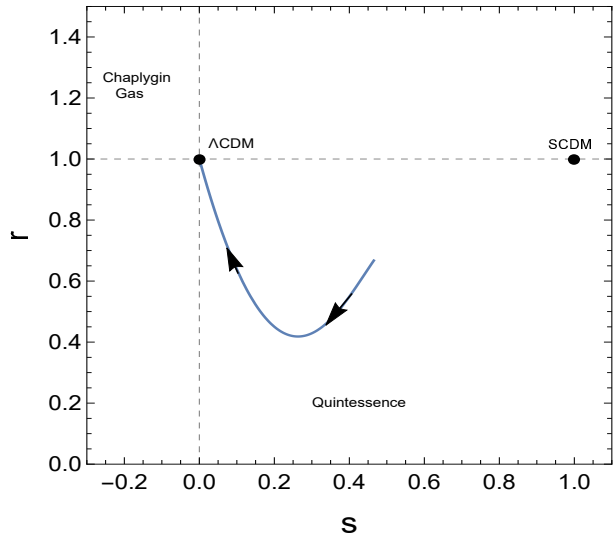

Figure 4.19: The plot of $\{r,s\}$ in the $s-r$ plane corresponding to the best-fit values of CHDE3 model. The arrow shows the direction of the evolution of the trajectory.

SCDM model of the Universe whereas $\{r,q\}=\{1,-1\}$ represents the steady-state (SS) model. The horizontal line $r=1$ represents the ΛCDM model. It is also observed from the figure that our model approaches the steady-state model in the late-time.

Now, we discuss some more general geometrical cosmological parameters, called cosmographic parameters (CP) defined by equation (1.12.2). To discuss the nature of the cosmographic parameters we plot their trajectories with respect to redshift z for the combined dataset of $SNeIa+HD+H_0$ as shown in Fig. 4.21. It can be observed from the figure that during the entire evolution of the Universe, the trajectories of j and l remain positive, and for l it decreases sharply from the high value at the early epoch. From the trajectory of s with respect to z we observe that it shows a transition from negative to positive. In the late-time, the trajectory of j approaches the value 1

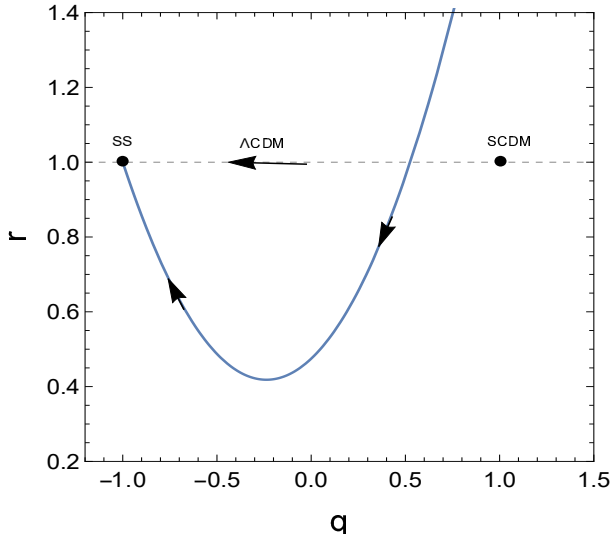

Figure 4.20: The plot of $\{r,q\}$ in the $q-r$ plane corresponding to the best-fitted parameters of CHDE3 model. The arrow shows the direction of the evolution of the trajectory.

which corresponds to the ΛCDM model. The trajectories of s and l also show similar behavior to that of j and approach 1 in the late-time of evolution. So, from the above analysis, we can conclude that at present time CHDE3 model is different from the ΛCDM model, but converges to the ΛCDM model as $z \to -1$.

Using (4.3.30) in (1.12.3), we can obtain Om-diagnostic as

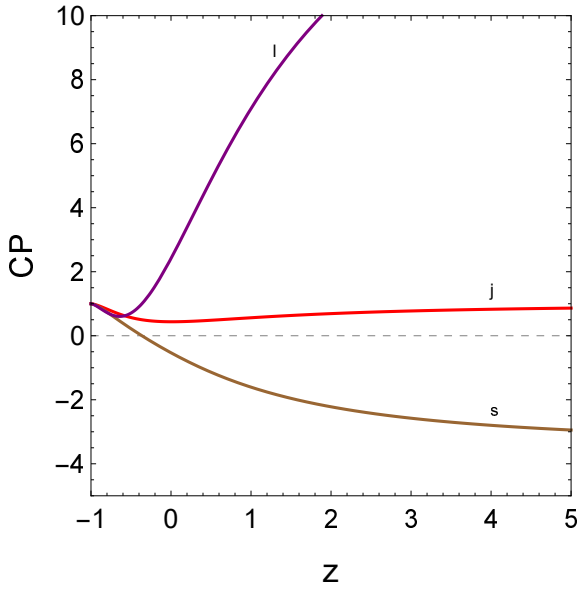

Figure 4.21: The cosmographic parameters j, s and l are plotted for best fit values of CHDE3 model.

$$Om(z) = \frac{\left[\frac{(1-b^2)\delta}{k_1} + \left(1 - \frac{(1-b^2)\delta}{k_1}\right)(1+z)^{\frac{3k_1}{2}}\right]^2 - 1}{(1+z)^3 - 1}. \tag{4.3.48}$$

We plot the trajectory of Om-diagnostic against the redshift z using best-fit values

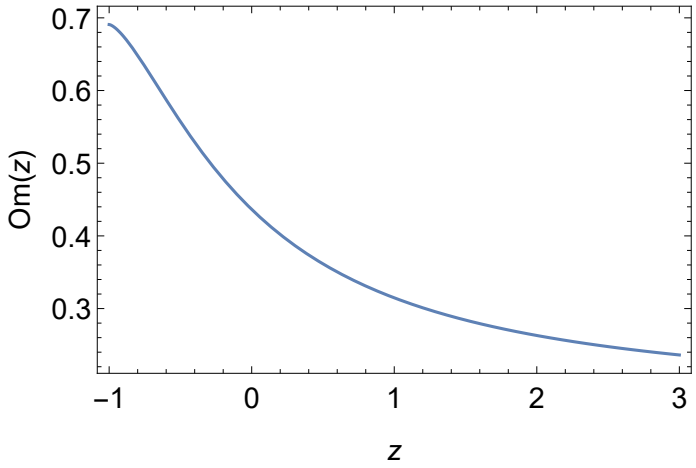

Figure 4.22: The $Om - z$ trajectory for best-fit values of CHDE3 model showing quintessence behavior.

obtained for the CHDE3 model. From Fig. 4.22, we find that the trajectory of Om shows the negative slope in the $Om(z) - z$ plane indicating that the behavior of the CHDE3 model is similar to the quintessence model.

Thermodynamics analysis

Let us now consider the entropy behavior of non-equilibrium thermodynamics of matter creation in CHDE3 model. The thermodynamic of the model depends on the rates of variation of the entropy per particle and of temperature. In adiabatic particle production, the total number of particles, N and entropy, $\mathbb{S}$ are produced in the space-time, but the specific entropy (per particle) $\sigma = \mathbb{S}/N$, remains constant, i.e., $\dot{\sigma} = 0$. This implies that

$$\frac{\dot{\mathbb{S}}}{\mathbb{S}} = \frac{\dot{N}}{N}. \tag{4.3.49}$$

Since $N = na^3$, using (1.10.1) and (4.3.26) into (4.3.49), we have

$$N = N_0 a^{3\beta}\, e^{3\delta H_0 (t-t_0)}, \tag{4.3.50}$$

where N_0 is the present value of particles. Using (4.3.50) in (4.3.49), we get

$$\mathbb{S} = S_0 a^{3\beta}\, e^{3\delta H_0 (t-t_0)}, \tag{4.3.51}$$

where S_0 is the present entropy. From (1.10.1) and (4.3.26), we get the particle number density as

$$n = n_0 a^{-3(1-\beta)}\, e^{3\delta H_0 (t-t_0)}, \tag{4.3.52}$$

where n_0 is the present particles number density. It is to be noted that in all the above equations the value of the scale factor, a is given by equation (4.3.29).

Further, we analyze the validity of generalized second law (GSL) of the CHDE3 model in a region enclosed by the apparent horizon. According to the second law of thermodynamics, the total entropy of the fluid components of the Universe plus that of the horizon must be greater than or equal to zero [330], i.e, $(\dot{\mathbb{S}}_m + \dot{\mathbb{S}}_d + \dot{\mathbb{S}}_h) > 0$, where $\mathbb{S}_m$ is the entropy of the dark matter, $\mathbb{S}_d$ is the entropy of HDE and $\mathbb{S}_h$ is entropy of the apparent horizon.

Now, we consider apparent horizon as the boundary for analyzing the validity of GSL. The entropy of apparent horizon is given by $\mathbb{S}_h = \frac{K_B \tilde{A}}{4 l_{Pl}^2}$, where $\tilde{A}$ and l_{Pl} are the area of the horizon and Planck's length, respectively, and K_B is the Boltzman constant. The area of the apparent horizon is given by $\tilde{A} = 4\pi r_h^2$, where the apparent horizon radius, $r_h = \frac{1}{\sqrt{(H^2 + k a^{-2})}}$. As we are restricting our analysis to a spatially flat model $(k = 0)$, this assumption yields $r_h = H^{-1}$ [331]. Therefore, the entropy of horizon reads as

$$\mathbb{S}_h = \frac{K_B \pi}{l_{Pl}^2 H^2}. \tag{4.3.53}$$

Using (4.3.30), the first order derivative of equation (4.3.53) can be written as

$$\dot{\mathbb{S}}_h = \frac{3 K_B \pi}{2 l_{Pl}^2} \frac{H_0}{H^2} \left[k_1 - (1 - b^2)\delta \right] \, a^{-3k_1/2}. \tag{4.3.54}$$

It can be observed that $\dot{\mathbb{S}}_h > 0$ if $k_1 - (1 - b^2)\delta > 0$. The entropy of the fluid within the horizon of the Universe is related to the Gibb's relation [332],

$$\mathbb{T} d\mathbb{S} = d(\rho V) + p dV, \tag{4.3.55}$$

where $\mathbb{T}$ is the temperature of the fluid within the horizon, where $\mathbb{T}_h = 1/2\pi r_h$ [333], and $V = \frac{4\pi}{3} r_h^3$ is the spatial volume enclosed by the horizon. From (4.3.55), the change in entropy for pressureless dark matter is given by

$$\dot{\mathbb{S}}_m = \frac{8\pi}{3} \frac{\rho_m H_0}{H^4} \left[3\delta + \frac{9}{2} \left(k_1 - (1 - b^2)\delta \right) a^{-3k_1/2} + 3(1 - \beta) \frac{H}{H_0} \right]. \tag{4.3.56}$$

Again, using (4.3.55), the change of entropy for CHDE3 model is given by

$$\dot{\mathbb{S}}_d = \frac{8\pi}{3} \frac{\rho_d H_0}{H^4} \left[\frac{9}{2} \left(k_1 - (1 - b^2)\delta \right) a^{-3k_1/2} + 3(1 + \omega_d) \frac{H}{H_0} \right]. \tag{4.3.57}$$

As H, ρ_m and ρ are always positive, adding equations (4.3.54), (4.3.56) and (4.3.57), we find that the GSL is satisfied at the apparent horizon provided $k_1 - (1-b^2)\delta > 0$.

4.4 Conclusion

In this chapter, we have presented three different HDE models with adiabatic matter creation process in the framework of homogeneous and isotropic flat FLRW Universe filled with HDE and pressureless dark matter with matter creation. We have discussed the basic terminology and solved the field equations by considering three different forms of particle creation rate Γ. We have discussed the observational analysis by employing the MCMC package EMCEE on a different combination of publicly available data sets. The best-fit values of model parameters have been obtained with different combinations of data sets. Figures 4.1 and 4.13 show the contour plots of model parameters at 1σ and 2σ confidence level using different observational data sets. The trajectories of the evolution of the scale factor, matter density parameter, deceleration parameter, Hubble parameter have been plotted with best-fit values and discussed their evolutions. We have studied the diagnostic parameters, such as statefinder parameters and $Om(z)$ to distinguish the models from the ΛCDM model. The cosmography analysis, like jerk, snap, etc., has been discussed to differentiate the models from other existing DE models. We summarize the result of different models as below:

- **In CHDE1 model**, we have assumed the particle creation rate $\Gamma = 3\beta H$ to solve the field equations. This assumption gives a power-law form of the scale factor. We have also calculated the deceleration parameter for this form of Γ which is constant and hence there is no transition redshift throughout the evolution. It has also been noted that the HDE model with Hubble horizon as an infrared cut-off also does not show the transition regime.

- **In CHDE2 model**, we have assumed the particle creation rate of the form $\Gamma = 3\delta H_0$. The exact solution for the scale factor has been obtained to discuss the evolution of the model. We have tested the viability of the model by employing the MCMC package EMCEE on different combinations of publicly available data sets of SNe, OHD, and BAO/CMB. The best-fit values of model parameters have been obtained with different combinations of data sets. Fig. 4.1 shows

the contour plot of model parameters at 1σ and 2σ confidence level using the observational data $SNe + OHD + BAO/CMB$. We have also performed the information criterion of AIC and BIC to discriminate CHDE2 model with ΛCDM model and presented in Table 4.2. The analysis of AIC indicates that there is average support for the CHDE2 model when compared to the ΛCDM model, while those based on the BIC indicates that there is positive evidence against the model with respect to the ΛCDM model when we use the combined dataset of $SNe + OHD$, while these selection criteria disfavor with other sets of data discussed here. The reduced χ^2_{red} listed in Table 4.2 shows that the model provides a very good fit to these data. It has been observed that the age of the Universe is found to be 13.393 Gyr which is very close to the observed value by the concordance model. In the CHDE2 model, the trajectory for the model deviates slightly from that of ΛCDM. It indicates that the CHDE2 model could really alleviate the age problem. This is due to the change in the energy conservation equation by the addition of matter creation which makes the matter dilution a little bit slower, and then the age problem is alleviated.

- **In CHDE3 model**, we have considered the particle creation rate of the form $\Gamma = 3\delta H_0 + 3\beta H$. The main advantage of considering HDE with this form of matter creation is the introduction of another free parameter, thus providing an extra degree of freedom in the process of constructing a physical interpretation of the solution. The evolution of such a model has been tested by the latest observational datasets. In this model, we have used the EMCEE python package to obtain the best-fit values of the model parameters through the MCMC method as listed in Table 4.4. Figure 4.13 shows the contour plot for the model parameters at $1\sigma(68.3\%)$ and $2\sigma(95.4\%)$ confidence level. We have also used the selection criterion of AIC and the BIC to assess the viability of our model against the ΛCDM model and presented the results in Table 4.5. These ICs tend to favor models that give a good fit with fewer parameters. Using the AIC and BIC for model comparison, it has been found that the concordance ΛCDM model remains the best one to explain current data. The HDE model with particle creation is punished by their large number of parameters, thus not favored by the ICs from a model selection point of view. However, the HDE model with matter creation gives a good fit to the data from a reduced chi-square point of

view because it does not contain the information of the complexity as ICs have. It has been found that the value $z_{tr} = 0.923$ between the two epochs is substantially higher than the concordance model ($z_{tr} = 0.66$). The current values of q are $q_0 = 0.34$, which is higher than the corresponding WMAP value $q_0 = 0.60$. We have also estimated the present age of the Universe and found it to be around 14.28 Gyr for best-estimate model parameters which are higher than the estimated value of ΛCDM model. We have analyzed the thermodynamics of the CHDE3 model. It has been observed that the GSL is valid with the apparent horizon as the boundary under certain conditions.

As the HDE models with a suitable form of particle production rate predicts the late time acceleration, we have analyzed the HDE models with matter creation using diagnostic parameters like statefinder and Om parameters, and some cosmographic parameters to discriminate from other standard DE models especially from ΛCDM model. The trajectories of statefinder $\{r, s\}$ show that the CHDE models lie in the region which corresponds to the quintessence model in early time and converges to the ΛCDM model in the late-time. Similar behavior has also been observed from the other cosmographic parameters which show that at present the CHDE models with matter creation are different from the ΛCDM model but converges to it in the late-time. The $Om(z)$ analysis also shows behavior similar to the quintessence model.

In conclusion, the present HDE models with matter creation successfully describe the expansion history of the evolution of the Universe from early decelerated phase to late time accelerated phase. The phenomenological model of matter creation as discussed in this chapter is good exploring. New constraints on the parameters from complementary observations need to be investigated in order to see whether the matter creation HDE models studied here provide a realistic description of the observed Universe.

****

Chapter 5

Holographic Ricci Dark Energy Model with Bulk Viscosity and Matter Creation

In this chapter [1]*, we extend the work carried out in chapter 2 by introducing matter creation with bulk viscosity to describe the evolution of the HRDE model. We consider bulk viscosity and matter creation as two independent irreversible processes. Assuming the suitable forms of the bulk viscous coefficient and matter creation rate, we find the exact solution of the field equations. We carry out fitting analysis on the cosmological parameters in the model by using* SNe*,* OHD*, and* BAO/CMB *datasets. We plot the trajectory of cosmological parameters with the best-fit values of model parameters and discuss all possible (deceleration, acceleration, and their transitions) evolutions of the model. We further discuss the geometrical diagnostic parameters such as statefinder,* Om*, and cosmographic parameters to distinguish the model from the* ΛCDM *model. Finally, we discuss the behavior of energy conditions for our model.*

[1] This chapter comprises the result of a research paper "Viscous Ricci dark energy model with matter creation: exact solution and observational tests, *Pramana Journal of Physics* **94**, 129 (2020)".

5.1 Introduction

It is well known that the content of the Universe as a perfect fluid is assertive since it suggests no dissipation, which actually exists widely, and intuitively plays an important role in the evolution of the Universe. To be more realistic, the Universe is assumed to be filled with dissipative media, therefore cosmology based on the imperfect fluid is proposed reasonably. Viscosity is a concept in fluid mechanics which is related to an exotic fluid with some thermodynamical features such as bulk and/or shear viscosities. To reduce the equilibrium pressure in an expanding Universe bulk viscosity can be useful. In cosmology, the viscosity concept was first discussed by Misner [200]. Several authors [99, 100, 193–196, 198, 199, 205–209, 334, 335] have discussed the effect of bulk viscosity to understand the DE phenomenon.

The study of matter creation in the relativistic cosmological models has drawn the attention of a number of authors. In the framework of GR, the adiabatic irreversible matter creation was first time studied by Prigogine et al. [225, 226]. In their papers, they discussed that the second law of thermodynamics may be modified to accommodate the flow of energy from the gravitational field to the created matter field. This phenomenon of matter creation has been studied by many authors in detail within the context of standard GR [227–229, 231, 234, 236, 240, 308, 336]. In the context of the recent acceleration, the concept of irreversible particle creation has been reconsidered due to its capability to produce an effective negative pressure. For more details, we refer to the Refs. [237, 238, 244, 246, 247, 307, 314, 337–339]. Prigogine et al. [225, 226] considered the viscous and matter creation processes as two independent processes. Some authors [197, 199, 243, 340–345] have studied these two dissipative processes by considering as two independent phenomena.

In chapter 2, we have discussed the effect of bulk viscosity on the HRDE model within the framework of the standard Eckart theory of relativistic thermodynamics. In the present chapter, we have extended our investigation by including gravitationally induced matter creation with bulk viscosity in the HRDE model within the framework of FLRW Universe. We have discussed the evolution of the Universe by constraining the model parameters through combined observational data. We have plotted the trajectory of the Hubble parameter and ΛCDM with an error bar from Hubble data. We have studied the dynamical properties of our model by calculating the deceleration parameter, jerk, snap, and lerk parameters analytically and geometrically. We have

further discussed the statefinder and Om diagnostics to discriminate the HRDE model with other standard dark energy models. We have also discussed the behavior of energy conditions for the HRDE model.

The chapter has been organized as follows: In Section 5.2, we have presented the Einstein field equations with bulk viscosity and matter creation for the HRDE model in the framework of a flat FLRW line element. In Section 5.3, we obtain the exact solution of the field equations to obtain the Hubble parameter and the scale factor. We have constrained the model parameters to the combined data set of Type Ia Supernovae, observational Hubble data, and combined data of baryon acoustic oscillations and cosmic microwave background, and have presented the fitting results in Subsection 5.3.1. Many interesting issues including the age of the Universe have been discussed in Subsection 5.3.2. We have compared the HRDE model with other DE models by calculating statefinder parameters, Om diagnostics, and cosmographic parameters in Subsection 5.3.3. In Subsection 5.3.4, we have discussed the energy conditions for our model. Finally, we have summarized our results in Sec. 5.4. It is to be noted that we have used matter creation and particle creation synonymously throughout the chapter.

5.2 The Cosmological Model

We consider a homogeneous and isotropic flat FLRW line element given by (2.2.1). We assume the Universe filled with pressureless dark matter and HRDE. The energy-momentum tensor in the presence of bulk viscosity and matter creation is given by [197, 242, 346]

$$T_{\mu\nu} = (\rho_m + \rho_d + p_{\text{eff}})u_\mu u_\nu + p_{\text{eff}}\, g_{\mu\nu}, \tag{5.2.1}$$

where ρ_m and ρ_d denote the energy densities of dark matter and HRDE, respectively, and p_{eff} is the effective pressure

$$p_{\text{eff}} = p_d + p_c + p_v, \tag{5.2.2}$$

where p_d is the pressure of HRDE, p_c is the pressure associated with the creation of particle out of the gravitational field [225, 226] and p_v represents the viscous pressure which is assumed as $p_v = -3\zeta H$, where ζ is bulk viscous coefficient [190]. The bulk viscous pressure, p_v represents only a small correction to the thermodynamical pres-

sure; it is a reasonable assumption that the inclusion of viscous term in the energy -momentum tensor does not change fundamentally the dynamics of the cosmic evolution. The pressure and density of HRDE are related by the equation of state (EoS) $p_d = \omega_d \rho_d$, where ω_d is the EoS parameter of HRDE.

In the background of the metric (2.2.1) in the general theory of relativity, EFEs (2.2.2) yield the following two independent equations:

$$3H^2 = \rho_m + \rho_d, \tag{5.2.3}$$

$$2\dot{H} + 3H^2 = -p_{\text{eff}} = -(p_d + p_c - 3\zeta H). \tag{5.2.4}$$

Let us now assume the particle creation rate Γ to discuss the HRDE model. The most natural choice is taken to be [231]

$$\Gamma = 3\beta H, \tag{5.2.5}$$

where β is a constant parameter which lies in the interval $0 \leq \beta < 1$. It has been found that this form of Γ does not favor the epoch in the evolution of the Universe. Lima et al. [236] have investigated the CDM model with this form of Γ, but with time-dependent dimensionless parameter β. However, we restrict ourself with β as a constant. We consider that these bulk viscosity and matter creation have independent physical phenomena as discussed by many others [197, 199].

Now, using (5.2.5) into (1.10.2), we obtain

$$p_c = -\beta \rho_m. \tag{5.2.6}$$

Using (5.2.5) into (1.10.1), we find the solution for the particle number density

$$n = n_0 \left(\frac{a_0}{a}\right)^{3(1-\beta)}, \tag{5.2.7}$$

where n_0 is the constant of integration and considered as the present value of particle number density. In adiabatic particle production, the particles and entropy are produced in the space-time, but the specific entropy (per particle) $\sigma = \mathbb{S}/N$, remains constant. This implies that $\dot{\mathbb{S}}/\mathbb{S} = \dot{N}/N$.

Using (1.8.5) and (5.2.6), a single evolution equation from (5.2.3) and (5.2.4) can be

obtained as

$$[2+3\alpha(\beta+\omega_d)]\dot{H}+3[1-\beta+2\alpha(\beta+\omega_d)]H^2-3\zeta H=0. \tag{5.2.8}$$

In the absence of bulk viscosity and matter creation, i.e., taking $\zeta=0$ and $\beta=0$, the solution of (5.2.8) for HRDE model is given by

$$H=H_0\left(\frac{a_0}{a}\right)^{B_1}, \tag{5.2.9}$$

where $B_1=3(1+2\alpha\omega_d)/(2+3\alpha\omega_d)$. The solution of the scale factor is obtained as

$$a=a_0\left[1+B_1H_0(t-t_0)\right]^{1/B_1}. \tag{5.2.10}$$

The scale factor shows the power-law expansion. The deceleration parameter gives $q=(B_1-1)$. Thus, the value of q is constant. Therefore, the HRDE model itself does not describe the transition redshift.

Further, let us consider the HRDE model with matter creation in the absence of bulk viscosity, i.e., $\zeta=0$. The solution of (5.2.8) in the presence of matter creation is given by

$$H=H_0\left(\frac{a_0}{a}\right)^{B_2}, \tag{5.2.11}$$

where $B_2=3[1-\beta+2\alpha(\beta+\omega_d)]/[2+3\alpha(\beta+\omega_d)]$. The solution of the scale factor is given by

$$a=a_0\left(1+B_2H_0(t-t_0)\right)^{1/B_2}. \tag{5.2.12}$$

The above equation again shows that the expansion of the Universe is of power-law form. The constant value of $q=(B_2-1)$ shows that the model does not transit from decelerated phase to accelerated phase. The model decelerates for $B_2>1$, marginal inflation at $B_2=1$ and accelerates for $B_2<1$. Therefore, the form of Γ defined in Eq. (5.2.5) does not explain the present-day Universe, i.e., the transition phase in the absence of bulk viscosity.

In what follows we find the solution of Eq. (5.2.8) with non-zero bulk viscosity and matter creation by assuming the suitable form of bulk viscous coefficient, ζ.

5.3 Solution with Viscosity and Matter Creation

Following [192, 273, 277], we consider the bulk viscosity coefficient ζ of the following form

$$\zeta = \zeta_0 + \zeta_1 H, \tag{5.3.1}$$

where ζ_0 and ζ_1 are positive constants. Equation (5.3.1) represents the general assumption as it is a combination of two forms, $\zeta = \zeta_0$ and $\zeta \propto H$. This motivation can be traced in fluid mechanics where the transport/viscosity phenomenon is involved with velocity $\dot{a}$ which is related to the expansion rate H. We define the dimensionless bulk viscous coefficients ξ, ξ_0 and ξ_1 as

$$\xi = \frac{\zeta}{H_0}, \ \ \xi_0 = \frac{\zeta_0}{H_0} \ \text{ and } \ \xi_1 = \zeta_1, \tag{5.3.2}$$

where H_0 is the current value of the Hubble parameter. Using the above transformation in (5.3.1), we obtain the dimensionless form of bulk viscosity as $\xi = \xi_0 + \xi_1 h$, where $h = H/H_0$ is the dimensionless Hubble parameter.

Using the relation $\frac{d}{dt} = \frac{\dot{a}}{a}\frac{d}{d\,ln\,a}$ in (5.2.8), a dimensionless evolution equation for $h = H/H_0$ is given by

$$\psi_2 h' + 3\psi_1 h - 3\xi_0 = 0, \tag{5.3.3}$$

where $\psi_1 = [1 - \beta - \xi_1 + 2\alpha(\beta + \omega_d)]$, $\psi_2 = [2 + 3\alpha(\beta + \omega_d)]$ and a prime denotes the differentiation with respect to the conformal time $ln\,a$.

Integration of Eq. (5.3.3) gives

$$h(a) = \frac{\xi_0}{\psi_1} + \left(1 - \frac{\xi_0}{\psi_1}\right)\left(\frac{a}{a_0}\right)^{-\frac{3\psi_1}{\psi_2}}, \quad \psi_1 \neq 0. \tag{5.3.4}$$

Now, using the relation $\frac{a_0}{a} = (1+z)$, we can write the Hubble parameter H in terms of redshift z as

$$H(z) = H_0\left[\frac{\xi_0}{\psi_1} + \left(1 - \frac{\xi_0}{\psi_1}\right)(1+z)^{\frac{3\psi_1}{\psi_2}}\right]. \tag{5.3.5}$$

We derive the $t - z$ relationship, which comes out as

$$t(z) = t_0 + \frac{\psi_2}{3\xi_0 H_0}\ln\left[1 + \frac{\xi_0}{\psi_1}\left\{(1+z)^{\frac{-3\psi_1}{\psi_2}} - 1\right\}\right]. \tag{5.3.6}$$

From (5.3.5), the scale factor $a(t)$ is obtained as

$$a(t) = a_0 \left[1 + \frac{\psi_1}{\xi_0}\left(e^{\frac{3\xi_0 H_0 (t-t_0)}{\psi_2}} - 1\right)\right]^{\frac{\psi_2}{3\psi_1}}, \quad \xi_0 \neq 0, \quad \psi_1 \neq 0 \tag{5.3.7}$$

For a better understanding of the evolution of the scale factor, we have plotted the graph of $a(t)$ with respect to $H_0(t-t_0)$ in Fig. 5.1 for the best-fitted values of the model parameters. The best fit values of the model parameters from the observations are given in Table 5.1 (discussed in subsect. 5.3.1). From Fig. 5.1, it is observed that the accelerated expansion starts earlier in the HRDE model with bulk viscosity and matter creation (magenta trajectory) than the HRDE model with bulk viscosity (blue trajectory) during the evolution of the Universe.

The Hubble parameter $H(t)$ in terms of t can be written as

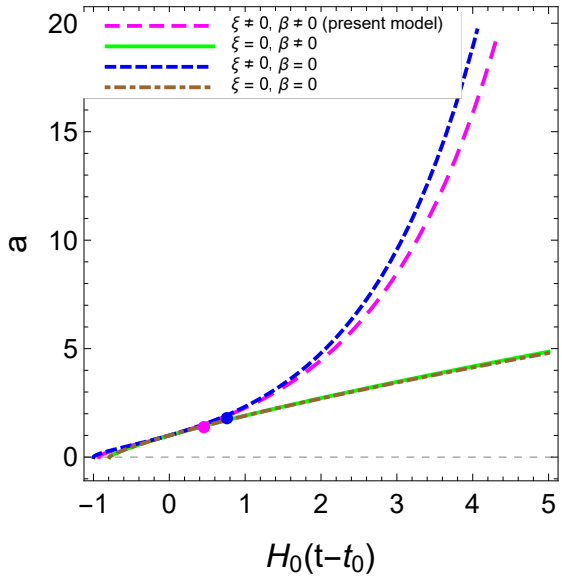

Figure 5.1: The evolution of the scale factor with respect to $H_0(t-t_0)$ for the best-fit values of free parameters. The dot denotes the transition value. The grey and green trajectories of the scale factor show decelerated expansion whereas blue and magenta trajectories show the accelerated expansion after the transition point.

$$H(t) = H_0\, e^{\frac{3\xi_0 H_0 (t-t_0)}{\psi_2}} \left[1 + \frac{\psi_1}{\xi_0}\left(e^{\frac{3\xi_0 H_0 (t-t_0)}{\psi_2}} - 1\right)\right]^{-1}. \tag{5.3.8}$$

The effective dark energy density ρ_{eff} and effective pressure p_{eff} are respectively given as

$$\rho_{\text{eff}} = 3H_0^2\, e^{\frac{6\xi_0 H_0 (t-t_0)}{\psi_2}} \left[1 + \frac{\psi_1}{\xi_0}\left(e^{\frac{3\xi_0 H_0 (t-t_0)}{\psi_2}} - 1\right)\right]^{-2}, \tag{5.3.9}$$

and

$$p_{\text{eff}} = -\frac{3H_0^2\xi_0\, e^{\frac{3\xi_0 H_0(t-t_0)}{\psi_2}}\left[\psi_2\, e^{\frac{3\xi_0 H_0(t-t_0)}{\psi_2}} + 2(\xi_0-\psi_1)\right]}{\psi_2\left[1+\frac{\psi_1}{\xi_0}\left(e^{\frac{3\xi_0 H_0(t-t_0)}{\psi_2}}-1\right)\right]^2}. \tag{5.3.10}$$

5.3.1 Parameters Estimation

We use the Hubble parameter obtained in equation (5.3.5) and estimate the best fit of the model parameters ξ_0, ξ_1, β, ω_d and α using the combined data set, consisting of the Type Ia supernova (SNe) data set, Observational Hubble Data (OHD) and the combined baryon acoustic oscillation (BAO) and cosmic microwave background (CMB) data, discussed in section 1.13. In order to figure out the observational constraints, we employ publicly available EMCEE codes [317] for implementing the Markov chain Monte Carlo (MCMC) method. We choose the current Hubble constant value as $H_0 = 67.8 Km/s/Mpc$ from Planck 2015 results [20].

Considering these cosmological data sets together, i.e. $SNe+OHD+BAO/CMB$, the total χ^2 function is then given by

$$\chi^2 = \chi^2_{SNe} + \chi^2_{OHD} + \chi^2_{BAO/CMB}, \tag{5.3.11}$$

where χ^2_{SNe}, χ^2_{OHD} and $\chi^2_{BAO/CMB}$ are given by equations (1.13.3), (1.13.4) and (1.13.8), respectively. The best fit values for the model parameters obtained by minimizing total χ^2 are given in Table 5.1 and the contour plot is shown in Fig. 5.2 with $1\sigma(68.3\%)$ and $2\sigma(95.4\%)$ confidence level.

Table 5.1: The best-fit values of the free parameters of HRDE model with bulk viscosity and matter creation using $SNe+OHD+BAO/CMB$ samples

Parameters	Best-fit values
ξ_0	5.223
ξ_1	0.485
β	0.777
ω_d	-0.240
α	8.078
M	24.95
χ^2_{min}	58.79
χ^2_{red}	0.77

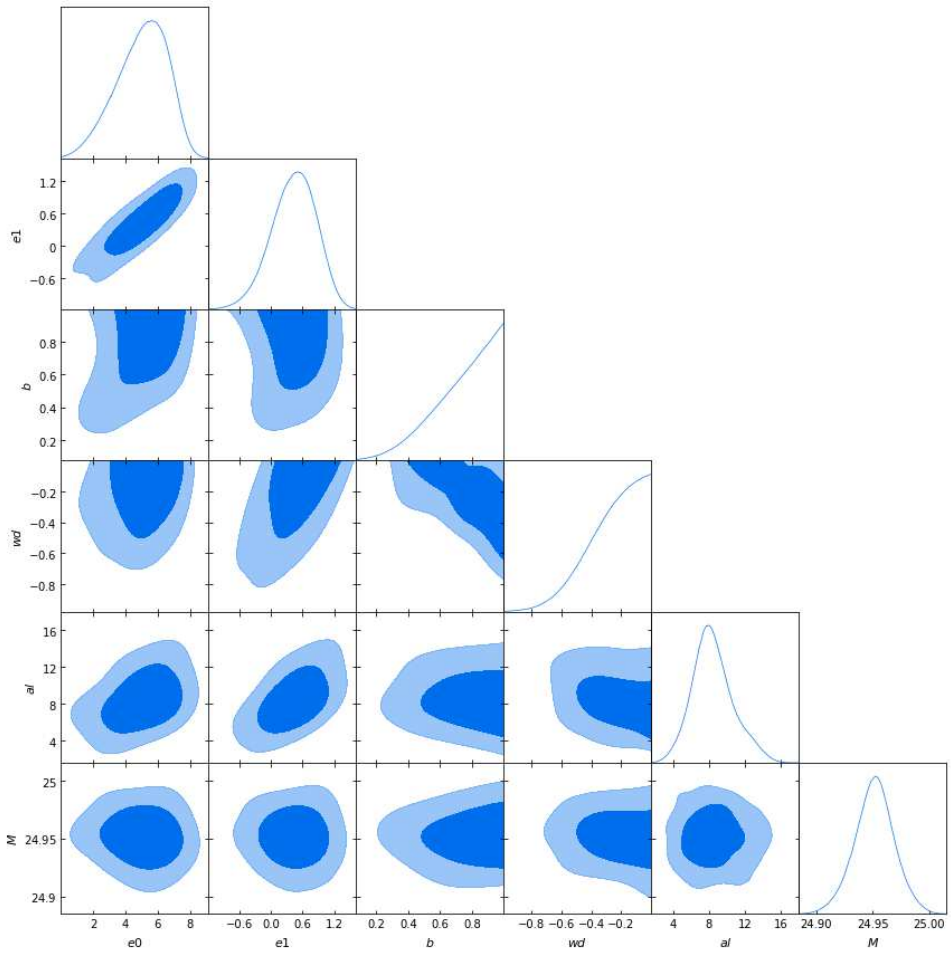

Figure 5.2: The contour plot for the free parameters using the observational data SNe+OHD+BAO/CMB for HRDE model with bulk viscosity and matter creation. The labels $e0$, $e1$, b, wd and al denote ξ_0, ξ_1, β, ω_d and α parameters, respectively.

5.3.2 Evolution of Cosmological Parameters

The Hubble parameter in equation (5.3.4) shows a decreasing behavior with the scale factor. It can have infinitely large value in the early stages and decreases as the Universe expands and finally saturated to a constant value as $a \to \infty$. Fig. 5.1 shows the behavior of the scale factor with cosmic time. The transition point is found to be $a_{tr} = 0.936$ where the model transits from decelerated phase to accelerated phase.

The deceleration parameter q is a geometric parameter which measures the state of acceleration/deceleration of the Universe. Using (5.3.7), we obtain

$$q(t) = -1 + \frac{3(\psi_1 - \xi_0)}{\psi_2} e^{\frac{-3\xi_0 H_0 (t-t_0)}{\psi_2}}. \tag{5.3.12}$$

Thus, the deceleration parameter (DP) in terms of z can be obtained as

$$q(z) = -1 + \frac{3(\psi_1 - \xi_0)}{\psi_2}\left[\frac{\psi_1}{\psi_1 + \xi_0\{(1+z)^{\frac{-3\psi_1}{\psi_2}} - 1\}}\right]. \tag{5.3.13}$$

The present value of deceleration parameter, q_0 corresponding to $z = 0$ is given by

$$q_0 = -1 + \frac{3(\psi_1 - \xi_0)}{\psi_2}. \tag{5.3.14}$$

For best fit values of parameters, $q_0 = -0.362$, which is higher than the corresponding

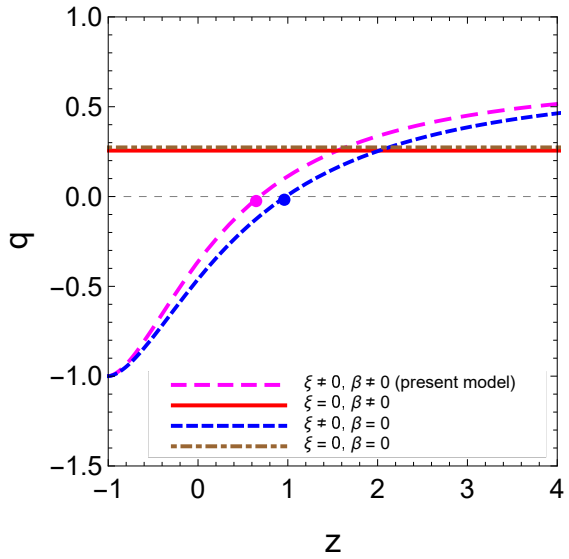

Figure 5.3: The $q - z$ relation diagram for best-fitted values of model parameters. The dot denotes the transition point from where the model transits from decelerated phase to accelerated phase. The horizontal red and grey trajectories show the constant deceleration values whereas the transition trajectories (blue and magenta) are due to the HRDE model with bulk viscosity, and the HRDE model with bulk viscosity and matter creation, respectively.

WMAP value $q_0 = -0.60$ [326]. In Fig. 5.3, we plot the deceleration parameter $q(z)$ relation with the cosmic redshift z for best-fitted values of the HRDE model. It is observed that q changes its sign from positive to negative showing the transition from decelerated phase to accelerated phase. The transition redshift, z_{tr} is found to be $z_{tr} = 0.68$ for HRDE model, which is within the range of the transition redshift $z_{tr} = 0.45$–0.73 in the concordance ΛCDM model [347].

We can obtain the effective equation of state parameter (EoS), ω_{eff} as

$$\omega_{\text{eff}} = -1 + \frac{2(\psi_1 - \xi_0)}{\psi_2}\left[\frac{\psi_1}{\psi_1 + \xi_0\{(1+z)^{\frac{-3\psi_1}{\psi_2}} - 1\}}\right]. \tag{5.3.15}$$

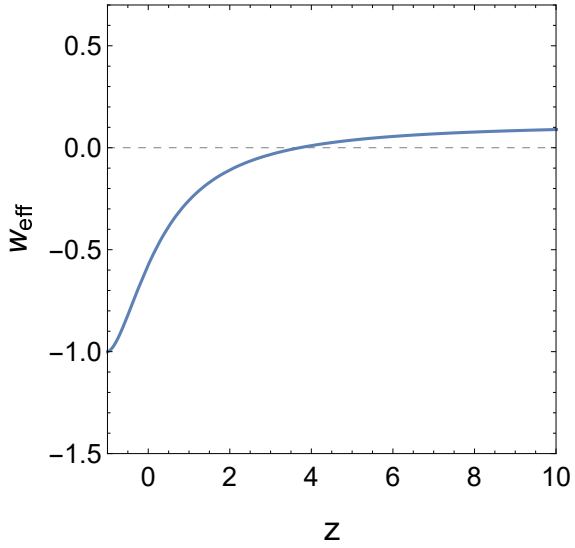

Figure 5.4: The $\omega_{\text{eff}} - z$ relation diagram for the best-fitted model parameters.

It can be observed that in the late-time as $z \to -1$, $\omega_{\text{eff}} \to -1$ which can also be verified from the Fig. 5.4. The late-time value $\omega_{\text{eff}} = -1$ implies that our model converges to ΛCDM model in future. It is also observed that the HRDE model does not cross phantom divide line and thus is free from big-rip singularity.

The present value of ω_{eff} can be found as

$$\omega_{\text{eff}}(z=0) = -1 + \frac{2(\psi_1 - \xi_0)}{\psi_2}. \tag{5.3.16}$$

The present value $\omega_{\text{eff}}(z=0) = -0.575$ can be calculated for the best-fit values of parameters. This value is comparatively higher than that predicted by the joint analysis of $WMAP + BAO + H_0 + SNe$ data which is around -0.93.

We can calculate and plot (Fig. 5.5) the age of the Universe with respect to the redshift z using equation (5.3.5) into equation (4.3.21) for the best-fit values. The current age of the Universe is found to be $t_0 = 13.397\ Gyr$ corresponding to combined $SNe + OHD + BAO/CMB$ data set, which is comparatively same as predicted by ΛCDM model.

The fitting achieved from our statistical analysis for combined data $SNe + OHD + BAO/CMB$ is compatible with the Hubble observational data for the HRDE model as shown in Fig. 5.6.

Also, the reduced $\chi^2_{red} = \chi^2_{min}/(\mathbb{N} - d)$, where $\mathbb{N}$ is the number of data and d is the degree of freedom, is calculated for our model and found to be $\chi^2_{red} = 0.77$ which shows that our HRDE model provides a very good fit to the considered observational data.

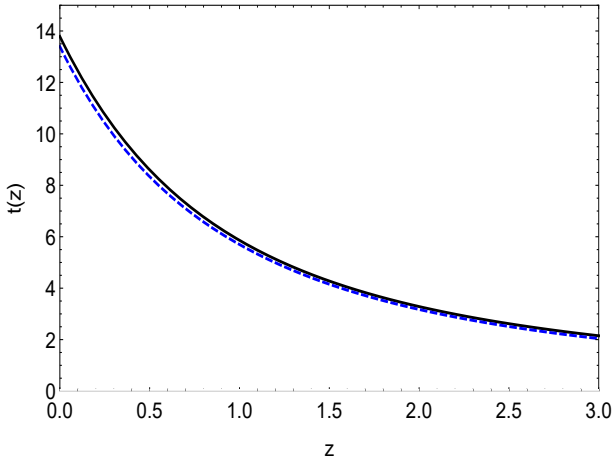

Figure 5.5: The age of Universe as a function of redshift where black line represents the age of ΛCDM model whereas blue dashed line represents the age of HRDE model.

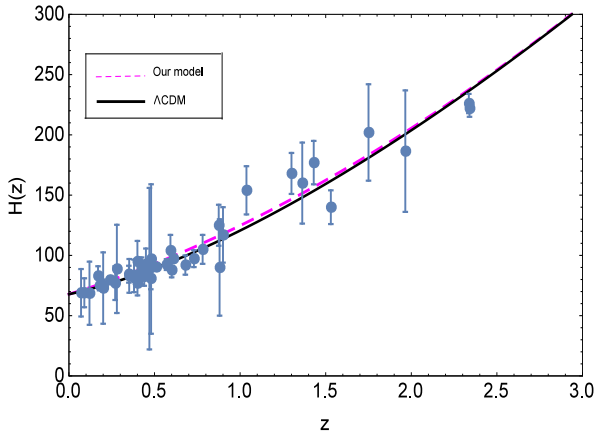

Figure 5.6: The best fit curves for HRDE model (dashed magenta) and ΛCDM model (black line). The navy blue points with uncertainty bars correspond to the OHD sample.

Using (5.3.5), we obtain the evolution of bulk viscosity as

$$\xi = \xi_0 + \xi_1 \left[\frac{\xi_0}{\psi_1} + \left(1 - \frac{\xi_0}{\psi_1}\right)(1+z)^{\frac{3\psi_1}{\psi_2}} \right] \tag{5.3.17}$$

The trajectory of the bulk viscous coefficient for best-fit values of model parameters (see, Table 5.1) is shown in Fig. 5.7. It can be observed that the bulk viscosity is negative at higher redshift (early time) and positive at lower redshift (late time) in the HRDE model with bulk viscosity (dashed blue curve). This means that the rate of entropy production is negative in the early epoch and positive in the later epoch. Hence, the entropy law violates in the early epoch and obeys in the later epoch. However, the bulk viscosity decreases at low redshift but always positive in the HRDE model with bulk viscosity and matter creation (solid magenta curve). Thus the model does not violate the law of entropy.

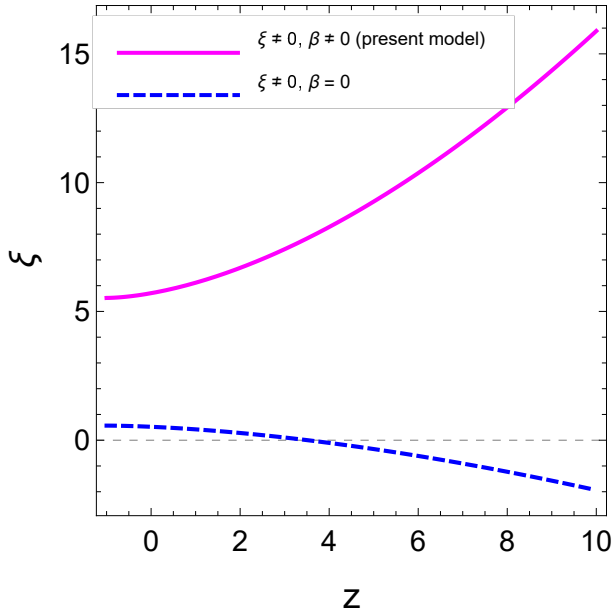

Figure 5.7: The behavior of bulk viscous coefficient with redshift for best-fit values of model parameters.

5.3.3 Geometrical Diagnostics

An important tool for investigating dark energy model characters nowadays is by the introduction of some geometry quantities, for instance the statefinder diagnostic parameters, defined by Eq. (1.12.1). The statefinder parameter pair $\{r,s\}$ of the model concerned is calculated explicitly to demonstrate the behavior of the HRDE model with bulk viscosity and matter creation which is obtained as

$$r = 1 + \frac{9(\xi_0 - \psi_1)\left(1 - \frac{\psi_1}{\psi_2}\right)}{\psi_2\, e^{\frac{3\xi_0 H_0 (t-t_0)}{\psi_2}}} + \frac{9(\xi_0 - \psi_1)^2}{\psi_2^2\, e^{\frac{6\xi_0 H_0 (t-t_0)}{\psi_2}}} \tag{5.3.18}$$

$$s = \frac{\frac{2(\xi_0-\psi_1)\left(1-\frac{\psi_1}{\psi_2}\right)}{\psi_2\, e^{\frac{3\xi_0 H_0 (t-t_0)}{\psi_2}}} + \frac{2(\xi_0-\psi_1)^2}{\psi_2^2\, e^{\frac{6\xi_0 H_0 (t-t_0)}{\psi_2}}}}{\frac{2(\psi_1-\xi_0)}{\psi_2\, e^{\frac{3\xi_0 H_0 (t-t_0)}{\psi_2}}} - 1} \tag{5.3.19}$$

By using (5.3.18) and (5.3.19), we plot the $r-s$ plane in Fig. 5.8 which shows that the trajectory starts evolving from the region $r > 1, s < 0$, which represents the behavior of the dark energy with chaplygin gas and evolves through the region $r < 1, s > 0$, which represents the quintessence model of dark energy and eventually approaches to the point of ΛCDM model represented by the point $\{1,0\}$. Thus, the HRDE model with bulk viscosity and matter creation discriminates with the ΛCDM model in early

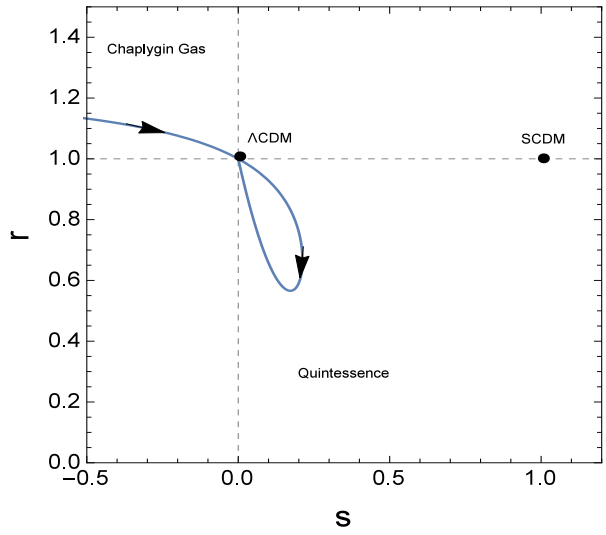

Figure 5.8: Evolution trajectory in $r-s$ plane to demonstrate the Universe evolution for best-fitted HRDE model. The fixed point $(0,1)$ corresponds to the ΛCDM model. The arrow shows the direction of the evolution of the trajectory.

time. However, the model behaves like ΛCDM model in the late time evolution of the Universe.

To illustrate more details for the HRDE model different from the ΛCDM model we also plot the function trajectory in the $r-q$ plane as shown in Fig. 5.9. The dashed line shows the time evolution of the ΛCDM model. The dashed line of the ΛCDM model divides the plane into two parts in which the upper part represents the phantom evolution of the model whereas the lower part represents the non-phantom phase. We can see that the model shows the phase transition from deceleration to acceleration as q changes its sign from positive to negative.

To examine the dynamics of the dark energy models one more diagnostic, called Om, is obtained with the help of Eq. (1.12.3) as

$$Om(z) = \frac{[\xi_0 + (\psi_1 - \xi_0)(1+z)^{\frac{3\psi_1}{\psi_2}}]^2 - \psi_1^2}{\psi_1^2[(1+z)^3 - 1]} \tag{5.3.20}$$

From the Fig. 5.10 we can observe that the negative slope of the trajectory of $Om(z)-z$ plane indicates the behavior similar to the quintessence model.

To study more about the evolution of the Universe we extend our study to the cosmographic parameters (CP), defined by Eq. (1.12.2). For our model, the variations of the jerk j, snap s and lerk l parameters is discussed by plotting their trajectories against the redshift z as shown in Fig. 5.11.

From the Fig. 5.11, we notice that the jerk parameter throughout remains positive

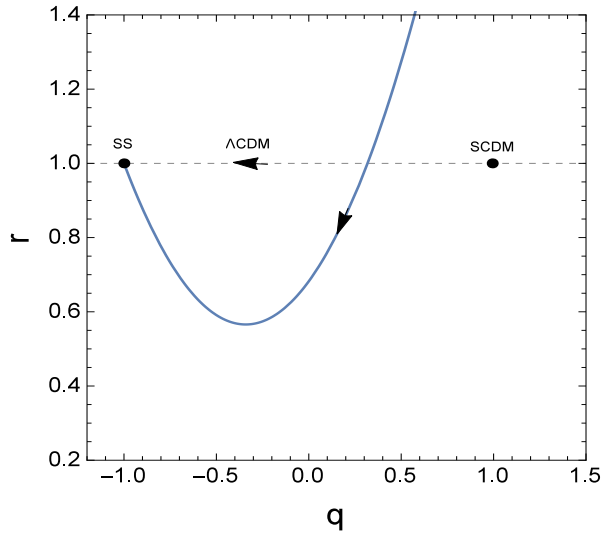

Figure 5.9: Evolution trajectory in $r-q$ plane to demonstrate the Universe evolution for best-fitted HRDE model. The horizontal dashed line indicates the ΛCDM model evolution trajectory. The arrow shows the direction of the evolution of the trajectory.

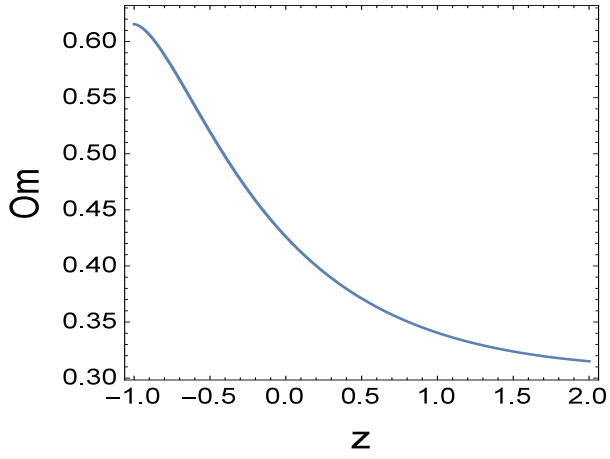

Figure 5.10: The $Om(z)-z$ diagram for HRDE model corresponding to the best-fit parameters.

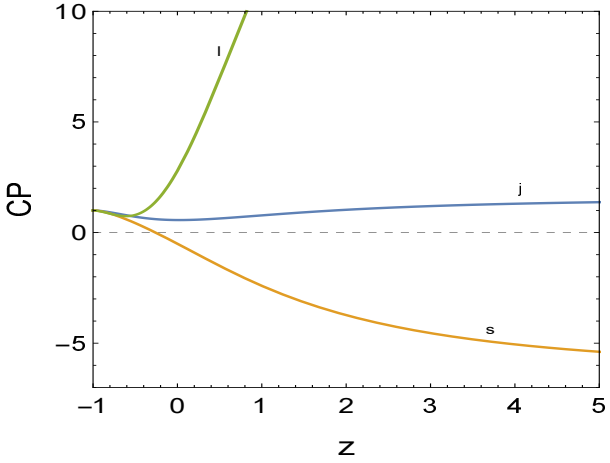

Figure 5.11: The evolution of the cosmographic parameters jerk j, snap s and lerk l for the best-fit model parameters.

and converges to 1 as z tends to -1 which corresponds to ΛCDM model. This may indicate that at present time our model is different from the ΛCDM model but at the late time converging to the ΛCDM model. The trajectory of snap parameter s shows the transition from negative to positive i.e. at the early time s takes the negative value whereas it becomes positive and approaches 1 in the late time evolution. The trajectory of l remains positive without any transition throughout the evolution and also approaches 1.

5.3.4 Energy Conditions

In general theory of relativity, the study of singularity theory of spacetime was based on energy conditions (ECs). The ECs take the form of various linear combinations of the stress-energy tensor components in such a way that the energy remains positive, or at least nonnegative [348]. The famous Raychaudhuri's equation for the expansion nature gives rise to the ECs [349]. Here it is to be noted that the Raychaudhuri's equation is purely geometric and it makes no reference to any gravitational theory under consideration. In FLRW Universe, the ECs takes the following forms:

$$\textbf{NEC} \Leftrightarrow \rho_{\text{eff}} + p_{\text{eff}} \geq 0, \tag{5.3.21}$$

$$\textbf{WEC} \Leftrightarrow \rho_{\text{eff}} \geq 0 \text{ and } \rho_{\text{eff}} + p_{\text{eff}} \geq 0, \tag{5.3.22}$$

$$\textbf{SEC} \Leftrightarrow \rho_{\text{eff}} + 3\, p_{\text{eff}} \geq 0 \text{ and } \rho_{\text{eff}} + p_{\text{eff}} \geq 0, \tag{5.3.23}$$

$$\textbf{DEC} \Leftrightarrow \rho_{\text{eff}} \geq 0 \text{ and } \rho_{\text{eff}} \geq |p_{\text{eff}}|, \tag{5.3.24}$$

where NEC, WEC, SEC and DEC correspond to the null, weak, strong and dominant energy conditions, respectively. Also in the Refs. [350–352], authors have analyzed the ECs in the general theory of relativity.

One can observe from the Figs. 5.12, 5.13, 5.14 and 5.15 that the NEC, WEC and DEC satisfied for our model while SEC is violated.

5.4 Conclusion

In the present chapter, we have discussed the holographic Ricci dark energy model while considering the effects of bulk viscosity and adiabatic matter creation within the framework of flat FLRW Universe. We have assumed the bulk viscosity coefficient as

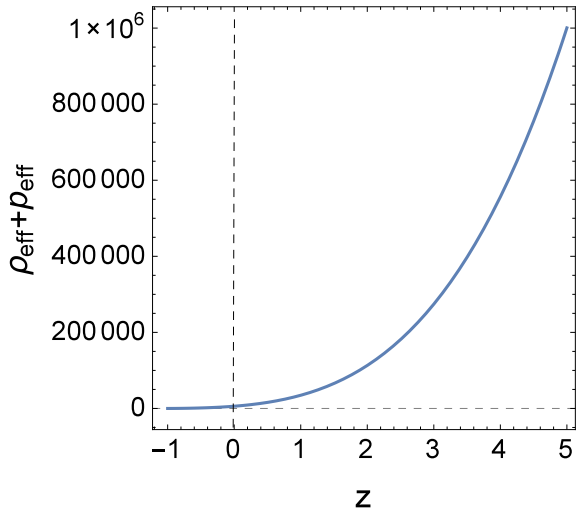

Figure 5.12: The plot of NEC against z for the best-fit model parameters.

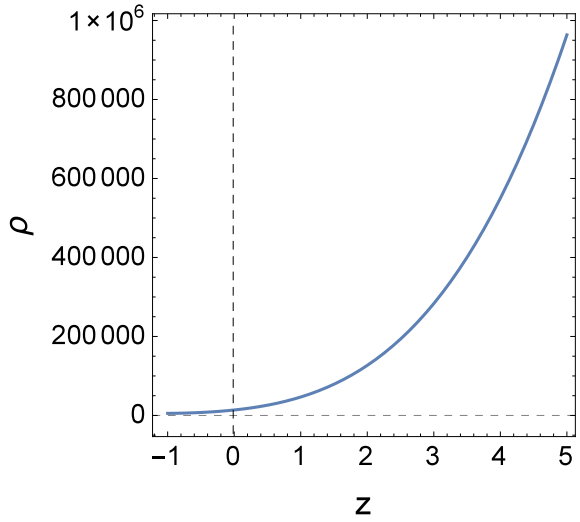

Figure 5.13: The plot of ρ against z for the best-fit model parameters.

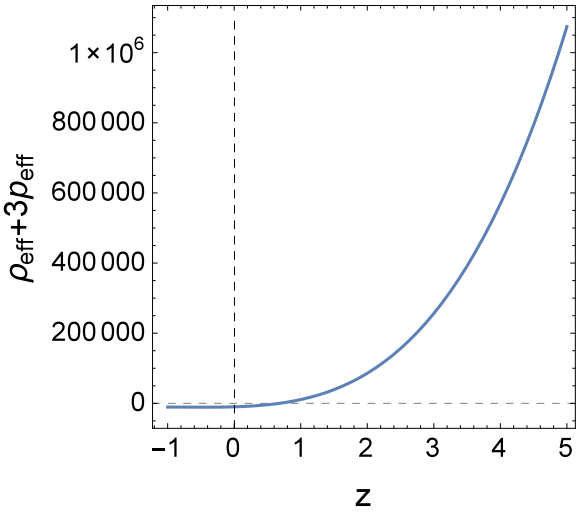

Figure 5.14: The plot of SEC against z for the best-fit model parameters.

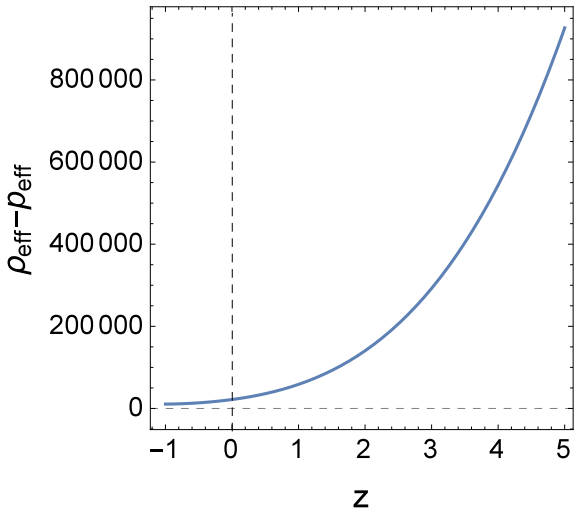

Figure 5.15: The plot of DEC against z for the best-fit model parameters.

$\zeta = \zeta_0 + \zeta_1 H$ and the particle creation rate as $\Gamma = 3\beta H$ to obtain the exact solutions for the scale factor and various physical quantities. We have considered these two dissipative phenomenons as independent irreversible processes. It has been observed that the assumption $\Gamma \propto H$ does not describe the present-day Universe (transition phase) in the absence of bulk viscosity. Also, the HRDE model without bulk viscosity and matter creation does not show transition redshift. Therefore, to overcome this problem we have introduced the bulk viscosity along with matter creation to observe the present-day Universe and we have succeeded to obtain such a model. We have obtained the function Hubble parameter in terms of redshift which is used to obtain the free parameters of the HRDE model.

We have performed the statistical analysis for our model in Sect. 5.3.1 using the latest observational data of SNe, OHD, and combined data of BAO and CMB. We have employed publicly available EMCEE codes for the implementation of the MCMC method. We have obtained the best fit values for the model parameters (see Table 5.1). Using best fit values we have found the transition value of the scale factor ($a_{tr} = 0.936$), the current value of the deceleration parameter ($q_0 = -0.362$) and EoS parameter ($\omega_{\text{eff}} = -0.575$).

To get further information about the behavior of the model we have presented the evolution of various cosmological parameters and studied various geometrical diagnostics and cosmographic parameters analytically and graphically. The deceleration parameter shows a signature flipping behavior thereby indicating the evolution of the Universe from early deceleration to present late-time acceleration (see Fig. 5.3). The behavior of effective EoS parameters (see Fig. 5.4) shows that the HRDE model be-

haves like de Sitter Universe in the late-time of evolution. It has also been observed that the trajectory of ω_{eff} does not cross the phantom divide line and thus is free from a big-rip singularity. Fig. 5.5 shows the age of the Universe with respect to redshift z for the best-fit values of the model parameters. The age of the Universe is found to be $13.397\ Gyr$ which is very close to that predicted by the ΛCDM model. From Fig. 5.6, it has been observed that these best-fit values of the model parameters are in good agreement with the predictions of the standard model. The reduced χ^2_{red} obtained for the HRDE model provides a very good fit to the considered observational data.

Furthermore, we have performed the statefinder diagnostic analysis to this HRDE model with bulk viscosity and matter creation to discriminate from the ΛCDM model. In Fig. 5.8, we have plotted the $r-s$ trajectory and observed that our model is finally approaching ΛCDM while in Fig. 5.9 there is a sign change of q from positive to negative which shows that our model changes the phase from deceleration to acceleration. In both the figures arrows show the direction of the trajectories in the plane. The Om diagnostic which is obtained from the Hubble parameter shows the negative slope in $Om(z)-z$ plane trajectory (Fig. 5.10) i.e. it shows the behavior similar to the quintessence model. We have also discussed cosmographic parameters like jerk j, snap s, lerk l to compare our model with the ΛCDM model. From the Fig. 5.11, we can observe from the trajectory of jerk j that at present our model is different from the ΛCDM model but in the late time, it converges to ΛCDM. We can observe from the trajectory of snap parameter s that it changes its sign from negative to positive during the evolution and finally converges to 1. Similarly, the lerk parameter l shows no transition with respect to z and reaches 1 in the late future.

Finally, we have examined the energy conditions of our model to analyze the physical viability of the model. It has been observed from the Figs. 5.12–5.15 that the NEC, WEC and DEC satisfied but SEC fails to hold for our model.

****

Chapter 6

Cosmology of Matter Creation in FLRW Model

In this chapter [1], we propose a new generalized form of the matter creation rate, $\Gamma = 3\delta H_0 + 3\beta H + 3\gamma\left(\frac{\dot{H}}{H} + H\right)$ to discuss the evolution of the Universe. The best fit of the model parameters is obtained from Markov Chain Monte Carlo (MCMC) analysis using the observational data of SNe, OHD, BAO/CMB. We apply Akaike information criterion (AIC) and Bayesian information criterion (BIC) to discriminate the model based on the penalization associated with the number of parameters. We also discuss the thermodynamics of the model.

---

[1] The work presented in this chapter comprises the results of a research paper entitled "Quintessence behavior via matter creation cosmology, *The European Physical Journal C* **80**, 106 (2020)".

6.1 Introduction

In general relativistic cosmology, the presence of negative pressure is the key ingredient to accelerate the expansion. This kind of stress occurs naturally in many different contexts when the physical systems depart from thermodynamic equilibrium states. In this connection, as first pointed out by Zeldovich [353], the process of cosmological particle creation at the expense of the gravitational field can phenomenologically be described by negative pressure and the associated entropy production. Prigogine et al. [225, 226] were first to put forward the self-consistent macroscopic formulation of the matter creation process. They used the generalized form of the first law of thermodynamics to describe the flow of energy from the gravitational field to the matter field, resulting in the creation of particles. The authors argued that the creation of matter can occur only as an irreversible process at the expense of the gravitational field.

It was also shown that matter creation, at the expense of the gravitational field, can effectively be discussed in the realm of relativistic non-equilibrium thermodynamics. It was also demonstrated that the matter creation is an irreversible process completely different from bulk viscosity mechanism [227, 354]. This formalism gives a balance equation for the number of created particles along with Einstein field equations. The combination of this equation with the second law of thermodynamics yields an additional negative pressure that depends on the rate of matter creation. Calvao et al. [228] proposed a generalization of this result to include the variation of specific entropy through a covariant formulation.

A model with adiabatic matter creation was proposed in order to interpret the cosmological entropy and to solve the Big-Bang singularity problem. However, after the discovery of the accelerating expansion of the Universe, this model was reconsidered to explain the expansion of the Universe and got some unexpected results. It has been pointed out that the matter creation can play the role of a dark energy component and lead to driving the accelerating expansion of the Universe.

In this context, Many authors [227, 229, 231, 244, 337, 355–358] have discussed FLRW line element with matter creation cosmology and analyzed the results through the observations. It has been shown that the matter creation models are consistent with the observations. Zimdahl et al. [359] tested the matter creation models with SNe data and got the result of accelerating Universe. Yuan et al. [360] studied the models with adiabatic matter creation and showed that the model is consistent with SNe data.

Many phenomenological models with matter creation have been proposed in the literature [237, 248, 310–312, 361] to study the late-time evolution of the Universe.

We are mainly interested in the paper of Prigogine and collaborators [225], in which the authors have applied the thermodynamics of open systems to cosmology, allowing both particle and entropy productions. Recently, it has been found that the matter creation cosmology successfully explains the current accelerated expansion [313]. Therefore, this field is very appealing as many important observations are carried out during the past many years with matter creation.

In this chapter, we have presented a matter-dominated cosmological model with matter creation within the framework of the FLRW line element. We have proposed a generalized form of matter creation rate and investigated the evolution equations by independent/combined observational data of SNe, OHD, and BAO/CMB. We have observed that the best-fit values of the model parameters give a smooth transition from decelerating phase to the accelerating phase. We have studied two independent diagnostic tests, namely, the statefinder parameter and the *Om* diagnostic to discriminate our model from the ΛCDM. We have applied AIC and BIC to discriminate the model. We have also performed a thermodynamic analysis based on the generalized second law (GSL) of thermodynamics and explore the restrictions on the free parameters of the cosmological model to satisfy the GSL.

The chapter has been organized as follows. In Section 6.2, we have presented a brief review of matter creation cosmology and the field equations. The solution of the field equations has been discussed in Section 6.3. In Section 6.4, we have presented the result and discussion of the model for the obtained best-fit values of the model parameters. In Section 6.5, we have discussed the model selection criteria to discriminate the model. We have discussed the thermodynamic of the model based on the generalized second law of thermodynamics in Section 6.6. Finally, we have summarized our findings in Section 6.7. It is to be noted that throughout the chapter, we use particle creation and matter creation synonymously.

6.2 Field Equations with Matter Creation

Let us start with the homogeneous and isotropic flat Friedmann-Lemaître-Robertson-Walker (FLRW) line element given by (2.2.1). The energy-momentum tensor for per-

fect fluid with particle creation is given by

$$T_{\mu\nu} = (\rho + P)\, u_\mu u_\nu + P\, g_{\mu\nu}, \tag{6.2.1}$$

satisfying the covariant conservation equation $T^{\mu\nu}{}_{;\nu} = 0$. In (6.2.1), u_μ is the fluid four-velocity, ρ is the energy density and P is the dynamics pressure which is given by

$$P = p + p_c, \tag{6.2.2}$$

where p is the equilibrium pressure and p_c is the pressure due to the matter creation. The particle flux vector has the form

$$N^\mu = nu^\mu, \tag{6.2.3}$$

where N is the total particle number in a comoving volume V, $n = N/V$ is the particle density and u^μ is the usual four velocity vector of the created particles. In the gravitationally induced particle creation mechanism, (6.2.3) satisfies the balance equation [225]

$$N^\mu{}_{;\mu} = \Gamma, \tag{6.2.4}$$

where Γ is the rate of matter creation from the gravitational field. In principle, $\Gamma > 0$ represents the matter creation, $\Gamma < 0$ is for matter annihilation, and $\Gamma = 0$ is the case when there is no matter creation. In general, the exact form of Γ is unknown, but it should be determined in the context of quantum processes in curved space time.

In this background, the field equations (2.2.2) for line element (2.2.1) and EMT (6.2.1) are given by [227, 228]

$$3H^2 = \rho, \tag{6.2.5}$$

$$2\dot{H} = -(\rho + p + p_c), \tag{6.2.6}$$

where ρ and p are energy density and pressure, respectively, of matter existing in the Universe in the form of cold dark matter during matter dominated era, and p_c is the pressure due to the matter creation. The dot denotes derivative with respect to cosmic time t. The energy conservation law is given by

$$\dot{\rho} + 3(\rho + p + p_c)H = 0. \tag{6.2.7}$$

As the particle number is not conserved (i.e., $N^{\mu}{}_{;\mu} \neq 0$), the conservation equation (6.2.4) takes the form

$$\frac{\dot{N}}{N} = \frac{\dot{n}}{n} + 3H = \Gamma. \tag{6.2.8}$$

It is to be noted that the creation pressure p_c must be defined in terms of the creation rate and other physical quantities. In the case of adiabatic particle production, the particles and entropy are generated but the entropy per particle does not vary. Under such 'adiabatic condition', the creation pressure can be written as [237]

$$p_c = -\frac{\Gamma}{3H}(\rho + p). \tag{6.2.9}$$

In what follows, we present the solution of the model with matter creation.

6.3 Solution of Field Equations

The discussion in previous section 6.2 shows that we can describe the dynamics of the Universe only if the matter creation rate is known. The nature of Γ is unknown as the associated quantum field theory (QFT) is yet to be developed. Steigman et al. [236,237] proposed a class of particle creation driven model of the form $\Gamma = 3\delta H_0 + 3\beta H$ to study the late-time evolution of the Universe.

In this chapter, we propose a new class of $\Gamma(t)$ cosmology in a spatially flat FLRW Universe where $\Gamma(t)$ is assumed to be the function of Hubble rate and its cosmic derivative. We cover a series of $\Gamma(t)$ (equivalently, $\Gamma(H_0, H, \dot{H})$) model in order to see their dynamical evolutions and viabilities. We propose the following general form of Γ:

$$\Gamma = 3\delta H_0 + 3\beta H + 3\gamma\left(\frac{\dot{H}}{H} + H\right), \tag{6.3.1}$$

which is a linear combination of three terms: the first term is a constant, the second term is proportional to the Hubble parameter, which characterizes the dependence of the matter creation on expansion rate, and the third term is proportional to $\ddot{a}/\dot{a}$, characterizing the effect of acceleration of the expansion. Here, δ, β and γ are dimensionless free parameters lying in the interval $[0,1]$ to be determined by observations, H_0 is the present value of the Hubble parameter and the factor 3 has been maintained for mathematical convenience.

The motivation of considering this form of Γ comes from the matter creation thermodynamics. We know that the transport phenomena is related to velocity, which is

related to the Hubble parameter, and the acceleration. Since we don't know the exact form of Γ, so a linear combination of three terms of parametrization of Γ is more physical. The existence of a transition redshift at late time also determines the form of matter creation rate.

We are interested in processes that occurred after radiation-dominated phase. Therefore, we neglect radiation and baryons, and consider only the presence (and creation) of pressureless $(p = 0)$ dark matter particles. In this case, Eq. (6.2.9) reduces to $p_c = -\rho\,\Gamma/3H$ for which equation (6.2.7) reduces to

$$\frac{\dot{\rho}}{\rho} + 3\left(1 - \frac{\Gamma}{3H}\right)H = 0, \tag{6.3.2}$$

Combining (6.2.5) and (6.3.2), and using (6.3.1), we obtain the following dimensionless equation

$$\frac{\dot{h}}{h} + \frac{3(1-\beta-\gamma)}{(2-3\gamma)}H_0\,h = \frac{3\delta}{(2-3\gamma)}H_0, \tag{6.3.3}$$

where $h = H/H_0$ is the dimensionless Hubble parameter. Using $\frac{d}{dt} = \frac{\dot{a}}{a}\frac{d}{d\,lna}$, the above equation can be written as

$$h' + \frac{3(1-\beta-\gamma)}{(2-3\gamma)}\,h = \frac{3\delta}{(2-3\gamma)}, \tag{6.3.4}$$

where a prime denotes the derivative with respect to conformal time $ln\,a$. Using $h(a_0) = 1$, (6.3.4) gives the solution as

$$h(a) = \frac{\delta}{(1-\beta-\gamma)} + \left(1 - \frac{\delta}{(1-\beta-\gamma)}\right)\left(\frac{a}{a_0}\right)^{-\frac{3(1-\beta-\gamma)}{(2-3\gamma)}}. \tag{6.3.5}$$

Equation (6.3.5) shows that when δ, β and γ are all zero, the Hubble parameter, $H = H_0(a/a_0)^{-3/2}$ which corresponds to the ordinary matter dominated Universe. On integration of (6.3.5), the scale factor $a(t)$ (or the redshift, z), normalized to unity at present epoch, evolves with time as

$$a(t) = \frac{1}{(1+z)} = \left[\frac{(1-\beta-\gamma)e^{\frac{3\delta H_0}{(2-3\gamma)}(t-t_0)} - 1 + (\delta+\beta+\gamma)}{\delta}\right]^{\frac{(2-3\gamma)}{3(1-\beta-\gamma)}}, \tag{6.3.6}$$

where $(\beta+\gamma) \neq 1$. We can study three different cases: $0 < \delta+\beta+\gamma < 1$, $\delta+\beta+\gamma = 1$ and $\delta+\beta+\gamma > 1$. In the case $0 < \delta+\beta+\gamma < 1$, we observe that in the early time as $t \to 0$, the scale factor $a(t) \to \left[1 + \frac{3(1-\beta-\gamma)H_0}{(2-3\gamma)}(t-t_0)\right]^{\frac{(2-3\gamma)}{3(1-\beta-\gamma)}}$, which corresponds to

an early decelerated expansion and in the late time as $t \to \infty$, the scale factor $a(t) \to e^{\frac{3\delta H_0}{(2-3\gamma)}(t-t_0)}$, corresponding to de Sitter like Universe. The model predicts a Big-Bang in the past at cosmic time: $t_B = t_0 + \frac{(2-3\gamma)}{3\delta H_0} \ln\left(\frac{1-(\delta+\beta+\gamma)}{1-\beta-\gamma}\right)$.

The transition time can be obtained by equating to zero the second derivative of scale factor given in (6.3.6) with respect to time which is given by

$$t_{tr} = t_0 + \frac{(2-3\gamma)H_0^{-1}}{3\delta}\, ln\left(\frac{(3-3(\delta+\beta+\gamma))}{(2-3\gamma)}\right). \tag{6.3.7}$$

The Hubble parameter in terms of redshift z, where $1+z = a^{-1}$, reads

$$H(z) = H_0\left[\frac{\delta}{(1-\beta-\gamma)} + \left(1 - \frac{\delta}{(1-\beta-\gamma)}\right)(1+z)^{\frac{3(1-\beta-\gamma)}{(2-3\gamma)}}\right]. \tag{6.3.8}$$

When $\gamma = 0$, i.e., $\Gamma = 3\delta H_0 + 3\beta H$ (See, Ref. [236]), (6.3.6) and (6.3.8) reduce to (14) and (13) of [236]. Further, In the limit $\delta \to 0$, the above equation reduces to (16) in [355].

To obtain the transition scale factor a_{tr} where the transition from decelerated phase to accelerated phase takes place, we take the derivative of (6.3.5) with respect to a,

$$\frac{d\dot{a}}{da} = \left[\frac{\delta}{1-\beta-\gamma} + \frac{(3\beta-1)(1-\delta-\beta-\gamma)}{(2-3\gamma)(1-\beta-\gamma)}\, a^{-\frac{3(1-\beta-\gamma)}{2-3\gamma}}\right]. \tag{6.3.9}$$

Equating (6.3.9) to zero, we obtain the transition scale factor, a_{tr} as

$$a_{tr} = \left[\frac{(1-3\beta)(1-\delta-\beta-\gamma)}{\delta(2-3\gamma)}\right]^{\frac{2-3\gamma}{3(1-\beta-\gamma)}}. \tag{6.3.10}$$

It is clear that for $\delta+\beta+\gamma = 1$ or $\beta = 1/3$, the transition from decelerated phase to accelerated phase occurs at a time corresponding to $a_{tr} \to 0$ closer to Big-Bang. In this case, $a = \exp(H_0(t-t_0))$, corresponds to de Sitter Universe. In this case the model predicts an accelerated expansion from the beginning. For $(\delta+\beta+\gamma) < 1$, the transition occurs in late-time whereas for $(\delta+\beta+\gamma) > 1$, there is no transition and in this case the model always accelerates from very early time.

An important cosmological quantity is the deceleration parameter q, which is an indicator of the accelerating/decelerating nature of the evolution of the Universe. It is straightforward to show from (6.3.6) that the deceleration parameter takes the following

form in terms of cosmic time t:

$$q = -1 + \frac{3(1-\delta-\beta-\gamma)}{2-3\gamma} e^{-\frac{3\delta H_0}{2-3\gamma}(t-t_0)}. \tag{6.3.11}$$

The redshift dependence of the deceleration parameter is obtained as

$$q = -1 + \frac{3(1-\delta-\beta-\gamma)}{(2-3\gamma)\left[1+\frac{\delta}{1-\beta-\gamma}\left((1+z)^{-\frac{3(1-\beta-\gamma)}{2-3\gamma}}-1\right)\right]}. \tag{6.3.12}$$

It can be observed that $q(z) \to -1$ as $z \to -1$, i.e., $q(z)$ approaches to -1 in future and for $z = 0$, we get $q_0 = \frac{1-3(\delta+\beta)}{2-3\gamma}$. This shows that for $\delta+\beta = 1/3$, the deceleration parameter $q_0 = 0$. This implies that the transition into accelerating phase would occur at the present time. In the absence of matter creation, i.e., for $\delta = \beta = \gamma = 0$, we get $q = 0.5$, a value of q in matter-dominated model. Putting $q = 0$ in (6.3.12), the transition redshift is given by

$$z_{tr} = \left[\frac{\delta(2-3\gamma)}{(1-3\beta)(1-\delta-\beta-\gamma)}\right]^{\frac{2-3\gamma}{3(1-\beta-\gamma)}} - 1. \tag{6.3.13}$$

It is to be noted that for $\delta = 0$, we get $z_{tr} = -1$, i.e., the transition would be in future which gives the contradiction with SNe data. From (6.2.5) and (6.3.5), we obtain the mass density parameter $\Omega_m = \rho/\rho_c$ and $\rho_c = 3H_0^2$ as,

$$\Omega_m(a) = \left[\left(1-\frac{\delta}{1-\beta-\gamma}\right)\left(\frac{a}{a_0}\right)^{-\frac{3(1-\beta-\gamma)}{2-3\gamma}} + \frac{\delta}{1-\beta-\gamma}\right]^2. \tag{6.3.14}$$

We observe that for $\delta = \beta = \gamma = 0$, the mass density parameter reduces to $\Omega_m \sim a^{-3}$, which corresponds to the matter dominated phase with null matter creation. It is also noted that as $a \to 0$, the mass density diverges.

In what follows we constrain the free parameters of the model coming from the background tests.

6.4 Parameter Estimation and Analysis

In this section we briefly present some details of the statistical method and observational sample that we adopt in order to constrain the model. We normalized $H(z)$ using the latest Planck data $H_0 = 67.8 \pm 0.9\ kms^{-1}Mpc^{-1}$ [20].

Using the observational data of SNe, OHD, BAO/CMB as discussed in section 1.13, we test the cosmological model with adiabatic matter creation, assuming a spatially flat Universe. We perform a global fitting to determine the model parameters using the MCMC method. We adopt a Python implementation of the ensemble sampler for MCMC, the 'emcee', introduced by Foreman-Mackey et al. [317]. The best fitting results of parameters are listed in Table 7.1. In our statistical analysis, the model parameters can be determined through the χ^2 minimization method. We minimize the function χ^2 of individual from (1.13.3), (1.13.4), (1.13.8) and jointly. A joint likelihood analysis is given by

$$\chi^2_{total} = \chi^2_{SNe} + \chi^2_{OHD} + \chi^2_{BAO}. \tag{6.4.1}$$

In statistical analysis, we find the best-fit values of model parameters at $1\sigma(68.3\%)$

Table 6.1: The best-fit results of model parameters and free normalization parameter M obtained from the analysis with different combinations of the data sets

Data set	δ	β	γ	M
SNe	$0.263^{+0.187}_{-0.170}$	$0.249^{+0.155}_{-0.161}$	$0.166^{+0.180}_{-0.113}$	$24.942^{+0.023}_{-0.028}$
SNe+OHD	$0.423^{+0.080}_{-0.117}$	$0.068^{+0.075}_{-0.048}$	$0.322^{+0.097}_{-0.084}$	$24.946^{+0.018}_{-0.020}$
SNe+BAO/CMB	$0.438^{+0.087}_{-0.153}$	$0.074^{+0.088}_{-0.058}$	$0.303^{+0.113}_{-0.077}$	$24.936^{+0.022}_{-0.022}$
SNe+OHD+BAO/CMB	$0.431^{+0.077}_{-0.131}$	$0.069^{+0.078}_{-0.048}$	$0.274^{+0.112}_{-0.076}$	$24.952^{+0.017}_{-0.018}$

and $2\sigma(95.4\%)$ of confidence level, respectively, satisfying the constraints $0 < \delta < 1$, $0 < \beta < 1$, $0 < \gamma < 1$ and $0 < (\delta + \beta + \gamma) < 1$. We can test the reliability by comparing the result with spatially flat ΛCDM model. We observe that the model provides a very good fit to these data. Figures 6.1–6.4 show confidence contours and the marginalized likelihood function of model at $1\sigma(68.3\%)$ (inner contour) and $2\sigma(95.4\%)$ (outer contour) using observational data of SNe, $SNe + OHD$, $SNe + BAO/CMB$ and $SNe + OHD + BAO/CMB$, respectively.

It can be observed from Table 7.1 that the result of the free parameters obtained from SNe data is a little different from $SNe + OHD$, $SNe + BAO/CMB$ and $SNe + OHD + BAO/CMB$. The error bars of free parameters are relatively large in the case of SNe data.

Figure 6.5 shows the evolution of the scale factor for best-fit values of model parameters. The trajectory of the best-fit values shows that the Universe starts its expansion

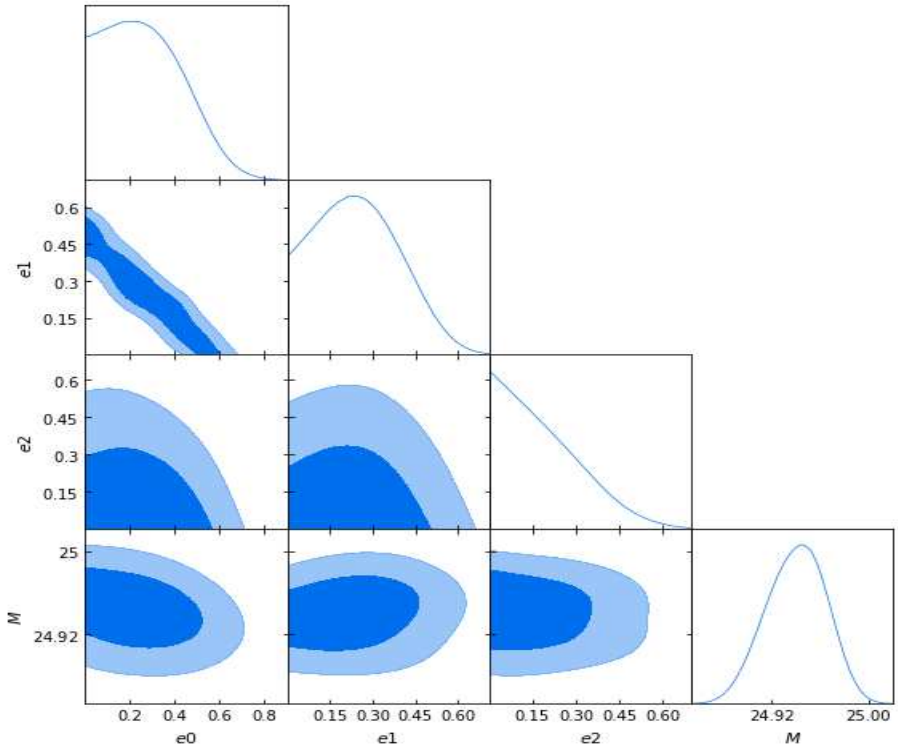

Figure 6.1: The contour map of matter creation model using data from SNe with marginalized probability for the parameters. The associated $1\sigma(68.3\%)$ and $2\sigma(95.4\%)$ confidence contours are shown. In Fig. the symbols $e0$, $e1$ and $e2$ denote the model parameters δ, β and γ, respectively.

at an accelerated rate at very early times for the best-fit values of model parameters obtained from different individual/combined observational data set. The trajectory (dotted curve) is also shown for a matter-dominated model in the absence of matter creation which shows decelerated expansion. The dots denote the transition point where the transition from decelerated phase to accelerated phase occurs. Using the best-fit values, the transition scale factor, a_{tr} and the corresponding redshift transition values, z_{tr} are listed in Table 6.2. It is observed that the value of $z_{tr} = 2.8619$ obtained from SNe and $z_{tr} = 1.0147$ from $SNe + BAO/CMB$ for the model are substantially higher than the values of z_{tr} from $SNe + OHD$, $SNe + OHD + BAO/CMB$ and ΛCDM model.

The evolution of the deceleration parameter, q with redshift for best-fit values is shown in Fig. 6.6. The deceleration parameter is a monotonically increasing function of z. It is observed that there is a sign change in each trajectory of $q(z)$ from positive to negative showing that the Universe transits from decelerated phase to accelerated phase (positive values of q indicate decelerating expansion while negative values indicate an accelerating evolution). We find that the model transits at around $z_{tr} = 0.8386$ and $z_{tr} = 0.8633$ through joint analysis of $SNe + OHD$ and $SNe + OHD + BAO/CMB$, respectively. These results are in good agreement with the concordance of Λ cosmol-

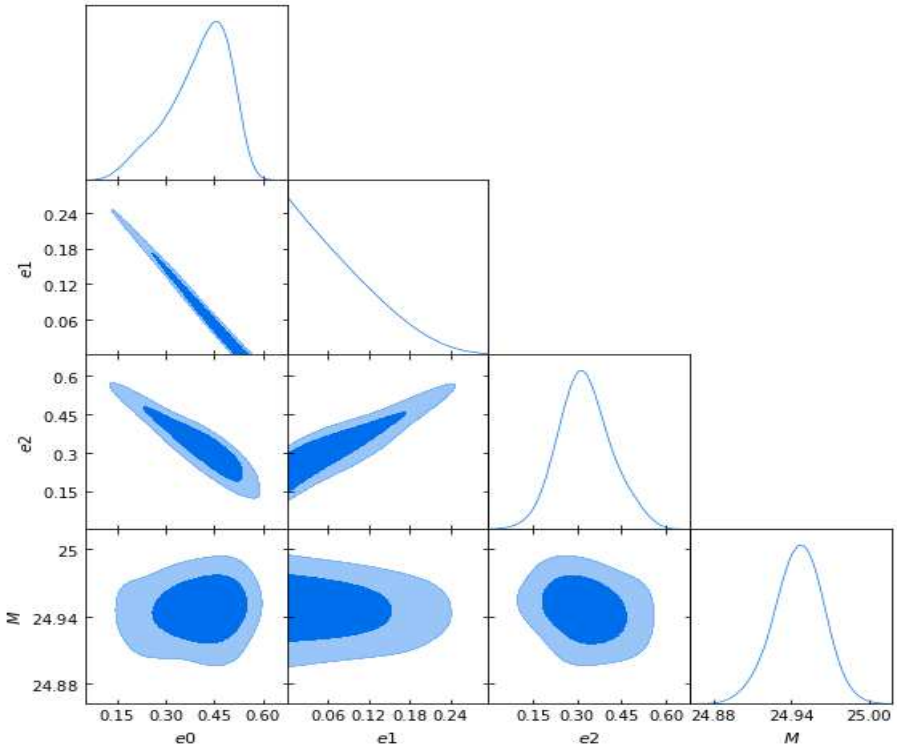

Figure 6.2: The contour map of matter creation model based on joint analysis of $SNe + OHD$ showing contours of $1\sigma(68.3\%)$ and $2\sigma(95.4\%)$ regions with marginalized probability for the parameters. In Fig. the symbols $e0$, $e1$ and $e2$ denote the model parameters δ, β and γ, respectively.

ogy [362]. The present-day value of q_0 and the transition redshift z_{tr} are listed in Table 6.2. The values of q_0 lie in range $-1 \leq q_0 < 0$ through each observational data set.

The effective equation of state (EoS) parameter, ω_{eff}, can be obtained by using (6.3.5) into (4.3.17) as

$$\omega_{\text{eff}} = -1 + \frac{2(1-\delta-\beta-\gamma)}{(2-3\gamma)\left[1+\frac{\delta}{1-\beta-\gamma}\left((1+z)^{-\frac{3(1-\beta-\gamma)}{2-3\gamma}}-1\right)\right]}. \tag{6.4.2}$$

As $z \to -1$, $(a \to \infty)$, we get $\omega_{\text{eff}} \to -1$, which can also be observed from Fig. 6.7. This can also be obtained if we take $\delta+\beta+\gamma = 1$. It means that the model corresponds to ΛCDM in future time. The EoS parameter does not cross the phantom divide line $\omega \leq -1$ which shows that the matter creation model is free from big-rip singularity.

The present value ($h = 1$) of ω_{eff} is found to be

$$\omega_{\text{eff}}(z=0) = -1 + \frac{2(1-\delta-\beta-\gamma)}{(2-3\gamma)}. \tag{6.4.3}$$

The present values of ω_{eff} are listed in Table 6.2 using different observational data

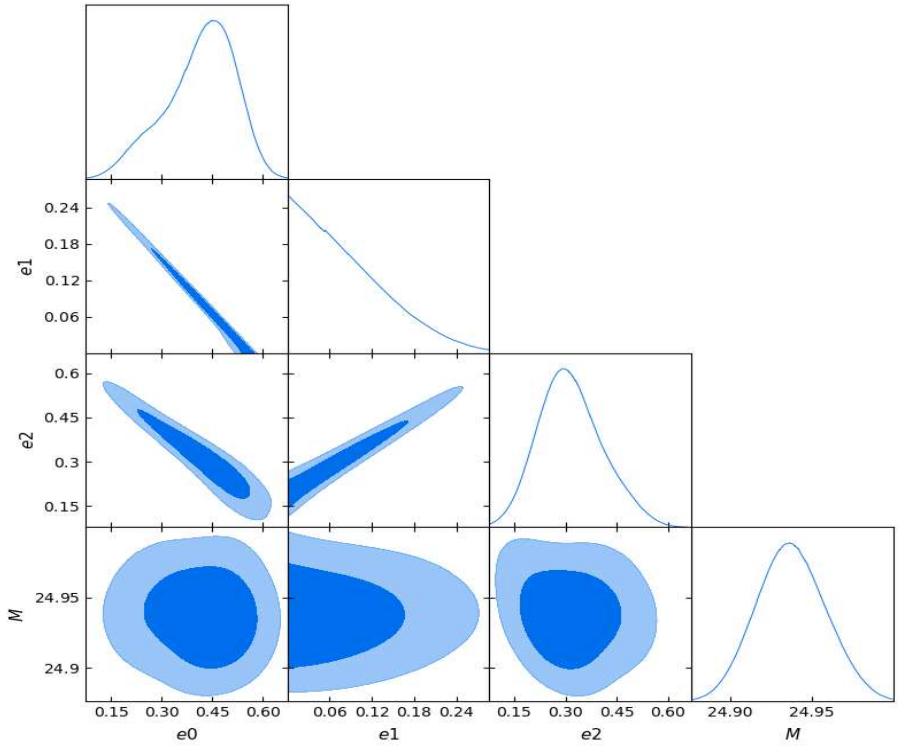

Figure 6.3: The contour map of matter creation model based on joint analysis of $SNe + BAO/CMB$ showing contours of $1\sigma(68.3\%)$ and $2\sigma(95.4\%)$ regions with marginalized probability for the parameters. In Fig. the symbols $e0$, $e1$ and $e2$ denote the model parameters δ, β and γ, respectively.

set. These values are comparatively higher than that predicted by the joint analysis of $WMAP + BAO + H_0 + SNe$ data which is around -0.93 [21].

Using (6.3.8) into (4.3.21), the trajectory of the age of the Universe with redshift for the best estimates of model parameters is shown in Fig. 6.8. The current age of the Universe is $t_0 \simeq 13.9\ Gyr$ while the transition point is located at $a_{tr} \simeq 0.58$ (hence at redshift $z_{tr} \simeq 0.72$. The ages of the Universe corresponding to $SNe + OHD$ and $SNe + OHD + BAO/CMB$ are found to be 13.9 Gyr. So, the age predicted by the present model is agreeing with the age deduced from ΛCDM model.

We compare our model with the ΛCDM model with the error bar plots of Hubble dataset in the range $z \in (0,2)$ as shown in Fig. 6.9. Although at the low redshifts, the cosmological evolution is practically independent on the best-fit values, at higher redshifts there is a significant effect of the parameter values on the cosmic expansion as can be observed from Fig. 6.9. The cosmic expansion of $SNe + OHD$ and $SNe + OHD + BAO/CMB$ differ appreciably in the case of SNe and $SNe + BAO/CMB$. It is possible to get a good fit using joint statistical analysis of $SNe+OHD$ and $SNe + OHD + BAO/CMB$. The Hubble function is a monotonically increasing function of the redshift (monotonically decreasing function of time) for all best-fit values of parame-

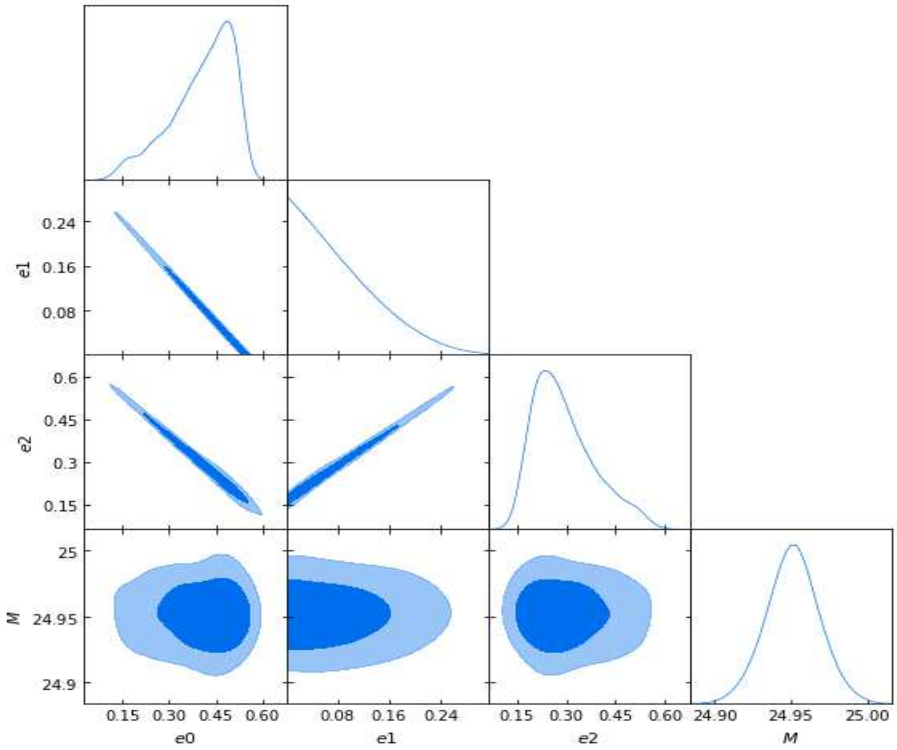

Figure 6.4: The contour map of matter creation model based on joint analysis of $SNe + OHD + BAO/CMB$, showing contours of $1\sigma(68.3\%)$ and $2\sigma(95.4\%)$ regions with marginalized probability for the parameters. In Fig. the symbols $e0$, $e1$ and $e2$ denote the model parameters δ, β and γ, respectively.

ters.

Now, we present our analysis on comparing the present model with other standard models of DE using the statefinder parameters $\{r,s\}$. For our model, $\{r,s\}$ are given by

$$r = 1 + \frac{9(1-\delta-\beta-\gamma)^2}{(2-3\gamma)^2\, e^{\frac{6\delta H_0(t-t_0)}{2-3\gamma}}} + \frac{9(1-\delta-\beta-\gamma)(-1-\beta+2\gamma)}{(2-3\gamma)^2\, e^{\frac{3\delta H_0(t-t_0)}{2-3\gamma}}}, \tag{6.4.4}$$

$$s = \frac{2(1-\delta-\beta-\gamma)\left[(1+\beta-2\gamma) - (1-\delta-\beta-\gamma)\, e^{\frac{-3\delta H_0(t-t_0)}{2-3\gamma}}\right]}{(2-3\gamma)\left[(2-3\gamma)\, e^{\frac{3\delta H_0(t-t_0)}{2-3\gamma}} - 2(1-\delta-\beta-\gamma)\right]}. \tag{6.4.5}$$

From the above equations, we observe that as $(t-t_0) \to \infty$, $\{r,s\} \to \{1,0\}$ which coincide with the ΛCDM model. This can also be achieved by assuming $\delta+\beta+\gamma = 1$ which gives the de Sitter behavior. The $s-r$ plane trajectory of the model for best-estimated values of parameters obtained by observational data set are shown in Fig. 6.10. The direction of trajectories is shown by the arrows. The trajectory obtained through SNe lies in the region $r < 1$, $s > 0$, which is the general behavior of any quintessence model. The other trajectories from $SNe + OHD$, $SNe + BAO/CMB$

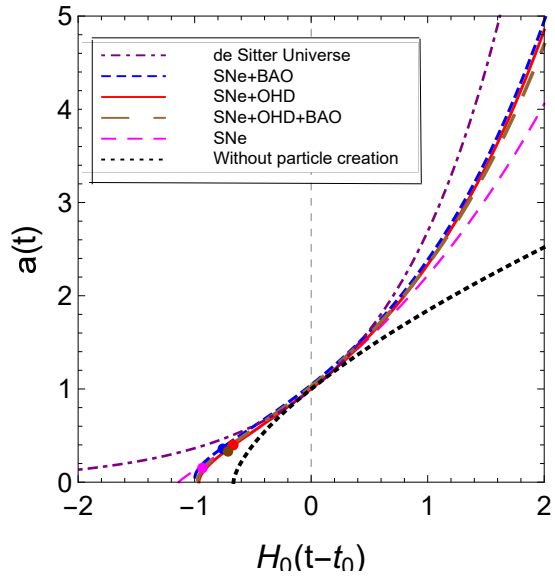

Figure 6.5: The scale factor as a function of time. A dot denotes the transition point where the transition from decelerated phase to accelerated phase occurs.

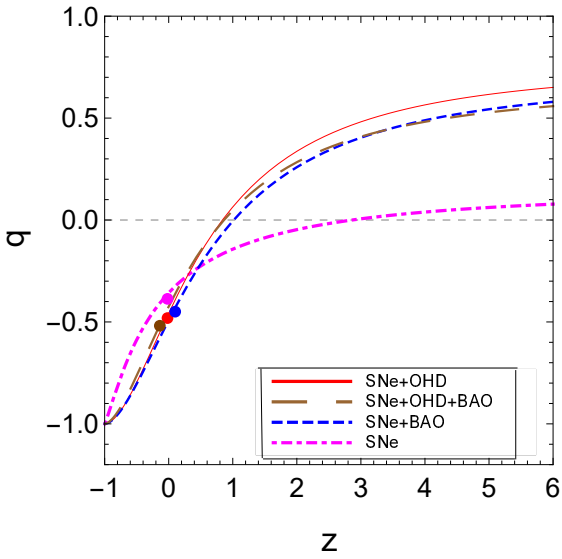

Figure 6.6: The deceleration parameter as a function of redshift for best-fit values of model parameters obtained from observational data. A dot denotes the current value of q (hence q_0).

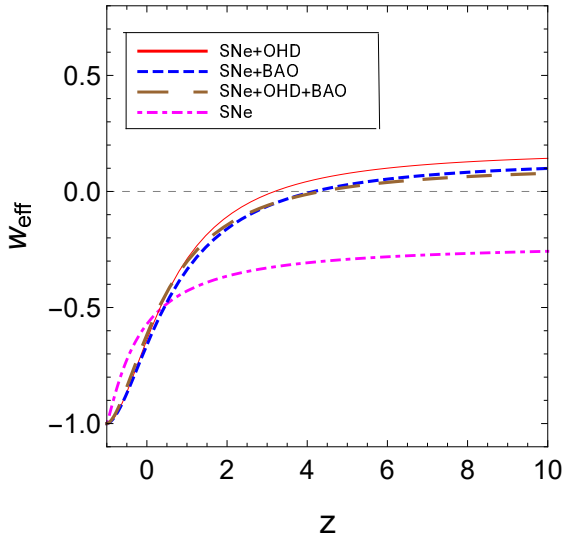

Figure 6.7: The variation of effective EoS parameter as a function of redshift for best-fit values of model parameters.

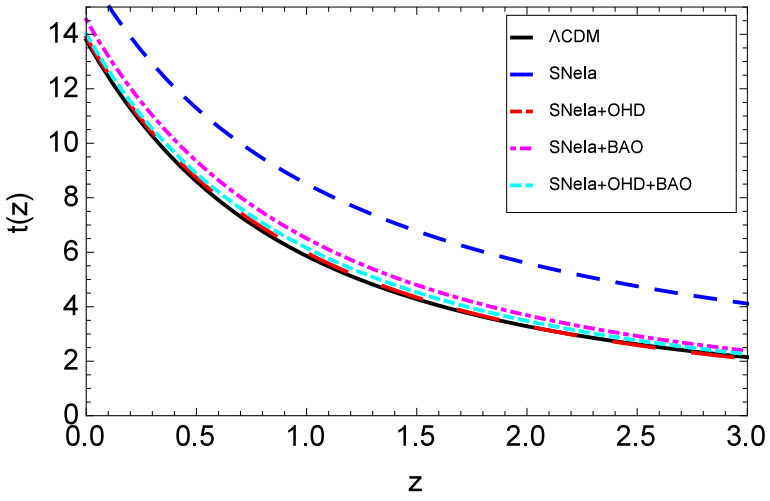

Figure 6.8: The age of the Universe as a function of redshift for best-fit values of model parameters.

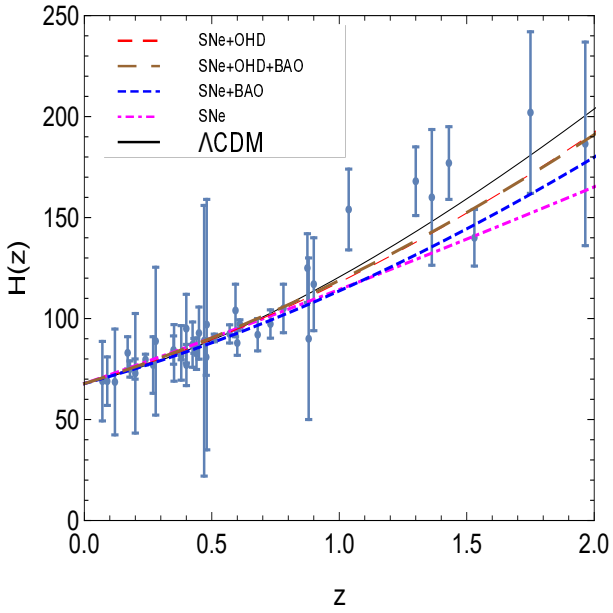

Figure 6.9: Variation of the Hubble function as a function of the redshift z for the best-fit values of the model. The observational 43 $H(z)$ points are shown with error bars (grey color). The variation of the Hubble function in the standard ΛCDM model is also represented as the solid curve.

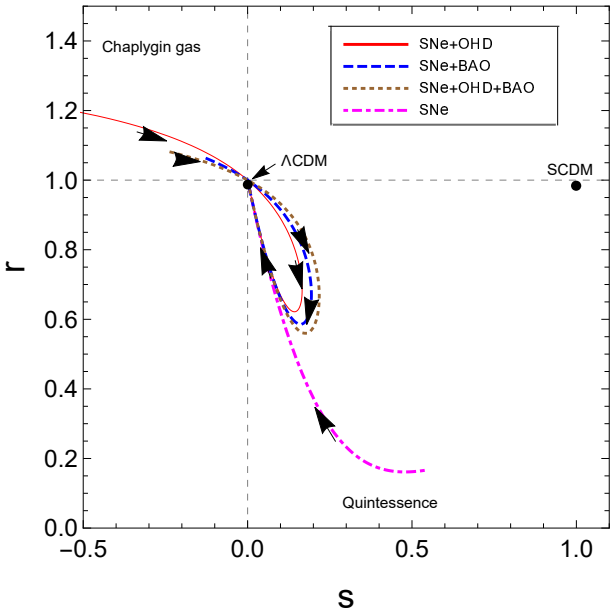

Figure 6.10: The trajectory of $\{r,s\}$ in $s-r$ plane corresponds to best-fitted parameters. The arrow shows the direction of the evolution of the trajectory.

Table 6.2: The numerical values of a_{tr}, z_{tr}, q_0, $\omega_{\text{eff}}(z=0)$ and t_0 using best-fit results of model parameters

Data	a_{tr}	z_{tr}	q_0	$\omega_{\text{eff}}(z=0)$	t_0
SNe	0.2589	2.8619	-0.356	-0.5712	16.4 Gyr
SNe+OHD	0.5438	0.8386	-0.457	-0.6382	13.8 Gyr
SNe+BAO/CMB	0.4963	1.0147	-0.424	-0.6608	14.5 Gyr
SNe+OHD+BAO/CMB	0.5366	0.8633	-0.491	-0.6162	13.98 Gyr

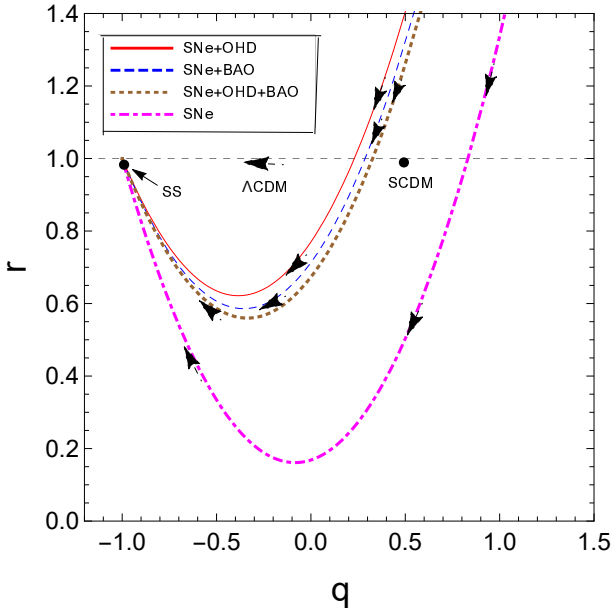

Figure 6.11: The trajectory of $\{r,q\}$ in $q-r$ plane for the best-fitted parameters. The arrow shows the direction of the evolution of the trajectory.

and $SNe+OHD+BAO/CMB$ start from the Chaplygin gas region $(r>1, s<0)$ at the early time and in intermediate time pass through quintessence and then ultimately approach to ΛCDM in late time.

The $\{r,q\}$ trajectory of the model is shown in Fig. 6.11. The *SCDM* model and steady state (SS) model correspond to fixed points $\{r,q\}=\{1,0.5\}$ and $\{r,q\}=\{1,-1\}$, respectively. The horizontal line at $r=1$ corresponds to the time evolution of ΛCDM model. Our model approaches to the standard model like ΛCDM and quintessence model ($Q-model$) [254] in late time.

The *Om* is another diagnostic approach to distinguish dark energy. Using (6.3.8) into (1.12.3), we can write the expression of *Om(z)*. Figure 6.12 exhibits the evolution of different trajectories of the function *Om(z)* with respect to the redshift z, corresponding to different best-fit values of model parameters. The negative slope of each trajectory

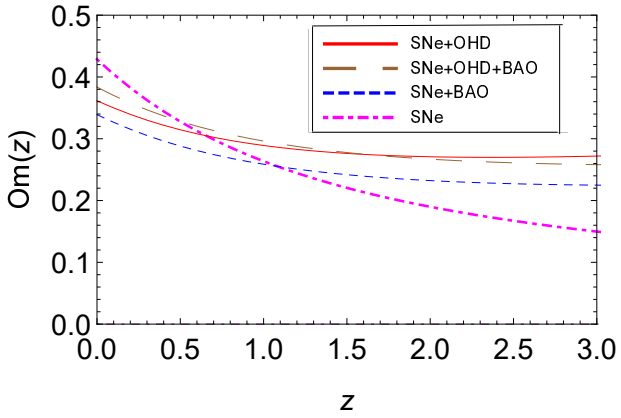

Figure 6.12: The trajectory of *Om(z)* for the best fitted parameters.

shows that the model behaves like quintessence.

6.5 Model Selection

We use two information criteria, namely the Akaike Information Criterion (AIC) and the Bayesian Information Criterion (BIC) to assess the model as discussed in section 1.13. For a cosmological model with d degrees of freedom in which $\mathbb{N}$ number of data points have been used to fit the model, the AIC and BIC parameters are defined through the relation (1.14.2) and (1.14.3).

Table 6.3 shows the χ^2_{min}s, χ^2_{red}s, AICs, BICs of the matter creation model with

Table 6.3: Summary of the reduced χ^2_{red}, ΔAIC and ΔBIC for ΛCDM model and matter creation model

Model	Data set	χ^2_{min}	χ^2_{red}	AIC	BIC	ΔAIC	ΔBIC
ΛCDM	SNe	17.027	0.587	21.027	23.894	0	0
	SNe+OHD	27.901	0.387	31.907	36.509	0	0
	SNe+BAO/CMB	18.131	0.518	22.131	25.352	0	0
	SNe+OHD+BAO/CMB	30.443	0.385	34.443	39.232	0	0
Matter creation model	SNe	17.417	0.622	23.417	27.718	2.390	3.824
	SNe+OHD	27.521	0.387	33.512	40.433	1.614	3.924
	SNe+BAO/CMB	17.416	0.512	23.416	28.249	1.285	2.897
	SNe+OHD+BAO/CMB	29.766	0.381	35.766	42.950	1.323	2.718

consideration of the ΛCDM as the referring model. It can be observed that the values of χ^2_{min}, AIC and BIC for matter creation model are very close to the values of ΛCDM model. Thus, the observational data strongly favor and support the matter creation model from AIC and BIC. The reduced χ^2_{red} also shows that it is very close to the values of ΛCDM model, which is less than one (the model is “over fitting” the data).

6.6 Thermodynamical Analysis

In this section, we find the condition of the thermodynamic stability for the present particle creation model. In [363], it has been demonstrated that cosmological apparent horizons are also endowed with thermodynamic properties. It can relate temperature and entropy to the apparent horizon like to the black hole event horizon.

According to the generalized second law (GSL) of thermodynamic, the total entropy $\mathbb{S}$ is the sum of entropy of all sources. Therefore, in this model the total entropy is contributed from the entropy of the apparent horizon ($\mathbb{S}_h$) and entropy of fluid ($\mathbb{S}_f$) inside the apparent horizon, i.e., $\mathbb{S} = \mathbb{S}_h + \mathbb{S}_f$. The entropy of apparent horizon is given by $\mathbb{S}_h = \kappa_B \tilde{A}/4l_{pl}^2$ [364], where κ_B is the Boltzmann's constant, $\tilde{A} = 4\pi r_h^2$ is the area of horizon in which $r_h = H^{-1}$ is the horizon radius for flat FLRW Universe and l_{pl} is the Planck's length.

Differentiating $\mathbb{S}_h$ with respect to cosmic time and using (6.3.8), we obtain

$$\dot{\mathbb{S}}_h = -\frac{2\pi\kappa_B}{l_{pl}^2}\frac{\dot{H}}{H^3} = \frac{6\pi\kappa_B}{l_{pl}^2 H^2}\frac{H_0(1-\delta-\beta-\gamma)}{(2-3\gamma)}\, a^{-\frac{3(1-\beta-\gamma)}{(2-3\gamma)}}. \tag{6.6.1}$$

It is observed from the above equation that $\dot{\mathbb{S}}_h \geq 0$ for $(\delta+\beta+\gamma) \leq 1$ and $\gamma < 2/3$.

Now, the Gibb's equation for the fluid is written as

$$\mathbb{T} d\mathbb{S}_f = d(\rho V) + p dV = V\dot{\rho} + \rho\dot{V} + p dV, \tag{6.6.2}$$

where $V = 4\pi r_h^3/3$ is the spatial volume enclosed by the horizon and $\mathbb{T}$ is the fluid temperature. Note that we are studying matter-dominated model $p = 0$. Using (6.3.8), the above equation gives

$$\dot{\mathbb{S}}_f = \frac{24\pi^2 H_0}{H^2}\frac{(1-\delta-\beta-\gamma)}{(2-3\gamma)} a^{-\frac{3(1-\beta-\gamma)}{2-3\gamma}}, \tag{6.6.3}$$

where $\mathbb{T} = \mathbb{T}_h = 1/2\pi r_h$, i.e., the temperature of the fluid becomes equal to that of the temperature of the horizon [333]. For $\dot{\mathbb{S}}_f \geq 0$, we must have $(\delta+\beta+\gamma) \leq 1$ and $\gamma < 2/3$.

Thus, from (6.6.1) and (6.6.3), we observe that $\dot{\mathbb{S}} = \dot{\mathbb{S}}_h + \dot{\mathbb{S}}_f \geq 0$ for $(\delta+\beta+\gamma) \leq 1$ and $\gamma < 2/3$. So, the entropy of the horizon plus fluid is an increasing function of the cosmic time.

Differentiating (6.6.1) again with respect to cosmic time, we get

$$\ddot{\mathbb{S}}_h = \frac{18\pi\kappa_B H_0}{l_{pl}^2}\frac{(1-\delta-\beta-\gamma)}{(2-3\gamma)^2}a^{-\frac{3(1-\beta-\gamma)}{2-3\gamma}}\left[\frac{2H_0}{H^2}a^{-\frac{3(1-\beta-\gamma)}{2-3\gamma}}-\frac{(1-\beta-\gamma)}{H}\right]. \tag{6.6.4}$$

Similarly, differentiating (6.6.3) with respect to cosmic time, we get

$$\ddot{\mathbb{S}}_f = 72\pi^2 H_0\frac{(1-\delta-\beta-\gamma)}{(2-3\gamma)^2}a^{-\frac{3(1-\beta-\gamma)}{2-3\gamma}}\left[\frac{2H_0}{H^2}a^{-\frac{3(1-\beta-\gamma)}{2-3\gamma}}-\frac{(1-\beta-\gamma)}{H}\right]. \tag{6.6.5}$$

Adding (6.6.4) and (6.6.5), one obtains

$$\begin{aligned}\ddot{\mathbb{S}} &= \ddot{\mathbb{S}}_h+\ddot{\mathbb{S}}_f \\ &= \left(\frac{18\pi\kappa_B}{l_{pl}^2}+72\pi^2\right)\frac{(1-\delta-\beta-\gamma)H_0}{(2-3\gamma)^2H}a^{-\frac{3(1-\beta-\gamma)}{2-3\gamma}}\times \\ &\quad\left[\frac{2H_0}{H}a^{-\frac{3(1-\beta-\gamma)}{2-3\gamma}}-(1-\beta-\gamma)\right].\end{aligned} \tag{6.6.6}$$

The sign of $\ddot{\mathbb{S}}$ is determined by last bracket in (6.6.6) and $\delta+\beta+\gamma<1$. Therefore, we find that the generalized second law of thermodynamics is always valid and hence the model is stable under the above constraints.

It is also interesting to discuss the model with adiabatic matter creation like irreversible process. In adiabatic process, the total entropy $\mathbb{S}$ increases, but, the specific entropy (per particle), $\sigma=\mathbb{S}/N$, remains constant, i.e., $\dot{\sigma}=0$ which implies that

$$\frac{\dot{\mathbb{S}}}{\mathbb{S}}=\frac{\dot{N}}{N}. \tag{6.6.7}$$

Using (6.3.1) into the relation $\frac{\dot{N}}{N}=\frac{\dot{n}}{n}+3H=\Gamma$, we get

$$N=N_0a^{3\beta}(\dot{a})^{3\gamma}e^{3\delta H_0(t-t_0)}, \tag{6.6.8}$$

where N_0 is the present number of particles. Now, from (6.6.7), we get

$$\mathbb{S}=S_0a^{3\beta}(\dot{a})^{3\gamma}e^{3\delta H_0(t-t_0)}, \tag{6.6.9}$$

where S_0 is the present entropy of matter fluid. It is to be noted that if $\delta=\beta=\gamma$, i.e., if there is no particle creation, we get $\mathbb{S}=S_0$, i.e., the standard conserved quantities are recovered.

6.7 Conclusion

We have discussed the matter-dominated model with matter creation cosmology as an alternative to explain the cosmic acceleration. As matter creation models are phenomenological and the literature contains a variety of models, so a generalized model could be a better choice to start for any study. Hence, in the present chapter, we have generalized the form of matter creation rate assumed by Lima et al. [236].

The assumption $\Gamma = 3\beta H$ [229] always gives accelerating model for $\beta > 1/3$ or decelerating for $\beta < 1/3$, that is, there is no transition redshift from a decelerating to an accelerating regime as required by observational data. In another paper, Abramo and Lima [248] proposed the form of Γ as $\Gamma = 3\beta H^2$, however, it also gives no transition redshift. In order to cure such difficulty, a constant term is added to this expression, i.e., $\Gamma = 3\delta H_0 + 3\beta H$ [236] to get the transition redshift. Basilakos and Lima [307] have also used the same form to constraints the model. They observed that the age of the Universe to be $t_0 \sim 14.8$ Gyr while the inflection point is located $a_{tr} \simeq 0.44$ which corresponds to $z_{tr} \simeq 1.26$. They have found that this form of matter creation rate is endowed with severe difficulties even for the set of background tests because it is unable to adjust simultaneously the observational data at low and high redshift.

In this chapter, we have generalized the form of Γ in order to produce a clear image about the matter creation models aiming to realize the early physics and its compatibility with the current astronomical data. It covers different matter creation rate, for instance, $\Gamma \propto H_0$, $\Gamma \propto H$ and $\Gamma \propto \ddot{a}/\dot{a}$. Lima et al. [236] have performed best-fit of the free parameters using only SNe data and best-fit values are $\beta = 0$ and $\delta = 0.65$. We have performed the fitting of free parameters using joint observational data of SNe, OHD, and BAO/CMB in which none free parameters is zero. However, In our model, the age of the Universe is found to be 13.9 Gyr from $SNe + OHD$ and $SNe + OHD + BAO/CMB$, but it is higher with SNe and $SNe + BAO/CMB$. Also, the transition redshift is less than one with $SNe + OHD$ and $SNe + OHD + BAO/CMB$, which are a good fit with the ΛCDM model. Our model also generalizes the work of the above references and it can be observed from the observational tests that our model gives best-fit values from joint observation of SNe with OHD, and OHD and BAO/CMB and fit the data very well with ΛCDM model. We have investigated the model analytically and numerically in which the matter creation process provides the late-time accelerating phase of the cosmic expansion without the need for any dark energy.

We have obtained the exact solutions for the scale factor, Hubble parameter, and deceleration parameter. These results have then contrasted with the ones obtained at the background level to find the model parameters. For the background tests, we have used SNe in combination with OHD and BAO/CMB at different redshifts. The nature of the cosmological evolution is strongly dependent on the numerical values of the model parameters. The best-fit values of model parameters have been listed in Table 7.1. Figure 6.1–6.4 show the confidence regions of parameters δ, β and γ for different sets of joint observational data. It has been found that the results of SNe and $SNe+BAO/CMB$ data are a little different from the other two data. However, the joint analysis of $SNe+OHD$ and $SNe+OHD+BAO/CMB$ constrain the model parameters very well and are in good agreement with observational data of the ΛCDM model. In what follows we summarize the results:

The evolution of the scale factor for best-fit values of model parameters have been plotted in Fig. 6.5. It has been observed that the model predicts early deceleration and late-time acceleration. The transition points a_{tr} where the Universe transits from decelerated phase to accelerated phase have been listed in Table 6.2.

Figure 6.6 plots the evolution of deceleration parameter with redshift for best-fit values obtained from independent/combined analysis of observational data. The present-day value of q and transition redshift z_{tr} have been listed in Table 6.2. The best-fit values of parameters obtained from different observational data give q_0 in the range of $-1 \leq q_0 < 0$. In general, $q \to -1$ as $z \to -1$, which corresponds to the de Sitter Universe. The deceleration parameter is time-dependent and hence shows the transition from positive to negative. The evolution of the Universe begins from a higher redshift, from a decelerating phase, with $q > 0$. The expansion of the Universe accelerates, and at a finite value of z it reaches the value $q = 0$, corresponding to the transition to the accelerated phase. The evolution of q is strongly dependent on the numerical values of the model parameters.

We have obtained the EoS parameter to discuss the evolution of the model. Figure 6.7 plots the evolution of the EoS parameter with redshift for best-fit values of parameters. It has been observed that the EoS does not cross the phantom-divide line $\omega = -1$. Irrespective of the values of parameters, $\omega_{\text{eff}} \to -1$ as $z \to -1$ which shows that the model behaves like ΛCDM in late time. The present values of ω_{eff} obtained from independent/combined observational data are listed in Table 6.2. These values are comparatively higher than that predicted by the joint analysis of $WMAP+BAO+H_0+SNe$ data which is around -0.93.

We have discussed the age of the Universe by plotting the trajectory with best-fit values of parameters as shown in Fig. 6.8. The trajectory shows that the age of the Universe obtained by $SNe+OHD$ and $SNe+OHD+BAO/CMB$ data are found to be approximately 13.9 Gyr. So, the age-predicted by the present model is agreeing with the age deduced from the ΛCDM model.

The Hubble function with the error bar fits into the ΛCDM model for best-fit values and has been plotted in Fig. 6.9. It has been observed that the curves coincide at low redshifts and differ appreciably at high redshifts. However, it is possible to get a good fit using joint analysis of $SNe+OHD$ and $SNe+OHD+BAO/CMB$.

We have studied two diagnostics parameters, namely, statefinder and *Om(z)* parameters to compare our model with ΛCDM model. In Fig. 6.10, the trajectories of $\{r,s\}$ have been plotted in $s-r$ plane for best-fit values obtained from different observational data set. The model corresponds to the ΛCDM model in late-time. The model also approaches the standard model in late time as shown in the $q-r$ plane (Fig. 6.11). The trajectory of *Om(z)* in Fig. 6.12 shows that the model behaves like quintessence.

We have performed the information criterion of AIC and BIC to discriminate our model with the ΛCDM model. The values of reduced Chi-square, ΔAIC and ΔBIC are calculated and have been listed in Table 6.3. The analysis based on the AIC and BIC indicates that there is positive support for the matter creation model when compared to the ΛCDM model. The reduced χ^2_{red} is less than one in each data points which shows that the model gives the best-fit values of model parameters and good support to ΛCDM model.

We have discussed the thermodynamic behavior of the model by calculating the total entropy for the matter creation. We have established the general conditions for any matter creation model that ensure the validity of the generalized second law of thermodynamics.

****

Chapter 7

Conclusion and Future Scope

7.1 Conclusion

In the thesis, we have studied the effects of bulk viscosity and matter creation on various cosmological models. In chapter 2, we have explored the possibility of bulk viscosity as a possible candidate of dark energy to explain the accelerating Universe. We have discussed the dissipative processes in the HRDE model within the framework of the standard Eckart theory of relativistic thermodynamics. We have observed that the accelerated expansion may be possible for a non-viscous case but the phase transition is not possible. For the viscous HRDE model, We have obtained the exponential expansion of the scale factor which gives the time-dependent deceleration parameter and statefinder pair. It is observed that the model shows the transition from the decelerated phase to the accelerated phase depending on the values of the viscous term and the results show that the recent acceleration is well explained with the viscous term.

In chapter 3, we extend the study of chapter 2 in the framework of modified $f(R,T)$ gravity theory. We have obtained the exact solutions of the field equations by assuming the simplest form of $f(R,T) = R + \lambda T$ with constant and variable bulk viscous coefficients. It is found that the behaviors concerning the cosmic expansion depend on the coupling parameter of $f(R,T)$ and bulk viscous term. Using statefinder parameters and Om diagnostic, it has been found that our model shows a similar behavior as the quintessence model and Chaplygin gas model for different values of the viscosity coefficient. We have also analyzed the time evolution of the total entropy and generalized second law of thermodynamics of the viscous HRDE model in $f(R,T)$ theory

inside the apparent horizon.

Further, chapter 4 deals with the adiabatic matter creation process in the HDE model with the motivation of considering it as an alternative choice to explain the recent accelerating phase of the Universe. We have considered three different forms of matter creation rate to discuss the evolution of the Universe. We have constrained the model parameters through the MCMC method by the use of the EMCEE python package on the latest observational data to discuss various cosmological parameters. We have used cosmographic parameters and Om to discriminate our model with other dark energy models. We have analyzed the model by applying information criterion AIC and BIC based on the penalization associated with the number of parameters. The generalized second law of thermodynamics is found to be valid for this model under certain conditions.

In chapter 5, we have explored the effect of bulk viscosity and matter creation in the HRDE model to observe the current accelerated phase. In the literature, both phenomena have been treated as the same cosmological phenomena and some papers treat both as different phenomena. We have considered these two dissipative phenomenons as independent irreversible processes. With the help of best-fitted model parameters, we have discussed the evolution of various cosmological parameters and also used geometric parameters to distinguish the model from other standard dark energy models. The behavior of energy conditions has also been discussed for the HRDE model. The result shows that the HRDE model with bulk viscosity and matter creation is in good agreement with current observational data.

Chapter 6 discusses the matter-dominated model with matter creation cosmology in the FLRW model as an alternative to explain the cosmic acceleration. We have proposed a new form of matter creation rate, which generalizes some of the previous models in the literature. We have performed the statistical analysis to obtain the best-fit values of the model parameter by employing the MCMC package EMCEE on a different combination of publicly available data sets of SNe, OHD, and BAO/CMB. Exact solutions of the scale factor and deceleration parameters have been obtained and discussed their evolution for the best-fit values of model parameter which shows the phase transition from deceleration to recent acceleration. We have also distinguished this model from other existing dark energy models using two geometrical diagnostics: statefinder parameter and Om diagnostic. We also used information criterion AIC and BIC to compare our model with the standard ΛCDM model. The thermodynamic

behavior have been discussed for this model by calculating the total entropy for the matter creation.

Table 7.1: Comparison of different models carried out in the thesis with the ΛCDM model

Model	z_{tr}	q_0	$\omega_{\text{eff}}(z=0)$	t_0 (Gyr)
ΛCDM	0.66	-0.60	-0.93	13.7
HDE with $\Gamma = 3\delta H_0$	0.61	-0.26	-0.50	13.39
HDE with $\Gamma = 3\delta H_0 + 3\beta H$	0.92	-0.34	-0.56	14.28
HRDE with $\zeta = \zeta_0 + \zeta_1 H$, $\Gamma = 3\beta H$	0.68	-0.36	-0.57	13.40
FLRW model with matter creation	0.86	-0.49	-0.62	13.98

7.2 Future Scope

This thesis as a whole can be considered as an extensive review on bulk viscosity and matter creation effects on cosmological models in the framework of GTR and modified $f(R,T)$ gravity theory, where not only detailed references to the literature have been furnished, but also new and original results have been obtained. We have analyzed the concepts of bulk viscosity and matter creation in HDE, HRDE, and matter-dominated models in GTR as well as in $f(R,T)$ gravity theory.

We have considered the bulk viscous coefficient as $\zeta = \zeta_0 + \zeta_1 H$ in this thesis, however a second-order bulk viscous coefficient as $\zeta = \zeta_0 + \zeta_1 H + \zeta_2(\frac{\dot{H}}{H} + H)$ may be considered to describe the late time evolution. In the forthcoming paper, we will try to assume such a form of ζ in GTR as well as in modified $f(R,T)$ gravity theory. The conservation of energy-momentum tensor is one of the main problems in $f(R,T)$ gravity. Harko has tried to explain the conservation equation through the thermodynamics of particle creation. We will try to resolve this problem in the future.

We have assumed various forms of particle creation rate Γ in our study of matter-dominated model and HDE model in this thesis. We have also proposed a new form of particle creation rate, $\Gamma = 3\delta H_0 + 3\beta H + 3\gamma(\frac{\dot{H}}{H} + H)$ to discuss the evolution of the Universe in flat FLRW line element. Therefore, it opens door to study the cosmological implications of this form in other aspects of evolution.

The modified $f(R,T)$ gravity theory presents a maximal coupling between matter and geometry which may be useful to explain the accelerated expansion of the Universe. Several cosmological models have been presented in $f(R,T)$ theory but there is a scope to do more work. We have studied only the first order Eckart theory of bulk viscosity in GTR and $f(R,T)$ gravity, therefore, it may be worthy to discuss the full causal theory of bulk viscosity which may provide better and more general results. Considerable discussion on observational cosmology also has not been discussed in this theory so there is a scope to do that. The study of structure formation and perturbation theory is another main field where considerable work can be done.

The field of cosmology is definitely worth following over the next decade since everything points toward significant advances. To ensure maximum benefit from future surveys, we still need to improve our theoretical understanding of cosmological models, and this thesis is one of many steps toward achieving this.

****

Bibliography

[1] A. Einstein; *The foundation of the general theory of relativity*, Annalen Phys. **49**, 769 (1916); Sitz. Preuss. Akad. Wiss. Phys. **1**, 142 (4) (1917); Annalen Phys. **69**, 436 (1922).

[2] S. Weinberg; *Gravitation and Cosmology: Principles and applications of the General Theory of Relativity*, John Wiley & Sons, ISBN-13: 978-0471925675, ISBN-10: 0471925675 (1972).

[3] H.P. Robertson; *Kinematics and world-structure*, Astrophys. J. **82**, 284 (1935).

[4] A.G. Walker; *On Milne's theory of world structure*, Proceedings of the London Mathematical Society **42**, 90 (1936).

[5] A. Friedmann; *Über die Krümmung des Raumes*, Zeitschriftfür Physik **10**, 377 (1922).

[6] G. Lemaître; *Un Univers homogène de masse constante et de rayon croissant rendant compte de la vitesse radiale des nébuleuses extra-galactiques*, Annales de la Société Scientifique de Bruxelles **47**, 49 (1927).

[7] E.P. Hubble; *A relation between distance and radial velocity among extra-galactic nebulae*, Proc. Nat. Acad. of Sci. USA **15**, 168 (1929).

[8] Planck Collaboration, N. Aghanim et. al., "Planck 2018 results. VI. Cosmological parameters," arXiv:1807.06209.

[9] A.H. Guth; *Inflationary Universe: A possible solution to the horizon and flatness problems*, Phys. Rev. D **23**, 347 (1981).

[10] A.D. Linde; *Chaotic inflation*, Phys. Lett. B **129**, 177 (1983).

[11] A.D. Linde; *Particle Physics and inflationary cosmology*, Contemp. Concepts Phys. **5**, 1 (2005); [arXiv:hep-th/0503203].

[12] A. Albrecht, P.J. Steinhardt; *Cosmology for grand unified theories with radiatively induced symmetry breaking*, Phys. Rev. Lett. **48**, 1200 (1982).

[13] A. Albrecht et al.; *Reheating an inflationary universe*, Phys. Rev. Lett. **48**, 1437 (1982).

[14] A.G. Riess et al.; *Observational evidence from supernovae for an accelerating Universe and a cosmological constant (Supernova Search Team Collaboration)*, Astron. J. **116**, 1009 (1998); [arXiv:astro-ph/9805201].

[15] S. Perlmutter et al.; *Measurements of Omega and Lambda from 42 high redshift supernovae (The Supernova Cosmology Project)*, Astrophys. J. **517**, 565 (1999); [arXiv:astro-ph/9812133].

[16] G. Hinshaw et al.; *Nine-Year Wilkinson Microwave Anisotropy Probe (WMAP) observations: Cosmological parameter results*, Astrophys. J. Suppl. **208**, 19 (2013); [arXiv:astro-ph/1212.5226].

[17] C.L. Bennett et al.; *Nine-Year Wilkinson Microwave Anisotropy Probe (WMAP) Observations: Final maps and results (WMAP Collaboration)*, Astrophys. J. Suppl. **208**, 20 (2013); [arXiv:astro-ph/1212.5225].

[18] L. Anderson et al.; *The clustering of galaxies in the SDSS-III Baryon Oscillation Spectroscopic Survey: Baryon Acoustic Oscillations in the data release 9 spectroscopic galaxy sample*, Mon. Not. Roy. Astron. Soc. **427**, 3435 (2013); [arXiv:astro-ph/1203.6594].

[19] P.A.R. Ade et al.; *Planck 2013 results. I. Overview of products and scientific results (Planck Collaboration)*, Astron. Astrophys. **571**, A1 (2014); [arXiv:astro-ph/1303.5062].

[20] P.A.R. Ade et al.; *Planck 2015 results*, Astron. Astrophys. **594**, A13 (2016).

[21] E. Komatsu et al.; *WMAP Collaboration, Seven-year Wilkinson Microwave Anisotropy Probe (WMAP) observations: Cosmological interpretation*, Astrophys. J. Suppl. **192**, 18 (2011).

[22] A.G. Sanchez et al.; *The clustering of galaxies in the SDSS-III Baryon Oscillation Spectroscopic Survey: cosmological implications of the large-scale two-point correlation function*, Mon. Not. Roy. Astron. Soc. **425**, 415 (2012).

[23] P.J.E. Peebles, B. Ratra; *The Cosmological constant and dark energy*, Rev. Mod. Phys. **75**, 559 (2003); [arXiv:astro-ph/0207347].

[24] S. Weinberg; *The cosmological constant problem*, Rev. Mod. Phys. **61**, 1 (1989).

[25] V. Sahni, A.A. Starobinsky; *The case for a positive cosmological Λ-term*, Int. J. Mod. Phys. D **9**, 373 (2000); [arXiv:astro-ph/9904398].

[26] T. Padmanabhan; *Cosmological constant: The weight of the vacuum*, Phys. Rept. **380**, 235 (2003); [arXiv:hep-th/0212290].

[27] T. Padmanabhan; *Dark Energy: the Cosmological Challenge of the Millennium*, Current Science **88**, 1057 (2005).

[28] E.J. Copeland, M. Sami, S. Tsujikawa; *Dynamics of dark energy*, Int. J. Mod. Phys. D **15**, 1753 (2006); [arXiv:hep-th/0603057].

[29] T. Padmanabhan; *Dark Energy and Gravity*, Gen. Relativ. Gravit. **40**, 529 (2008).

[30] P. Steinhardt; Critical Problems in Physics, edited by V.L. Fitch, D.R. Marlow (Princeton University Press, Princeton, NJ, 1997).

[31] I. Zlatev, L.M. Wang, P.J. Steinhardt; *Quintessence, cosmic coincidence, and the cosmological constant*, Phys. Rev. Lett. **82**, 896 (1999); [arXiv:astro-ph/9807002].

[32] L.H. Ford; *Cosmological-constant damping by unstable scalar fields*, Phys. Rev. D **35**, 2339 (1987).

[33] R.R. Caldwell, R. Dave, P.J. Steinherdt; *Cosmological imprint of an energy component with general equation of state*, Phys. Rev. Lett. **80**, 1582 (1998).

[34] E.J. Copeland, A.R. Liddle, D. Wands; *Exponential potentials, scaling solutions and inflation*, Ann. N. Y. Acad. Sci. **688**, 647 (1993).

[35] P.J. Steinhardt, L.M. Wang, I. Zlatev; *Cosmological tracking solutions*, Phys. Rev. D **59**, 123504 (1999); [arXiv:astro-ph/9812313].

[36] T. Chiba; *Quintessence, the gravitational constant, and gravity*, Phys. Rev. D **60**, 083508 (1999); [arXiv:gr-qc/9903094].

[37] L. Wang, R.R. Caldwell, J.P. Ostriker, P.J. Steinhardt; *Cosmic concordance and quintessence*, Astrophys J. **530**, 17 (2000); [arXiv:astro-ph/9901388].

[38] W. Zimdahl, D. Pavón, L.P. Chimento; *Interacting Quintessence*, Phys. Lett. B **521**, 133 (2001).

[39] J. Martin; *Quintessence: a mini-review*, Mod. Phys. Lett. A **23**, 1252 (2008); [arXiv:astro-ph/0803.4076].

[40] P.J. Peebles, R. Ratra; *Cosmology with a time-variable cosmological "constant"*, Astrophys J. **325**, L17 (1988).

[41] C. Wetterich; *The cosmon model for an asymptotically vanishing time-dependent cosmological "constant"*, Astron. and Astrophys. **301**, 321 (1995); [arXiv:hep-th/9408025].

[42] R. Ratra, P.J. Peebles; *Cosmological consequences of a rolling homogeneous scalar field*, Phys. Rev. D **37**, 3406 (1988).

[43] J.D. Barrow, P. Saich; *Scalar field cosmologies*, Class. Quantum Grav. **10**, 279 (1993).

[44] A.B. Burd, J.D. Barrow; *Inflationary models with exponential potentials*, Nucl. Phys. B **308**, 929 (1988).

[45] J.W. Lee, I.G. Koh; *Galactic halos as boson stars*, Phys. Rev. D **53**, 2236 (1996); [arXiv:hep-ph/9507385].

[46] V. Sahni; *Dark matter and dark energy*, Lect. Notes Phys. **653**, 141 (2004); [arXiv:astro-ph/0403324].

[47] V. Sahni, A. Starobinsky; *Reconstructing dark energy*, Int. J. Mod. Phys. D **15**, 2105 (2006); [arXiv:astro-ph/0610026].

[48] A. Melchiorri et al.; *The state of the dark energy equation of state*, Phys. Rev. D **68**, 043509 (2003); [arXiv:astro-ph/0211522].

[49] B.A. Bassett, P.S. Corasaniti, M. Kunz; *The essence of quintessence and the cost of compression*, Astrophys. J. **617**, L1 (2004); [arXiv:astro-ph/0407364].

[50] U. Alam et al.; *Is there Supernova evidence for dark energy metamorphosis?*, Mon. Not. Roy. Astron. Soc. **354**, 275 (2004); [arXiv:astro-ph/0311364].

[51] D. Huterer, A. Cooray; *Uncorrelated estimates of dark energy evolution*, Phys. Rev. D **71**, 023506 (2005); [arXiv:astro-ph/0404062].

[52] G.B. Zhao, X. Zhang; *Probing dark energy dynamics from current and future cosmological observations*, Phys. Rev. D **81**, 043518 (2010); [arXiv:astro-ph/0908.1568].

[53] R.R. Caldwell; *A Phantom Menace? Cosmological consequences of a dark energy component with super-negative equation of state*, Phys. Lett. B **545**, 23 (2002); [arXiv:astro-ph/9908168].

[54] V. Faraoni; *Superquintessence*, Int. J. Mod. Phys. D **11**, 471 (2002).

[55] R.R. Caldwell, M. Kamionkowski, N.N. Weinberg; *Phantom energy and Cosmic Doomsday*, Phys. Rev. Lett. **91**, 071301 (2003); [arXiv:astro-ph/0302506].

[56] Z.K. Guo, Y.S. Piao, X.M. Zhang, Y.Z. Zhang; *Cosmological evolution of a quintom model of dark energy*, Phys. Lett. B **608**, 177 (2005); [arXiv: astro-ph/0410654].

[57] T. Padmanabhan; *Accelerated expansion of the Universe driven by tachyonic matter*, Phys. Rev. D **66**, 021301 (2002); [arXiv:hep-th/0204150].

[58] G.W. Gibbons; *Cosmological evolution of the rolling tachyon*, Phys. Lett. B **537**, 1 (2002); [arXiv:hep-th/0204008].

[59] S. Tsujikawa, M. Sami; *A unified approach to scaling solutions in a general cosmological background*, Phys. Lett. B **603**, 113 (2004); [arXiv:hep-th/0409212].

[60] T. Chiba, T. Okabe, M. Yamaguchi; *Kinetically driven quintessence*, Phys. Rev. D **62**, 023511 (2000); [arXiv:astro-ph/9912463].

[61] C. Armendariz-Picon, V.F. Mukhanov, P.J. Steinhardt; *Essentials of k-essence*, Phys. Rev. D **63**, 103510 (2001); [arXiv:astro-ph/0006373].

[62] A. Kamenshchik, U. Moschella, V. Pasquier; *An alternative to quintessence*, Phys. Lett. B **511**, 265 (2001); [arXiv:gr-qc/0103004].

[63] M.C. Bento, O. Bertolami, A.A. Sen; *Generalized Chaplygin gas, accelerated expansion and dark energy-matter unification*, Phys. Rev. D **66**, 043507 (2002); [arXiv:gr-qc/0202064].

[64] E. Elizalde, S. Nojiri, S.D. Odintsov; *Late-time cosmology in (phantom) scalar-tensor theory: dark energy and the cosmic speed-up*, Phys. Rev. D **70**, 043539 (2004); [arXiv:hep-th/0405034].

[65] M. Sami, A. Toporensky; *Phantom field and the fate of Universe*, Mod. Phys. Lett. A **19**, 1509 (2004); [arXiv:gr-qc/0312009].

[66] M. Li; *A model of holographic dark energy*, Phys. Lett. B **603**, 1 (2004).

[67] G. 't Hooft; *Dimensional reduction in quantum gravity*, [arXiv:gr-qc/9310026].

[68] L. Susskind; *The world as a hologram*, J. Math. Phys. **36**, 6377 (1995).

[69] R. Bousso; *The holographic principle for general backgrounds*, Class. Quantum Grav. **17**, 997 (2000).

[70] A.G. Cohen, D.B. Kaplan, A.E. Nelson; *Effective field theory, black holes, and the cosmological constant*, Phys. Rev. Lett. **82**, 4971 (1999).

[71] F. Canfora, G. Vilasi; *The Holographic Principle and the Early Universe*, Phys. Lett. B **625**, 171 (2005).

[72] Q.G. Huang, M. Li; *The holographic dark energy in a non-flat universe*, JCAP **08**, 013 (2004).

[73] Q.G. Huang, M. Li; *Anthropic principle favours the holographic dark energy*, JCAP **03**, 001 (2005).

[74] K. Enqvist, M.S. Sloth; *Possible Connection between the Location of the Cutoff in the Cosmic Microwave Background Spectrum and the Equation of State of Dark Energy*, Phys. Rev. Lett. **93**, 221302 (2004).

[75] K. Ke, M. Li; *Cardy-Verlinde formula and holographic dark energy*, Phys. Lett. B **606**, 173 (2005).

[76] X. Zhang; *Statefinder diagnostic for holographic dark energy model*, Int. J. Mod. Phys. D **14**, 1597 (2005).

[77] B. Wang, Y. Gong, E. Abdalla; *Transition of the dark energy equation of state in an interacting holographic dark energy model*, Phys. Lett. B **624**, 141 (2005).

[78] H. Kim, H.W. Lee, Y.S. Myung; *Equation of state for an interacting holographic dark energy model*, Phys. Lett. B **632**, 605 (2006).

[79] B. Hu, Y. Ling; *Interacting dark energy, holographic principle, and coincidence problem*, Phys. Rev. D **73**, 123510 (2006).

[80] Y.S. Myung, M.G. Seo; *Origin of holographic dark energy models*, Phys. Lett. B **671**, 435 (2009).

[81] E.N. Saridakis; *Restoring holographic dark energy in brane cosmology*, Phys. Lett. B **660**, 138 (2008).

[82] J. Zhang, X. Zhang, H. Liu; *Holographic dark energy in a cyclic universe*, Eur. Phys. J. C **52**, 693 (2007).

[83] Y.S. Myung; *Holographic principle and dark energy*, Phys. Lett. B **610**, 18 (2005).

[84] M.R. Setare; *Bulk-Brane Interaction and Holographic Dark Energy*, Phys. Lett. B **642**, 421 (2006).

[85] Y.S. Myung; *Instability of holographic dark energy models*, Phys. Lett. B **652**, 223 (2007).

[86] S.D.H. Hsu; *Entropy bounds and dark energy*, Phys. Lett. B **594**, 13 (2004).

[87] M. Li, X.D. Li, S. Wang, X. Zhang; *Holographic dark energy models: A comparison from the latest observational data*, JCAP **06**, 036 (2009).

[88] H. Wei, S.N. Zhang; *Age Problem in the Holographic Dark Energy Model*; [arXiv:0707.2129].

[89] D. Pavón, W. Zimdahl; *Holographic dark energy and cosmic coincidence*, Phys. Lett. B **628**, 206 (2005).

[90] S. Nojiri, S.D. Odintsov; *Unifying phantom inflation with late-time acceleration: scalar phantom non-phantom transition model and generalized holographic dark energy*, Gen. Relativ. Gravit. **38**, 1285 (2006).

[91] M.R. Setare; *Holographic tachyon model of dark energy*, Phys. Lett. B **653**, 116 (2007).

[92] M.R. Setare; *Interacting holographic generalized Chaplygin gas model*, Phys. Lett. B **654**, 1 (2007).

[93] E.N. Saridakis; *Holographic Dark Energy in Braneworld Models with a Gauss-Bonnet Term in the Bulk. Interacting Behavior and the* $w = -1$ *Crossing*, Phys. Lett. B **661**, 335 (2008).

[94] R.G. Cai; *A Dark Energy Model Characterized by the Age of the Universe*, Phys. Lett. B **657**, 228 (2007).

[95] H. Wei, R.G. Cai; *A new model of agegraphic dark energy*, Phys. Lett. B **660**, 113 (2008).

[96] C. Gao, F. Wu, X. Chen, Y.G. Shen; *Holographic dark energy model from Ricci scalar curvature*, Phys. Rev. D **79**, 043511 (2009).

[97] C.P. Singh, P. Kumar; *Holographic dark energy in Brans-Dicke theory with logarithmic form of scalar field*, Int. J. Theor. Phys. **56**, 3297 (2017).

[98] P. Kumar, C.P. Singh; *New agegraphic dark energy model in Brans-Dicke theory with logarithmic form of scalar field*, Astrophys. Space Sci. **362**, 52 (2017).

[99] C.P. Singh, M. Srivastava; *Viscous cosmology in new holographic dark energy model and the cosmic acceleration*, Eur. Phys. J. C **78**, 190 (2018).

[100] M. Srivastava, C.P. Singh; *New holographic dark energy model with constant bulk viscosity in modified $f(R,T)$ gravity theory*, Astrophys. Space Sci. **363**, 117 (2018).

[101] X. Zhang, F.Q. Wu; *Constraints on holographic dark energy from type Ia supernova observations*, Phys. Rev. D **72**, 043524 (2005).

[102] C. Feng et al.; *Testing the viability of the interacting holographic dark energy model by using combined observational constraints*, J. Cosmol. Astropart. Phys. **09**, 005 (2007).

[103] M. Li, X.D. Li, S. Wang, X. Zhang; *Holographic dark energy models: a comparison from the latest observational data*, J. Cosmol. Astropart. Phys. **06**, 036 (2009).

[104] O. Luongo; *A thermodynamic approach to holographic dark energy*, Adv. High Energy Phys. **2017**, 1424503 (2017).

[105] M. Malekjani et al.; *Can holographic dark energy models fit the observational data?*, Phys. Rev. D **98**, 063533 (2018).

[106] M. Suwa, T. Nihei; *Observational constraints on the interacting Ricci dark energy model*, Phys. Rev. D **81**, 023519 (2010).

[107] C.J. Feng; *Statefinder diagnosis for Ricci dark energy*, Phys. Lett. B **670**, 231 (2008).

[108] M. Bouhmadi-López, Y. Tavakoli; *Why is the running vacuum energy more benign than the holographic Ricci dark energy?*, Phys. Rev. D **87**, 023515 (2013).

[109] M. Suwa, K. Kobayashi, H. Oshima; *The Interacting Generalized Ricci Dark Energy Model in Non-Flat Universe*, J. Mod. Phys. **6**, 327 (2015).

[110] S. Ghaffari, A. Sheykhi, M.H. Dehghani; *Statefinder diagnosis for holographic dark energy in the DGP braneworld*, Phys. Rev. D **91**, 023007 (2015).

[111] L. Xu, W. Li, J. Lu; *Cosmic constraint on Ricci dark energy model*, Mod. Phys. Lett. A **24**, 1355 (2009).

[112] C.J. Feng, X.Z. Li; *Ricci dark energy in braneworld models with a Gauss-Bonnet term in the bulk*, Phys. Lett. B **679**, 151 (2009).

[113] C.J. Feng; *Reconstructing $f(R)$ theory from Ricci dark energy*, Phys. Lett. B **676**, 168 (2009).

[114] C.J. Feng, X.Z. Li; *Scalar perturbation and stability of Ricci dark energy*, Phys. Lett. B **680**, 184 (2009).

[115] C.J. Feng, X. Zhang; *Holographic Ricci dark energy in Randall-Sundrum braneworld: Avoidance of big rip and steady state future*, Phys. Lett. B **680**, 399 (2009).

[116] C.J. Feng; *Reconstructing quintom from Ricci dark energy*, Phys. Lett. B **672**, 94 (2009).

[117] X. Zhang; *Holographic Ricci dark energy: Current observational constraints, quintom feature, and the reconstruction of scalar-field dark energy*, Phys. Rev. D **79**, 103509 (2009).

[118] S. Chattopadhyay; *Interacting Ricci dark energy and its statefinder description*, Eur. Phys. J. Plus **126**, 130 (2011).

[119] K.Y. Kim, H.W. Lee, Y.S. Myung; *On the Ricci dark energy model*, Gen. Relativ. Gravit. **43**, 1095 (2011).

[120] I. Durán, D. Pavón; *Model of interacting holographic dark energy at the Ricci scale*, Phys. Rev. D **83**, 023504 (2011).

[121] H. Saadat; *Holographic Ricci Dark Energy Model*, Int. J. Theor. Phys. **51**, 731 (2012).

[122] T.F. Fu et al.; *Holographic Ricci dark energy: interacting model and cosmological constraints*, Eur. Phys. J. C **72**, 1932 (2012).

[123] L.P. Chimento, M.G. Richarte; *Dark radiation and dark matter coupled to holographic Ricci dark energy*, Eur. Phys. J. C **73**, 2352 (2013).

[124] S. del Campo, J.C. Fabris, R. Herrera, W. Zimdahl; *Cosmology with Ricci dark energy*, Phys. Rev. D **87**, 123002 (2013).

[125] S. Chattopadhyay; *A Study on the Interacting Ricci Dark Energy in $f(R,T)$ Gravity*, Proc. Natl. Acad. Sci., India, Sect. A Phys. Sci. **84**, 87 (2014).

[126] H. Weyl; *A new extension of Relativity Theory (In German)*, Annalen Phys. **59**, 101 (1919); Surveys High Energy Phys. **5**, 237 (1986); Annalen Phys. **364**, 101 (1919).

[127] A.S. Eddington; *The Mathematical Theory of Relativity*, Cambridge University Press, (1923).

[128] T. Kaluza; *Zum Unitätsproblem der Physik*, Sitz. Preuss. Akad. Wiss. Phys. Math. **K1**, 966 (1921); T. Appelquist, A. Chodos and P.G.O. Freund; *Modern Kaluza-Klein theories*, Addison-Wesley, (1987).

[129] O. Klein; *Quantentheorie und fünfdimensionale Relativitätstheorie*, Zeits. Phys. **37**, 895 (1926); Nature **118**, 516 (1926); T. Appelquist, A. Chodos and P.G.O. Freund; *Modern Kaluza-Klein theories*, Addison-Wesley, (1987).

[130] E. Witten; *String theory dynamics in various dimensions*, Nucl. Phys. B **443**, 85 (1995); [arXiv:hep-th/9503124].

[131] K. Becker, M. Becker, J.H. Schwarz; *String theory and M-theory: A modern introduction*, Cambridge University Press, ISBN: 978-0-512-86069-7 (2007).

[132] P.G. Bergmann; *Unified field theory with fifteen variables*, Ann. Math **49**, 225 (1948).

[133] G.W. Horndeshe; *Second order scalar tensor field equations in a four-dimensional space*, Int. J. Theor. Phys. **10**, 363 (1974).

[134] R. Utiyama, B.S. DeWitt; *Renormalization of a classical gravitational field interacting with quantized matter fields*, J. Math. Phys. **3**, 608 (1962).

[135] A. Starobinsky; *A new type of isotropic cosmological models without singularity*, Phys. Lett. B **91**, 99 (1980).

[136] H.A. Buchdahl; *Non-linear Lagrangians and cosmological theory*, Mon. Not. Roy. Astron. Soc. **150**, 1 (1970).

[137] A.A. Starobinsky; *Disappearing cosmological constant in $f(R)$ gravity*, JETP Lett. **86**, 157 (2007); [arXiv:astro-ph/0706.2041].

[138] T.P. Sotiriou, V. Faraoni; *$f(R)$ theories of gravity*, Rev. Mod. Phys. **82**, 451 (2010); [arXiv:gr-qc/0805.1726].

[139] S. Nojiri, S.D. Odintsov; *Unified cosmic history in modified gravity: From $f(R)$ theory to Lorentz non-invariant models*, Phys. Rept. **505**, 59 (2011); [arXiv:gr-qc/1011.0544].

[140] S. Capozziello, V.F. Cardone, S. Carloni, A. Troisi; *Quintessence without scalar fields*, Rec. Res. Dev. Astron. Astrophys. **1**, 625 (2003); [arXiv:astro-ph/0303041].

[141] S. Capozziello, V.F. Cardone, A. Troisi; *Dark energy and dark matter as curvature effects?*, J. Cosmo. Astropart. Phys. **08**, 001 (2006); [arXiv:astro-ph/0602349].

[142] S. Capozziello, V.F. Cardone, A. Troisi; *Low surface brightness galaxy rotation curves in the low energy limit of R^n gravity: No need for dark matter?*, Mon. Not. Roy. Astron. Soc. **375**, 1423 (2007); [arXiv:astro-ph/0603522].

[143] C.G. Boehmer, T. Harko, F.S.N. Lobo; *Dark matter as a geometric effect in $f(R)$ gravity*, Astropart. Phys. **29**, 386 (2008); [arXiv:gr-qc/0709.0046].

[144] S. Capozziello, M. Francaviglia; *Extended theories of gravity and their cosmological and astrophysical applications*, Gen. Rel. Grav. **40**, 357 (2008); [arXiv:astro-ph/0706.1146].

[145] F.S.N. Lobo; *The dark side of gravity: Modified theories of gravity, dark energy: Current advances and ideas (Research Signpost)*, 173 (2009); [arXiv:gr-qc/0807.1640].

[146] S. Capozziello, M. de Laurentis; *Extended theories of gravity*, Phys. Rep. **509**, 167 (2011); [arXiv:gr-qc/1108.6266].

[147] M.C.B. Abdalla, S. Nojiri, S.D. Odintsov; *Consistent modified gravity: Dark energy, acceleration and the absence of cosmic doomsday*, Class. Quantum Grav. **22**, L35 (2005); [arXiv:hep-th/0409177].

[148] T. Clifton, P.G. Ferreira, A. Padilla, C. Skordis; *Modified gravity and cosmology*, Phys. Rept. **513**, 1 (2012); [arXiv:astro-ph/1106.2476].

[149] A. de Felice, S. Tsujikawa; $f(R)$ *theories*, Living Rev. Rel. **13**, 3 (2010); [arXiv:gr-qc/1002.4928].

[150] S. Nojiri, S.D. Odintsov; *Introduction to modified gravity and gravitational alternative for dark energy*, Int. J. Geom. Math. Mod. Phys. **4**, 115 (2007); [arXiv:hep-th/0601213].

[151] S. Nojiri, S.D. Odintsov; *Modified Gauss-Bonnet theory as gravitational alternative for dark energy*, Phys. Lett. B **631**, 1 (2005); [arXiv:hep-th/0508049].

[152] G. Cognola et al.; *Dark energy in modified Gauss-Bonnet gravity: Late-time acceleration and the hierarchy problem*, Phys. Rev. D **73**, 084007 (2006); [arXiv:hep-th/0601008].

[153] C. Brans, R.H. Dicke; *Mach's principle and a relativistic theory of gravitation*, Phys. Rev. **124**, 925 (1961).

[154] D. La, P.J. Steinhardt; *Extended infationary cosmology*, Phys. Rev. Lett. **62**, 376 (1989).

[155] Z. Berezhiania et al.; *Vanishing of cosmological constant and fully localized gravity in a brane world with extra time(s)*, Phys. Lett. B **517**, 387 (2001).

[156] R. Maartens, K. Koyama; *Brane-world gravity*, Living Rev. Rel. **13**, 5 (2010).

[157] P. Horava; *Quantum gravity at a Lifshitz point*, Phys. Rev. D **79**, 084008 (2009); [arXiv:hep-th/0901.3775].

[158] P. Horava; *Membranes at quantum criticality*, JHEP **0903**, 020 (2009); [arXiv:hep-th/0812.4287].

[159] Y. Zhang et al.; *Notes on f(T) theories*, J. Cosmol. Astropart. Phys **07**, 015 (2011).

[160] E.V. Linder; *Einstein's other gravity and the acceleration of the Universe*, Phys. Rev. D **81**, 127301 (2010); [arXiv:astro-ph/1005.3039].

[161] T. Harko et al.; $f(R,T)$ *gravity*, Phys. Rev. D **84**, 024020 (2011).

[162] A. Pasqua, S. Chattopadhyay, I. Khomenkoc; *A reconstruction of modified holographic Ricci dark energy in* $f(R,T)$ *gravity*, Canadian J. Phys. **91**, 632 (2013); [arXiv:gen-ph1305.1873].

[163] T.P. Sotiriou, V. Faraoni, S. Liberati; *Theory of gravitation theories: A no-progress report*, Int. J. Mod. Phys. D **17**, 399 (2008); [arXiv:gr-qc/0707.2748].

[164] O. Bertolami, P.J. Martins; *Nonminimal coupling and quintessence*, Phys. Rev. D **61**, 064007 (2000).

[165] T. Harko; *Modified gravity with arbitrary coupling between matter and geometry*, Phys. Lett. B **669**, 376 (2008).

[166] T. Harko, F.S.N. Lobo; $f(R,L_m)$ gravity, Eur. Phys. J. C **70**, 373 (2010).

[167] L.D. Landau, E.M. Lifshitz; *The classical theory of field*, Butterwash Heinemann, Oxford (1998).

[168] M.J.S. Houndjo, C.E.M. Batista, J.P. Campos, O.F. Piattella; *Finite-time singularities in* $f(R,T)$ *gravity and the effect of conformal anomaly*, Canadian J. Phys. **91**, 548 (2013); [arXiv:gr-qc/1203.6084].

[169] M. Sharif, M. Zubair; *Thermodynamics in* $f(R,T)$ *theory of gravity*, J. Cosmo. Astropart. Phys. **21**, 28 (2012); [arXiv:gr-qc/1204.0848].

[170] T. Azizi; *Wormhole geometries in* $f(R,T)$ *gravity*, Int. J. Theor. Phys. **52**, 3486 (2013); [arXiv:gr-qc/1205.6957].

[171] S. Chakraborty; *An alternative* $f(R,T)$ *gravity theory and the dark energy problem*, Gen. Rel. Grav. **45**, 2039 (2013); [arXiv:gen-ph/1212.3050].

[172] F.G. Alvarenga et al.; *Dynamics of scalar perturbations in $f(R,T)$ gravity*, Phys. Rev. D **87**, 103526 (2013); [arXiv:gr-qc/1302.1866].

[173] E.H. Baffou et al.; *Cosmological viable f(R,T) dark energy model: dynamics and stability*, Astrophys. Space Sci. **356**, 173 (2014).

[174] H. Shabani, M. Farhoudi; *Cosmological and solar system consequences of $f(R,T)$ gravity models*, Phys. Rev. D **90**, 044031 (2014).

[175] V. Fayaz et al.; *Anisotropic cosmological models in $f(R,T)$ gravity according to holographic and new agegraphic dark energy*, Astrophys. space Sci. **353**, 301 (2014).

[176] T. Harko; *Thermodynamic interpretation of the generalized gravity models with geometry-matter coupling*, Phys. Rev. D **90**, 044067 (2014).

[177] M. Jamil, D. Momeni, M. Raza, R. Myrzakulov; *Reconstruction of some cosmological models in $f(R,T)$ gravity*, Eur. Phys. J. C **72**, 1999 (2012); [arXiv:gen-ph/1107.5807].

[178] M.J.S. Houndjo; *Reconstruction of $f(R,T)$ gravity describing matter-dominated and accelerated phases*, Int. J. Mod. Phys. D **21**, 1250003 (2012); [arXiv:astro-ph/1107.3887].

[179] M.J.S. Houndjo, O.F. Piattella; *Reconstructing $f(R,T)$ gravity from holographic dark energy*, Int. J. Mod. Phys. D **2**, 1250024 (2012); [arXiv:gr-qc/1111.4275].

[180] C.P. Singh, V. Singh; *Reconstruction of modified $f(R,T)$ gravity with perfect fluid cosmological models*, Gen. Relativ. Gravit. **46**, 1696 (2014).

[181] M. Sharif, S. Rani, R. Myrzakulov; *Analysis of $f(R,T)$ gravity models through energy conditions*, Eur. Phys. J. Plus **128**, 123 (2013); [arXiv:gr-qc/1210.2714].

[182] F.G. Alvarenga, M.J. Houndjo, A.V. Monwanou, J.B. Chabi Oron; *Testing some $f(R,T)$ gravity models from energy conditions*, J. Mod. Phys. **4**, 130 (2013); [arXiv:gr-qc/1205.4678].

[183] M. Sharif, M. Zubair; *Anisotropic Universe models with perfect fluid and scalar field in $f(R,T)$ gravity*, J. Phys. Soc. Jpn. **81**, 114005 (2012); [arXiv:gr-qc/1301.2251].

[184] K.S. Adhav; *LRS Bianchi type-I cosmological model in $f(R,T)$ theory of gravity*, Astrphys. Space Sci. **339**, 365 (2012).

[185] M. Sharif, M. Zubair; *Energy conditions constraints and stability of power law solutions in $f(R,T)$ gravity*, J. Phys. Soc. Jpn. **82**, 014002 (2013); [arXiv:gr-qc/1210.3878].

[186] H. Shabani, M. Farhoudi; *$f(R,T)$ cosmological models in phase space*, Phys. Rev. D **88**, 044048 (2013); [arXiv:gr-qc/1306.3164].

[187] V.U.M. Rao, D. Neelima; *Bianchi type-VI_0 perfect fluid cosmological model in a modified theory of gravity*, Astrophys. Space Sci. **345**, 427 (2013).

[188] N. Ahmed, A. Pradhan; *Bianchi Type-V cosmology in $f(R,T)$ gravity with $\Lambda(T)$*, Int. J. Theor. Phys. **53**, 289 (2014); [arXiv:.gen-ph/1303.3000].

[189] T. Harko, P.H.R.S. Moraes; *Comment on "Reexamining $f(R,T)$ gravity", Phys. Rev. D 100, 064059 (2019)*, Phys. Rev. D **101**, 108501 (2020).

[190] C. Eckart; *The thermodynamics of irreversible processes. III. relativistic theory of the simple fluid*, Phys. Rev. **58**, 919 (1940).

[191] L.D. Landau, E.M. Lifshitz; *Fluid Mechanics, Vol. 6* (Butterworth Heinermann Ltd. Oxford, 1987).

[192] X.H. Meng, J. Ren, M.G. Hu; *Friedmann cosmology with a generalized equation of state and bulk viscosity*, Commun. Theor. Phys. **47**, 379 (2007).

[193] J. Ren, X.H. Meng; *Cosmological model with viscosity media (dark fluid) described by an effective equation of state*, Phys. Lett. B **633**, 1 (2006).

[194] M.G. Hu, X.H. Meng; *Bulk viscous cosmology: Statefinder and entropy*, Phys. Lett. B **635**, 186 (2006).

[195] C.P. Singh, S. Kumar, A. Pradhan; *Early viscous universe with variable gravitational and cosmological constants*, Class. Quantum Grav. **24**, 455 (2007).

[196] C.P. Singh; *Bulk viscous cosmology in early universe*, Pramana J. Phys. **71**, 33 (2008).

[197] C.P. Singh; *Viscous FRW models with particle creation in early universe*, Mod. Phys. Lett. A **27**, 1250070 (2012).

[198] C.P. Singh, P. Kumar; *Friedmann model with viscous cosmology in modified $f(R,T)$ gravity theory*, Eur. Phys. J. C **74**, 3070 (2014).

[199] P. Kumar, C.P. Singh; *Viscous cosmology with matter creation in modified $f(R,T)$ gravity*, Astrophys. Space Sci. **357**, 120 (2015).

[200] W. Misner, *The Isotropy of the Universe*, Astrophysical J. **151**, 431 (1968).

[201] W. Israel, J. Stewart; *Transient relativistic thermodynamics and kinetic theory*, Ann. Phys. **118**, 341 (1979).

[202] R. Maartens; *Dissipative cosmology*, Class. Quantum Phys. **12**, 1455 (1995).

[203] G.L. Murphy; *Big-Bang model without singularities*, Phys. Rev. D **8**, 4231 (1973).

[204] J.D. Barrow; *String-driven inflationary and deflationary cosmological models*, Nucl. Phys. B **310**, 743 (1988).

[205] Y.D. Xu, Z.G. Huang, X.H. Zhai; *Generalized Chaplygin gas model with or without viscosity in the $w-w'$ plane*, Astrophys. Space Sci. **337**, 493 (2012).

[206] C.J. Feng, X.Z. Li; *Viscous Ricci dark energy*, Phys. Lett. B **680**, 355 (2009).

[207] S. Nojiri, S.D. Odintsov; *Inhomogeneous equation of state of the universe: Phantom era, future singularity, and crossing the phantom barrier*, Phys. Rev. D **72**, 023003 (2005).

[208] S. Capozziello et al.; *Observational constraints on dark energy with generalized equations of state*, Phys. Rev. D **73**, 043512 (2006).

[209] N. Cruz, S. Lepe, F. Peña; *Dissipative generalized Chaplygin gas as phantom dark energy*, Phys. Lett. B **646**, 177 (2007).

[210] M. Cataldo, N. Cruz, S. Lepe; *Viscous dark energy and phantom evolution*, Phys. Lett. B **619**, 5 (2005).

[211] B. Saha; *Bianchi type Universe with viscous fluid*, Mod. Phys. Lett. A **20**, 2127 (2005).

[212] L. Sebastiani; *Dark viscous fluid coupled with dark matter and future singularity*, Eur. Phys. J. C **69**, 547 (2010).

[213] M.R. Setare, A. Sheykhi; *Viscous dark energy and generalized second law of thermodynamics*, Int. J. Mod. Phys. D **19**, 1205 (2010).

[214] I. Brevik; *Viscosity in modified gravity*, Entropy **14**, 2302 (2012).

[215] M. Zeyauddin, B. Saha; *Bianchi type V bulk viscous cosmological models with particle creation in general relativity.*, Eur. Phys. J. Plus **129**, 177 (2014).

[216] I. Brevik, V.V. Obukhov, A.V. Timoshkin; *Cosmological Models Coupled with Dark Matter in a Dissipative Universe* , Astrophys. Space Sci. **359**, 11 (2015).

[217] I. Brevik, V.V. Obukhov, A.V. Timoshkin; *Dark Energy Coupled with Dark Matter in Viscous Fluid Cosmology*, Astrophys. Space Sci. **355**, 399 (2015).

[218] I. Brevik et al.; *Viscous Cosmology for Early- and Late-Time Universe*, Int. J. Mod. Phys. D **26**, 1730024 (2017).

[219] I. Brevik, A.N. Makarenko, A.V. Timoshkin; *Viscous accelerating universe with nonlinear and logarithmic equation of state fluid* , Int. J. Geom. Meth. Mod. Phys. **16**, 1950150 (2019).

[220] I. Brevik, A.V. Timoshkin; *Viscous fluid holographic bounce*, Int. J. Geom. Meth. Mod. Phys. **17**, 2050023 (2020).

[221] I. Brevik, B.D. Normann; *Remarks on cosmological bulk viscosity in different epochs*, Symmetry **12**, 1085 (2020).

[222] I. Brevik, A.V. Timoshkin; *Rip brane cosmology from a viscous holographic dark fluid*, Int. J. Geom. Meth. Mod. Phys. **17**, 2050087 (2020).

[223] J.S. Gagnon, J. Lesgourgues; *Dark goo: Bulk viscosity as an alternative to dark energy*, J. Cosmol. Astropart. Phys. **09**, 026 (2011); [arXiv:astro-ph/1107.1503v2].

[224] L. Parker; *Quantized Fields and Particle Creation in Expanding Universes. I*, Phys. Rev. **183**, 1057 (1969).

[225] I. Prigogine et al.; *Thermodynamics of cosmological matter creation*, Proc. Natl. Acad. Sci. USA **85**, 7428 (1988).

[226] I. Prigogine et al.; *Thermodynamics and cosmology*, Gen. Relativ. Gravit. **21**, 8 (1989).

[227] J.A.S. Lima, A.S.M. Germano; *On the equivalence of bulk viscosity and matter creation*, Phys. Lett. A **170**, 373 (1992).

[228] M.O. Calvão, J.A.S. Lima, I. Waga; *On the thermodynamics of matter creation in cosmology*, Phys. Lett. A **162**, 223 (1992).

[229] J.A.S. Lima, A.S.M Germano, L.R.W. Abramo; *FRW-type cosmologies with adiabatic matter creation*, Phys. Rev. D **53**, 4287 (1996).

[230] E. Gunzig, R. Maartens, A.V. Nesteruk; *Inflationary cosmology and thermodynamics*, Class. Quantum Grav. **15**, 923 (1998).

[231] J.S. Alcaniz, J.A.S. Lima; *Closed and open FRW cosmologies with matter creation: kinematic tests*, Astron. Astrophys. **349**, 729 (1999).

[232] T. Harko, F.S.N. Lobo, J.P. Mimoso, D. Pavon; *Irreversible matter creation processes through a non-minimal curvature matter coupling*, [arXiv:1508.03069].

[233] T. Harko, F.S.N. Lobo, J.P. Mimoso, D. Pavon; *Gravitational induced particle production through a non-minimal curvature-matter coupling*, Eur. Phys. J. C **75**, 386 (2015).

[234] W. Zimdahl, D.J. Schwarz, A.B. Balakin, D. Pavón; *Cosmic antifriction and accelerated expansion*, Phys. Rev. D **64**, 063501 (2001).

[235] Y. Qiang, T.J. Zhang, Z.L. Yi; *Constraint on cosmological model with matter creation using complementary astronomical observations*, Astrophys. Space Sci. **311**, 407 (2007).

[236] J.A.S. Lima, F.E. Silva, R.C. Santos; *Accelerating cold dark matter cosmology ($\Omega_\Lambda = 0$)*, Class. Quantum Grav. **25**, 205006 (2008).

[237] G. Steigman, R.C. Santos, J.A.S. Lima; *An accelerating cosmology without dark energy*, J. Cosmol. Astropart. Phys. **06**, 033 (2009), [arXiv:astro-ph/0812.3912].

[238] J.A.S. Lima, J.F. Jesus, F.A. Oliveira, *CDM accelerating cosmology as an alternative to LCDM model*, J. Cosmol. Astropart. Phys. **11**, 027 (2010), [arXiv:astro-ph/0911.5727]

[239] V.H. Cárdenas; *Dark energy, matter creation and curvature*, Eur. Phys. J. C **72**, 2149 (2012).

[240] T. Harko, F.S.N. Lobo; *Irreversible thermodynamic description of interacting dark energy-dark matter cosmological models*, Phys. Rev. D **87**, 044018 (2013).

[241] T. Padmanabhan, S.M. Chitre; *Viscous universes*, Phys. Lett. A **120**, 433 (1987).

[242] J. Triginer, D. Pavón; *Particle production in a viscous cosmological fluid*, Gen. Relativ. Gravit. **26**, 513 (1994).

[243] I. Brevik, G. Stokkan; *Viscosity and matter creation in the early universe*, Astrophys. Space Sci. **239**, 89 (1996).

[244] C.P. Singh, A. Beesham; *Early universe cosmology with particle creation: kinematics tests*, Astrophys. Space Sci. **336**, 469 (2011).

[245] C.P. Singh; *Viscous FRW models with particle creation in early universe*, Mod. Phys. Lett. A **27**, 1250070 (2012).

[246] J. de Haro, S. Pan; *Gravitationally induced adiabatic particle production: From Big Bang to de Sitter*, Class. Quant. Grav. **33**, 165007 (2016).

[247] S. Pan, S. Chakraborty; *Will There Be Future Deceleration? A Study of Particle Creation Mechanism in Nonequilibrium Thermodynamics*, Adv. High Energy Phys. **201**, 654025 (2015).

[248] L.R.W. Abramo, J.A.S. Lima; *Inflationary Models Driven by Adiabatic Matter Creation*, Class. Quantum Grav. **13**, 2953 (1996).

[249] S. Pan, J. de Haro, A. Paliathanasis, R.J. Slagter; *Evolution and Dynamics of a Matter creation model*, Mon. Not. Roy. Astron. Soc. **460**, 1445 (2016).

[250] V. Sahni, T.D. Saini, A.A. Starobinsky, U. Alam; *Statefinder-A new geometrical diagnostic of dark energy*, JETP Lett. **77**, 201 (2003).

[251] U. Alam, V. Sahni, T.D. Saini, A.A. Starobinsky; *Exploring the expanding universe and dark energy using the statefinder diagnostic*, Mon. Not. R. Astron. Soc. **344**, 1057 (2003).

[252] M. Visser; *Jerk, snap, and the cosmological equation of state*, Class. Quant. Grav. **21**, 2603 (2004).

[253] M. Visser; *Cosmography: Cosmology without the Einstein equations*, Gen. Relativ. Gravit. **37**, 1541 (2005).

[254] V. Sahni, A. Shafieloo, A.A. Starobinsky; *Two new diagnostics of dark energy*, Phys. Rev. D **78**, 103502 (2008).

[255] M.L. Tong, Y. Zhang; *Cosmic age, statefinder, and Om diagnostics in the decaying vacuum cosmology*, Phys. Rev. D **80**, 023503 (2009).

[256] J.B. Lu, L.X. Xu; *Geometrical diagnostic for the generalised chaplygin gas model*, Int. J. Mod. Phys. D **18**, 1741 (2009).

[257] Z.G. Huang, H.Q. Lu, K. Zhang; *Om diagnostic for dilaton dark energy*, Astrophys. Space Sci. **331**, 331 (2011).

[258] M. Betoule et al.; *Improved cosmological constraints from a joint analysis of the SDSS-II and SNLS supernova samples*, Astron. Astrophys. **568**, A22 (2014).

[259] R. Jimenez, A. Loeb; *Constraining Cosmological Parameters Based on Relative Galaxy Ages*, Astrophys. J. **573**, 37 (2002).

[260] S.L. Cao et al.; *Testing backreaction effects with observational Hubble parameter data*, Eur. Phys. J. C **78**, 170 (2018).

[261] M.V. dos Santos, R.R.R. Reis, I. Waga; *Constraining the cosmic deceleration-acceleration transition with type Ia supernova, BAO/CMB and H(z) data*, J. Cosmol. Astropart. Phys. **02**, 066 (2016).

[262] N. Padmanabhan et al.; *A 2 per cent distance to* $z = 0.35$ *by reconstructing baryon acoustic oscillations-I. Methods and application to the Sloan Digital Sky Survey*, Mon. Not. Roy. Astron. Soc. **427**, 2132 (2012).

[263] F. Beutler et al.; *The 6dF Galaxy Survey: baryon acoustic oscillations and the local Hubble constant*, Mon. Not. Roy. Astron. Soc. **416**, 3017 (2011).

[264] L. Anderson et al.; *The clustering of galaxies in the SDSS-III Baryon Oscillation Spectroscopic Survey: baryon acoustic oscillations in the Data Releases 10 and 11 Galaxy samples*, Mon. Not. Roy. Astron. Soc. **441**, 24 (2014).

[265] C. Blake et al.; *The WiggleZ Dark Energy Survey: joint measurements of the expansion and growth history at* $z < 1$, Mon. Not. Roy. Astron. Soc. **425**, 405 (2012).

[266] H. Akaike; *A new look at the statistical model identification*, IEEE Transactions on Automatic Control **19**, 716 (1974).

[267] G. Schwarz; *Estimating the Dimension of a Model*, Ann. Statist. **6**, 461 (1978).

[268] A.R. Liddle; *Information criteria for astrophysical model selection*, Mon. Not. R. Astron. Soc. **377**, L74 (2007).

[269] B. Cheng; *Bulk viscosity in the early universe*, Phys. Lett. A **160**, 329 (1991).

[270] J.C. Fabris, S.V.B. Goncalves, R. de Sa Ribeiro; *Bulk viscosity driving the acceleration of the Universe*, Gen. Rel. Grav. **38**, 495 (2006).

[271] B. Li, J.D. Barrow; *Does bulk viscosity create a viable unified dark matter model?*, Phys. Rev. D **79**, 103521 (2009).

[272] A. Avelino, U. Nucamendi; *Can a matter-dominated model with constant bulk viscosity drive the acceleraterd expansion of the universe?*, J. Cosmol. Astropart. Phys. **04**, 006 (2009).

[273] A. Avelino, U. Nucamendi; *Exploring a matter-dominated model with bulk viscosity to drive the accelerated expansion of the Universe*, J. Cosmol. Astropart. Phys. **08**, 009 (2010).

[274] A. Avelino et al.; *Bulk Viscous Matter-dominated Universes: Asymptotic Properties*, J. Cosmol. Astropart. Phys. **08**, 012 (2013).

[275] A. Sasidharan, T.K. Mathew; *Bulk viscous matter and recent acceleration of the Universe*, Eur. Phys. J. C **75**, 348 (2015); [arXiv:gr-qc/1411.5154].

[276] J.A.S. Lima, F.E. Silva, R.C. Santos; *Accelerating Cold Dark Matter Cosmology ($\Omega_\Lambda \equiv 0$)*, Class. Quant. Grav. **25**, 205006 (2008); [arXiv:gr-qc/1411.5154].

[277] X.H. Meng, X. Dou; *Friedmann cosmology with bulk viscosity: a concrete model for dark energy*, Commun. Theor. Phys. **52**, 377 (2009).

[278] B. Wu Ya, S. Li, M.H. Fu, J. He; *A modified Chaplygin gas model with interaction*, Gen. Relativ. Gravit. **39**, 653 (2007).

[279] K. Bamba, S. Capozziello, S. Nojiri, S.D. Odintsov; *Dark energy cosmology: the equivalent description via different theoretical models and cosmography tests*, Astrophys. Space Sci. **342**, 155 (2012); [arXiv:gr-qc/1205.3421].

[280] M. Sharif, M. Zubair; *Thermodynamics in $f(R,T)$ theory of gravity*, J. Cosmol. Astropart. Phys. **03**, 028 (2012).

[281] D. Momeni, P.H.R.S. Moraes, R. Myrzakulov; *Generalized second law of thermodynamics in $f(R,T)$ theory of gravity*, Astrophys. Space Sci. **361**, 228 (2016).

[282] C.P. Singh, P. Kumar; *Statefinder diagnosis for holographic dark energy models in modified $f(R,T)$ gravity theory*, Astrophys. Space Sci. **361**, 157 (2016).

[283] Ø. Grøn; *Viscous inflationary universe models*, Astrophys. Space Sci. **173**, 191 (1990).

[284] I. Brevik, S.D. Odintsov; *Cardy-Verlinde entropy formula in viscous cosmology*, Phys. Rev. D **65**, 067302 (2002).

[285] I. Brevik, O. Gorbunova; *Dark Energy and Viscous Cosmology*, Gen. Relativ. Gravit. **37**, 2039 (2005).

[286] J. Ren, X.H. Meng; *Modified equation of state, scalar field, and bulk viscosity in Friedmann universe*, Phys. Lett. B **636**, 5 (2006).

[287] I. Brevik, E. Elizalde, O. Gorbunova, A.V. Timoshkin; *A FRW dark fluid with a non-linear inhomogeneous equation of state*, Eur. Phys. J. C **52**, 223 (2007).

[288] I. Brevik, O. Gorbunova, D. Saez-Gomez; *Casimir effects near the big rip singularity in viscous cosmology*, Gen. Relativ. Gravit. **42**, 1513 (2010).

[289] I. Brevik, V.V. Obukhov, A.V. Timoshkin; *Dark energy coupled with dark matter in viscous fluid cosmology*, Astrophys. Space Sci. **355**, 399 (2015).

[290] I. Brevik, S. Nojiri, S.D. Odintsov, D. Saez-Gomez; *Cardy-Verlinde formula in FRW Universe with inhomogeneous generalized fluid and dynamical entropy bounds near the future singularity*, Eur. Phys. J. C **69**, 563 (2010); [arXiv:hep-th/1002.1942].

[291] W.A. Hiscock, J. Salmonson; *Dissipative Boltzmann-Robertson-Walker cosmologies*, Phys. Rev. D **43**, 3249 (1991).

[292] E.H. Baffou, M.J.S. Houndjo, M. Hamani-Daouda; *Late-time cosmological approach in mimetic $f(R,T)$ gravity*, Eur. Phys. J. C **77**, 708 (2017).

[293] E.H. Baffou, M.J.S. Houndjo, I.G. Salako; *Viscous generalized Chaplygin gas interacting with $f(R,T)$ gravity*, Int. J. Geom. Method. Mod. Phys. **14**, 1750051 (2017).

[294] H. Shabani; *Cosmological consequences and statefinder diagnosis of a non-interacting generalized Chaplygin gas in $f(R,T)$ gravity*, Int. J. Mod. Phys. D **26**, 1750120 (2017).

[295] T. Harko, F.S.N. Lobo; *Generalized curvature-matter couplings in modified gravity*, Galaxies **2**, 410 (2014).

[296] D.J. Liu, X.Z. Li; *Dynamics of quintessence with thermal interactions*, Phys. Lett. B **611**, 8 (2005).

[297] C.W. Misner, K.S. Thorne, J.A. Wheeler; *Gravitation*, W.H. Freeman and Company, U.S.A. (1973).

[298] S. Nojiri, S.D. Odintsov, S. Tsujikawa; *Properties of singularities in (phantom) dark energy Universe*, Phys. Rev. D **71**, 063004 (2005); [arXiv:hep-th/0501025].

[299] S. Capozziello, M. de Laurentis, S. Nojiri, S.D. Odintsov; *Classifying and avoiding singularities in the alternative gravity dark energy models*, Phys. Rev D **79**, 124007 (2009).

[300] S. Myrzakul, R. Myrzakulov, L. Sebastiani; *Inhomogeneous viscous fluids in FRW universe and finite-future time singularities*, Astrophys. Space Sci. **350**, 845 (2014).

[301] G.S. Khadekar, D. Raut, V.G. Miskin; *FRW viscous cosmology with inhomogeneous equation of state and future singularity*, Mod. Phys. Lett. A **29**, 1550144 (2015).

[302] R. Brustein, D. Gorbonos, M. Hadad; *Wald's entropy is equal to a quarter of the horizon area in units of the effective gravitational coupling*, Phys. Rev. D **79**, 044025 (2009).

[303] M. Akbar; *Generalized Second Law of Thermodynamics in Extended Theories of Gravity*, Int. J. Theor. Phys. **48**, 2665 (2009).

[304] T.K. Mathew, M.B. Aswathy, M. Manoj; *Cosmology and thermodynamics of FLRW universe with bulk viscous stiff fluid*, Eur. Phy. J. C **74**, 3188 (2014).

[305] S.M. Carroll; *The cosmological constant*, Living Rev. Rel. **4**, 1 (2001); [arXiv:astro-ph/0004075].

[306] B. Chen, M. Li, Y. Wang; *Inflation with holographic dark energy*, Nucl. Phys. B **774**, 256 (2007).

[307] S. Basilakos, J.A.S. Lima; *Constraints on cold dark matter accelerating cosmologies and cluster formation*, Phys. Rev. D **82**, 023504 (2010).

[308] J.A.S. Lima, M.O. Calvao, I. Waga; Cosmology, Thermodynamics and Matter Creation, vol. 317, World Scientific, Singapore (1991).

[309] R.C. Nunes, S. Pan; *Cosmological consequences of an adiabatic matter creation process*, Mon. Not. R. Astron. Soc. **459**, 673 (2016).

[310] J.A.S. Lima, L.L. Graef, D. Pavón, S. Basilakos; *Cosmic acceleration without dark energy: background tests and thermodynamic analysis*, J. Cosmol. Astropart. Phys. **10**, 042 (2014).

[311] R.O. Ramos, M.V. dos Santos, I. Waga; *Matter creation and cosmic acceleration*, Phys. Rev. D **89**, 083524 (2014); [arXiv:1404.2604].

[312] R.C. Nunes, D. Pavón; *Phantom behavior via cosmological creation of particles*, Phys. Rev. D **91**, 063526 (2015); [arXiv:1503.04113].

[313] S. Pan, B.K. Pal, S. Pramanik; *Gravitationally influenced particle creation models and late-time cosmic acceleration*, Int. J. Geom. Methods Mod. Phys. **15**, 1850042 (2018).

[314] C.P. Singh, S. Kaur, *Matter creation cosmology in Brans-Dicke theory: Observational tests and thermodynamic analysis*, Phys. Rev. D **100**, 084057 (2019).

[315] V. Salzano et al.; *Linear dark energy equation of state revealed by supernovae?*, Mod. Phys. Lett. A **29**, 145008 (2014).

[316] P. Praseetha, T.K. Mathew; *Interacting modified holographic Ricci dark energy model and statefinder diagnosis in flat universe*, Int. J. Mod. Phys. D **23**, 1450024 (2014).

[317] D. Foreman-Mackey, D. Hogg, D. Lang and J. Goodman; *emcee: The MCMC Hammer*, Publications of the Astronomical Society of the Pacific **125**, 306 (2012).

[318] M. Li et al.; *Planck constraints on holographic dark energy*, J. Cosmol. Astropart. Phys. **09**, 021 (2013).

[319] D.M. Scolnic et al.; *The Complete Light-curve Sample of Spectroscopically Confirmed SNe Ia from Pan-STARRS1 and Cosmological Constraints from the Combined Pantheon Sample*, Astrophys. J. **859**, 101 (2018).

[320] A. Conley et al.; *Supernova constraints and systematic uncertainties from the first three years of the supernova legacy survey*, Astrophys. J. Suppl. Ser. **192**, 1 (2011).

[321] M. Moresco et al.; *Improved constraints on the expansion rate of the Universe up to* $z \sim 1.1$ *from the spectroscopic evolution of cosmic chronometers*, J. Cosmol. Astropart. Phys. **08**, 006 (2012).

[322] S. Alam et al.; *The clustering of galaxies in the completed SDSS-III Baryon Oscillation Spectroscopic Survey: cosmological analysis of the DR12 galaxy sample* , Mon. Not. R. Astron. Soc. **470**, 2617 (2017).

[323] T. Delubac et al.; *Baryon acoustic oscillations in the Ly*α *forest of BOSS DR11 quasars*, Astron. Astrophys. **574**, A59 (2015).

[324] A. Font-Ribera et al.; *Quasar-Lyman* α *forest cross-correlation from BOSS DR11: Baryon Acoustic Oscillations*, J. Cosmol. Astropart. Phys. **05**, 027 (2014).

[325] M.J. Reid, D.W. Pesce, A.G. Riess; *An Improved Distance to NGC 4258 and its Implications for the Hubble Constant*, Astrophys. J. **886 (2)**, L27 (2019).

[326] G. Hinshaw et al.; *Five-Year Wilkinson Microwave Anisotropy Probe (WMAP) Observations: Data Processing, Sky Maps, and Basic Results*, Astrophys. J. Suppl. **180**, 225 (2009).

[327] Y. Wang, L. Xu; *Current observational constraints to the holographic dark energy model with a new infrared cutoff via the Markov chain Monte Carlo method*, Phys. Rev. D **81**, 083523 (2010).

[328] I.A. Akhlaghi, M. Malekjani, S. Basilakos, H. Haghi; *Model selection and constraints from Holographic dark energy scenarios*, Mon. Not. R. Astron. Soc. **477**(3), 3659 (2018). [arXiv:1804.02989].

[329] L.P. Chimento, M.G. Richarte; *Interacting dark matter and modified holographic Ricci dark energy induce a relaxed Chaplygin gas*, Phys. Rev. D **84**, 123507 (2011).

[330] G.W. Gibbons, S.W. Hawking; *Cosmological event horizons, thermodynamics, and particle creation*, Phys. Rev. D **15**, 2738 (1977).

[331] A. Sheykhi; *Thermodynamics of interacting holographic dark energy with the apparent horizon as an IR cutoff*, Class. Quantum Grav. **27**, 025007 (2010).

[332] G. Izquierdo, D. Pavón; *The generalized second law in phantom dominated universes in the presence of black holes*, Phys. Lett. B **639**, 1 (2006).

[333] M. Akbar, R.G. Cai; *Thermodynamic behavior of the Friedmann equation at the apparent horizon of the FRW universe*, Phys. Rev. D **75**, 084003 (2007).

[334] C.P. Singh, A. Kumar; *Observational constraints on viscous Ricci dark energy model*, Astrophys. Space Sci. **364**, 94 (2019).

[335] C.P. Singh, S. Kaur; *Probing bulk viscous matter-dominated model in Brans-Dicke theory*, Astrophys. Space Sci. **365**, 2 (2019).

[336] W. Zimdahl, P. Pavón; *Reheating and adiabatic particle production*, Mon. Not. Roy. Astron. Soc. **266**, 872 (1994).

[337] C.P. Singh; *FRW models with particle creation in Brans-Dicke theory*, Astrophys. Space Sci. **338**, 411 (2012).

[338] S. Basilakos, M. Plionis; *Could dark matter interactions be an alternative to dark energy?*, Astron. Astrophys. **507**, 47 (2009).

[339] S. Chakraborty, S. Pan, S. Saha; *A third alternative to explain recent observations: Future deceleration*, Phys. Lett. B **738**, 424 (2014).

[340] D. Pavón, J. Gariel, G. Le Denmat; *Particle decay and bulk dissipative stress in the early universe*, Gen. Relativ. Gravit. **28**, 573 (1996).

[341] K. Desikan; *Cosmological Models with Bulk Viscosity in the Presence of Particle Creation*, Gen. Relativ. Grav. **29**, 435 (1997).

[342] G.P. Singh, A. Beesham; *Bulk viscosity and particle creation in Brans-Dicke theory*, Aust. J. Phys. **52**, 1039 (1999).

[343] V.B. Johri, S.K. Pandey; *Cosmological Models with Matter Creation in Open Thermodynamic Systems*, Int. J. Theor. Phys. **38**, 1981 (1999).

[344] G.P. Singh, R.V. Deshpande, T. Singh; *Viscous cosmological models with particle creation in Brans-Dicke theory*, Astrophys. Space Sci. **282**, 489 (2002).

[345] G.P. Singh, A.Y. Kale; *Anisotropic bulk viscous cosmological models with particle creation*, Astrophys. Space Sci. **331**, 207 (2011).

[346] R. Sudharsan, V.B. Johri; *Cosmological models with particle creation and bulk viscosity*, Gen. Relativ. Gravit. **26**, 41 (1994).

[347] U. Alam, V. Sahni, A.A. Starobinsky; *The case for dynamical dark energy revisited*, J. Cosmol. Astropart. Phys. **08**, 0406 (2004).

[348] M. Visser, C. Barcelo; *Energy conditions and their cosmological implications*, COSMO-99, 98 (2000); [arXiv:gr-qc/0001099].

[349] S. Carroll, *Spacetime and Geometry: An Introduction to General Relativity*, Addison Wesley (2004).

[350] J. Santos, J.S. Alcaniz; *Energy Conditions and Segre Classification of Phantom Fields*, Phys. Lett. B **619**, 11 (2005).

[351] J. Santos et al.; *Lookback time bounds from energy conditions*, Phys. Rev. D **76**, 043519 (2007).

[352] A.A. Sen, R.J. Scherrer; *The weak energy condition and the expansion history of the Universe*, Phys. Lett. B **659**, 457 (2008).

[353] Ya. B. Zeldovich; *Particle production in cosmology*, JETP Lett. **12**, 307 (1970).

[354] J. Gariel, G. le Denmat; *Matter creation and bulk viscosity in early cosmology*, Phys. Lett. A **200**, 11 (1995).

[355] J.A.S. Lima, J.S. Alcaniz; *Flat FRW cosmologies with adiabatic matter creation: Kinematic tests*, Astron. Astrophys. **348**, 1 (1999).

[356] W. Zimdahl, J. Triginer, D. Pavón; *Collisional equilibrium, particle production, and the inflationary universe*, Phys. Rev. D **54**, 6101 (1996).

[357] V.B. Johri, K. Desikan; *An Extended Class of FRW Models with Creation of Particles out of Gravitational Energy*, Astrophys. lett. Commun. **33**, 287 (1996).

[358] V. Singh, C.P. Singh; *Friedmann cosmology with particle creation in modified* $f(R,T)$ *gravity*, Int. J. Theor. Phys. **55**, 1257 (2016).

[359] W. Zimdahl, D.J. Schwarz, A.B. Balakin, D. Pavón; *Cosmic anti-friction and accelerated expansion*, Phys. Rev. D **64**, 063501 (2001).

[360] Y. Qiang, T.J. Zhang, Z.L. Yi; *Constraint on cosmological model with matter creation using complementary astronomical observations*, Astrophys. Space Sci. **311**, 407 (2007).

[361] J.A.S. Lima, S. Basilakos, F.E.M. Costa; *New cosmic accelerating scenario without dark energy*, Phys. Rev. D **86**, 103534 (2012).

[362] M. Kowalski et al.; *Improved Cosmological Constraints from New, Old and Combined Supernova Datasets*, Astrophys. J. **686**, 749 (2008).

[363] R.G. Cai, L.M. Cao, Y.P. Hu; *Hawking Radiation of Apparent Horizon in a FRW Universe*, Class. Quantum Grav. **26**, 155018 (2009); [arXiv:0809.1554].

[364] D. Bak, S.J. Rey; *Cosmic Holography*, Class. Quantum Grav. **17**, L83 (2000).

****

List of Publications

1. C.P. Singh and **Ajay Kumar**; *Ricci dark energy model with bulk viscosity*, The European Physical Journal Plus **133**, 312 (2018). **Impact Factor (3.911)**

2. C.P. Singh and **Ajay Kumar**; *Viscous Ricci dark energy and generalized second law of thermodynamics in modified* $f(R,T)$ *gravity*, Modern Physics Letters A **33**, 1850225 (2018). **Impact Factor (2.066)**

3. C.P. Singh and **Ajay Kumar**; *Holographic Ricci dark energy with constant bulk viscosity in modified* $f(R,T)$ *gravity*, Gravitation and Cosmology **25**, 58 (2019). **Impact Factor (1.173)**

4. C.P. Singh and **Ajay Kumar**; *Quintessence behavior via matter creation cosmology*, The European Physical Journal C **80**, 106 (2020). **Impact Factor (4.590)**

5. **Ajay Kumar** and C.P. Singh; *Observational constraints on holographic dark energy with matter creation*, Astrophysics and Space Science **365**, 84 (2020). **Impact Factor (1.830)**

6. **Ajay Kumar** and C.P. Singh; *Viscous Ricci dark energy model with matter creation: exact solution and observational tests*, Pramana Journal of Physics **94**, 129 (2020). **Impact Factor (2.219)**

7. C.P. Singh and **Ajay Kumar**, *Holographic dark energy, matter creation, and cosmic acceleration*, Physical Review D **102**, 123537 (2020). **Impact Factor (5.296)**

****